WORLD METEOROLOGICAL ORGANIZATION

GUIDE TO WAVE ANALYSIS AND FORECASTING

1998

(second edition)

WMO-No. 702

WORLD METEOROLOGICAL ORGANIZATION

GUIDE
TO
WAVE ANALYSIS
AND FORECASTING

1998

(second edition)

WMO-No. 702

Secretariat of the World Meteorological Organization – Geneva – Switzerland
1998

ISBN 92-63-12702-6

NOTE

The designations employed and the presentation of material in this publication do not imply the expression of any opinion whatsoever on the part of the Secretariat of the World Meteorological Organization concerning the legal status of any country, territory, city or area, or of its authorities or concerning the delimitation of its fontiers or boundaries.

CONTENTS

Page

FOREWORD

The national Meteorological Services of a large number of maritime countries have, for many years now, been engaged in the provision of ocean wave forecast and hindcast services in support of the requirements of users in the whole range of maritime activities (shipping, fisheries, offshore mining, commerce, coastal engineering, construction, recreation, and so on). In recognition of this, and of the relative lack of easily accessible guidance material on wave forecasting methodology suitable for use by national Meteorological Services in developing countries, the WMO *Guide to wave analysis and forecasting* was prepared by a group of experts and published in 1988 as publication WMO-No. 702. This formal WMO *Guide* updated and replaced the earlier, very popular, WMO *Handbook* on the same subject, first published in 1976.

In further recognition, both of the requirements of national Meteorological Services for the provision of ocean wave-related services and also of the rapid developments which were occurring in wave measurement, analysis and forecast techniques, the WMO Commission for Marine Meteorology (CMM) established in 1984 a WMO wave programme. The various elements of this programme are implemented, reviewed and updated by the CMM Sub-group on Wave Modelling and Forecasting. One of these elements involves the continuous review and revision, as necessary, of the *Guide to wave analysis and forecasting*. To this end, the sub-group established, in 1991, an *ad hoc* group of experts, under the chairmanship of Dr A. K. Laing (New Zealand), to undertake a complete revision and updating of the *Guide*, in the light of new developments and especially of feedback from users of the first edition.

The international team of experts, directed by Dr Laing, individually prepared substantially revised versions of the different chapters of the *Guide*. These individual contributions were subsequently coordinated, assembled and edited by Dr Laing into a draft, which was then submitted to a wide network of wave experts for review and comment. Reviewers' comments were incorporated to the extent possible and a final editing of a new, second edition of the *Guide* was made by Dr Laing.

No publication such as this can ever be perfect, particularly in such a continuously developing field of science and technology, and further additions and modifications will undoubtedly be required in the future. Nevertheless, it is firmly believed that this second edition of the *Guide to wave analysis and forecasting* will continue to prove a very valuable publication in support of the marine services provided by WMO's maritime Members. It is also believed that it continues to meet very well its two-fold objectives: to provide introductory but self-sufficient guidance material for use in the provision of basic wave forecast services, while at the same time acting as a source text and a guide to further reading on the subject.

Detailed acknowledgements to authors are given with each section and chapter as appropriate, but I should like here, on behalf of the World Meteorological Organization, to express my sincere appreciation to all the experts (authors, reviewers and particularly Dr Laing) who have contributed so much to this important and valuable publication.

(G. O. P. Obasi)
Secretary-General

ACKNOWLEDGEMENTS

The revision of this *Guide to wave analysis and forecasting* has been very much a team effort, involving a number of experts from several countries in various aspects of ocean waves. Overall direction of the project has been undertaken by Dr Andrew Laing (New Zealand). The chapter editors/authors have had overall responsibility for the revision of each chapter and, in cases where substantial assistance has been given, co-authors are acknowledged.

Much of the material is derived from the first edition of the *Guide* and the present editor would like to once again acknowledge the efforts put into that publication by the editor E. Bouws, and the chapter editors E. Bouws, L. Draper, A. K. Laing, D. J. T. Carter, L. Eide and J .A. Battjes.

The present edition has been produced with specific attributions due to:

- Overall direction and introduction:
  A. K. Laing, National Institute of Water and Atmospheric Research (NIWA), Wellington, New Zealand
- Chapter 1:
  A. K. Laing, NIWA, Wellington, New Zealand
- Chapter 2:
  W. Gemmill, National Meteorological Center (NMC), Washington D.C., USA
- Chapter 3:
  A. K. Magnusson, Norwegian Meteorological Institute (DNMI), Bergen, Norway
  M. Reistad, DNMI, Bergen, Norway
- Chapter 4:
  L. Burroughs, National Meteorological Center (NMC), Washington D.C., USA
- Chapter 5:
  M. Reistad, DNMI, Bergen, Norway
  A. K. Magnusson, DNMI, Bergen, Norway
- Chapter 6:
  M. Khandekar, Atmospheric Environment Service (AES), Toronto, Canada
- Chapter 7:
  L. Holthuijsen, Delft Technical University, Delft, the Netherlands
- Chapter 8:
  J. A. Ewing, United Kingdom
  D. J. T. Carter, Satellite Observing Systems, Godalming, Surrey, United Kingdom
- Chapter 9:
  D. J. T. Carter, Satellite Observing Systems, Godalming, Surrey, United Kingdom
  V. Swail, Atmospheric Environment Service (AES), Toronto, Canada

Illustrations have been acknowledged in the captions. Otherwise they have been taken from the previous edition of the *Guide* or specially prepared for this edition.

Contact with contributors can be made through the Ocean Affairs Division of the WMO Secretariat.

The Editor would like to thank the Secretariat staff who assisted in the preparation of this publication.

INTRODUCTION

Overview

The subject of this *Guide* is ocean waves, and specifically those generated by the wind. Such waves affect our coasts and activities of all kinds which we pursue at the coast, near the coast and out to sea. At any given time the waves are a result of the recent history of winds over often quite broad expanses of ocean. Indeed, knowledge of the winds allows us to diagnose the wave conditions. Just as the winds vary considerably in time and space, so do the waves. Hence, because there is some short-term predictability in the winds, there is an associated predictability for wind waves, enabling operational forecasts to be made. On the other hand, longer term estimates of wave conditions must be based on climatological information for which measurements, observations or "synthetic" data are needed. Estimates of likely future conditions or extremes may be required and there are often limited data to work with, making the correct choice of technique critical.

The objective of this *Guide* is to provide basic information and techniques in the analysis and forecasting of ocean waves. The *Guide* is not intended to be a comprehensive theoretical treatment of waves, nor does it contain details of present research activity, rather it focuses on providing a general overview with more detail on aspects considered useful in the practice of wave analysis and forecasting. The latest research into wave processes and modelling is given a thorough treatment in the recently published book, *Dynamics and modelling of ocean waves* (Komen et al., 1994), and an extensive treatment of problems related to wave data and their use is provided in *Waves in ocean engineering: measurement, analysis, interpretation* (Tucker, 1991). For problems specifically related to coastal engineering, a comprehensive reference is the *Shore protection manual* (CERC 1973, 1984).

The primary users of this publication are seen as being professionals and technicians involved in operations which are affected by ocean waves, that is a fairly wide community of marine operators and those providing specialized services to them. Marine weather forecasters form a key group, but the *Guide* is equally intended for the potential users of wave data analyses, forecasts and climatological products.

This edition of the WMO *Guide to wave analysis and forecasting* replaces the 1988 edition of the same name, which in turn replaced the 1976 WMO *Handbook on wave analysis and forecasting*. In all editions it has been recognized that the interpretation of wave data and products demands a good understanding of the processes by which these products are derived. An overview of the elementary theory is therefore necessary in this *Guide* and, wherever a technique or source of data is introduced, sufficient background information has been included to make this publication as self-contained as possible.

Whilst many of the basics have remained consistent between editions, there are developments which are creating new opportunities in wave information services. In recent years, an increasing number of wave products incorporate data from satellites or are synthesized from simulations using numerical wave models. Indeed, many forecasting centres are operationally using numerical models. Effective use of these products is only possible if the forecasters and other users have sufficient knowledge about the physical background of wave modelling and satellite observations.

Wave modelling was given prominence in the 1988 *Guide*, an emphasis which has been retained in this edition. The concerted international effort of the 1980s to develop physically realistic wave models has culminated in a generation of wave models which have been thoroughly researched, tested and are now becoming operational tools. Wave modelling has "come of age" with this development. This does not mean that the problem is solved, far from it. For example, dissipation plays a critical role in the energy balance, but is poorly known and is generally formulated to satisfy closure of the energy-balance equation. Further, for computational reasons, operational models must all use parameterizations of the wave-wave interactions which control the distribution of energy within the wave spectrum. The problems of wave evolution in shallow water and interaction with surface currents also require continuing efforts.

The present edition also includes a catalogue describing present day operational wave models and it is worth noting that regular updates of such models are given in WMO Marine Meteorology and Related Oceanographic Activities Report No. 12 and its supplements (see WMO, 1994(*a*)). Further, wave modelling has now been used extensively in synthesizing wave data for climatological purposes. Hence, in the chapter on wave statistics specific treatment of wave climatologies is presented, including the use of wave models in hindcasting.

Another exciting development since the last edition has been the increase in wave and wind data available from satellites. Thus, new material on this source of data

has been included particularly in the chapters on wind fields, wave data, climate and statistics. These data are also now being used in conjunction with wave models to provide improved initializations and to validate hindcast data. Reference is given to some of the work being carried out.

Notwithstanding such advances, it is recognized that many wave products are based on visual observations and manual analyses and forecasts are still widely used. Hence, material on manual methods has been retained in the present *Guide*. These manual methods are linked with the numerical by demonstrating their joint physical basis.

Terminology

Analysis of waves is used in this *Guide* to refer to a broad range of procedures. The conventional meteorological context of an analysis involves data assimilation and this has had limited application in deriving wave products since wave data have been too scarce. That is until recently, when the large volume of data from satellites has brought to the fore the problem of assimilating wave data into numerical models.

In this *Guide*, wave analysis incorporates the procedures for estimating, calculating or diagnosing wave conditions. There is a direct relationship between wind and waves which, in principle, is a matter of calculation by manual or automatic means. Sometimes this relationship is quite simple and can be represented by a table showing the wave height for a given wind speed (and possibly wind direction). In many cases, however, a more complicated approach is required, depending on (*a*) the amount of detail that is needed, i.e. information on wave periods, wave steepness, etc.; (*b*) the environmental conditions of the forecasting area, including the geometry of coastlines, bathymetry and currents; and (*c*) the nature of the wind which can sometimes be quite variable, i.e. with changes taking place before a stationary wave condition has been reached.

Forecasting has a meaning here which is slightly different from that which is common in meteorology. When issuing a wave forecast, one can forecast the propagation of wave energy, but the evolution (growth) of the wave energy is dependent on the wind and so a major part of the procedure is actually referring to the forecast of the winds that cause the waves. The wave growth is in fact *diagnosed* from the forecast wind.

Hindcasting, on the other hand, refers to the diagnosis of wave information based on historical wind data. A computation based on present wind data is commonly referred to as wave analysis. The term *nowcast* is increasingly used in meteorology in a similar context.

A number of conventions have been adopted in the formulations used in the *Guide*. In particular, vector quantities are written in bold italic type (e.g. $\boldsymbol{a}$) to distinguish them from scalar quantities (e.g. a). A glossary of variables, symbols and acronyms is included as Annex I.

Climatological issues

Whatever the main objective of the wave analysis or forecast, an appreciation of wave climatology is essential. The aim of some readers may be to derive the wave climate and estimate extremes, and for others to produce operational wave forecasts. For the latter it must be noted that verification of an estimate of wave conditions is often not possible due to the lack of wave observations. Hence, as with all computations, sensible results are more likely if the local wave *climate* is known, particularly the ranges and likelihood of various wave parameters (for example, height and period) in the sea or ocean area of interest. Furthermore, experience should give a feeling for the probable values which might occur under the given wind conditions. It is of great importance, therefore, that any investigation, including training for wave forecasting, starts with a detailed study of the geography and climatology of the area of interest, in order to appreciate the limitations of wind fetch for certain wind directions, the existence of strong ocean currents, the typical configuration of wind fields in the weather patterns prevailing over the area and the climatological probability of wind speeds and directions.

It is useful to know the range of wave heights and periods which may occur at sea in general: individual waves higher than 20 m are very rare — the highest wave reported and checked being 33 m (North Pacific, 1933) — which implies that characteristic or significant wave heights will rarely exceed 10 m; characteristic wave periods usually vary between four and 15 seconds and are seldom greater than 20 seconds. Furthermore, one should be aware that waves can travel long distances and still retain appreciable height and energy; for instance, waves generated in mid-latitude storms in the North Atlantic Ocean have been observed as swell in the South Atlantic, and certain atolls in the equatorial Pacific have been damaged by swell waves which must have travelled several thousands of kilometres.

If regular wave forecasting is required for a fixed position or area (e.g. in support of coastal or offshore engineering or other marine operations such as ship loading) it is preferable to arrange for regular wave measurements at suitable points. This provides data for verification of wave forecasts or validation of models for hindcasting. In a few instances it may even be possible to develop a sufficiently homogeneous set of measured data for determining the wave climate from statistical analysis. In many applications, the only way to obtain a satisfactory data set is to hindcast the waves for a sufficiently long time period, using wind fields derived from historical weather charts or archived air-pressure data from atmospheric models. However, the current availability of upwards of 10 years of satellite altimeter data globally allows wave height climatology to be accurately described, at least in areas of the world's oceans not affected by tropical storms, down to the spatial resolution of the satellite data.

Structure of the *Guide*

The *Guide* has been organized into three sections. ***The first section***, Chapters 1 to 4, comprises general background material, leading to a chapter on traditional manual wave forecasting techniques. An overview of the theory of free water waves is given in Chapter 1. Simple linear waves are introduced and their behaviour is described. These are the building blocks for more complex descriptions of wave fields, especially the frequency-directional spectrum. Other topics introduced include: the concepts of wave energy and group velocity, which are particularly important in discussions of the propagation of surface wave energy; the effects of depth on simple waves, providing an introduction to Chapter 7; and elementary statistical descriptions of wave records, for which a more complete description is provided in Chapter 9. Many textbooks are available which may provide extension of the concepts introduced here, see, for example, Lighthill (1978) and Crapper (1984).

Chapter 2 is devoted solely to the specification of the winds which drive wave generation. Due to the high sensitivity of wave growth to wind speed, reliable wave forecasts are only possible if the wind input is of sufficient accuracy. An overview of sources of surface wind data, and winds derived from meteorological analyses is given. The complication of the marine boundary layer is also discussed. Unfortunately, there are important outstanding problems in specifying the surface wind (see also Cavaleri, 1993). Of particular interest are the resolution required of the wind-field analysis, and the behaviour of the boundary layer. For example, the temperature difference between water and air is often used to specify the stability of the air directly over the water, but additional factors associated with the gustiness of the wind may also be important. A large body of opinion among wave modellers now agrees that wind forcing should be parameterized by means of wind stress rather than wind speed. However, this again leaves us with the problem of determining wind stress from measurements or, indirectly, from properties of the atmospheric boundary layer such as wind speed and stability. Chapter 2 concludes with a brief description of some statistical methods for deducing the surface wind.

In Chapter 3 the reader is introduced to the physical background of processes which control the evolution of wave conditions. Primarily these are wave generation by the wind, propagation across the ocean surface, dissipation and the reshuffling of energy within the wave spectrum caused by weakly non-linear wave-wave interactions. The formulation of these processes is given for application in both manual forecasting procedures and numerical modelling.

Whilst numerical wave modelling has become the norm in many centres, there is still widespread use of manual methods. These methods have been in operational use for more than 40 years and are well proven. Hence, Chapter 4 has survived largely intact from the original *Handbook*. Manual procedures are described for determining wind waves and a series of examples illustrates how the procedures are applied in progressively more complicated situations. The chapter is completed with a section illustrating simple manual methods for estimating the bottom influence on wave height.

The second section of the *Guide* focuses on wave modelling and also on the complications arising from waves either entering or being generated in finite depth or shallow waters.

Chapter 5 describes the general structure of numerical wave models based on an equation describing the energy balance of a surface wave field. Each of the identified elements is formulated and its use in wave models discussed. Full calculation of all these processes is not computationally viable in an operational environment and so wave models do not necessarily treat all of the components explicitly. Certain trade-offs are employed to improve operability. Some of these trade-offs are historical, arising from an era when computational power was limited and the dominant mechanisms were not as well attributed. The classes of wave model arising from this evolution are described.

The operation of numerical wave models is given further attention in Chapter 6. Important operational considerations are the model outputs, including a range of charts and coded formats, and the verification of the model products. This chapter also contains tables listing models known to WMO. A section on the use of these models in generating climatologies is a precursor to further discussion in Chapter 9.

The complicating factors of limited water depth and coastal geometry are discussed in Chapter 7. Here, methods for determining shoaling, refraction and diffraction are discussed. Also considered are the generation of new waves in shallow water and the formulation of dissipation due to bottom friction for inclusion in numerical wave models. The chapter also addresses some of the problems encountered in the nearshore zone, such as breaking waves and wave-induced set-up and currents.

The third section of the *Guide* deals with wave data, its use in deriving wave statistics and in the evaluation of the wave climate.

Chapter 8 encompasses a wide range of sources of observed and measured wave data. A significant development in recent years has been the satellite-borne instrumentation which provides large quantities of wave information. This is a large and expanding field and many of the details are beyond the scope of this *Guide*. Hence, the treatment is limited to an overview of remote-sensing techniques.

Finally, Chapter 9 is devoted to wave climate and the statistics used to describe it. Much of the statistical material may not be found collected together in any one textbook, particularly in relation to waves. The estimation of return values for extremes in wave height is given

considerable attention. Annex III, which is related to this chapter, contains a list of various distribution functions and their properties. It has been noted that knowledge of the wave climate is important in operational forecasting as well as in the estimation of extremes. Hence, the second part of Chapter 9 is devoted to the derivation of wave climatologies, from hindcasts as well as wave data. In respect to hindcasts we still face the problem of generating reliable historical wind fields, particularly from the time before the introduction of fine-mesh models in the early 1970s. The chapter includes tables identifying sources of major climatologies, both from measured and observed data and from hindcast wave data.

It is acknowledged that material has been included that is dated and "perishable". It is inevitable that information on the status of data acquisition, models being used, products being delivered, studies in progress and other activities, which was correct at the time of writing, is going to change. However, inclusion of these items is necessary in a publication of this type.

This publication is intended to provide guidance in solving day-to-day problems. In some cases, however, the problems concerned go beyond the scope of this *Guide*. If the reader wishes to pursue particular topics then sufficient references are included to provide a gateway to the open literature. The editor of the relevant chapter may also be contacted; the names and affiliations are listed in the "Acknowledgments". Further, the *Guide* is not intended to be a self-contained training course. In particular, specialist training courses are recommended for marine forecasters who are required to make wave forecasts. For example, the interpretation of the guidance which the output from a particular wave model provides for a particular national forecast service goes well beyond the scope of this *Guide*.

CHAPTER 1

AN INTRODUCTION TO OCEAN WAVES

A. K. Laing: editor

1.1 Introduction

Ocean surface waves are the result of forces acting on the ocean. The predominant natural forces are pressure or stress from the atmosphere (especially through the winds), earthquakes, gravity of the Earth and celestial bodies (the Moon and Sun), the Coriolis force (due to the Earth's rotation) and surface tension. The characteristics of the waves depend on the controlling forces. Tidal waves are generated by the response to gravity of the Moon and Sun and are rather large-scale waves. Capillary waves, at the other end of the scale, are dominated by surface tension in the water. Where the Earth's gravity and the buoyancy of the water are the major determining factors we have the so-called gravity waves.

Waves may be characterized by their *period*. This is the time taken by successive wave crests to pass a fixed point. The type and scale of forces acting to create the wave are usually reflected in the period. Figure 1.1 illustrates such a classification of waves.

On large scales, the ordinary tides are ever present but predictable. Less predictable are tsunamis (generated by earthquakes or land movements), which can be catastrophic, and storm surges. The latter are associated with the movement of synoptic or meso-scale atmospheric features and may cause coastal flooding.

Wind-generated gravity waves are almost always present at sea. These waves are generated by winds somewhere on the ocean, be it locally or thousands of kilometres away. They affect a wide range of activities such as shipping, fishing, recreation, coastal and offshore industry, coastal management (defences) and pollution control. They are also very important in the climate processes as they play a large role in exchanges of heat, energy, gases and particles between the oceans and atmosphere. It is these waves which will be our subject in this *Guide*.

To analyse and predict such waves we need to have a model for them, that is we need to have a theory for how they behave. If we observe the ocean surface we note that the waves often form a rather complex pattern. To begin we will seek a simple starting model, which is consistent with the known dynamics of the ocean surface, and from this we will derive a more complete picture of the wind waves we observe.

The model of the ocean which we use to develop this picture is based on a few quite simple assumptions:

- The incompressibility of the water. This means that the density is constant and hence we can derive a continuity equation for the fluid, expressing the conservation of fluid within a small cell of water (called a water particle);
- The inviscid nature of the water. This means that the only forces acting on a water particle are gravity and pressure (which acts perpendicular to the surface of the water particle). Friction is ignored;
- The fluid flow is irrotational. This means that the individual particles do not rotate. They may move around each other, but there is no twisting action. This allows us to relate the motions of neighbouring particles by defining a scalar quantity, called the velocity potential, for the fluid. The fluid velocity is determined from spatial variations of this quantity.

From these assumptions some equations may be written to describe the motion of the fluid. This *Guide* will not present the derivation which can be found in most textbooks on waves or fluids (see for example Crapper, 1984).

1.2 The simple linear wave

The simplest wave motion may be represented by a sinusoidal, long-crested, progressive wave. The sinusoidal descriptor means that the wave repeats itself and has the smooth form of the sine curve as shown in Figure 1.2. The long-crested descriptor says that the wave is a series of

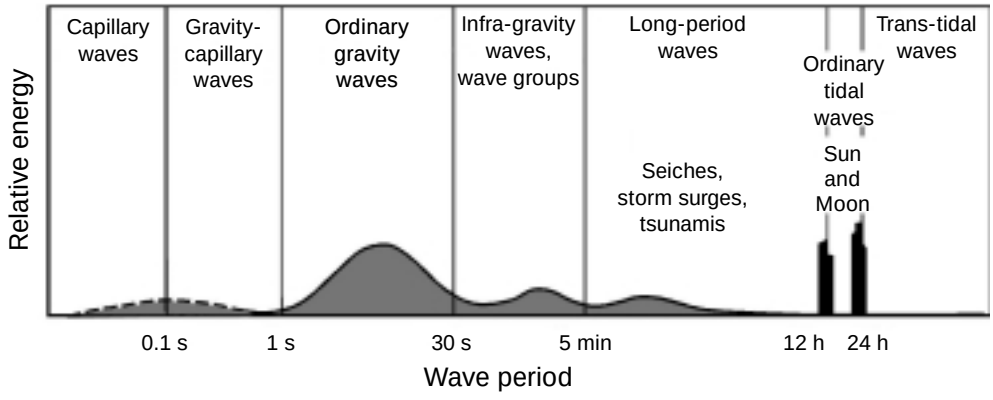

Figure 1.1 — Classification of ocean waves by wave period (*derived from Munk, 1951*)

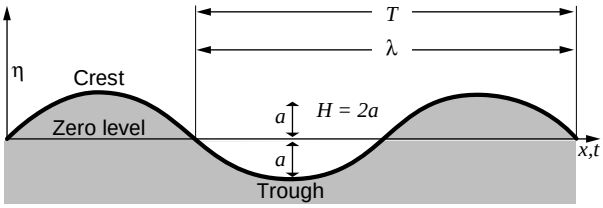

Figure 1.2 — A simple sinusoidal wave

long and parallel wave crests which are all equal in height, and equidistant from each other. The progressive nature is seen in their moving at a constant speed in a direction perpendicular to the crests and without change of form.

1.2.1 *Basic definitions**

The *wavelength*, λ, is the horizontal distance (in metres) between two successive crests.

The *period*, T, is the time interval (in seconds) between the passage of successive crests passed a fixed point.

The *frequency*, f, is the number of crests which pass a fixed point in 1 second. It is usually measured in numbers per second (Hertz) and is the same as $1/T$.

The *amplitude*, a, is the magnitude of the maximum displacement from mean sea-level. This is usually indicated in metres (or feet).

The *wave height*, H, is the difference in surface elevation between the wave crest and the previous wave trough. For a simple sinusoidal wave $H = 2a$.

The rate of propagation, c, is the speed at which the wave profile travels, i.e. the speed at which the crest and trough of the wave advance. It is commonly referred to as wave speed or *phase speed*.

The *steepness* of a wave is the ratio of the height to the length (H/λ).

1.2.2 *Basic relationships*

For all types of truly periodic progressive waves one can write:

$$\lambda = cT \,, \qquad (1.1)$$

i.e. the wavelength of a periodic wave is equal to the product of the wave speed (or phase speed) and the period of the wave. This formula is easy to understand. Let, at a given moment, the first of two successive crests arrive at a fixed observational point, then one period later (i.e. T seconds later) the second crest will arrive at the same point. In the meantime, the first crest has covered a distance c times T.

The wave profile has the form of a sinusoidal wave:

$$\eta(x,t) = a \sin (kx - \omega t) \,. \qquad (1.2)$$

In Equation 1.2, $k = 2\pi/\lambda$ is the *wavenumber* and $\omega = 2\pi/T$, the *angular frequency*. The wavenumber is a cyclic measure of the number of crests per unit distance and the angular frequency the number of radians per second. One wave cycle is a complete revolution which is 2π radians.

Equation 1.2 contains both time (t) and space (x) coordinates. It represents the view as may be seen from an aircraft, describing both the change in time and the variations from one point to another. It is the simplest solution to the equations of motion for gravity wave motion on a fluid, i.e. linear surface waves.

The wave speed c in Equation 1.1 can be written as λ/T or, now that we have defined ω and k, as ω/k. The variation of wave speed with wavelength is called *dispersion* and the functional relationship is called the *dispersion relation*. The relation follows from the equations of motion and, for deep water, can be expressed in terms of frequency and wavelength or, as it is usually written, between ω and k:

$$\omega^2 = gk \,, \qquad (1.3)$$

where g is gravitational acceleration, so that the wave speed is:

$$c = \frac{\lambda}{T} = \frac{\omega}{k} = \sqrt{\frac{g}{k}} \,.$$

If we consider a snapshot at time $t = 0$, the horizontal axis is then x and the wave profile is "frozen" as:

$$\eta(x) = a \sin (kx) \,.$$

However, the same profile is obtained when the wave motion is measured by means of a wave recorder placed at the position $x = 0$. The profile then recorded is

$$\eta(t) = a \sin (-\omega t) \,. \qquad (1.4)$$

Equation 1.4 describes the motion of, for instance, a moored float bobbing up and down as a wave passes by.

The important parameters when wave forecasting or carrying out measurements for stationary objects, such as offshore installations, are therefore wave height, wave period (or wave frequency) and wave direction. An observer required to give a visual estimate will not be able to fix any zero level as in Figure 1.2 and cannot therefore measure the amplitude of the wave. Instead, the vertical distance between the crest and the preceding trough, i.e. the wave height, is reported.

In reality, the simple sinusoidal waves described above are never found at sea; only swell, passing through an area with no wind, may come close. The reason for starting with a description of simple waves is that they represent the basic solutions of the physical equations which govern waves on the sea surface and, as we shall see later, they are the "building blocks" of the real wave fields occurring at sea. In fact, the concept of simple sinusoidal waves is frequently used as an aid to understanding and describing waves on the sea surface. In spite of this simplified description, the definitions and formulae derived from it are extensively used in practice and have proved their worth.

* See also key to symbols in Annex I.

1.2.3 *Orbital motion of water particles*

It is quite evident that water particles move up and down as waves travel through water. By carefully watching small floating objects, it can be seen that the water also moves backwards and forwards; it moves forward on the crest of a wave and backward in the trough. If the water is not too shallow relative to the wavelength, the displacements are approximately as large in the horizontal as in the vertical plane. In fact, during one cycle of a simple wave (i.e. a wave period) the particles describe a circle in a vertical plane. The vertical plane is the cross-section which we have drawn in Figure 1.2. In shallow water the motion is an ellipse. Figure 1.3 illustrates this particle motion for a simple sinusoidal wave in deep water.

Consider the speed at which a water particle completes its path. The circumference of the circle is equal to πH. This circumference is covered by a particle within a time equal to one period T. The speed of the water is therefore $\pi H/T$. This is also the greatest forward speed reached in the crests. The speed of individual water particles should not be confused with the speed at which the wave profile propagates (wave speed). The propagation rate of the wave profile is usually far greater, as it is given by λ/T, and the wavelength λ is generally much greater than πH.

Figure 1.3 has been slightly simplified to show the progression of wave crests and troughs as the result of water particle motion. In reality, depending on the wave steepness, a water particle does not return exactly to the starting point of its path; it ends up at a slightly advanced position in the direction in which the waves are travelling (Figure 1.4). In other words, the return movement in the wave trough is slightly less than the forward movement in the wave crest, so that a small net forward shift remains. This difference increases in steep waves (see Section 1.2.7).

1.2.4 *Energy in waves*

We have noted that waves are associated with motion in the water. Therefore as a wave disturbs the water there is kinetic energy present which is associated with the wave, and which moves along with the wave. Waves also displace particles in the vertical and so affect the potential energy of the water column. This energy also moves along with the wave. It is an interesting feature of the waves that the total energy is equally divided between kinetic energy and potential energy. This is called the equipartition of energy.

It is also important to note that the energy does **not** move at the same speed as the wave, the phase speed. It moves with the speed of groups of waves rather than individual waves. The concept of a group velocity will be discussed in Section 1.3.2 but it is worth noting here that, in deep water, group velocity is half the phase speed.

The total energy of a simple linear wave can be shown to be $\rho_w g a^2/2$ which is the same as $\rho_w g H^2/8$, where ρ_w is the density of water. This is the total of the

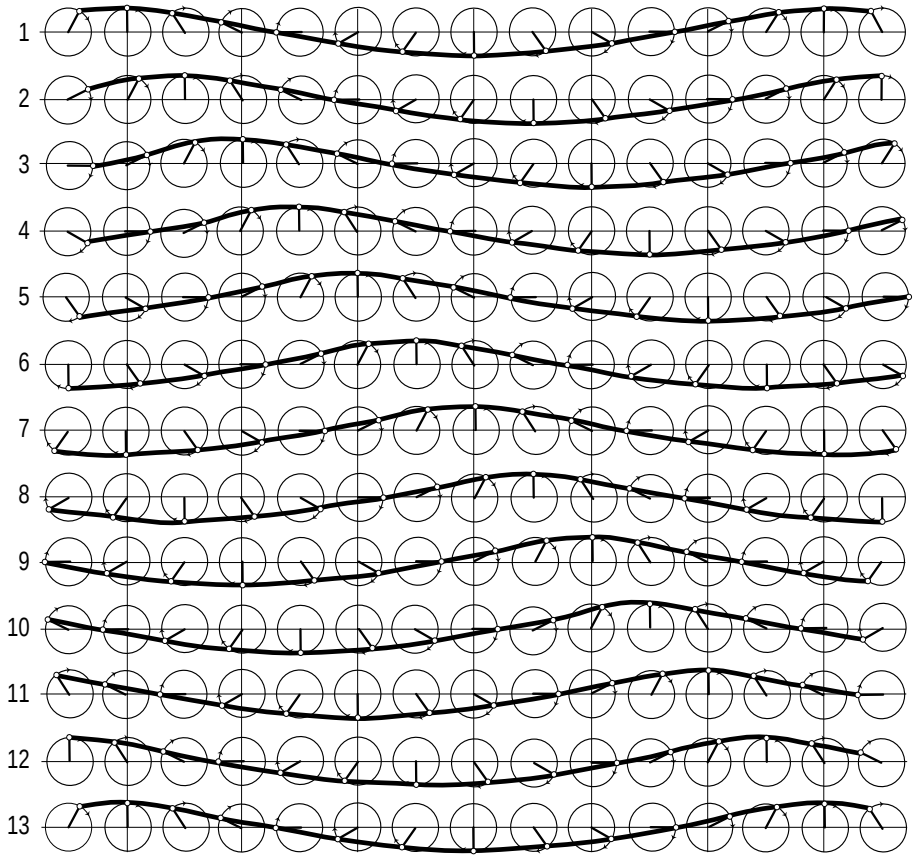

Figure 1.3 — Progression of a wave motion. Thirteen snapshots each with an interval of 1/12th period (*derived from Gröen and Dorrestein, 1976*)

Figure 1.4 — Path shift of a water particle during two wave periods

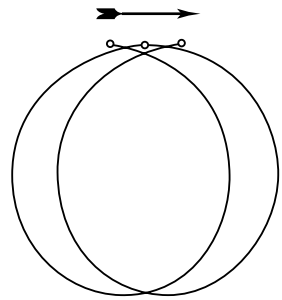

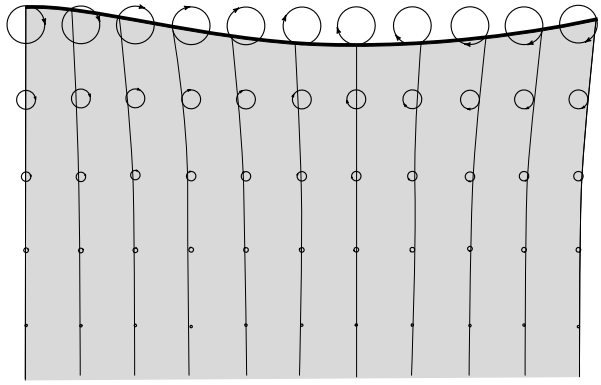

Figure 1.5 — Paths of the water particles at various depths in a wave on deep water. Each circle is one-ninth of a wavelength below the one immediately above it

potential and kinetic energies of all particles in the water column for one wavelength.

1.2.5 *Influence of water depth*

As a wave propagates, the water is disturbed so that both the surface and the deeper water under a wave are in motion. The water particles also describe vertical circles, which become progressively smaller with increasing depth (Figure 1.5). In fact the decrease is exponential.

Below a depth corresponding to half a wavelength, the displacements of the water particles in deep water are less than 4 per cent of those at the surface. The result is that, as long as the actual depth of the water is greater than the value corresponding to $\lambda/2$, the influence of the bottom on the movement of water particles can be considered negligible. Thus, the water is called deep with respect to a given surface wave when its depth is at least half the wavelength.

In practice it is common to take the transition from deep to transitional depth water at $h = \lambda/4$. In deep water, the displacements at this depth are about 20 per cent of those at the surface. However, so long as the water is deeper than $\lambda/4$, the surface wave is not appreciably deformed and its speed is very close to the speed on deep water. The following terms are used to characterize the ratio between depth (h) and wavelength (λ):

- Deep water $h > \lambda/4$;
- Transitional depth $\lambda/25 < h < \lambda/4$;
- Shallow water $h < \lambda/25$.

Note that wave *dissipation* due to interactions with the bottom (friction, percolation, sediment motion) is not yet taken into account here.

When waves propagate into shallow water, for example when approaching a coast, nearly all the characteristics of the waves change as they begin to "feel" the bottom. Only the period remains constant. The wave speed decreases with decreasing depth. From the relation $\lambda = cT$ we see that this means that the wavelength also decreases.

From linearized theory of wave motion, an expression relating wave speed, c, to wavenumber, $k = 2\pi/\lambda$, and water depth, h, can be derived:

$$c^2 = \frac{g}{k} \tanh kh \,, \tag{1.5}$$

where g is the acceleration of gravity, and tanh x denotes the hyperbolic tangent:

$$\tanh = \frac{e^x - e^{-x}}{e^x + e^{-x}}.$$

The dispersion relation for finite-depth water is much like Equation 1.5. In terms of the angular frequency and wavenumber, we have then the generalized form for Equation 1.3:

$$\omega^2 = gk \tanh kh \,. \tag{1.3a}$$

In deep water ($h > \lambda/4$), tanh kh approaches unity and c is greatest. Equation 1.5 then reduces to

$$c^2 = \frac{g}{k} = \frac{g\lambda}{2\pi} \tag{1.6}$$

or, when using $\lambda = cT$ (Equation 1.1)

$$T = \sqrt{\frac{2\pi\lambda}{g}} \tag{1.7}$$

and

$$\lambda = \frac{gT^2}{2\pi} \tag{1.8}$$

and

$$c = \frac{gT}{2\pi} = \frac{g}{2\pi f} = \frac{g}{\omega} \,. \tag{1.9}$$

Expressed in units of metres and seconds (m/s), the term $g/2\pi$ is about equal to 1.56 m/s^2. In this case, one can write $\lambda = 1.56\ T^2$ m and $c = 1.56\ T$ m/s. When, on the other hand, c is given in knots, λ in feet and T in seconds, these formulae become $c = 3.03\ T$ knots and $\lambda = 5.12\ T^2$ feet.

When the relative water depth becomes shallow ($h < \lambda/25$), Equation 1.6 can be simplified to

$$c = \sqrt{gh} \,. \tag{1.10}$$

This relation is of importance when dealing with long-period, long-wavelength waves, often referred to as long waves. When such waves travel in shallow water, the wave speed depends only on water depth. This relation can be used, for example, for tsunamis for which the entire ocean can be considered as shallow.

If a wave is travelling in water with transitional depths ($\lambda/25 < h < \lambda/4$), approximate formulae can be used for the wave speed and wavelength in shallow water:

$$c = c_0 \sqrt{\tanh k_0 h} \,, \tag{1.11}$$

$$\lambda = \lambda_0 \sqrt{\tanh k_0 h} \,, \tag{1.12}$$

with c_0 and λ_0 the deep-water wave speed and wavelength according to Equations 1.6 and 1.8, and k_0 the deep-water wavenumber $2\pi/\lambda_0$.

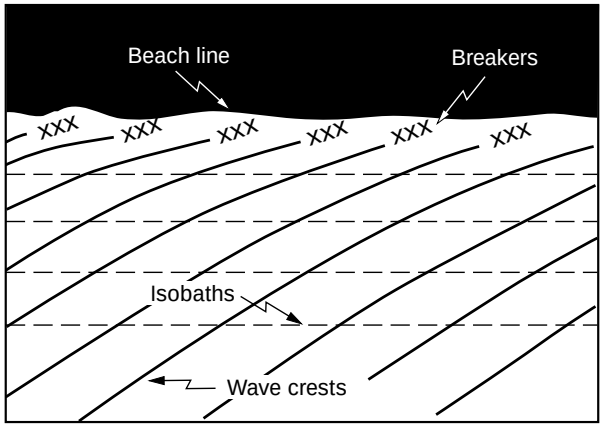

Figure 1.6 — Refraction along a straight beach with parallel bottom contours

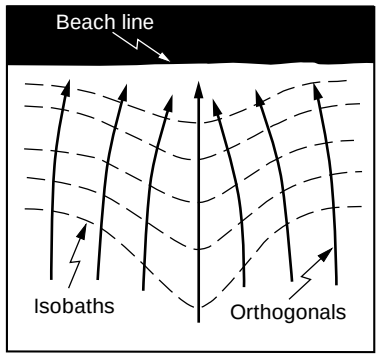

Figure 1.7(*a*) — Refraction by a submarine ridge

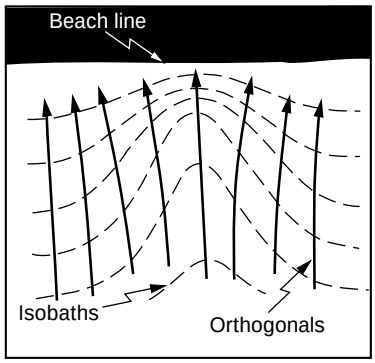

Figure 1.7(*b*) — Refraction by a submarine canyon

Figure 1.8 — Refraction along an irregular shoreline

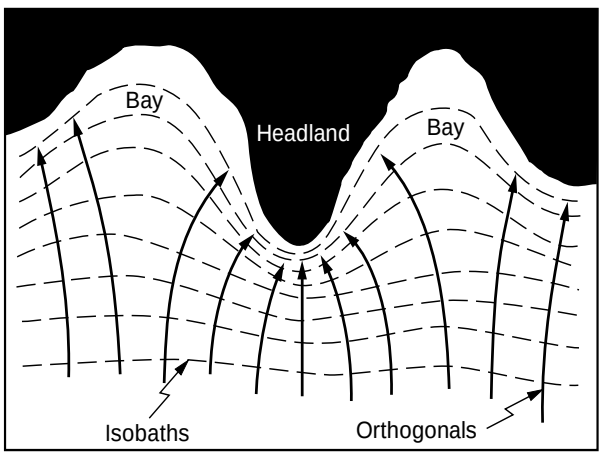

A further feature of changing depth is changing wave height. As a wave approaches the shore its height increases. This is a result of the changes in group velocity. The energy propagating towards the coast must be conserved, at least until friction becomes appreciable, so that if the group velocity decreases and wavelength decreases, the energy in each wavelength must increase. From the expression for energy in Section 1.2.4 we see that this means that the height of the wave must increase.

1.2.6 *Refraction and diffraction*

As waves begin to feel the bottom, a phenomenon called refraction may occur. When waves enter water of transitional depth, if they are not travelling perpendicular to the depth contours, the part of the wave in deeper water moves more rapidly than the part in shallower water, according to Equation 1.11, causing the crest to turn parallel to the bottom contours. Some examples of refraction patterns are shown in Figures 1.6, 1.7 and 1.8.

Generally, any change in the wave speed, for instance due to gradients of surface currents, may lead to refraction, irrespective of the water depth. In Section 4.5.1 a few examples are given to illustrate refraction under simplified conditions. A more complete description of methods for the analysis of refraction and diffraction can be found in Sections 7.3 and 7.4, and in CERC (1984).

Finally, the phenomenon of wave diffraction should be mentioned. It most commonly occurs in the lee of obstructions such as breakwaters. The obstruction causes energy to be transformed along a wave crest. This transfer of energy means that waves can affect the water in the lee of the structure, although their heights are much reduced. An example is illustrated in the photograph in Figure 1.9.

1.2.7 *Breaking waves*

In Section 1.2.3, it was noted that the speed of the water particles is slightly greater in the upper segment of the orbit than in the lower part. This effect is greatly magnified in very steep waves, so much so that the maximum forward speed may become not $\pi H/T$ but $7H/T$. Should $7H$ become equal to the wavelength λ (i.e. $H/\lambda = 1/7$), the forward speed of the water in the crest would then be equal to the rate of propagation which is λ/T. There can be no greater forward speed of the water because the water would then plunge forward out of the wave: in other words, the wave would break.

According to a theory of Stokes, waves cannot attain a height of more than one-seventh of the wavelength without breaking. In reality, the steepness of waves is seldom greater than one-tenth. However, at values of that magnitude, the profile of the wave has long ceased to be a simple undulating line and looks more like a trochoid (Figure 1.10). According to Stokes' theory, at the limiting steepness of one-seventh, the forward and backward slopes of the wave meet in the crest under an angle of 120° (Figure 1.11).

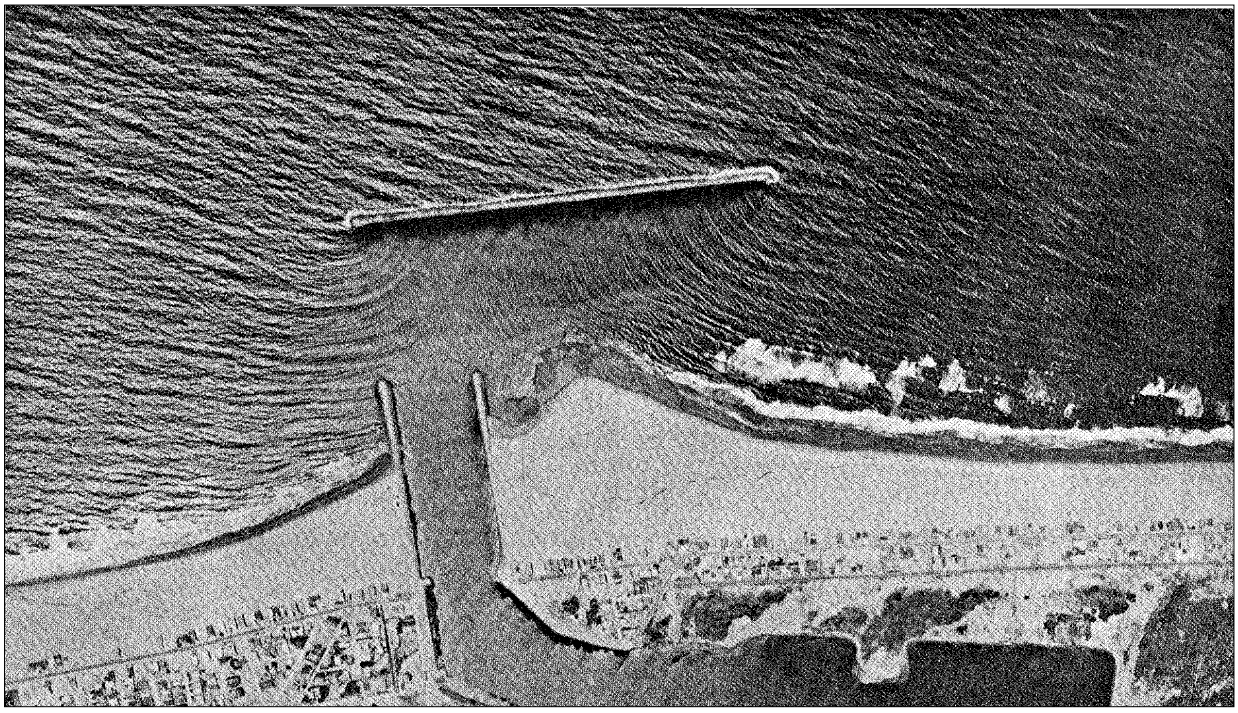

Figure 1.9 — Wave diffraction at Channel Islands harbour breakwater (California) (*from CERC, 1977*)

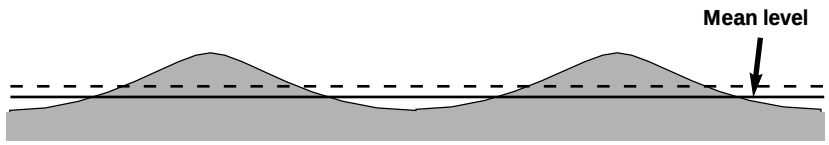

Figure 1.10 — Trochoidal wave profile. Here the crests project farther above the mean level than the troughs sink under it

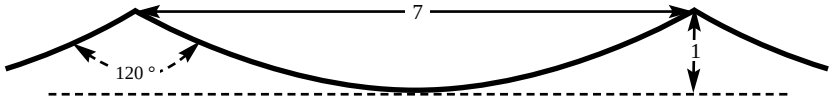

Figure 1.11 — Ultimate form which water waves can attain according to Stokes' theory

When waves propagate into shallow water their characteristics change as they begin to feel the bottom, as we have already noted in Section 1.2.5. The wave period remains constant, but the speed decreases as does the wavelength. When the water depth becomes less than half the wavelength, there is an initial slight decrease in wave height*. The original height is regained when the ratio h/λ is about 0.06 and thereafter the height increases rapidly, as does the wave steepness, until breaking point is reached:

$$h_b = 1.28\, H_b \qquad (1.13)$$

in which h_b is termed the breaking depth and H_b the breaker wave height.

1.3 Wave fields on the ocean

1.3.1 *A composition of simple waves*

Actual sea waves do not look as simple as the profile shown in Figure 1.2. With their irregular shapes, they appear as a confused and constantly changing water surface, since waves are continually being overtaken and crossed by others. As a result, waves at sea are often short-crested. This is particularly true for waves growing under the influence of the wind (*wind sea*).

A more regular pattern of long-crested and nearly sinusoidal waves can be observed when the waves are no longer under the influence of their generating winds. Such waves are called *swell* and they can travel hundreds and thousands of kilometres after having left the area in which they were generated. Swell from distant generating areas often mixes with wind waves generated locally.

* Tracking a wave into shallow water, the wavelength decreases and the wave slows down but, initially, its energy does not. The energy then spreads over relatively more waves and the height reduces This is only temporary. The wave energy soon also slows and the height begins to increase.

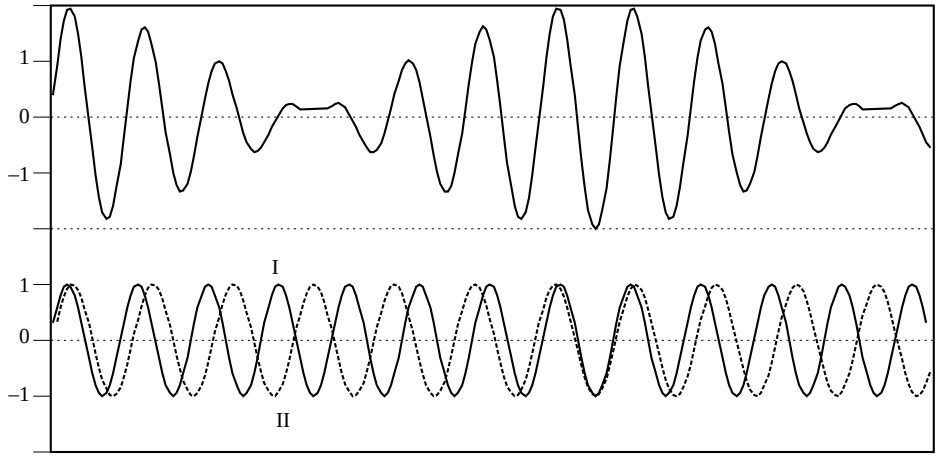

Figure 1.12 — The upper profile is equal to the sum (superposition) of two simple waves, I and II, shown in the lower part of the figure. The horizontal dimensions are greatly shortened with respect to the vertical ones

The simple waves, which have been described in Section 1.2, can be shown to combine to compose the observed patterns. To put it differently, any observed wave pattern on the ocean can be shown to comprise a number of simple waves, which differ from each other in height, wavelength and direction.

As a first step, let us consider waves with long, parallel crests but which differ in height, for example, the profile as shown in the top curve of Figure 1.12. Although this curve looks fairly regular, it is certainly no longer the profile of a simple sinusoidal wave, because the height is not everywhere the same, nor are the horizontal distances between crests. This profile, however, can be represented as the sum of two simple wave profiles of slightly different wavelength (see I and II in Figure 1.12). In adding the vertical deviations of I and II at corresponding points of the horizontal axis, we obtain the vertical deviations of the sum of wave I and wave II, represented by the top wave profile in Figure 1.12.

Thus, the top profile can be broken down, or decomposed, into two simple waves of different wavelength. The reason why the crests are of varying height in the sum of I and II is that at one place waves I and II are "in phase" and their heights therefore add up, whereas the resulting height is reduced at those places where the waves are out of phase.

Taking this idea one step further, we can see how an irregular pattern of wind waves can be thought of as a superposition of an infinite number of sinusoidal waves, propagating independently of each other. This is illustrated in Figure 1.13, which shows a great number of sinusoidal waves piled up on top of each other. Think, for example, of a sheet of corrugated iron as representing a set of simple sinusoidal waves on the surface of the ocean and caught at an instant in time. Below this, there is another set of simple sinusoidal waves travelling in a slightly different direction from the one on top. Below that again is a third one and a fourth one, etc. — all with different directions and wavelengths. Each set is a classic example of simple sinusoidal waves.

It can be shown that, as the number of different sinusoidal waves in the sum is made larger and larger and the heights are made smaller and smaller, and the periods and directions are packed closer and closer together (but never the same and always over a considerable range of values), the result is a sea surface just like the one actually observed. Even small irregularities from the sinusoidal shape can be represented by superpositions of simple waves.

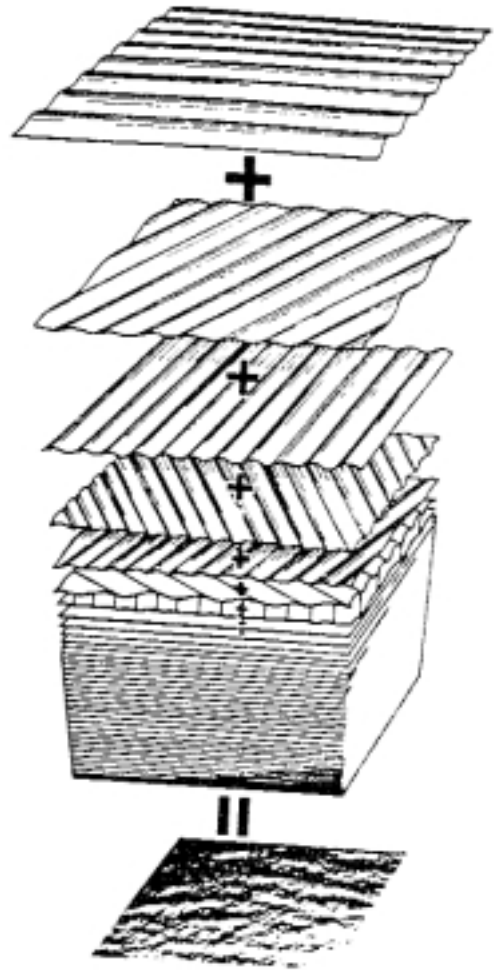

Figure 1.13 — The sea surface obtained from the sum of many sinusoidal waves (*derived from Pierson, Neumann and James, 1955*)

1.3.2 *Wave groups and group velocity*

We have seen how waves on the ocean are combinations of simple waves. In an irregular sea the number of differing wavelengths may be quite large. Even in regular swell, there are many different wavelengths present but they tend to be grouped together. In Figure 1.12 we see how simple waves with close wavelengths combine to form groups of waves. This phenomenon is common. Anyone who has carefully observed the waves of the sea will have noticed that in nature also the larger waves tend to come in groups.

Although various crests in a group are never equidistant, one may speak of an average distance and thus of an average wavelength. Despite the fact that individual crests or wave tops advance at a speed corresponding to their wavelength, the group, as a coherent unit, advances at its own velocity — the *group velocity*. For deep water this has magnitude (group speed):

$$c_g = \frac{c}{2}. \qquad (1.14)$$

A more general expression also valid in finite depth water is:

$$c_g = \frac{c}{2}\left(1 + \frac{2kh}{\sinh 2kh}\right). \qquad (1.15)$$

The general form for the group speed can be shown to be:

$$c_g = \frac{d\omega}{dk}.$$

Derivations may be found in most fluid dynamics texts (e.g. Crapper, 1984).

We can also show that the group velocity is the velocity at which wave energy moves. If we consider the energy flow (flux) due to a wave train, the kinetic energy is associated with the movement of water particles in nearly closed orbits and is not significantly propagated. The potential energy however is associated with the net displacement of water particles and this moves along with the wave at the phase speed. Hence, in deep water, the effect is as if half of the energy moves at the phase speed, which is the same as the overall energy moving at half the phase speed. The integrity of the wave is maintained by a continuous balancing act between kinetic and potential energy. As a wave moves into previously undisturbed water potential energy at the front of the wave train is converted into kinetic energy resulting in a loss of amplitude. This leads to waves dying out as they outrun their energy. At the rear of the wave train kinetic energy is left behind and is converted into potential energy with the result that new waves grow there.

One classical example of a wave group is the band of ripples which expands outwards from the disturbance created when a stone is cast into a still pond. If you fix your attention on a particular wave crest then you will notice that your wave creeps towards the outside of the band of ripples and disappears. Stating this slightly differently, if we move along with waves at the phase velocity we will stay with a wave crest, but the waves ahead of us gradually disappear. Since the band of ripples is made up of waves with components from a narrow range of wavelengths the wavelength of our wave will also increase a little (and there will be fewer waves immediately around us). However, if we travel at the group velocity, the waves ahead of us may lengthen and those behind us shorten but the total number of waves near us will be conserved.

Thus, the wave groups can be considered as carriers of the wave energy (see also Section 1.3.7), and the group velocity is also the velocity with which the wave energy is propagated. This is an important consideration in wave modelling.

1.3.3 *Statistical description of wave records*

The rather confusing pattern seen in Figure 1.13 can also be viewed in terms of Equation 1.4 as the motion of the water surface at a fixed point. A typical wave record for this displacement is shown in Figure 1.14, in which the vertical scale is expressed in metres and the horizontal scale in seconds. Wave crests are indicated with dashes and all zero-downcrossings are circled. The wave period T is the time distance between two consecutive downcrossings (or upcrossings*), whereas the wave height H is the vertical distance from a trough to the next crest as it appears on the wave record. Another and more commonly used kind of wave height is the zero-crossing wave height H_z, being the vertical distance between the highest and the lowest value of the wave record between two zero-downcrossings (or upcrossings). When the wave record contains a great variety of wave periods, the number of crests becomes greater than the number of zero-downcrossings. In that case, there will be some difference between the crest-to-trough wave height and H_z. In this chapter, however, this difference will be neglected and H_z will be used implicitly. A simple and commonly used method for analysing wave records by hand is the Tucker-Draper method which gives good approximate results (see Section 8.7.2).

A measured wave record never repeats itself exactly, due to the random appearance of the sea surface. But if the sea state is "stationary", the statistical properties of the distribution of periods and heights will be similar from one record to another. The most appropriate parameters to describe the sea state from a measured wave record are therefore statistical. The following are frequently used:

---

* There is no clear convention on the use of either zero-upcrossings or downcrossings for determining the wave height and period of zero-crossing waves. Generally, if the record in sufficiently long, no measurable differences will be found among mean values.

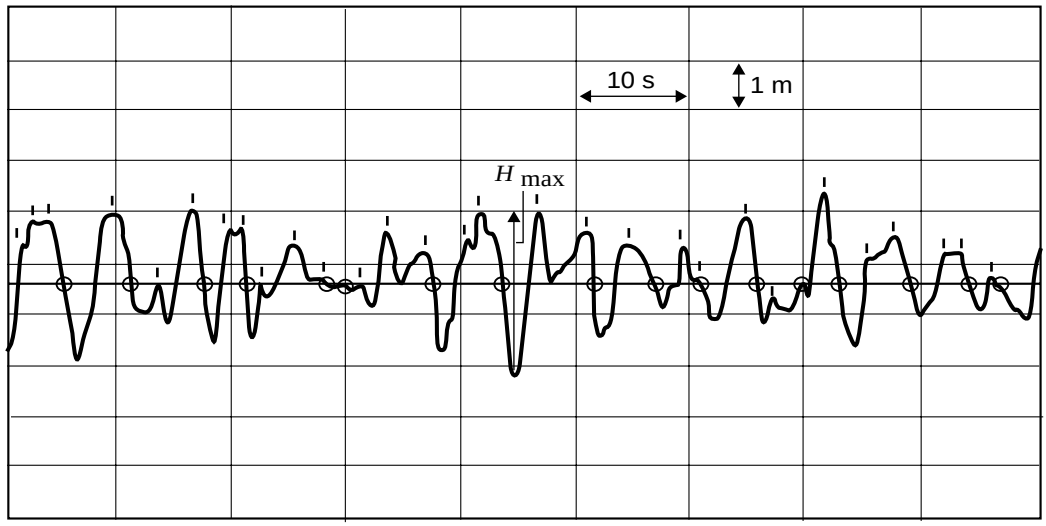

Figure 1.14 — Sample of a wave record (dashes show wave crests; zero down-crossings are circled)

$\bar{H}$ = Average wave height;

H_{max} = Maximum wave height occurring in a record;

$\bar{T}_z$ = Average zero-crossing wave period; the time obtained by dividing the record length by the number of downcrossings (or upcrossings) in the record;

$\bar{H}_{1/n}$ = The average height of the 1/n highest waves (i.e. if all wave heights measured from the record are arranged in descending order, the one-nth part, containing the highest waves, should be taken and $\bar{H}_{1/n}$ is then computed as the average height of this part);

$\bar{T}_{H_{1/n}}$ = The average period of the 1/n highest waves.

A commonly used value for n is 3:

$\bar{H}_{1/3}$ = Significant wave height (its value roughly approximates to visually observed wave height);

$\bar{T}_{H_{1/3}}$ = Significant wave period (approximately equal to the wave period associated with the spectral maximum, see Section 1.3.8).

1.3.4 *Duration of wave records*

The optimal duration of wave records is determined by several factors. First of all, for a correct description of the sea state, conditions should be statistically stationary during the sampling period. In fact, this will never be achieved completely as wave fields are usually evolving (i.e. growing or decaying). On the other hand, to reduce statistical scatter, the wave record should contain at least 200 zero-downcrossing waves. Hence, the optimal time over which waves are usually measured is 15–35 minutes, as this reasonably accommodates both conditions.

So far, we have introduced the manual analysis of analogue "stripchart" records. Most analyses are performed by computer for which digital records are used, i.e. the vertical displacement of the ocean surface (or the position of the pen at the chart recorder) is given with a sampling rate of 1–10 times per second (1–10 Hz). For example, a record of 20 minutes duration with a sampling rate of 4 Hz contains 4 800 values.

When wave records are processed automatically, the analysis is always preceded by checks on the quality of the recorded data points to remove outliers and errors due to faulty operation of sensors, in data recording equipment, or in data transmission.

1.3.5 *Notes on usage of statistical parameters*

In this *Guide*, the term sea state is used as a wave condition which is described by a number of statistical parameters. It is common to use the significant wave height, $\bar{H}_{1/3}$, and the average zero-crossing period, $\bar{T}_z$, or some other characteristic period, to define the sea state. The corresponding maximum wave height can be deduced as shown in Section 1.3.6.

The use of the average zero-crossing period, $\bar{T}_z$, has its drawbacks. The distribution of individual zero-downcrossing periods of a record is usually very wide and is also somewhat sensitive to noise, in contrast with the distribution of periods of, say, the highest one-third of waves. Moreover, the average period of the highest waves of a record is usually a good approximation of the period associated with the peak of the wave spectrum (see Section 1.3.8). It has been found that average wave periods of the 1/n highest waves with n > 3 are not essentially different from $\bar{T}_{H_{1/n}}$, but exhibit a larger scatter.

In this *Guide*, as elsewhere, various definitions of wave steepness are used. The general form is $\xi = H/\lambda$ which becomes, using Equation 1.8:

$$\xi = \frac{2\pi H}{g T^2},$$

where H represents a wave height (e.g. $\bar{H}_{1/3}$, H_{m0}, H_{rms}, $\sqrt{m_0}$) and T the wave period (e.g. $\bar{T}_z$, $\bar{T}_{H_{1/3}}$, T_p, T_{m02}). Some of these parameters are introduced in Section 1.3.8.

1.3.6 *Distribution of wave heights*

The elevation of the sea surface is denoted $\eta(x,t)$. This formulation expresses the variations of sea surface in space and time for both simple waves (see Equation 1.2) and more complicated sea states. If the range of

wavelengths in a given sea state is not too broad, it has been shown (Longuet-Higgins, 1952) that the elevation, η, has a statistical distribution which is Gaussian (i.e. normal).

For a normally distributed parameter, such as η, the maximum values are known to be distributed with a Rayleigh distribution. For a sea state these maximum values are directly related to the wave heights. Hence, the distribution of (zero-downcrossing) wave heights can be represented by the Rayleigh distribution. This feature has been shown theoretically and verified empirically. If $F(H)$ denotes the probability of heights not exceeding a given wave height H_1 in a sea state characterized by a known value of $\bar{H}_{1/3}$, $F(H)$ is given by:

$$F(H_1) = 1 - \exp\left[-2\,(H_1/\bar{H}_{1/3})^2\right] . \qquad (1.16)$$

The probability $Q(H_1)$ of heights exceeding H_1 is then

$$Q(H_1) = 1 - F(H_1) . \qquad (1.17)$$

Example:

Given a sea state for which $\bar{H}_{1/3}$ = 5 m,
what is the probability of observing waves higher than 6 m?

Since $F(H_1) = 1 - \exp\left[-2\,(6/5)^2\right] = 0.94$,
the probability of heights exceeding 6 m is
$Q(H_1) = 1 - 0.94 = 0.06$.

If $\bar{H}_{1/3}$ is computed from a wave record of finite length, the record length or the number of waves used for the computation should be taken into account. If, on a record containing N waves, n ($n \le N$) waves exceed a given height H_1, the probability of heights exceeding H_1 is:

$$Q(H_1) = \frac{n}{N} . \qquad (1.18)$$

Inserting the relationships from Equations 1.16 and 1.17 into Equation 1.18 leads to:

$$\bar{H}_{1/3} = H_1\,(0.5 \ln \frac{N}{n})^{-0.5} . \qquad (1.19)$$

Equation 1.19 provides a quick method for the determination of $\bar{H}_{1/3}$ from a wave record. On the other hand, if $\bar{H}_{1/3}$ is known, the distribution of a wave record can be compared with the Rayleigh distribution by using:

$$H_1 = \bar{H}_{1/3} \sqrt{0.5 \ln \frac{N}{n}}. \qquad (1.19a)$$

For the prediction of the maximum wave height H_{max} for a sequence of N waves with known $\bar{H}_{1/3}$, it is common to take the mode of the distribution of maximum values:

$$H_{max} = \bar{H}_{1/3} \sqrt{0.5 \ln N}. \qquad (1.20)$$

Alternatively, if the 50-percentile of the distribution of maximum values is taken, we get a more conservative estimate of H_{max} because of the asymmetry of the distribution, i.e. about 5 per cent greater than according to Equation 1.20:

$$H_{max} = \bar{H}_{1/3}\, 0.5 \ln \sqrt{1.45\ N}. \qquad (1.21)$$

The prediction of H_{max} must be based on a realistic duration, e.g. six hours, apart from the usual confidence limits of the $\bar{H}_{1/3}$ forecast. This implies N = 2 000–5 000 (in 6 hours there are about 2 700 waves if the peak period is 8 seconds). Using Equation 1.20 we get*:

$$H_{max} \cong 2.0\ \bar{H}_{1/3} \cong 1.9\ H_{m0}.$$

1.3.7 *The wave spectrum*

We have noted in Section 1.3.1 that a sea surface with a random appearance may be regarded as the sum of many simple wave trains. A way of formalizing this concept is to introduce the wave spectrum. A wave record may be decomposed by means of harmonic (or Fourier) analysis into a large number of sinusoidal waves of different frequencies, directions, amplitudes and phases. Each frequency and direction describes a wave component, and each component has an associated amplitude and phase.

The harmonic (Fourier) analysis thus provides an approximation to the irregular but quasi-periodic form of a wave record as the sum of sinusoidal curves. For a surface elevation varying in time in a single direction:

$$\eta(t) = \eta_0 + \sum_{j=1}^{n} a_j \sin(j\omega_0 t + \phi_j)$$

in which:

$\eta(t)$ = recorded elevation of the water surface at time t;
η_0 = mean elevation (as shown for instance in Figure 1.14);
ω_0 = angular wave frequency of the longest wave fitted to the record;
j = number of wave component;
a_j = amplitude of the jth component;
ϕ_j = phase angle of the jth component;
n = total number of components.

The phase angle allows for the fact that the components are not all in phase, i.e. their maxima generally occur at different times. The high frequency components tend to become insignificant and hence there is a reasonable limit to n.

Each wave component travels at its own speed (which depends on the wave frequency — or period — as expressed in Equation 1.10). Hence, the spectrum of wave components is continuously changing across the sea surface as the low frequency (large period or long wavelength) components travel faster than the high frequency components.

The expected values of the squares of the amplitudes a_j are the contribution to the variance of the surface elevation (η) from each of the wave components (i.e. the

---

* See Section 1.3.8 for definition of H_{m0} and its relation with $\bar{H}_{1/3}$.

variance is $E\,[\Sigma_j a_j^2]$). The resulting function is known as the *wave-variance spectrum* $S(f)$*. Typical spectra of wave systems have a form as shown in Figure 1.15 where the squared amplitudes for each component are plotted against their corresponding frequencies. The figure shows the spectrum from a measured wave record, along with a sample of the data from which it was calculated†. On the horizontal axis, the wave components are represented by their frequencies (i.e. 0.1 Hertz (Hz) corresponds to a period of ten seconds).

In actual practice, wave spectra can be computed by different methods. The most commonly used algorithm is the fast-Fourier transform (FFT), developed by Cooley and Tukey (1965). A much slower method, now superseded by the FFT, is the auto-correlation approach according to the Wiener-Kinchine theorem, introduced for practical use by Blackman and Tukey (1959) (see also Bendat and Piersol, 1971). Experience has shown that the difference between spectra computed by any two methods does not exceed confidence limits of each of them.

Since the wave energy E equals $\rho_w g H^2/8$ or $\rho_w g a^2/2$ ($H = 2a$), wave spectra in the earlier literature were expressed in terms of E and called *wave-energy spectra*. However, it has become common practice to drop the term $\rho_w g$ and to plot $a^2/2$ or, simply, a^2 along the vertical axis. The wave-energy spectrum is thus usually regarded synonymously with the "variance spectrum".

Wave spectra are usually given as a continuous curve connecting the discrete points found from the Fourier analysis and systems typically have a general form like that shown in Figure 1.16. The curve may not always be so regular. Irregular seas give rise to broad spectra which may show several peaks. These may be clearly separated from each other or merged into a very broad curve with several humps. Swell will generally give a very narrow spectrum concentrating the energy in a narrow range of frequencies (or wavelengths) around a peak value. Such a narrow spectrum is associated with the relatively "clean" appearance of the waves. Recall from Section 1.3.2 (and Figure 1.12) that this was often a condition where wave groups were clearly visible.

It is important to note that most measurements do not provide information about the wave direction and therefore we can only calculate an "energy" distribution over wave frequencies, $E(f)$. On the vertical axis, a measure for the wave energy is plotted in units of m^2/Hz. This unit is usual for "frequency spectra". We have seen

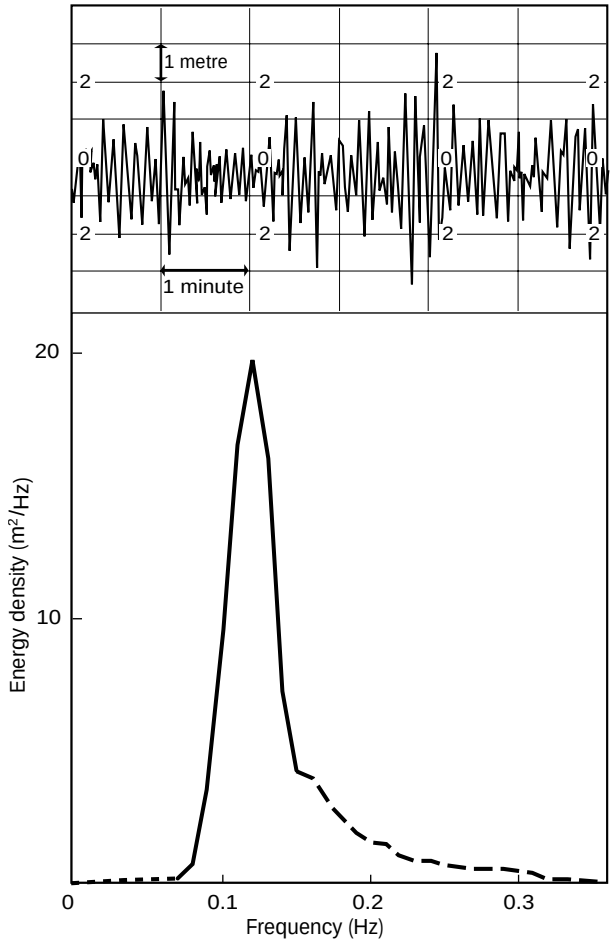

Figure 1.15 — Example of a wave spectrum with the corresponding wave record (12 November 1973, 21 UTC, 53°25'N, 4°13'E, water depth 25 m, wave height 4.0 m, wave period 6.5 s, West wind 38 kn (19.6 m/s) (*derived from KNMI*)

earlier that, although the spectrum may be continuous in theory, in practice the variances (or energies) are computed for discrete frequencies. Even when a high-speed computer is used, it is necessary to regard the frequency domain (or the frequency-directional domain) as a set of distinct or discrete values. The value of a^2 at,

Figure 1.16 — Typical wave-variance spectrum for a single system of wind waves. By transformation of the vertical axis into units of $\rho_w g S(f)$, a wave-energy $E(f)$ spectrum is obtained

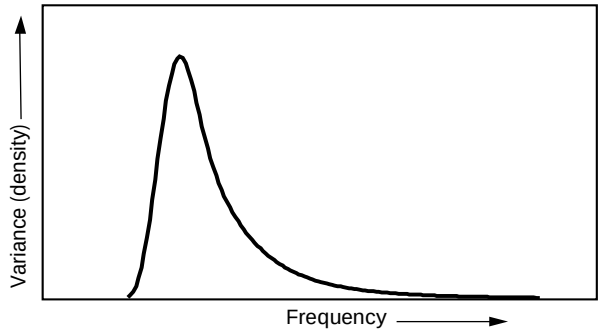

* The variance of a wave record is obtained by averaging the squares of the deviations of the water surface elevation, η, from its mean η_0. In Section 1.3.8, this variance is related to the area, m_0, under the spectral curve.

† This example shows a case with pure wind sea. However, the spectrum may often have a more complicated appearance, with one or more peaks due to swell.

for instance, a frequency of 0.16 Hz is considered to be a mean value in an interval which could be 0.155 to 0.165 Hz. This value, divided by the width of the interval, is a measure for the energy density and expressed in units of m^2/Hz (again omitting the factor $\rho_w g$). In fact the wave spectrum is often referred to as the *energy-density spectrum*.

Thus, this method of analysing wave measurements yields a distribution of the energy of the various wave components, $E(f,\theta)$. It was noted in Section 1.3.2 that wave energy travels at the group velocity c_g, and from Equation 1.15 we see that this is a function of both frequency and direction (or the wavenumber vector) and possibly water depth. The energy in each spectral component therefore propagates at the associated group velocity. Hence it is possible to deduce how wave energy in the local wave field *disperses* across the ocean.

It is important to note that a wave record and the spectrum derived from it are only samples of the sea state (see Section 1.3.4). As with all statistical estimates, we must be interested in how good our estimate is, and how well it is likely to indicate the true state. There is a reasonably complete statistical theory to describe this. We will not give details in this *Guide* but refer the interested reader to a text such as Jenkins and Watts (1968). Suffice to say that the validity of a spectral estimate depends to a large extent on the length of the record, which in turn depends on the consistency of the sea state or statistical stationarity (i.e. not too rapidly evolving). The spectral estimates can be shown to have the statistical distribution called a χ^2 distribution for which the expected spread of estimates is measured by a number called the "degrees of freedom". The larger the degrees of freedom, the better the estimate is likely to be.

1.3.8 *Wave parameters derived from the spectrum*

A wave spectrum is the distribution of wave energy (or variance of the sea surface) over frequency (or wavelength or frequency and direction, etc.). Thus, as a statistical distribution, many of the parameters derived from the spectrum parallel similar parameters from any statistical distribution. Hence, the form of a wave spectrum is usually expressed in terms of the moments* of the distribution (spectrum). The nth-order moment, m_n, of the spectrum is defined by:

$$m_n = \int_0^\infty f^n E(f)\, df \qquad (1.22)$$

(sometimes $\omega = 2\pi f$ is preferred to f). In this formula, $E(f)$ denotes the variance density at frequency, f, as in Figure 1.16, so that $E(f)\, df$ represents the variance $a_i^2/2$ contained in the ith interval between f and $f + df$. In practice, the integration in Equation 1.22 is approximated by a finite sum, with $f_i = i\, df$:

$$m_n = \sum_{i=0}^{N} f_i^n \frac{a_i^2}{2}. \qquad (1.22a)$$

From the definition of m_n it follows that the moment of zero-order, m_0, represents the area under the spectral curve. In finite form this is:

$$m_0 = \sum_{i=0}^{N} \frac{a_i^2}{2} = \frac{a^2}{2},$$

which is the total variance of the wave record obtained by the sum of the variances of the individual spectral components. The area under the spectral curve therefore has a physical meaning which is used in practical applications for the definition of wave-height parameters derived from the spectrum. Recalling that for a simple wave (Section 1.2.4) the wave energy (per unit area), E, was related to the wave height by:

$$E = \frac{1}{8}\rho_w g H^2 ,$$

then, if one replaces the actual sea state by a single sinusoidal wave having the same energy, its equivalent height would be given by:

$$H_{rms} = \sqrt{\frac{8E}{\rho_w g}},$$

the so-called *root-mean-square wave height*. E now represents the total energy (per unit area) of the sea state.

We would like a parameter derived from the spectrum and corresponding as closely as possible to the significant wave height $\bar{H}_{1/3}$ (as derived directly from the wave record) and, equally, the characteristic wave height H_c (as observed visually). It has been shown that H_{rms} should be multiplied by the factor $\sqrt{2}$ in order to arrive at the required value. Thus, the spectral wave height parameter commonly used can be calculated from the measured area, m_0, under the spectral curve as follows:

$$H_{m0} = \sqrt{2}\sqrt{\frac{8E}{\rho_w g}} = 4\sqrt{m_0} .$$

Note that we sometimes refer to the total variance of the sea state (m_0) as the total energy, but we must be mindful here that the total energy E is really $\rho_w g m_0$. In theory, the correspondence between H_{m0} and $\bar{H}_{1/3}$ is valid only for very narrow spectra which do not occur often in nature. However, the difference is relatively small in

---

* The first moment of a distribution of N observations $X_1, X_2, \ldots, X_n$ is defined as the average of the deviations $x_1, x_2, \ldots, x_n$ from the given value X_0. The second moment is the average of the squares of the deviations about X_0; the third moment is the average of the cubes of the deviations, and so forth. When X_0 is the mean of all observations, the first moment is obviously zero, the second moment is then known as the "variance" of X and its square root is termed the "standard deviation".

most cases, with $H_{m0} = 1.05\ \bar{H}_{1/3}$ on average. The significant wave height is also frequently denoted by H_s. In that case, it must be indicated which quantity ($4\sqrt{m_0}$ or $\bar{H}_{1/3}$) is being used.

The derivation of parameters for wave period is a more complicated matter, owing to the great variety of spectral shapes related to various combinations of sea and swell. There is some similarity with the problem about defining a wave period from statistical analysis (see Section 1.3.5). Spectral wave frequency and wave period parameters commonly used are:

f_p = Wave frequency corresponding to the peak of the spectrum (modal or peak frequency);

T_p = Wave period corresponding to f_p: i.e. $T_p = f_p^{-1}$;

T_{m01} = Wave period corresponding to the mean frequency of the spectrum:

$$T_{m01} = \frac{m_0}{m_1}; \qquad (1.24)$$

T_{m02} = Wave period theoretically equivalent with mean zero-downcrossing period $\bar{T}_z$:

$$T_{m02} = \sqrt{\frac{m_0}{m_2}}; \qquad (1.25)$$

T_{m-10} = Energy wave period, so-called for its role in computing wave power, J, in wave energy studies:

$$T_{m-10} = \frac{m_{-1}}{m_0};$$

where J, the wave power in kW/m of wave front, is computed as $J = 0.49\ H_{m0}{}^2 T_{m-10}$.

Note that the wave period T_{m02} is sensitive to the high frequency cut-off in the integration (Equation 1.22) which is used in practice. Therefore this cut-off should be noted when presenting T_{m02} and, in particular, when comparing different data sets. For buoy data, the cut-off frequency is typically 0.5 Hz as most buoys do not accurately measure the wave spectrum above this frequency. Fitting a high frequency tail before computing the spectral moments can be a useful convenience when high frequency information is not available (for example in a wave model hindcast).

Goda (1978) has shown that, for a variety of cases, average wave periods of the higher waves in a record, e.g. $\bar{T}_{H_{1/3}}$ (see Section 1.3.5), remain within a range of 0.87 T_p to 0.98 T_p.

Finally, the width of the spectral peak can be used as a measure of the irregularity of the sea state. The *spectral width parameter* ε is defined by:

$$\varepsilon = \sqrt{\frac{m_0 m_4 - m_2{}^2}{m_0 m_4}}\ .$$

Parameter ε varies between 0 (very narrow spectrum; regular waves) and 1 (very broad spectrum; many different wave periods present; irregular wave pattern).

The use of ε is **not recommended**, however, because of its sensitivity to noise in the wave record due to the higher order moments, in particular m_4. Rye (1977) has shown that the peakedness parameter, Q_p, by Goda (1970) is a good alternative:

$$Q_p = \frac{2}{m_0{}^2}\int_0^\infty f S(f)^2\ df\ . \qquad (1.26)$$

$Q_p = 1$ corresponds with $\varepsilon = 1$, while Q_p becomes very large for very narrow spectra. Under natural conditions, Q_p usually remains within the interval 1.5–5.

1.3.9 *Model forms for wave spectra*

The concept of a wave spectrum is commonly used for modelling the sea state. Models of the spectrum enable the spectrum to be expressed as some functional form, usually in terms of frequency, $E(f)$, frequency and direction, $E(f,\theta)$, or alternatively in terms of the wavenumber, $E(k)$. Since the wavenumber and frequency are related by the dispersion relation (see Equations 1.3 and 1.3a), the frequency and wavenumber forms can be transformed from one to the other.

Models of the spectrum are used to obtain an estimate of the entire wave spectrum from known values of a limited number of parameters such as the significant wave height and wave period. These may be obtained by hindcast calculations, by direct measurement or visual observation. To give an idea of the various factors which need to be taken into account, a few models are given below as examples. In the first three models no bottom effects have been taken into account. The TMA spectrum (see p. 14) is proposed as a general form for a model spectrum in depth-limited waters. In all cases E is used to represent the variance density spectrum.

The ***Phillips' spectrum*** describes the shape particularly of the high frequency part of the spectrum, above the spectral peak. It recognizes that the logarithm of the spectrum is generally close to a straight line, with a slope that is about –5. Hence, the general form:

$$E(f) = 0.005\frac{g^2}{f^5}\ ,\ \text{if}\ f \geq \frac{g}{u}$$
$$= 0 \qquad \text{elsewhere.} \qquad (1.27)$$

The ***Pierson-Moskowitz spectrum*** (Pierson and Moskowitz, 1964) is often used as a model spectrum for a fully developed sea, an idealized equilibrium state reached when duration and fetch are unlimited. This spectrum is based on a subset of 420 selected wave measurements recorded with the shipborne wave recorder — developed by Tucker (1956) — on board British ocean weather ships during the five-year period 1955–1960. In its original form, this model spectrum is:

$$E(f) = \frac{\alpha g^2}{(2\pi)^4\ f^5}\ e^{-0.74\left(\frac{g}{2\pi u f}\right)^4} \qquad (1.28)$$

in which $E(f)$ is the variance density (in m^2/s), f the wave frequency (Hz), u the wind speed (m/s) at 19.5 m above the sea surface, g the acceleration due to gravity (m/s^2) and α a dimensionless quantity, $\alpha = 0.0081$.

It can be shown that the peak frequency of the Pierson-Moskowitz spectrum is:

$$f_p = 0.877 \frac{g}{2\pi u} . \qquad (1.29)$$

Equation 1.28, together with Equations 1.22 and 1.23, allows us to calculate m_0 as a function of wind speed. Hence H_{m0} (the significant wave height) for a fully grown sea is:

$$H_{m0} = 0.0246\, u^2 , \qquad (1.30)$$

with H_{m0} in metres and u in m/s, with the wind speed now related to 10 m height*. This agrees well with limiting values of wave-growth curves in Chapter 4 (e.g. Figure 4.1). Equations 1.29 and 1.30 are valid for fully developed sea only, as is their combination:

$$H_{m0} = 0.04\, f_p^{-2} . \qquad (1.31)$$

The ***JONSWAP spectrum*** is often used to describe waves in a growing phase. Observations made during the Joint North Sea Wave Project (JONSWAP) (Hasselmann et al., 1973) gave a description of wave spectra growing in fetch-limited conditions, i.e. where wave growth under a steady offshore wind was limited by the distance from the shore. The basic form of the spectrum is in terms of the peak frequency rather than the wind speed, i.e as in Equation 1.28 but after the substitution for $g/(2\pi u)$ using Equation 1.29:

$$E(f) = \frac{\alpha g^2}{(2\pi)^4 f^5} \mathrm{e}^{-1.25\left(\frac{f}{f_p}\right)^4} \gamma(f). \qquad (1.32)$$

The function γ is the peak enhancement factor, which modifies the interval around the spectral peak making it much sharper than in the Pierson-Moskowitz spectrum. Otherwise, the shape is similar. The general form of the JONSWAP spectrum is illustrated in Figure 1.17.

Using JONSWAP results, Hasselmann et al. (1976) proposed a relation between wave variance and peak frequency for a wide range of growth stages. Transforming their results into terms of H_{m0} and f_p we get:

$$H_{m0} = 0.0414\, f_p^{-2} (f_p u)^{1/3} , \qquad (1.33)$$

again with H_{m0} in m, f_p in Hz and u in m/s at 10 m above mean water level.

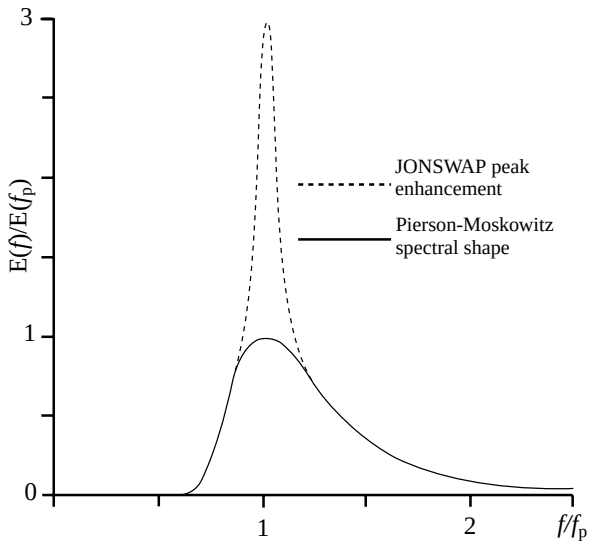

Figure 1.17 — General form of a JONSWAP spectrum as a function of f/f_p

This equation is connected with developing waves and so is not exactly comparable with Equation 1.30 for fully developed waves. The peak frequency can be obtained by reversing Equation 1.33:

$$f_p = 0.148\, H_{m0}^{-0.6}\, u^{0.2} . \qquad (1.34)$$

Equation 1.34 can be applied for estimating the approximate spectrum and characteristic wave periods when wave height and wind speed are known. This is common practice when predicting waves using growth curves relating wave height to wind speed and fetch or duration.

The ***TMA*** (Texel-Marsen-Arsloe) ***spectrum***, proposed as a model in depth-limited waters, takes the form:

$$E(f) = E_{\mathrm{JONSWAP}}(f)\, \Phi(f,h) , \qquad (1.35)$$

where Φ is a function of frequency, f, and depth, h (see Bouws et al., 1985).

Finally, it should be noted that the spectra shown here are all of the type

$$E(f) = E(f, \textit{parameters}),$$

with no account taken of the directional distribution of the sea state. Further information on directionality can be found in Section 3.3.

---

* The usual reference height for wind speeds is 10 m. Wind speed at 19.5 m is reduced to 10 m height by applying a correction factor; in this case the wind speed has been divided by 1.075 (see Section 2.4.1).

CHAPTER 2

OCEAN SURFACE WINDS

W. Gemmill: editor

2.1 Introduction

In order to be able to make good wave forecasts, it is essential that accurate surface wind analyses and forecasts are available. A detailed analysis of the wind field and of its development from the past into the future is required.

The effects of erroneous wind speeds are cumulative in time, and the effect on forecast wave heights may be appreciable. For example, the wave-growth diagram in Figure 3.1 shows that a wind of 15 m/s (29 knots) is capable of raising a sea of 4 m height after 12 h and of 5 m height after 24 h. If the wind speed was assumed to be 17.5 m/s (34 knots), the forecast would indicate wave heights of 4.9 m and 6.3 m, respectively. An initial error of 16 per cent in the wind speed would thus give rise to errors of 25–30 per cent in the forecast wave heights.

If, in the above example, the "forecast" was in fact an analysis of the current situation and the analysis was used as a basis for forecasts of future wave conditions, the error would tend to become still greater and errors in wave height of 2 m or even more would be the result. Wave-height differences of this magnitude are generally of great importance to marine operations and, for this reason, the wave forecaster must be aware of the sources of errors in his forecast and he should also be able to make an assessment of their magnitude.

Ocean surface wind fields can be determined from:

- Manual analysis of the marine meteorological observations with extrapolation in time;
- Automated numerical objective analysis and prediction models; or
- A combination of both — the "man-machine mix".

The physical processes that determine the ocean surface wind field are contained in the basic equations of motion. But, these equations are mathematically very complex and can only be solved by using numerical methods on high-speed, large-scale computers. This approach is commonly referred to as weather prediction by numerical methods, pioneered originally by L. F. Richardson (1922). A hierarchy of numerical weather prediction models are currently used by various countries. For a description of the basic principles see Haltiner and Williams (1980), for example. For operational requirements it would, of course, be preferable to use the automated procedures of a numerical model since they provide the ocean surface winds in a quick and efficient manner.

When numerical weather prediction models are employed, the ocean surface wind field can be obtained from the lowest layer of the analysis and forecast model system. However, additional diagnostic calculations may be necessary to adjust the model winds to obtain the wind at a pre-assigned height over the ocean surface (10 or 20 m). The closer the lowest level of the model is to the ocean, the smaller is the potential for introducing errors when extrapolating from that level to the near surface.

If one does not have access to a large computer system with a real-time observational database, it will be necessary to perform a manual analysis of marine variables to construct the wind fields with the aid of some simple dynamical relationships. These can be derived from the more complex and complete set of equations of motion. Although time consuming, manual analyses can produce more detailed wind fields than models. For hindcast studies, where accuracy is particularly important and more time may be available, the combined use of models and manual intervention provides perhaps the best wind fields (see also Section 9.6.2). Statistical techniques can also be used to infer surface winds from selected model outputs. This approach is particularly useful for site specific areas where local effects can be important in determining the wind field.

The basic force that drives ocean waves is the surface stress imparted by the wind. However, that parameter is not measured directly. It is estimated by knowing the wind at a specified height (10 or 20 m) and applying an appropriate value for drag coefficient. The drag coefficient is dependent on height and stability (air minus sea temperature difference) of the atmosphere above the ocean surface. In unstable conditions the sea is warmer than the overlying air and there is more turbulent mixing in the lower atmosphere. This increases the stress on the surface, so for the same wind speed at a given height, waves will become higher under unstable conditions than under stable conditions. Hence, characterizing friction and the stability in the lower boundary layer is an important step in deriving winds or surface stresses suitable for use in wave estimation.

In the following sections, a brief discussion on the sources of marine data is first presented (2.2). This is followed by a discussion on the methods to obtain the ocean surface wind field using simple dynamical relations (between pressure gradient, Coriolis and frictional forces, 2.3), with particular attention to characterizing the marine boundary layer (2.4), and statistical approaches (2.5).

2.1.1 *Wind and pressure analyses — general considerations*

The wind field is usually analysed by indirect means, starting with a surface pressure analysis in mid- and higher latitudes, or a streamline analysis in low latitudes. In routine analyses of weather charts, the analyst uses the latest available analysis from which to obtain a first guess. An isobaric pattern is drawn using pressure observations, and hopefully some satellite imagery. The observations of wind speed are used as a check on the pressure gradient, and those of wind direction on the orientation of the isobars. Both pressure and wind direction are used for streamline analysis (see the end of this section for more discussion on wind analysis in the tropics). At best the analyses are coarse because of sparseness of the surface data.

It takes time to carefully examine and fit the pressure and wind data in the final analysis. Sanders (1990) has shown that producing a good subjective analysis of pressure, even when sufficient surface pressure data are available, is a time consuming activity and requires careful editing for quality control. Then, to prepare the wind field analysis, an additional step is required. Wind observations are used to specify the wind speed and direction at observation locations. However, over large areas of the ocean where no (or very few) observations are available, one must resort to determining wind speed and direction from parameters which can be obtained from weather charts (i.e. pressure gradients, curvature of isobars, and air-sea temperature differences). The corresponding wind speeds and directions are analysed in such a way that a consistent pattern emerges which shows the characteristic features of wind fields associated with weather disturbances over the ocean.

Thus, determining the wind field requires an analysis of a weather chart in two consecutive steps. First, a standard analysis of the isobaric pattern is performed to determine the main locations of weather systems. Then follows a close examination of the exact position of the isobars, with a view to adjusting their position at places where that is needed to arrive at a logical and consistent wind-isotach field. In such reviews, one soon finds that, even in areas where the network of ship observations is comparatively dense, local adjustments to the isobar spacing can be made which may easily result in gradient-wind correction of about 2 m/s. Without observations the potential for error is much higher. Hence, the main errors in determining the wind field result from a lack of pressure and wind observations over the oceans.

Today, operational meteorologists generally use numerical forecast guidance as the starting point to produce ocean wind charts. Figure 2.1(*a*) shows a sample 48-hour forecast extracted from the NCEP (National Center for Environment Prediction, USA) global forecast model of 10 m surface winds and sea-level pressures for the north-west Atlantic Ocean. The forecaster studies the movement and development of weather systems through the forecast period (out to 72 hours at 12-hour increments), as well as the consistency of the forecasts from run cycle to run cycle. Many forecast centres also maintain statistics on their own forecast model performance (i.e. the accuracy of movement and intensity of weather systems) so that this information can be used to improve the forecasts. Meteorologists can either accept the guidance as is, or use the additional information to modify the forecasts. Figure 2.1(*b*) shows the final interpretation for the ocean surface weather forecast chart using the information in Figure 2.1(*a*). Of course, the work is all done within restrictive deadlines. The forecast chart is "broadcast" in "real time" to the marine community through various distribution systems including marine radio facsimile and private companies.

In the tropics it is not possible to determine the wind field directly from the pressure analyses. This is because the geostrophic relationship is weaker in the lower latitudes and breaks down completely at the Equator. Also, errors in pressure measurements can become significant compared to the pressure gradients which are to be analysed. Direct analysis of the wind in the form of streamlines and isotachs gives a useful depiction of the low-level wind field.

The procedure for streamline analysis is similar to pressure analysis in that all weather systems have consistency over time and they need to be located and tracked from chart to chart. Each system should be followed from genesis, to maturity and decay, and its movement tracked. A knowledge of conceptual models of weather systems is required to carry this out so that streamlines and isotachs can be correctly analysed where there are few observations. It is particularly important for the analyst to monitor the evolution of the anticyclones in the subtropical ridge as sudden increases in intensity can result in surges of wind penetrating well into the tropics, with resultant increases in wave and swell height. A useful reference for analysis in the tropics is the *Forecasters guide to tropical meteorology* (AWS, 1995).

2.2 Sources of marine data

There are three sources of surface observations that are generally used to make analyses of pressure and winds over the ocean. These are observations taken routinely at six-hour synoptic intervals by ships, ocean buoys (fixed and drifting) and land (coastal) weather stations. They are disseminated worldwide via the Global Telecommunication System (GTS) to be available in real time for use in operational centres. In addition, remote measurements of winds using active and passive microwave sensors on board satellites are now available and used by the operational meteorological world.

2.2.1 *Ship weather reports*

Today, ship weather reports provide the standard source of marine data. They are prepared by deck officers as part of their routine duties. Wind speed and direction are

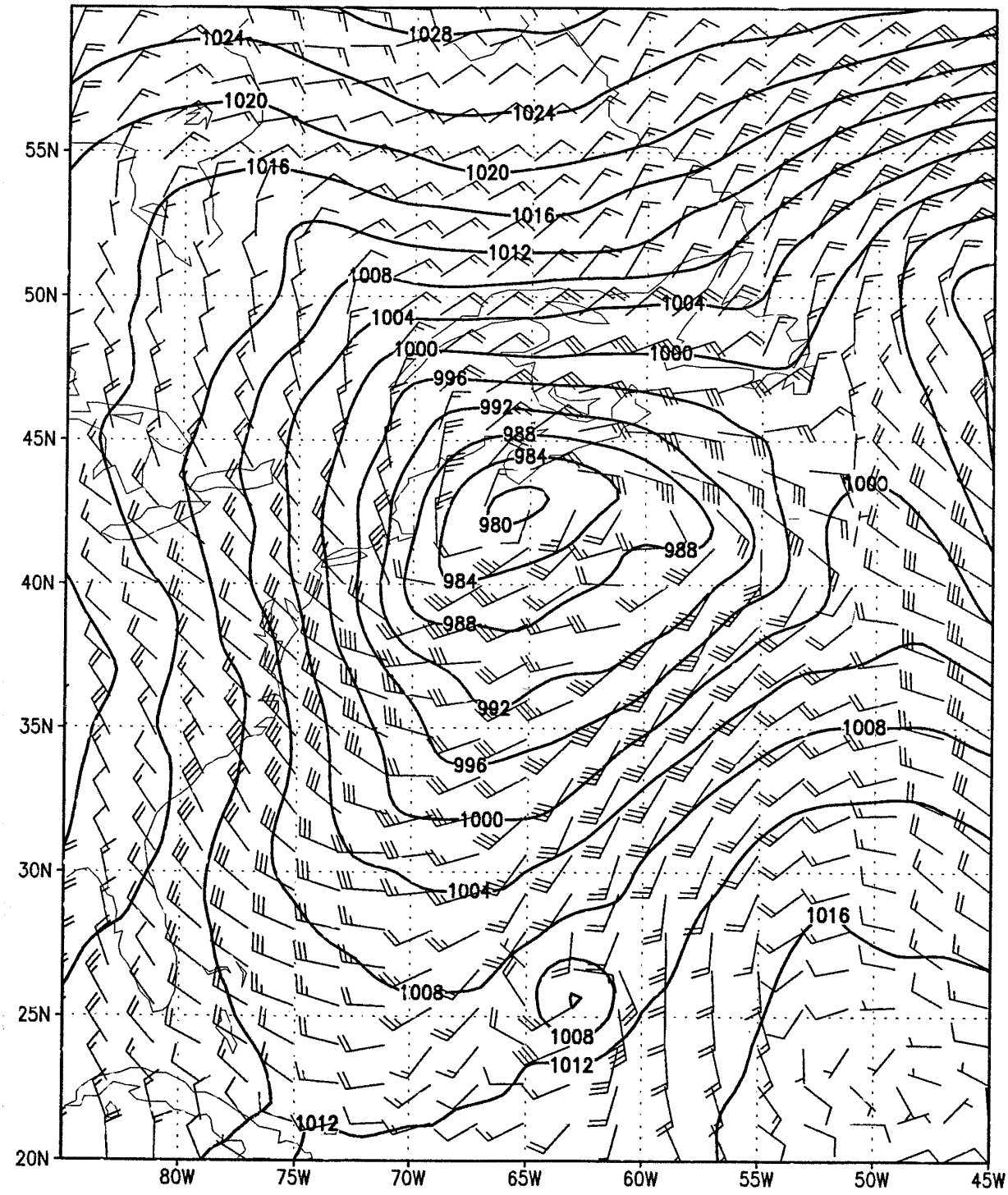

Figure 2.1(*a*) — Numerical model forecast from the NCEP global forecast model. The output shows isobars of surface pressure (hPa) and wind barbs for 10 m winds (knots (kn), 1.94 kn = 1 m/s) for the 48-hour forecast valid at 00 UTC on 21 December 1995

estimated either indirectly, by the observer using sea state and feel of the wind, or directly by anemometer if the vessel is so equipped.

Estimated wind observations are subject to a wide variety of errors. Such reports are often made by first determining the wind speed in terms of the Beaufort scale, where each scale number represents a range of possible wind speeds. Then, a single speed is chosen for reporting purposes. The scale is based on the appearance of the sea state. However, a substantial time lag may occur for the sea to reach a state that truly reflects the prevailing wind conditions. In addition, it is obvious that night-time wind reports based on visual sea state will be subject to great error.

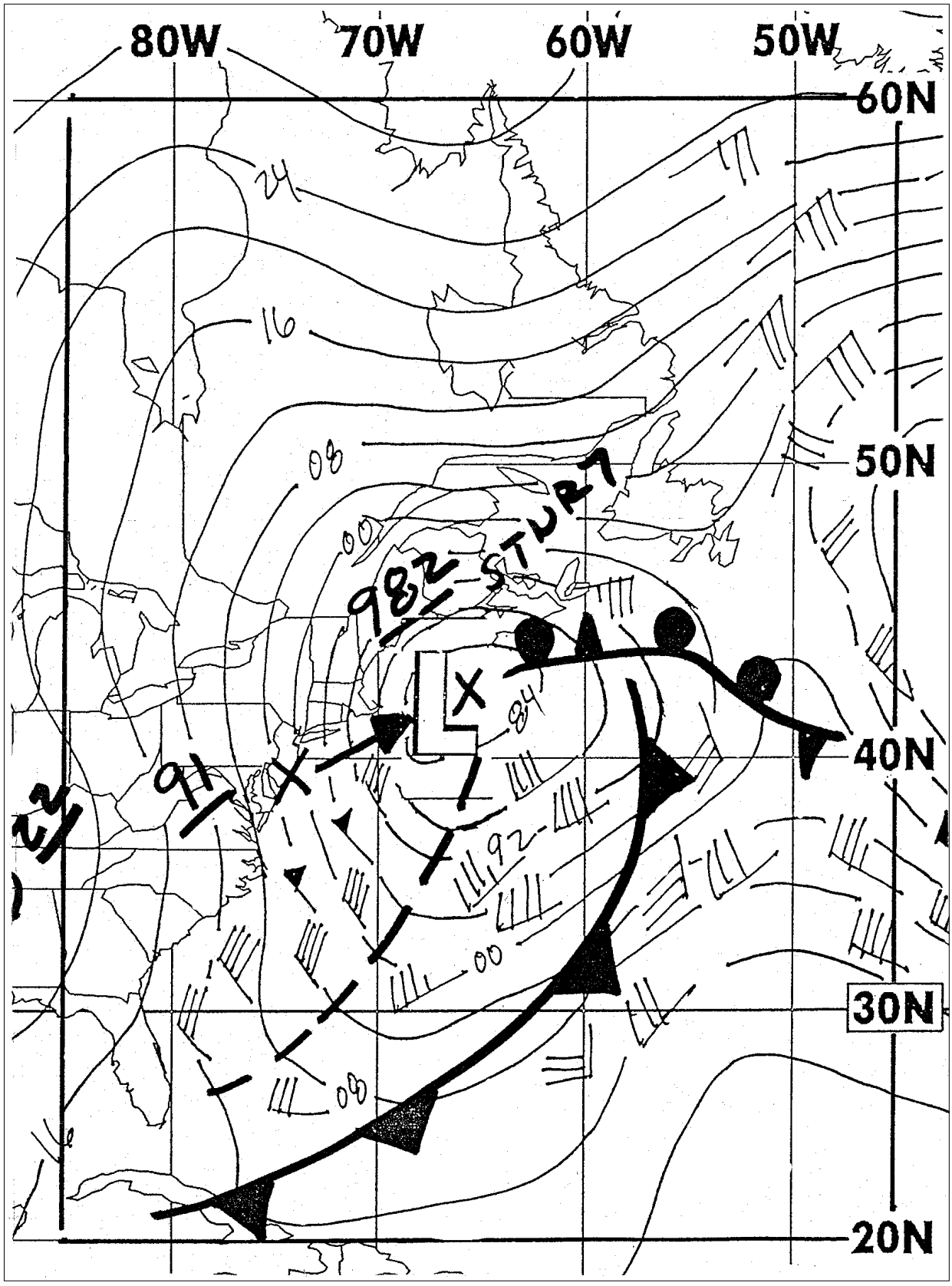

Figure 2.1(*b*) — Surface weather 48-hour forecast based on information in Figure 2.1(*a*). Valid at 00 UTC, 21 December 1995 (*from National Meteorological Center, Marine Forecast Branch, US Department of Commerce/NOAA/NWS*)

The descriptions of wind effects on the sea surface which are used by mariners for observing the various intensities of the wind have not been chosen arbitrarily. The criteria are the result of long experience and represent individually distinguishable steps on a specific scale. Originally, these steps were characterized by descriptive terms, such as light breeze and moderate breeze, or gale and strong gale. When, in the last century, weather reporting became an operational practice, the steps were given numbers, and the wind scale was named after Admiral Beaufort who introduced this coding system in 1814 in the British navy. The Beaufort scale was recommended for international use in 1874.

Since it is possible for an experienced observer to distinguish one step from another, a wind observation should be accurate to within a half of one scale interval — a fact which has indeed been verified empirically. However, wind effects on the sea surface are sometimes modified by other phenomena, of which the observer may be unaware. The plankton content of the sea water has an influence on foam forming, air stability affects the steepness of waves to some extent, while strong currents may also change the form of waves and hence the general appearance of the sea state. As a result, the standard deviation of a wind observation is, on the average, somewhat greater than a half of one scale interval: it amounts to 0.58 I (I being the width of the scale interval) for each of the steps 1–10 of the Beaufort scale. This means that the standard deviation of an individual wind-speed observation varies from 0.76 m/s at step 1 (wind speed 2.0 m/s) to 1.34 m/s at step 5 (wind speed 10.2 m/s) and 2.6 m/s at step 10 (wind speed 24.2 m/s) (Verploegh, 1967).

It should be stressed that wave height is not a criterion used in wind observations at sea. Any mariner is all too well aware that wave height depends on other factors as well — such as the duration and fetch of the wind. The influence of fetch, for instance, is clearly noticeable when the ship is in the lee of land, or when there are abrupt wind changes in open seas.

Many studies have been made to determine wind speeds equivalent to the steps of the Beaufort scale (WMO, 1970) and such studies are continuing at present (Lindau, 1994). A scale recommended for scientific use is given in Table 2.1. It shows the equivalent wind speed for each Beaufort number and equivalent scale intervals in metres/second (m/s) and in knots.

Since this scientific scale has not been introduced for the operational reporting of wind speeds from ships, ships' observers use an older conversion table which was introduced internationally in 1948. This table (using knots) is given in Table 2.2 (WMO, 1990). For the purpose of wave forecasting, therefore, a wind report (expressed in knots) should be converted back into the original Beaufort scale number and then converted into the correct wind speed of the scientific scale. This slightly complicates the work, but many years of wave-forecasting practices have shown that important systematic errors are avoided in this way.

TABLE 2.1

Conversion scales for Beaufort wind force

Beaufort number	*Descriptive term*	*Scale recommended for use in wave forecasting*		
		Equivalent wind speed (m/s)	*Intervals*	
			m/s	*kn*
0	Calm	0.8	1 or 0	0–2
1	Light air	2.0	2	3–5
2	Light breeze	3.6	3–4	6–8
3	Gentle breeze	5.6	5–6	9–12
4	Moderate breeze	7.8	7–9	13–16
5	Fresh breeze	10.2	9–11	17–21
6	Strong breeze	12.6	12–14	22–26
7	Near gale	15.1	14–16	27–31
8	Gale	17.8	17–19	32–37
9	Strong gale	20.8	19–22	38–43
10	Storm	24.2	23–26	44–50
11	Violent storm	28.0	26–30	51–57
12	Hurricane	-	31 and above	58 and above

The wind direction is much easier to determine from the orientation of the crests of wind waves. The standard deviation of an individual observation of wind direction amounts to 10° (Verploegh, 1967) and appears to be independent of wind speed. The direction of constant trade or monsoon winds can be determined with greater accuracy.

The mix of wind observations between visual estimates and anemometers varies considerably from one ocean area to another. Anemometer winds are prevalent in the Pacific whereas most observations in the Atlantic are visual estimates. Surprisingly, a study by

TABLE 2.2

Scales in use in international reports

Beaufort number	*Descriptive term*	*Range of values reported by observers (kn)*
0	Calm	<1
1	Light air	1–3
2	Light breeze	4–6
3	Gentle breeze	7–10
4	Moderate breeze	11–16
5	Fresh breeze	17–21
6	Strong breeze	22–27
7	Near gale	28 –33
8	Gale	34–40
9	Strong gale	41–47
10	Storm	48–55
11	Violent storm	56–63
12	Hurricane	64 and above

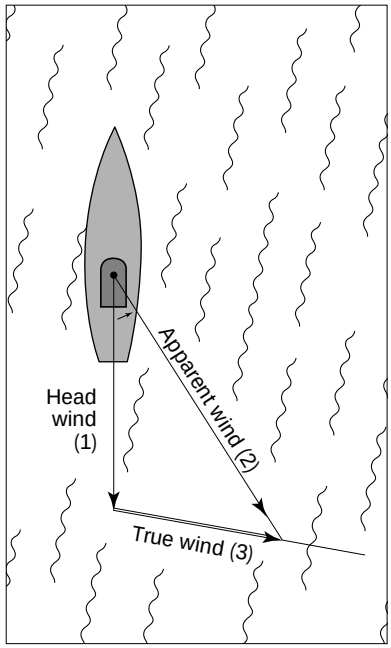

Figure 2.2(*a*) (*right*) — Usual way of computing the true wind (3) from a diagram plot of head wind (1) and measured (apparent) wind speed and direction (2)

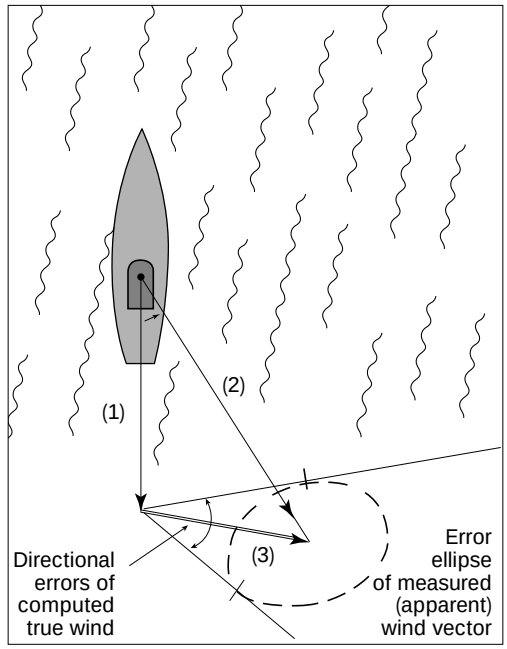

Figure 2.2(*b*) (*far right*) — The computed true wind may be erroneous both as regards direction and speed

Wilkerson and Earle (1990) shows that the quality of wind reports from ships with anemometers is not much better than those without. Pierson (1990) also reported on the characteristics of ship wind observations made with and without anemometers and concluded that ship reports, with or without anemometers, were inferior to buoy measurement. Errors from anemometer measurements on board ships are generally introduced by poor instrument exposure, improper reading of wind speed and direction indicators, vessel motion and maintenance problems.

Winds measured by an anemometer on board ship will be the combined effect of the wind over the ocean and the ship's motion. Therefore, in order to obtain a best estimate of the prevailing (true) wind over the sea, the measured wind must be corrected to exclude the ship's movement. This is done by means of a vector diagram as illustrated in Figure 2.2(*a*).

Whilst an anemometer may give an accurate representation of the air flow at the location of the anemometer, the main problem with measuring wind on board ship is that a fixed anemometer cannot always be properly exposed to all wind directions. The vessel's superstructure may interfere with the flow of air, and consequently the measurement may not be representative of the true air flow over the ocean surface. It should be obvious that errors in the apparent wind, and/or the incorrect application of the vector diagram will produce poor quality wind reports, as illustrated in Figure 2.2(*b*).

On larger ships, anemometers are usually installed at great heights: heights of 40 m above the surface of the sea are by no means uncommon. The wind speed normally increases with height, but the rate of speed increase depends on stability of the air. However, routine observations are not corrected for height, and that is yet another source of error when comparing wind data from many platforms. For a more detailed review of problems of wind measurements at sea, see Dobson (1982) and also Taylor et al. (1994).

2.2.2 *Fixed buoy reports*

Since 1967, moored buoys equipped with meteorological instruments have provided surface atmospheric and oceanographic data. Buoys can be expected to provide better quality data than those reported by ships for several reasons:

- The sensor's location on the buoy is carefully considered to avoid exposure problems;
- Sampling and averaging periods for the measurements are determined after accounting for buoy motion;
- Duplicate sensors are used for redundancy and each is calibrated before deployment;
- Monitoring in near-real time allows detection of instrument errors. (This is the practice in the USA for all data gathered by buoys deployed by the National Data Buoy Center.)

Buoys are presently providing measurements which are within the original accuracy specification. The National Data Buoy Center's specified accuracy requires that winds, averaged for 8.5 minutes, should have a root-mean-square error for speed of less than 1.0 m/s (or 10 per cent) and for direction of less than 10°. This has been verified through field calibration studies (Gilhousen, 1987).

2.2.3 *Land (coastal) stations*

Land (coastal) reporting stations provide data of variable quality and applicability. In some cases they may provide reliable data (NOAA, 1990). However, using these reports requires knowledge of the exposure, local topography, proximity to the coast and type of station: whether it is a buoy, light tower, or coastguard station. Consideration should be given also to the time of day

(for the possible influence of land-sea breezes) and level of station maintenance.

2.2.4 *Satellite data*

During the past decade or so, there have been a number of oceanographic satellites on which active and passive microwave sensors, such as scatterometers and radiometers (1978 on SEASAT) and radar altimeters (1985–89 on GEOSAT), have demonstrated the capability of measuring ocean surface winds. Since 1987, the Special Sensor Microwave/Imager (SSM/I) (US Defense Meteorological Satellite Program spacecraft) has been providing surface wind speed data over the global oceans in real time. These microwave measurements, from polar-orbiting satellites in 102-minute orbits around the Earth, provide several orders of magnitude greater surface wind observations compared to conventional ship and buoy data. Most recently the European Space Agency also has started to provide vector wind data from scatterometers and wind speed and wave data from radar altimeters on board the ERS-1 satellite and its successor ERS-2 launched in April 1995.

Research efforts now are concentrating on how best to use these remotely sensed ocean surface wind data in improving the initial ocean surface wind analyses and subsequent forecasts. Table 2.3 is a summary of the current operational wind data available from satellites*.

An example of an ocean surface wind data plot using SSM/I wind speed data is shown in Figure 2.3. This plot represents data centred at 00 UTC with a ± 3-hour window. The wind directions are assigned using the lowest level winds (about 45 m) from the US National Meteorological Center global operational analysis system. Winds are missing either where there is precipitation or where wind speeds are in excess of 50 kn (~ 25 m/s) (the satellite sensor's upper limit).

It should be noted that the quality of the wind measurements obtained from satellite-borne sensors depends on the accuracy of the algorithms used to derive wind-related parameters (speed and, if applicable, direction) from the sensor measurements (brightness temperatures from passive microwave sensors, and radar backscatter cross-section and antenna parameters from active microwave sensors) and various corrections that need to be applied for atmospheric water vapour and liquid water contamination. Furthermore, the sensor response may drift in time and careful quality-control procedures should be used to monitor the retrievals.

* The altimeter footprint depends on the pulse duration, satellite height, the sea state and the method for retrieving the backscatter value. The footprint is about 10 km. Measurements are reported as one second averages (so the area sampled is effectively about 17 km x 10 km) centred at about 7 km intervals along the sub-satellite track.

TABLE 2.3
Satellite derived winds

Instrument	*Mode*	*Swath*	*Footprint*	*Measurement*
Altimeter	Active microwave	Nadir	≈10 km	Surface wind speed
Scatterometer	Active microwave	500 km	50 km	Surface wind speed and direction
Special Sensor Microwave/ Imager	Passive microwave	1 500 km	25 km	Surface wind speed

2.2.5 *Common height adjustment*

In order to perform wind and pressure analyses, the data must be adjusted to a standard height. However, there is no fixed height at which the observations are made. Anemometer heights on fixed buoys range between 3 m and 14 m, on ships they range from 15 m to over 40 m, and on platforms or at coastal stations the heights may range up to 200 m or more above the sea.

The theory of Monin-Obukhov (1954) is well known for calculating the shape of the wind profile through the lowest part of the atmosphere — known as the constant flux layer. The calculation requires the wind speed, at a known height within the layer, and the stability, which is derived from the air-sea temperature difference. Methods for adjusting winds to a standard height are reviewed and wind adjustment ratios are presented in table form in a WMO document by Shearman and Zelenko (1989). In practice, when an ocean surface wind field is being analysed from observations, the wind field is assumed to be prescribed at 10 m. For further discussion of wind profiles in the lower atmospheric boundary layer see Section 2.4.

2.3 Large-scale meteorological factors affecting ocean surface winds

In common practice a forecaster may have to work from surface weather maps, because prognostic or diagnostic models for producing ocean surface wind fields may not be available. The forecaster can subjectively produce an ocean surface wind chart based on a knowledge of a few principles of large-scale atmospheric motions and some knowledge of boundary-layer theory.

The simplest approach to obtain ocean surface winds would be to:

- Calculate the geostrophic wind speed;
- Correct it for curvature to derive the gradient wind speed;
- Simulate the effect of friction by reducing this wind to approximately 75 per cent and rotating the wind direction by approximately 15° (anti-clockwise in the northern hemisphere and clockwise in the southern hemisphere). In relation to the geostrophic wind that is towards the region of lower pressure.

Figure 2.3 — Example of a combined Aviation Model (global spectral model) — Special Sensor Microwave/Imager (SSM/I) ocean surface wind analysis, valid at 00 UTC on 6 April 1992 for the area of the Grand Banks, North Atlantic (*from NWS*)

As a quick approximation of ocean surface winds this approach may be satisfactory. However, there are several important factors which should be considered when particular meteorological situations are identified.

Some important meteorological relationships that govern the speed and direction of ocean surface winds are:

(1) Surface-pressure gradient — geostrophic wind;
(2) Curvature of isobars — gradient wind;
(3) Vertical wind shear of the geostrophic wind — thermal wind;
(4) Rapidly changing pressure gradient in time — isallobaric wind;
(5) Rapidly changing pressure gradient downstream — difluence and confluence;
(6) Friction — Ekman and Prandtl layers;
(7) Stability of air over the sea — air-sea temperature difference.

These relationships (discussed in the following sections) may be considered independently and then combined to give an estimate of the wind field. It should

be noted that this approach is an over-simplification because each relationship yields a wind component which is derived from rather specific assumptions but then combined under very general conditions in order to approximate the wind field.

2.3.1 *Geostrophic wind*

The primary driving force for atmospheric motions is the pressure gradient force. One of the most important balances in large-scale atmospheric motions is that between the Coriolis force and the pressure gradient force, with the resulting balanced motion called the geostrophic wind. This balance is generally valid:

- For large-scale flows;
- In the free atmosphere above the friction layer;
- Under steady state conditions; and
- With straight isobars.

The geostrophic flow is parallel to the isobars and is expressed by the following relationship:

$$\left(u_g, v_g\right) = \frac{1}{f\rho_a}\left(-\frac{\delta p}{\delta y}, \frac{\delta p}{\delta x}\right), \qquad (2.1)$$

where p is the atmospheric pressure, f is the Coriolis parameter ($f = 2\,\Omega \sin \Theta$), ρ_a is the air density, Ω is the angular speed of the Earth's rotation and Θ is the latitude. u_g and v_g are the geostrophic winds in the x (positive towards east), and y (positive towards north) directions.

Equation 2.1 shows that the wind blows in such a manner that, looking downwind, the high pressure is to the right and the low pressure is to the left in the northern hemisphere ($f > 0$) and vice versa in the southern hemisphere ($f < 0$). It should be observed that, for a given pressure gradient, the geostrophic wind will increase with decreasing latitude and, in fact, goes to infinity at the Equator. The geostrophic wind relation is assumed to be not valid in low latitudes, between approximately 20°N and 20°S. Also, over the ocean, air density decreases about 10 per cent from cold high pressure systems to warm low pressure systems. The geostrophic wind speed can be estimated from a pressure analysis using Table 2.4.

2.3.2 *Gradient wind*

Generally atmospheric flow patterns are not straight, but move along curved trajectories. This implies an additional acceleration along the radius of curvature, i.e. the addition of centripetal force to balance the flow. This balanced motion is known as the gradient wind. The gradient wind (Gr) equation is given by:

$$Gr = \frac{fr}{2}\left[-1 + \sqrt{1 + \frac{4G}{fr}}\right], \qquad (2.2)$$

where f is the Coriolis force, G is the geostrophic wind speed (which is used as proxy for the pressure gradient as seen from Equation 2.1) and r is the radius of curvature of an isobar at the point of interest.

For a low pressure system (cyclone), the circulation is in a counter-clockwise direction in the northern hemisphere and in a clockwise direction in the southern hemisphere. The sense of direction around a high pressure system (anticyclone) is opposite to that of a cyclone in each of the hemispheres.

Around a low pressure centre, the Coriolis and centrifugal forces act together to balance the pressure gradient force, compared to geostrophic flow where only the Coriolis force balances the pressure gradient. Consequently, the speed of the gradient wind around a cyclone is less than that of a geostrophic wind corresponding to the same pressure gradient. The balance of forces shows that for a high pressure system the Coriolis force is balanced by pressure gradient and centrifugal forces acting together. Hence, the gradient flow around a high is larger (in magnitude) than the geostrophic flow corresponding to the same pressure gradient.

There is an upper limit to the anticyclonic gradient wind which is obtained when the pressure gradient term reaches:

$$\frac{1}{\rho_a}\frac{\delta p}{\delta r} = -\frac{rf^2}{4}. \qquad (2.3)$$

When the pressure gradient reaches this value, the quantity under the square root in Equation 2.2 becomes zero, resulting in a maximum (in magnitude) gradient wind speed of:

$$Gr = \left|\frac{fr}{2}\right|. \qquad (2.4)$$

Using the geostrophic relation with Equation 2.3 and combining with Equation 2.4, the upper limit for the gradient wind speed for anticyclonic flow is twice the geostrophic wind speed:

$$Gr \le 2\,G. \qquad (2.5)$$

There is no such corresponding lower limit to the cyclonic gradient wind speed in relation to the pressure gradient.

The gradient wind speed can be estimated using Table 2.5 by measuring the radius of curvature of an isobar from a weather map and using the geostrophic wind speed determined from Table 2.4.

The balance diagrams for the simple frictionless flows reviewed above are illustrated in Figure 2.4.

2.3.3 *Thermal wind*

So far, the sea-level pressure field has been considered to be constant from the ocean surface to the top of the boundary layer. However, if there are non-zero horizontal temperature gradients at the surface, it can be shown through the thermal wind equation that the pressure gradient will change with height. This results in a change of the geostrophic wind with height so that the geostrophic wind at the top of the boundary layer will differ from that at the surface. The vertical shear of the geostrophic wind is given by:

TABLE 2.4

Geostrophic wind table

Speed is given (in knots) as a function of latitude and distance (in degrees of latitude) for 4 hPa change in pressure; pressure is 1015.0 hPa; temperature is 285 K; density is 0.001241 gm/cm^3

Dist.	*Latitude (°)*										
(°lat.)	*20*	*25*	*30*	*35*	*40*	*45*	*50*	*55*	*60*	*65*	*70*
1.0	113	92	77	68	60	55	51	47	45	43	41
1.1	103	83	70	61	55	50	46	43	41	39	37
1.2	94	76	65	56	50	46	42	39	37	36	34
1.3	87	70	60	52	46	42	39	36	34	33	32
1.4	81	65	55	48	43	39	36	34	32	31	29
1.5	75	61	52	45	40	37	34	32	30	28	27
1.6	71	57	48	42	38	34	32	30	28	27	26
1.7	67	54	46	40	35	32	30	28	26	25	24
1.8	63	51	43	38	33	30	28	26	25	24	23
1.9	60	51	43	38	33	30	28	26	25	24	23
2.0	57	46	39	34	30	27	25	24	22	21	21
2.1	54	44	37	32	29	26	24	23	21	20	20
2.2	51	42	35	31	27	25	23	21	20	19	19
2.3	49	40	34	29	26	24	22	21	19	19	18
2.4	47	38	32	28	25	23	21	20	19	18	17
2.5	45	37	31	27	24	22	20	19	18	17	16
2.6	44	35	30	26	23	21	19	18	17	16	16
2.7	42	34	29	25	22	20	19	18	17	16	15
2.8	40	33	28	24	22	20	18	17	16	15	15
2.9	39	32	27	23	21	19	17	16	15	15	14
3.0	38	31	26	23	20	18	17	16	15	14	14
3.1	37	30	25	22	19	18	16	15	14	14	13
3.2	35	29	24	21	19	17	16	15	14	13	13
3.3	34	28	23	20	18	17	15	14	14	13	12
3.4	33	27	23	20	18	16	15	14	13	13	12
3.5	32	26	22	19	17	16	14	14	13	12	12
3.6	31	25	22	19	17	15	14	13	12	12	11
3.7	31	25	21	18	16	15	14	13	12	12	11
3.8	30	24	20	18	16	14	13	12	12	11	11
3.9	29	23	20	17	15	14	13	12	11	11	11
4.0	28	23	20	17	15	14	13	12	11	11	10
4.2	27	22	18	16	14	13	12	11	11	10	10
4.4	26	21	18	15	14	12	11	11	10	10	9
4.6	25	20	17	15	13	12	11	10	10	9	9
4.8	24	19	16	14	13	11	11	10	9	9	9
5.0	23	18	15	14	12	11	10	9	9	9	8
5.2	22	18	15	13	12	11	10	9	9	8	8
5.4	21	17	14	13	11	10	9	9	8	8	8
5.6	20	16	14	12	11	10	9	8	8	8	7
5.8	20	16	13	12	10	9	9	8	8	7	7
6.0	19	15	13	11	10	9	8	8	7	7	7
6.2	18	15	12	11	10	9	8	8	7	7	7
6.4	18	14	12	11	9	9	8	7	7	7	6
6.6	17	14	12	10	9	8	8	7	7	6	6
6.8	17	13	11	10	9	8	7	7	7	6	6
7.0	16	13	11	10	9	8	7	7	6	6	6
8.0	14	11	10	8	8	7	6	6	6	5	5
9.0	13	10	9	8	7	6	6	5	5	5	5
10.0	11	9	8	7	6	5	5	5	4	4	4

TABLE 2.5

Gradient wind table

Wind speeds (in knots) are shown at latitude 40°N for given geostrophic wind speed (from Table 2.4) and radius of curvature (° lat.).
(Note: for any other latitude, ϕ, the winds should be scaled by the ratio f_ϕ/f_{40}, where f is the value of the Coriolis parameter.)

Radius of curvature (° lat.)	*Geostrophic wind (kn)*														
	5	***10***	***15***	***20***	***25***	***30***	***35***	***40***	***45***	***50***	***55***	***60***	***65***	***70***	***75***
							Anticyclonic flow								
25	5	10	15	21	26	32	38	44	50	56	63	70	77	84	92
24	5	10	15	21	26	32	38	44	50	57	63	70	77	85	93
23	5	10	16	21	27	32	38	44	51	57	64	71	78	86	94
22	5	10	16	21	27	32	38	44	51	57	64	72	79	87	96
21	5	10	16	21	27	32	39	45	51	58	65	72	80	89	97
20	5	10	16	21	27	33	39	45	52	58	66	73	81	90	100
19	5	10	16	21	27	33	39	45	52	59	67	75	83	92	102
18	5	10	16	21	27	33	39	46	53	60	68	76	85	95	106
17	5	10	16	21	27	33	40	46	53	61	69	78	87	98	111
16	5	10	16	21	27	33	40	47	54	62	70	80	90	103	119
15	5	10	16	22	28	34	40	47	55	63	72	83	95	110	138
14	5	10	16	22	28	34	41	48	56	65	75	87	102	129	0
13	5	10	16	22	28	35	42	49	58	67	79	93	120	0	0
12	5	10	16	22	28	35	42	51	60	71	85	111	0	0	0
11	5	10	16	22	29	36	44	52	63	76	102	0	0	0	0
10	5	11	16	23	29	37	45	55	68	92	0	0	0	0	0
9	5	11	17	23	30	38	47	60	83	0	0	0	0	0	0
8	5	11	17	23	31	40	51	74	0	0	0	0	0	0	0
7	5	11	17	24	32	43	65	0	0	0	0	0	0	0	0
6	5	11	18	25	35	55	0	0	0	0	0	0	0	0	0
5	5	11	18	28	46	0	0	0	0	0	0	0	0	0	0
4	5	12	20	37	0	0	0	0	0	0	0	0	0	0	0
3	6	13	28	0	0	0	0	0	0	0	0	0	0	0	0
2	6	18	0	0	0	0	0	0	0	0	0	0	0	0	0
1	9	0	0	0	0	0	0	0	0	0	0	0	0	0	0
							Cyclonic flow								
25	5	10	15	19	24	28	33	37	42	46	50	54	58	62	66
24	5	10	15	19	24	28	33	37	41	46	50	54	58	62	66
23	5	10	15	19	24	28	33	37	41	46	50	54	58	62	66
22	5	10	15	19	24	28	33	37	41	45	49	54	58	61	65
21	5	10	15	19	24	28	33	37	41	45	49	53	57	61	65
20	5	10	14	19	24	28	32	37	41	45	49	53	57	61	65
19	5	10	14	19	24	28	32	37	41	45	49	53	57	60	64
18	5	10	14	19	23	28	32	36	40	45	49	52	56	60	64
17	5	10	14	19	23	28	32	36	40	44	48	52	56	60	63
16	5	10	14	19	23	28	32	36	40	44	48	52	55	59	63
15	5	10	14	19	23	27	32	36	40	44	48	51	55	59	62
14	5	10	14	19	23	27	31	36	39	43	47	51	54	58	62
13	5	10	14	19	23	27	31	35	39	43	47	50	54	57	61
12	5	10	14	19	23	27	31	35	39	43	46	50	53	57	60
11	5	10	14	18	23	27	31	35	38	42	46	49	53	56	59
10	5	10	14	18	22	27	30	34	38	41	45	48	52	55	58
9	5	10	14	18	22	26	30	34	37	41	44	48	51	54	57
8	5	9	14	18	22	26	30	33	37	40	43	47	50	53	56
7	5	9	14	18	22	25	29	33	36	39	42	45	48	51	54
6	5	9	13	17	21	25	28	32	35	38	41	44	47	50	52
5	5	9	13	17	21	24	27	31	34	37	40	42	45	48	50
4	5	9	13	17	20	23	26	29	32	35	38	40	43	45	47
3	5	9	12	16	19	22	25	27	30	33	35	37	39	41	44
2	4	8	12	15	17	20	22	25	27	29	31	33	35	37	38
1	4	7	10	12	15	16	18	20	22	23	25	26	27	29	30

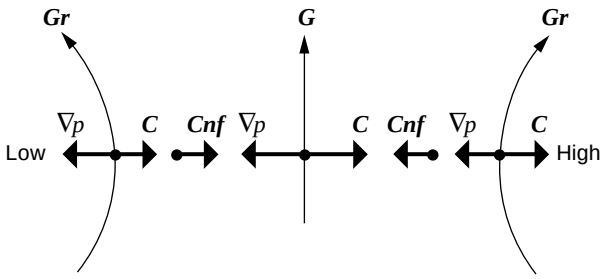

Figure 2.4 — Balance of forces for basic types of frictionless flow (northern hemisphere) (***Gr*** = gradient wind, ***G*** = geostrophic wind, ∇*p* = pressure gradient force; ***C*** = Coriolis force and ***Cnf*** = centrifugal force)

$$\left(\frac{\delta u_g}{\delta z}, \frac{\delta v_g}{\delta y}\right) = \frac{g}{T}\left(-\frac{\delta T}{\delta y}, \frac{\delta T}{\delta x}\right). \qquad (2.6)$$

In the southern hemisphere the left hand side of the equation needs to be multiplied by –1.

It is clear from Equation 2.6 that the geostrophic wind increases with height if higher pressure coincides with higher temperatures (as in the case of mid-latitude westerlies) and decreases with height if higher pressure coincides with lower temperatures. Furthermore, if the geostrophic wind at any level is blowing towards warmer temperatures (cold advection), the wind turns to the left (backing) as the height increases and the reverse happens (veering) if the geostrophic wind blows towards lower temperatures (warm advection).

The vector difference in the geostrophic wind at two different levels is called the "thermal wind". It can be shown geometrically that the thermal wind vector represents a flow such that high temperatures are located to the right and low temperatures to the left. The thermal wind, through linear vertical wind shear, can be incorporated directly into the solution of the Ekman layer, and thus incorporated in the diagnostic models which will be described in more detail below.

2.3.4 *Isallobaric wind*

In the above discussions, the wind systems have been considered to be evolving slowly in time. However, when a pressure system is deepening (or weakening) rapidly, or moving rapidly, so that the local geostrophic wind is changing rapidly, an additional wind component becomes important. This is obtained through the isallobaric wind relation. An isallobar is a line of equal pressure tendency (time rate of change of pressure). The strength of the isallobaric wind is proportional to the isallobaric gradient, and its direction is perpendicular to the gradient — away from centres of rises in pressure and toward centres of falls in pressure. Normally, this component is less than 5 kn (2.5 m/s), but can become greater than 10 kn (5 m/s) during periods of rapid or explosive cyclogenesis.

The isallobaric wind component is given by:

$$(u_i, v_i) = -\frac{1}{\rho_a f^2}\left[\frac{\delta\left(\frac{\delta p}{\delta t}\right)}{\delta x}, \frac{\delta\left(\frac{\delta p}{\delta t}\right)}{\delta y}\right]. \qquad (2.7)$$

The modification of the geostrophic wind field around a moving low pressure system is illustrated in Figure 2.5.

2.3.5 *Difluence of wind fields*

Difluence (confluence) of isobars also creates flows that make the winds deviate from a geostrophic balance. When a difluence of isobars occurs (isobars spread apart), the pressure gradient becomes weaker than its upstream value, so that as an air parcel moves downstream, the pressure gradient is unbalanced by the Coriolis force associated with the flow speed. This then results in the flow being deflected towards high pressure in an effort to restore the balance of forces through an increase in the pressure gradient force. In the case of converging isobars, the pressure gradient increases from it upstream value. Hence, the pressure gradient force becomes larger than the Coriolis force and the flow turns towards the low pressure in a effort to decrease the pressure gradient force. In either case, it is clear that a non-geostrophic cross-isobaric flow develops of a magnitude $U\,dG/ds$ (Haltiner and Martin, 1957), where G is the geostrophic speed, U is the non-geostrophic component normal to the geostrophic flow that has developed in response to the confluence or difluence of the isobars, and s is in the direction of the geostrophic flow.

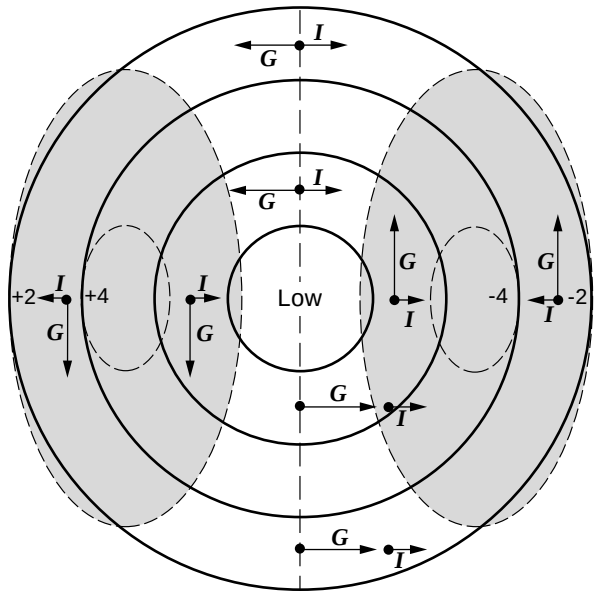

Figure 2.5 — Examples of the isallobaric wind field. Solid line = isobar, dashed line = isallobar, ***G*** = (u_g, v_g) = geostrophic wind, and ***I*** = (u_i, v_i) = isallobaric wind

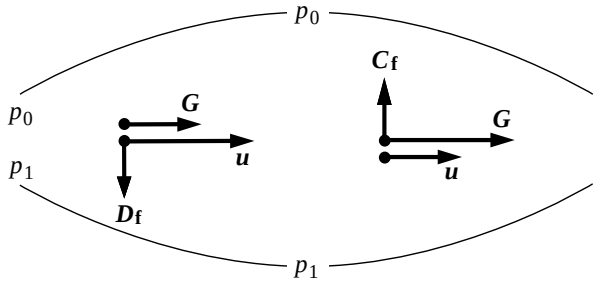

Figure 2.6 — Examples of difluent/confluent wind fields (p_0 and p_1 are isobars. $\boldsymbol{D}_\mathbf{f}$ and $\boldsymbol{C}_\mathbf{f}$ are the difluent and confluent wind components, respectively, and $\boldsymbol{G}$ and $\boldsymbol{u}$ are the geostrophic and surface winds)

In reality, since surface friction turns the flow towards low pressure, confluence will increase the inflow angle over the effect of friction alone, and difluence will decrease the inflow angle, with the result that flow towards high pressure will seldom exist. Figure 2.6 illustrates the modification to geostrophic wind due to effects by difluence and confluence.

2.3.6 *Surface friction effects*

The effect of friction is to reduce the speed of the free air flow. As a result of the balance of forces this will turn the direction of flow toward lower pressure, which is to the left in the northern hemisphere and to the right in the southern hemisphere. As one approaches the surface of the Earth the wind speed tends to zero, and the inflow angle tends to reach a maximum. A simple balance between the pressure gradient, Coriolis and frictional forces (Figure 2.7) describes this effect through the well-known Ekman spiral. The lower part of the atmosphere in which this effect is prominent is called the Ekman layer. In nature the predicted 45° angle of turning at the surface is too large, and predicted speeds near the surface are too low.

These effects of friction on the geostrophic flow in the Ekman layer are further influenced by the thermal wind discussed above. Studies have shown the importance of the thermal wind in explaining deviations from the typical Ekman spiral (Mendenhall, 1967). A result of the thermal wind influence is larger surface cross-isobaric (inflow) flow angles during cold advection, and smaller inflow angles during warm advection, as described above. An illustration of the effect of thermal wind on the wind in the Ekman layer is shown for a low pressure system in Figure 2.8.

In order to represent the effects of friction in a more realistic manner several approaches have been developed that relate the free atmospheric wind to a stress at the ocean surface. These often use the concept of a two-regime boundary layer; a constant flux layer at the surface, and the Ekman layer (spiral) above. Observations fit much better with this representation of the planetary boundary layer, with a turning angle of 10–15° predicted over the ocean for a neutrally stable atmosphere in contact with the ocean.

2.3.7 *Stability effects*

Stability within the boundary layer is important in determining the wind speed near the ocean surface. Over much of the oceans, the surface air temperature is in equilibrium with the sea-surface temperature so that near-neutral stability dominates. Under these conditions the structure of the wind profile in the constant flux layer is dominated by friction and can be described by a logarithmic profile.

For unstable cases (air temperature colder than the water temperature) convection becomes active and the higher wind speeds aloft are brought to the surface quickly, reducing dissipation by friction, and increasing the stress on the ocean surface. A stable atmosphere (warm air over cold water) acts to increase the friction forces in the boundary layer, resulting in lighter winds and a weaker wind stress. Table 2.6 shows the effects of stability on wind profiles above the ocean.

Stability effects are most important for ocean areas near large land masses, which act as source areas for air masses with very different physical properties from oceanic air masses. An expanded discussion of the theory of friction and stability in the boundary layer is presented in the next section.

2.4 A marine boundary-layer parameterization

The boundary layer of the atmosphere is that region which extends from the surface to the free atmosphere (at approximately 1 km height). At the surface frictional forces dominate. In the free atmosphere frictional forces become less important and, to a first order of approximation, the atmospheric flow is close to being in geostrophic balance.

Because all flows in nature are turbulent, the frictional forces we are concerned with are those arising from turbulent fluctuations — the so-called Reynolds stresses. A fundamental difficulty of the turbulence theory is to relate these turbulent stresses to the properties of the mean flow. Through extensive research some insights into these relationships have evolved, at least in

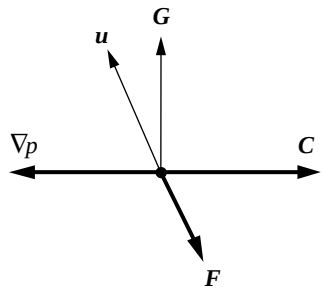

Figure 2.7 — Balances of friction, pressure gradient and Coriolis forces (northern hemisphere) ($\boldsymbol{u}$ = surface wind; $\boldsymbol{G}$ = geostrophic wind, ∇p = pressure gradient force; $\boldsymbol{C}$ = Coriolis force and $\boldsymbol{F}$ = friction)

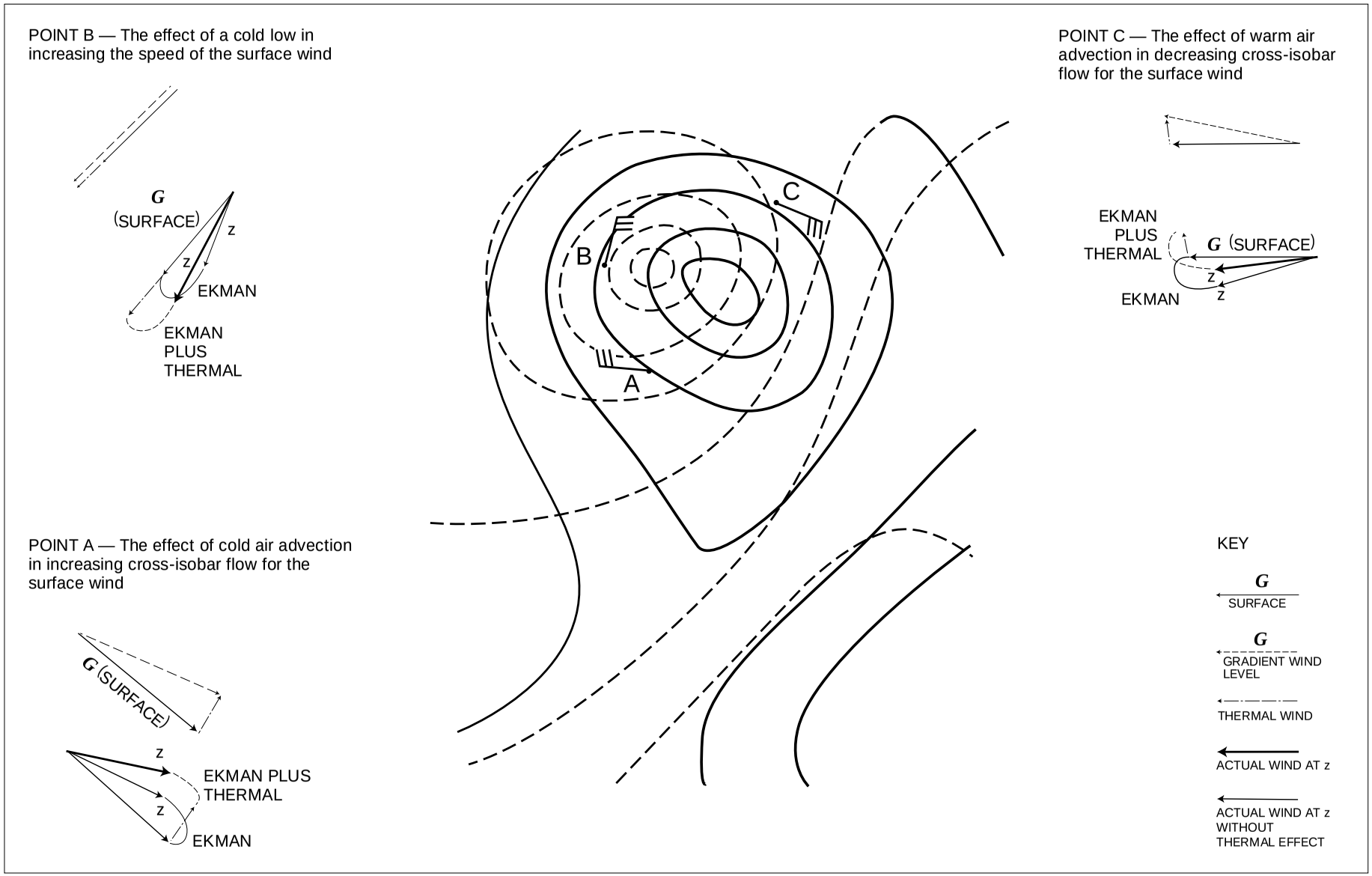

Figure 2.8 — The thermal wind. Sketch of surface winds, surface isobars (solid contours) and a constant pressure surface (dashed contours) for an extra-tropical cyclone (*after Pierson, 1979*)

TABLE 2.6

The effects of stability on wind profiles

Wind speed profiles are shown (in m/s) for a range of stabilities (characterized by the air-sea temperature difference). Profiles are given both for a fixed wind speed at 50 m and for a fixed surface friction velocity (0.36 m/s)

Height (m)	*Air-sea temperature difference (°C)*														
	–10	*–8*	*–6*	*–4*	*–3*	*–2*	*–1*	*0*	*1*	*2*	*3*	*4*	*6*	*8*	*10*
	Fixed wind speed at 50 m														
50	10.0	10.0	10.0	10.0	10.0	10.0	10.0	10.0	10.0	10.0	10.0	10.0	10.0	10.0	10.0
45	10.0	10.0	10.0	10.0	10.0	10.0	9.9	9.9	9.8	9.8	9.7	9.7	9.7	9.7	9.7
40	9.9	9.9	9.9	9.9	9.9	9.9	9.9	9.8	9.6	9.5	9.4	9.4	9.4	9.4	9.4
35	9.9	9.9	9.9	9.9	9.8	9.8	9.8	9.7	9.4	9.2	9.1	9.1	9.1	9.1	9.1
30	9.8	9.8	9.8	9.8	9.8	9.8	9.7	9.6	9.2	8.9	8.8	8.7	8.7	8.7	8.7
28	9.8	9.8	9.8	9.8	9.7	9.7	9.7	9.5	9.1	8.8	8.6	8.6	8.5	8.5	8.6
26	9.8	9.8	9.7	9.7	9.7	9.7	9.6	9.4	9.0	8.6	8.5	8.4	8.3	8.4	8.4
24	9.7	9.7	9.7	9.7	9.7	9.6	9.6	9.4	8.9	8.5	8.3	8.2	8.2	8.2	8.2
22	9.7	9.7	9.7	9.6	9.6	9.6	9.5	9.3	8.7	8.4	8.1	8.0	8.0	8.0	8.0
20	9.7	9.6	9.6	9.6	9.6	9.5	9.5	9.2	8.6	8.2	8.0	7.8	7.8	7.8	7.8
18	9.6	9.6	9.6	9.5	9.5	9.5	9.4	9.1	8.5	8.0	7.8	7.6	7.5	7.5	7.6
16	9.6	9.5	9.5	9.5	9.4	9.4	9.3	9.0	8.4	7.9	7.6	7.4	7.3	7.3	7.3
14	9.5	9.5	9.5	9.4	9.4	9.3	9.2	8.9	8.2	7.7	7.4	7.2	7.0	7.0	7.0
12	9.4	9.4	9.4	9.3	9.3	9.2	9.1	8.8	8.1	7.5	7.1	6.9	6.7	6.7	6.7
10	9.3	9.3	9.3	9.2	9.2	9.1	9.0	8.6	7.9	7.3	6.9	6.6	6.4	6.4	6.4
9	9.3	9.2	9.2	9.1	9.1	9.0	8.9	8.5	7.8	7.2	6.7	6.5	6.2	6.2	6.2
8	9.2	9.2	9.1	9.1	9.0	8.9	8.8	8.4	7.7	7.0	6.6	6.3	6.1	6.0	6.0
7	9.1	9.1	9.1	9.0	8.9	8.8	8.7	8.3	7.6	6.9	6.4	6.2	5.9	5.8	5.7
6	9.0	9.0	9.0	8.9	8.8	8.7	8.6	8.2	7.4	6.7	6.3	6.0	5.7	5.5	5.5
5	8.9	8.9	8.8	8.7	8.7	8.6	8.5	8.0	7.3	6.6	6.1	5.8	5.4	5.3	5.2
4	8.8	8.7	8.7	8.6	8.5	8.4	8.3	7.8	7.1	6.4	5.9	5.5	5.2	5.0	4.9
3	8.6	8.5	8.5	8.4	8.3	8.2	8.0	7.6	6.9	6.2	5.6	5.3	4.9	4.7	4.5
2	8.3	8.2	8.1	8.0	8.0	7.9	7.7	7.2	6.6	5.9	5.3	5.0	4.5	4.3	4.1
1	7.7	7.6	7.5	7.4	7.4	7.3	7.1	6.7	6.1	5.4	4.9	4.5	4.0	3.7	3.6
	Friction velocity fixed (0.36 m/s)														
50	8.2	8.3	8.5	8.7	8.8	9.0	9.3	10.0	11.1	12.0	12.8	13.5	14.5	15.2	16.1
45	8.1	8.3	8.4	8.6	8.8	9.0	9.2	9.9	10.9	11.8	12.5	13.1	14.1	14.9	15.6
40	8.1	8.3	8.4	8.6	8.7	8.9	9.2	9.8	10.7	11.5	12.1	12.7	13.7	14.5	15.1
35	8.1	8.2	8.4	8.6	8.7	8.9	9.1	9.7	10.4	11.2	11.8	12.3	13.2	13.9	14.6
30	8.0	8.2	8.3	8.5	8.6	8.8	9.0	9.6	10.2	10.8	11.4	11.9	12.7	13.4	13.9
28	8.0	8.2	8.3	8.5	8.6	8.8	9.0	9.5	10.1	10.7	11.2	11.7	12.5	13.1	13.7
26	8.0	8.1	8.3	8.5	8.6	8.7	9.0	9.4	10.0	10.6	11.1	11.5	12.2	12.9	13.4
24	8.0	8.1	8.2	8.4	8.6	8.7	8.9	9.4	9.9	10.4	10.9	11.3	12.0	12.6	13.1
22	8.0	8.1	8.2	8.4	8.5	8.7	8.9	9.3	9.7	10.2	10.7	11.1	11.7	12.3	12.8
20	7.9	8.1	8.2	8.4	8.5	8.6	8.8	9.2	9.6	10.1	10.5	10.8	11.5	12.0	12.5
18	7.9	8.0	8.2	8.3	8.4	8.6	8.7	9.1	9.5	9.9	10.3	10.6	11.2	11.7	12.1
16	7.9	8.0	8.1	8.3	8.4	8.5	8.7	9.0	9.3	9.7	10.1	10.4	10.9	11.4	11.8
14	7.8	8.0	8.1	8.2	8.3	8.4	8.6	8.9	9.2	9.5	9.8	10.1	10.6	11.0	11.4
12	7.8	7.9	8.0	8.2	8.2	8.4	8.5	8.8	9.0	9.3	9.6	9.8	10.2	10.6	11.0
10	7.7	7.9	7.9	8.1	8.2	8.3	8.4	8.6	8.8	9.1	9.3	9.5	9.9	10.2	10.5
9	7.7	7.8	7.9	8.0	8.1	8.2	8.3	8.5	8.7	8.9	9.1	9.3	9.7	10.0	10.2
8	7.6	7.8	7.8	8.0	8.0	8.1	8.2	8.4	8.6	8.8	9.0	9.1	9.4	9.7	10.0
7	7.6	7.7	7.8	7.9	8.0	8.0	8.1	8.3	8.5	8.6	8.8	8.9	9.2	9.5	9.7
6	7.5	7.7	7.7	7.8	7.9	8.0	8.0	8.2	8.3	8.5	8.6	8.7	9.0	9.2	9.4
5	7.4	7.6	7.6	7.7	7.8	7.8	7.9	8.0	8.1	8.3	8.4	8.5	8.7	8.9	9.1
4	7.3	7.5	7.5	7.6	7.6	7.7	7.8	7.8	7.9	8.0	8.1	8.2	8.4	8.5	8.7
3	7.2	7.3	7.3	7.4	7.4	7.5	7.5	7.6	7.7	7.8	7.8	7.9	8.0	8.1	8.3
2	7.1	7.1	7.1	7.1	7.2	7.2	7.2	7.2	7.3	7.4	7.4	7.5	7.6	7.6	7.7
1	6.6	6.6	6.6	6.7	6.7	6.7	6.7	6.7	6.8	6.8	6.8	6.8	6.9	6.9	7.0

a general sense, and can be applied to the atmosphere. These concepts have been developed to formulate diagnostic models that allow us to deduce surface turbulent flow fields from the free atmospheric flow.

The marine boundary layer itself can be separated into two regimes: the constant flux (or constant stress) layer (from the surface to about 50 m) and the Ekman layer (from about 50 m up to the free atmosphere ≈ 1 km). In the surface layer it can be assumed that the frictional forces contributing to turbulence are constant with height, and the effects of the Coriolis and pressure gradient forces, as well as the horizontal gradient of turbulent fluxes, are negligible. The wind direction is consequently constant with height. Using the mixing length theory developed by Prandtl, it can be shown that the flow in the constant flux layer (or Prandtl layer) depends only on the surface roughness length.

2.4.1 *Constant flux layer*

Under neutral conditions, Prandtl's solution shows that the horizontal flow over the ocean surface follows the well known "log" (logarithmic) profile in the vertical direction,

$$u = \frac{u_*}{\kappa} \ln\left(\frac{z}{z_0}\right), \qquad (2.8)$$

where κ is the von Kármán constant, z_0 is the constant of integration, known as the roughness length, and $\boldsymbol{u_*}$ is the friction velocity, which has magnitude:

$$u_* = \sqrt{\frac{\tau}{\rho_a}}, \qquad (2.9)$$

τ is the magnitude of the surface stress, and ρ_a the density of air. $\boldsymbol{u_*}$ can be thought of as a proxy for the surface stress.

It is common also to express stress (τ) through the bulk transfer relation:

$$\tau = \rho_a C_d u^2, \qquad (2.10)$$

where C_d is the drag coefficient. In general, C_d and u are both functions of height. Determining C_d has been the objective of many field research programmes over the years.

One of the problems of specifying the wind in the turbulent layer near the ocean is the formulation of z_0 and its relationship to u_*. Using dimensional argument, Charnock (1955) related the roughness length of the sea surface to the friction velocity of the wind as follows:

$$z_0 = \frac{\alpha {u_*}^2}{g}, \qquad (2.11)$$

where α is the Charnock constant, with a value as determined by Wu (1980) of 0.0185 , and g is the acceleration by gravity.

If the boundary layer is in a state of neutral stratification, the drag coefficient, which is a function of height, can be expressed as:

$$C_d(z) = \kappa^2 / \left(\ln\left[\frac{z}{z_0}\right]\right)^2, \qquad (2.12)$$

or

$$C_d(z) = \left(\frac{u_*}{u(z)}\right)^2. \qquad (2.13)$$

However, the boundary layer over the ocean is not necessarily neutral. A stability dependence was originally derived by Monin-Obukhov (1954) from profile similarity theory. This is used to modify the simple log relation provided above:

$$u = \frac{u_*}{\kappa}\left[\ln\left(\frac{z}{z_0}\right) - \psi\left(\frac{z}{L}\right)\right] \qquad (2.14)$$

$$C_d(z) = \left(\kappa / \left[\ln\left(\frac{z}{z_0}\right) - \psi\left(\frac{z}{L}\right)\right]\right)^2. \qquad (2.15)$$

The function ψ has been derived for both stable and unstable conditions. L is the Monin-Obukhov mixing length. For neutral conditions $\psi(z/L) = 0$. Businger et al. (1971) proposed functional relationships between the non-dimensional wind shear and z/L which can be used to determine the stability function $\psi(z/L)$ in Equation 2.14.

2.4.2 *The use of the drag coefficient*

In the above discussion, we developed the concept of the drag coefficient, as defined in Equation 2.10. There have been many studies to determine C_d under varying wind speeds and stabilities and a summary can be found in Roll (1965). More recently, Wu (1980, 1982) has shown through empirical studies that the drag coefficient at a given height depends linearly on the wind speed, and that the following formulation holds for a wide range of winds under near neutrally stable conditions:

$$10^3 C_{10} = (0.8 + 0.65\, U_{10}) \qquad (2.16)$$

where: C_{10} = Drag coefficient at the 10 m level; and
U_{10} = Wind speed (m/s) at the 10 m level.

This simple linear empirical relationship, however, needs to be modified when temperature stratification is present. Stratification affects turbulent momentum transport, thereby causing the wind profile to deviate from the logarithmic form.

Schwab (1978) determined C_d over water for a wide range of wind speeds and atmospheric stabilities. Figure 2.9 shows the results of his calculation. A crucial issue to be addressed at this juncture concerns the effect of changing stability and wind stress on the prediction of wave growth. It can be inferred from Figure 2.9 that, for a given 10 m level wind speed, unstable conditions result in higher drag coefficients (or surface stress) and hence larger wave growth than stable conditions. Liu et al. (1979) have developed a set of equations which compute the surface variables $\boldsymbol{u_*}$, z_0 and the boundary-layer stability length (L), so that the wind profile of

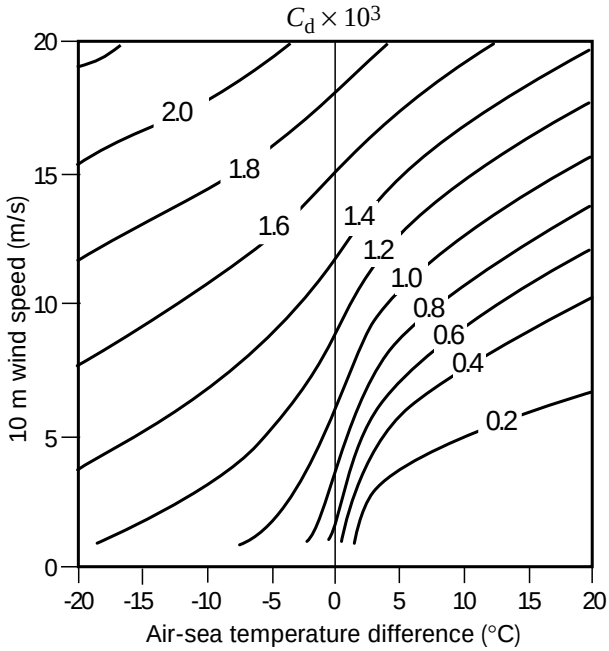

Figure 2.9 — Drag coefficient as a function of stability (air-sea temperature difference) and 10 m wind speed (*derived from Schwab, 1978*)

the constant flux layer including stability can be determined.

For wave forecast models, it appears appropriate to express the input wind in terms of $\boldsymbol{u}_*$. This is calculated taking stability into account. The wind is then expressed at some nominal height by applying the neutral logarithmic profile (Equation 2.8, given $\boldsymbol{u}_*$ with stability effect already taken into account and $\psi = 0$). This wind is then called the "equivalent neutral" wind at that height.

However, if winds are given at heights above the constant flux layer (above 50 m), i.e. well into the Ekman spiral, the above techniques should not be used. Instead one needs to deal with the more complicated two-regime (constant flux and Ekman) boundary layer. Several approaches have been developed using the two-regime boundary-layer model, whereby the surface stress and its direction are determined using the free atmospheric parameters.

2.4.3 *Analytic models*

One analytic approach is to solve the equations for both the constant flux and Ekman layers with a matching of the wind speed, wind direction and stress across the interface between the layers. This enables the surface variables to be related to variables in the free atmosphere. This type of model was initially developed by Blackadar (1965) over land, and modified for use over the ocean by Cardone (1969, 1978), Brown and Liu (1982) and Krishna (1981).

Overland and Gemmill (1977) compared the Cardone model to observations from fixed buoys in the New York Bight and found mean absolute speed errors of about 3 m/s. Brown and Liu (1982) compared their model with data taken during two large-scale experiments, JASIN and GOASEX. They indicate that the overall accuracy of their model compared to observations was 2 m/s and 20°.

2.4.4 *Rossby number similarity theory*

The other common approach is based on Rossby number similarity theory. The governing equations are the same as before, but the matching is by using two similarity approximations: one for the flow of the Ekman layer, and another for the constant flux layer (Stull, 1988). Clark and Hess (1974) have produced a modified version of the Rossby number similarity theory which gives relations for $\boldsymbol{u}_*$ and the turning angle at the ocean surface in terms of the geostrophic wind, ocean current, surface roughness and similarity functions $A(\mu,m)$ and $B(\mu,m)$, where m is related to the thermal wind and μ is related to stability. $A(\mu,m)$ and $B(\mu,m)$ have been evaluated using the measurements taken during the Wangara Experiment (Clark, et al., 1971). Possible inconsistencies in the wind fields produced by the two approaches described above may be traced to at least three sources:

(*a*) The non-dimensional wind shear, and hence the stability function ψ (analytic approach) and the functions A and B (Rossby number similarity) are empirically based;

(*b*) The specification of the depth of the constant flux layer by the analytic approach is not well known;

(*c*) Significant error is introduced by the large-scale model which provides the wind and temperature fields.

Figure 2.10 summarizes the properties of the two-regime boundary layer.

2.4.5 *Prognostic boundary-layer models*

Prognostic boundary-layer models, with generally high horizontal and vertical resolution, are potentially the most accurate. However, the very high spatial resolution required makes it difficult to run such models in an operational setting because of the large computational resources required.

A typical prognostic boundary-layer model will describe the space and time evolution of wind, temperature and moisture fields from prescribed initial distribution of these fields over the domain of interest. At the upper boundary, typically around 2 km, boundary conditions are prescribed from an overlying large-scale model. If the model covers a limited area, lateral boundaries must also be prescribed. An example of such an operationally run model is the US National Weather Service atmospheric boundary-layer model (Long et al., 1978). Unfortunately, the model has only limited use as a forecast tool for ocean surface winds because its domain covers only a small part of the coastal area of the USA.

Another approach is to incorporate sophisticated boundary-layer physics in large-scale atmospheric models. This permits the forecasting of more

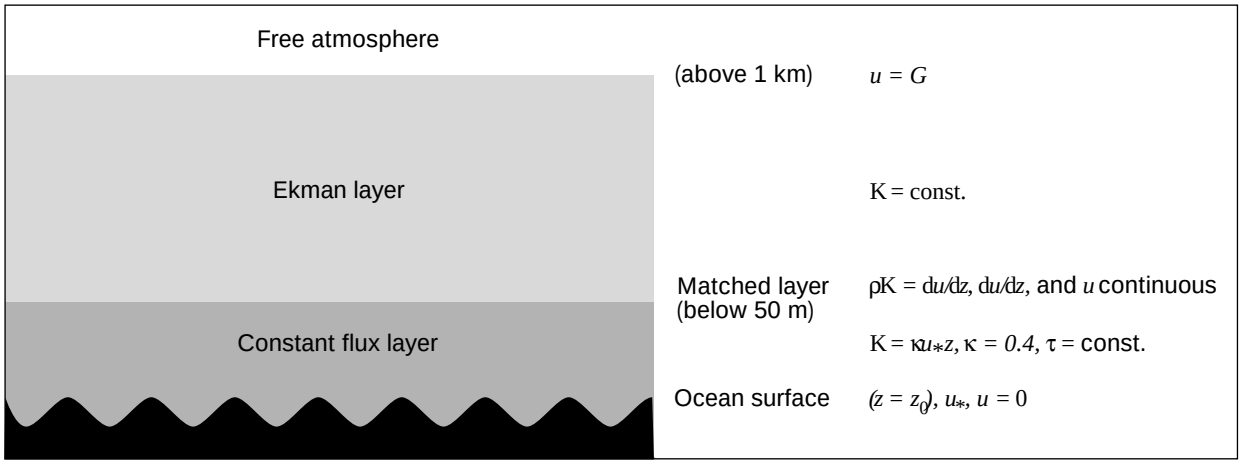

Figure 2.10 — Schematic of the two-regime boundary layer, K is the mixing coefficient

representative ocean surface winds as input to ocean forecast models. Examples may be found in the ECMWF model (Tiedtke, et al., 1979; Simmons et al., 1988) and the US National Meteorological Center spectral forecast model (Sela, 1982; Kanamitsu et al., 1991). It should be emphasized that, even with these improvements, a large-scale model cannot be considered a true boundary-layer model because of its incomplete formulation of boundary-layer physics and horizontal and vertical resolution. In order to obtain wind forecasts in the boundary layer, one generally takes the wind forecast from the lowest level of these large-scale models and applies the diagnostic boundary-layer considerations discussed earlier. In this approach, there is a tacit assumption that the winds in the boundary layer are in instantaneous equilibrium with those from the model first level.

A new generation of regional models, with high horizontal resolution and several additional vertical levels in the boundary layer, are currently under development with greater emphasis on boundary-layer physics. One such model is the so-called ETA model (Mesinger et al., 1988), which has a horizontal resolution of 20 km and 40 layers in the vertical. The model is centred over the North American continental domain of the USA. It also covers large ocean areas adjacent to the continent. When this model becomes operational, the winds in the boundary layer are directly given by the forecast model itself at the ocean surface (20 m) and there is no need to perform the above diagnostic calculations separately. A special advantage of this model is that it is easily portable to any other region of the world to produce meteorological forecasts, provided the lateral boundary conditions are supplied by some means.

2.5 Statistical methods

Statistical methods provide another approach to generate surface wind fields from large-scale forecast models. These techniques do well in situations where forecast models do not or cannot depict the surface winds with adequate accuracy.

In general, the statistical approach to the generation of wind analyses and forecasts calls for the derivation of a mathematical relationship between a dependent variable (the predictand) and selected independent variables (the predictors). The predictors may either be made available to forecasters for manual use or may be entered directly to computers for automated use.

2.5.1 *Extrapolation*

In the simplest approach, observed surface winds over the land can be compared with concurrent winds over the water and a relationship derived, usually in the form of a simple ratio. Forecasts of wind over water can then be made from the projected values of wind over land. Examples of this approach can be found in Richards et al. (1966), Overland and Gemmill (1977), Phillips and Irbe (1978) and Burroughs (1984). An advantage of this approach is that it can easily be applied manually.

Clearly, the technique would be most effective when used in situations only requiring estimations of winds relatively near the coast. It may also be useful on enclosed bodies of water, such as the Great Lakes, where the surrounding wind field is sufficiently specified. For producing wind forecast fields that extend from coastal areas to far distances on the high seas, however, this type of approach has only limited usefulness.

2.5.2 *Perfect prognosis*

A more sophisticated approach is to derive a relationship between analysed atmospheric parameters and the winds at the ocean surface. The predictors are obtained directly from gridded analysed fields and include parameters which are directly available, such as winds, geopotential height or pressure, etc. at various model levels. Computed parameters such as gradients, vorticity, divergence, etc. are also included. Values of the predictors anywhere on the grid may be considered in addition to values collocated with the predictand.

This approach to statistical forecasting is called “perfect prognosis” because it is assumed that, when the scheme is put into operation, the predictors supplied

from the numerical models as input will approach a perfect simulation of the actual atmosphere.

The predictands are the wind direction and speed obtained from either fixed locations, such as moored buoys and ocean weather ships, or from voluntary observing ships.

A number of different statistical techniques for developing relationships between predictors and predictands are available. The most prominent among them is called step-wise screening multiple linear regression and results in equations of the following form:

$$Y = C_0 + C_1X_1 + \ldots + C_nX_n , \qquad (2.17)$$

where: Y = Predictand (dependent variable);
C_n = Constants;
X_n = Predictors (independent variables).

An example of the use of this approach over marine areas can be found in Thomasell and Welsh (1963). When tested against independent data, their system achieved RMS errors of 3.7 m/s and 35° in speed and direction, respectively.

An important consideration in using this type of technique is that the wind-specification equations are independent of the model supplying the predictors. Because of this the accuracy will improve as better models are developed.

2.5.3 *Model output statistics*

This approach (Glahn and Lowry, 1972) is similar to the perfect prognosis technique, i.e. a relationship is derived between observed ocean surface winds and independent predictors. However, predictors are not derived from an analysis of the actual observations but from a particular numerical forecast model. This has a number of important implications:

- Biases associated with the particular numerical model used to supply the predictors are suppressed;
- The number of potential predictors available is greatly enlarged since predictors may include those from different forecast times; but
- As the model producing the predictors is changed and improved, the wind-specification equations must also be re-derived using the latest version of the numerical model as a predictor source.

An example of this technique is given by Feit and Pore (1978) for use on the Great Lakes.

TABLE 2.7

Data requirements for various statistical approaches

Approach	*Development data*		*Operational data*
	Dependent	*Independent*	*Independent*
Extrapolation	Observations	Observations	Manual or model forecast output
Perfect prognosis	Observations	Analyses	Model forecast output
Model output statistics	Observations	Model forecast output	Model forecast output

Table 2.7 summarizes the data requirement for each of the approaches described above.

The major difference between the approaches lies in the type of independent data used in the development stage. In the extrapolation approach observations are used as potential predictors, in the perfect prognosis approach analyses are used and in the model output statistics approach model forecasts are used. Another difference to note is that during actual operations of the extrapolation approach the predictors may be manually applied, while in the operations of the perfect prognosis and model output statistics approach the predictors are derived in an automated fashion from model forecasts.

CHAPTER 3

WAVE GENERATION AND DECAY

A. K. Magnusson with M. Reistad: editors

3.1 Introduction

This chapter gives an overview of the processes involved in wave generation and decay. An indication of how these processes are formulated is given.

Wave forecasting is the process of estimating how waves evolve as changing wind fields act on the surface of the ocean. To understand this we need to identify the processes affecting the energy of the waves. In simple terms, wave energy at a given location is changed through advection (rate of energy propagated into and away from the location), the wave energy gains from the external environment and wave energy losses due to dissipation. In wave modelling, the usual approach is to represent these influences as a wave energy conservation equation, as presented in Chapter 5 (Equation 5.1), and then to solve it.

The sources of wave energy (gains and losses) are identified as three major processes, the external gains (S_{in}), the dissipative loss (S_{ds}) and the shifting of energy within the spectrum due to weakly non-linear wave-wave interactions (S_{nl}). A description of these terms as well as of propagation are presented in this chapter.

3.2 Wind-wave growth

The only input of energy to the sea surface over the time-scales we are considering comes from the wind. Transfer of energy to the wave field is achieved through the surface stress applied by the wind and this varies roughly as the square of the wind speed. Thus, as already noted in Section 2.1, an error in wind specification can lead to a large error in the wave energy and subsequently in parameters such as significant wave height.

After the onset of a wind over a calm ocean there are thought to be two main stages in the growth of wind waves. First, the small pressure fluctuations associated with turbulence in the airflow above the water are sufficient to induce small perturbations on the sea surface and to support a subsequent linear growth as the wavelets move in resonance with the pressure fluctuations. This mechanism is called the Phillips' resonance (see Phillips, 1957). Formulations can be found in Barnett (1968) and Ewing (1971). However, this mechanism is only significant early in the growth of waves on a calm sea.

Most of the development commences when the wavelets have grown to a sufficient size to start affecting the flow of air above them. The wind now pushes and drags the waves with a vigour which depends on the size of the waves themselves.

This growth is usually explained by what is called a shear flow instability: the airflow sucking at the crests and pushing on the troughs (or just forward of them). A useful theory has been presented by Miles (1957). The rate of this growth is exponential as it depends on the existing state of the sea. This is usually described in terms of the components of the wave energy-density spectrum (see Section 1.3.7).

From the formulation of Miles (1960):

$$E(f,\theta) = \frac{k}{4\pi f\, {\rho_w}^2 \mu g}\, P(\boldsymbol{k}, f)\left(e^{2\pi f t\mu} - 1\right)$$

or

$$S_{in}(f,\theta) = \frac{\delta E(f,\theta)}{\delta t} = 2\pi f \mu\, E(f,\theta),$$

where $E(f,\theta)$ is a frequency-direction component, $\boldsymbol{k}$ is the wavenumber, $P(\boldsymbol{k},f)$ is the spectrum of wave-induced turbulence, μ is a coupling coefficient to be defined, g is gravitational acceleration and ρ_w is the water density.

It has been noted that the rates of growth predicted by Miles are much smaller than observed growth rates from laboratory and field studies. Based on a field experiment, Snyder and Cox (1966) proposed a simple form:

$$\mu = \frac{\rho_a}{\rho_w}\left[\frac{u}{c}\cos(\theta - \psi) - 1\right],$$

where c and θ are the phase speed and the direction, respectively, of the component being generated, ψ and u are the direction and speed of the wind and ρ_a is the air density.

Measurements made in the Bight of Abaco in the Bahamas in 1974 enabled Snyder et al. (1981) to propose a revision which can be expressed by:

$$S_{in}(f,\theta) = E(f,\theta)\, \max\left[0, K_1 2\pi f \frac{\rho_a}{\rho_w}\left(\frac{U_5}{c}\cos(\theta - \psi) - 1\right)\right].$$

The height at which the wind speed was specified in the original work was 5 m. Since application of this to other situations can be affected by the structure of the lower part of the atmospheric boundary layer (see Section 2.4), it may be better to express the wind input in terms of the friction velocity u_* with magnitude:

$$u_* = \sqrt{\frac{\tau}{\rho_a}} = u\sqrt{C_d}$$

where τ is the magnitude of the wind stress and C_d is the drag coefficient.

The drag coefficient, which relates u_* to u, varies with u. Komen et al. (1984) have used an approximate form to write the wind input term as:

$$S_{in}(f,\theta) = E(f,\theta) \max\left[0, K_1 \frac{\rho_a}{\rho_w} 2\pi f \left(K_2 \frac{u_*}{c}\cos(\theta-\psi)-1\right)\right]. \quad (3.1)$$

The constants K_1 (≈ 0.25) and K_2 (≈ 28) allow for some flexibility in specifying this term.

Later research has shown that the aerodynamic drag on the sea surface depends on the state of the waves. Janssen (1991) and Jenkins (1992), using quasi-linear theories, have found that the drag coefficient depends on the wave age parameter defined as c_p/u_*, where c_p is the phase velocity of the peak frequency of the actual wave spectrum. These theories imply that the aerodynamic drag and the growth rate of the waves are higher for young wind sea than for old wind sea. This result is in good agreement with experimental data by Donelan (1982) and Maat et al. (1991).

There are also many empirical formulae for wave growth which have been derived from large data sets. These formulae make no attempt to separate the physical processes involved. They represent net wave growth from known properties of the wind field (wind speed and direction, fetch and duration). In representing such relations, it simplifies comparisons if the variables are all made dimensionless:

Peak frequency	f_p^*	=	uf_p/g
Fetch	X^*	=	gX/u^2
Duration	t^*	=	gt/u
Height	H^*	=	gH/u^2
Energy	E^*	=	Eg^2/u^4 etc.

For example, from the JONSWAP 1973 data (see Hasselmann et al., 1973, 1976; and Section 1.3.9), the peak frequency and total energy in the spectrum are related to the fetch (X) and wind speed at 10 m (U_{10}) by the following:

$$f_p^* = 3.5\, X^{*-0.33}, \quad E^* = 1.6 \times 10^{-7}\, X^* \quad (3.2)$$

Operationally useful graphical presentations of such empirical relations have existed since the mid-1940s and the Sverdrup and Munk (1947) and Pierson-Neumann-James (1955) curves have been widely used (see Annex IV). Such relationships may also need to consider the depth (see Section 7.5); since wave growth is affected by the depth, with additional dissipative processes in play, the deep water curves will over-estimate the wave growth in shallow water.

A more recent set of curves are those developed by Gröen and Dorrestein (1976). These comprise a variety of formats for calculating wave height and period, given the wind speed, fetch length and wind duration, and the effects of refraction and shoaling. In Figure 3.1, the basic non-dimensional graphs are displayed, showing characteristic height and period versus fetch and duration. It should be noted that these graphs have been constructed to fit visually assessed wave heights and periods (see Section 8.3) and are thus called "characteristic" height (H_c) and period (T_c), as distinct from significant height ($\bar{H}_{1/3}$) and mean period ($\bar{T}_z$). The set of curves and the applications of them are given in Section 4.1.

There is some uncertainty about the relationship between the visually and instrumentally derived quantities, but it appears that some bias (H_c and T_c both being slightly higher than $\bar{H}_{1/3}$ and $\bar{T}_z$, respectively) may need to be kept in mind when using this type of graph. On the other hand, the systematic errors are generally small compared to random errors in individual observations.

So far, we have considered wind waves which are in the process of growing. When the wind stops or when the waves propagate out of the generating area, they are often called "swell". Swell looks different from an ordinary running sea. The backs of the waves are smoother and the crests are long. Whereas wind waves grow under the influence of the wind, swell waves decrease in its absence. Since propagation is the most important characteristic of swell waves, they are discussed more fully in the next section.

3.3 Wave propagation

A disturbance on the water will travel away from the point at which it was generated. For a wave train with period T (frequency $f = 1/T$) and wavelength λ, the wave speed (phase speed) is $c = \lambda/T$. This can be written also as ω/k, where ω is the angular frequency ($2\pi f$) and k is the wavenumber $2\omega/\lambda$ (the number of crests per unit distance). *Wave energy travels at the group velocity*, which is not in general the same. For the dispersive waves in deep water, the group velocity ($\boldsymbol{c_g}$) is only half of the phase velocity. As given in Section 1.3.2, this can be worked out from the dispersion relation by using $c_g = d\omega/dk$. In very shallow water, the waves are non-dispersive as the bottom dominates the fluid's response to a perturbation and the group velocity equals the phase velocity.

In general, for water of finite depth, h, the dispersion relation is:

$$\omega^2 = gk \tanh kh$$

and the group speed is:

$$c_g = \frac{1}{2}\frac{\omega}{k}\left(1 + \frac{2kh}{\sinh 2kh}\right)$$

(see also Section 1.3.2). For large h, this reduces to $\omega k/2$ and, for very small h, to ω/k [$= \sqrt{(gh)}$].

In wave modelling, we are interested in how a local average of the energy moves. This is not as simple as moving the energy at one point in a straight line (or more correctly a great circle path) across the ocean. For any one location the energy is actually spread over a

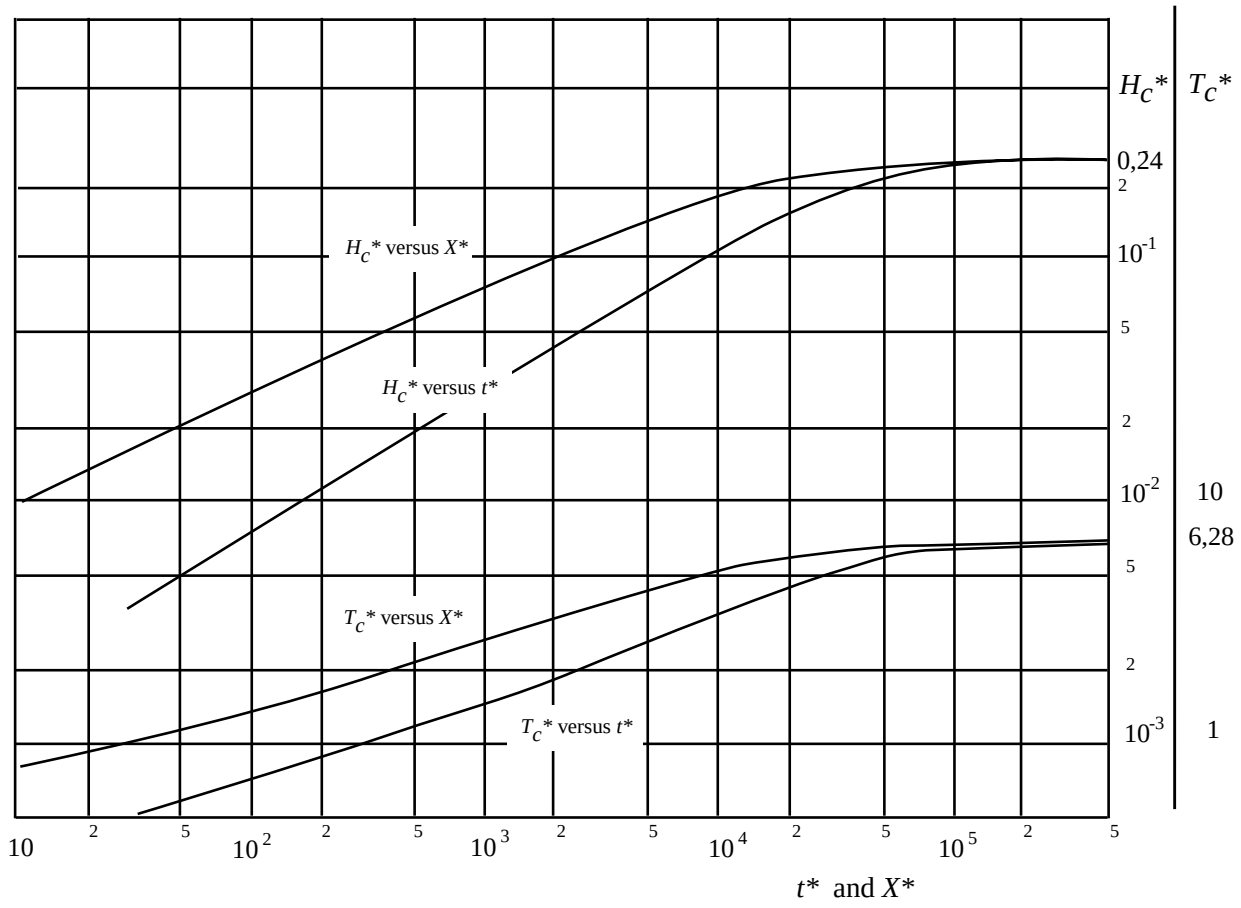

Figure 3.1 — Basic diagram for manual wave forecasting. The curves are drawn for non-dimensional parameters ($H_c^* = gH_c/u^2$; $T_c^* = gT_c/u$) (*derived from Gröen and Dorrestein, 1976*)

range of directions. Also, waves at different frequencies will propagate at different speeds. Thus, from a point source, each component of the spectrum $E(f,\theta)$ can be propagated in the direction θ with a speed $c_g(f,\theta)$.

3.3.1 *Angular spreading*

It is often assumed that the directional part of the wind-wave distribution has a $\cos^2(\theta - \psi)$ form where ψ is the predominant direction of the waves and θ is the direction of the spectral component concerned. Most of the energy is propagated in the mean direction of the sea. At deviating angles, less energy is transported and, for all practical purposes, the energy propagated at right angles to the mean direction is negligible. There is considerable evidence indicating that the spread is dependent on the lengths of waves. Several such formulations for the directional distribution based on observations have been given. Using the form $\cos^{2s}(\theta - \psi)/2$, Mitsuyasu et al. (1975) and Hasselmann et al. (1980) give functional forms for s which are dependent on the ratio of frequency to peak frequency. These indicate the narrowest spread at the peak of the spectrum, with widening at both lower and higher frequencies. However, there is still uncertainty with respect to the real functional form of the s parameter in simple sea states (e.g. wind-sea generation and long swells). This is due to the fact that different directional wave instruments located very close to one another give widely different results (see for example, Allender et al., 1989).

Waves which have left the generating area (i.e. swell) are reduced by the angular spreading. Numerical models automatically take care of this by splitting the spectrum into components and propagating each of the components independently. Manual methods require more action by the operator. Angular spreading and dispersion factors must be applied.

As illustrated in Figure 3.2, a point P will receive wave energy from points all along the front of the fetch. It is possible to compute the sum of all the contributions. For a cosine-squared distribution of energy at the fetch front, results are shown in Figure 3.3. At any fixed frequency, the curved lines in this diagram represent the percentages of the wave energy from the fetch front which reach there. These are the angular spreading factors. The spatial coordinates are expressed in terms of the width AB of the fetch area. For example, at a distance of 2.5 AB along the predominant swell direction, the wave energy has decreased to about 25 per cent of the energy per unit area which was present at the fetch front AB. The reduction in wave height due to

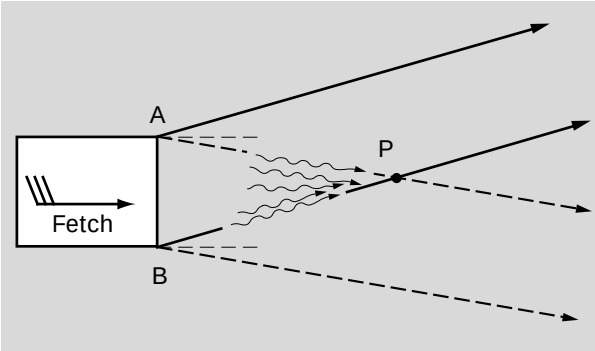

Figure 3.2 — Possible directions for swell originating at a storm front, AB, and incident on a point P

angular spreading is by the square root of this factor. These heights are the maximum heights which the swell may attain.

3.3.2 *Dispersion*

A further reduction needs to be applied to account for dispersion. It has been explained how long waves and their energy travel faster than short waves and their energy. The wave field leaving a generating area has a mixture of frequencies. At a large distance from the generating fetch, the waves with low frequencies (long waves) will arrive first, followed by waves of increasing frequency. If the spectrum at the front edge of the generating fetch is that represented in Figure 3.4, then, given the distance from this edge and the time elapsed, it is easy to work out the speed of the slowest wave which could possibly reach your point of observation. Hence, we know the maximum frequency we would observe. Similarly, the length of fetch and the time at which generation ceases may limit the low frequencies: all the fastest waves may have passed through the monitoring point. The swell spectrum is therefore limited to a narrow band of frequencies (indicated by the shaded areas of the spectra in Figure 3.4). The shaded portion of the spectrum is the maximum that can be expected at the point of observation. The ratio of this area to the total area under the spectrum is called the wave-energy dispersion factor. A consequence of this dispersion effect is that by analysing the way in which swell arrives at an observing point, and noting the changes in the frequencies in the swell spectrum, it is possible to get an idea of the point of origin of the waves.

Thus, given the spectrum of wave energy exiting a generating area and a point at which you wish to calculate the swell, you can calculate the angular spreading factor and the dispersion factor to get an estimate of the swell.

Dispersion and spreading can be considered the main causes of a gradual decrease of swell waves. Some energy is also lost through internal friction and air resistance. This acts on all components of the wave spectrum, but is strongest on the shorter waves (higher frequencies), contributing to the lengthening of swell at increasing distances from the source. This dissipation is often

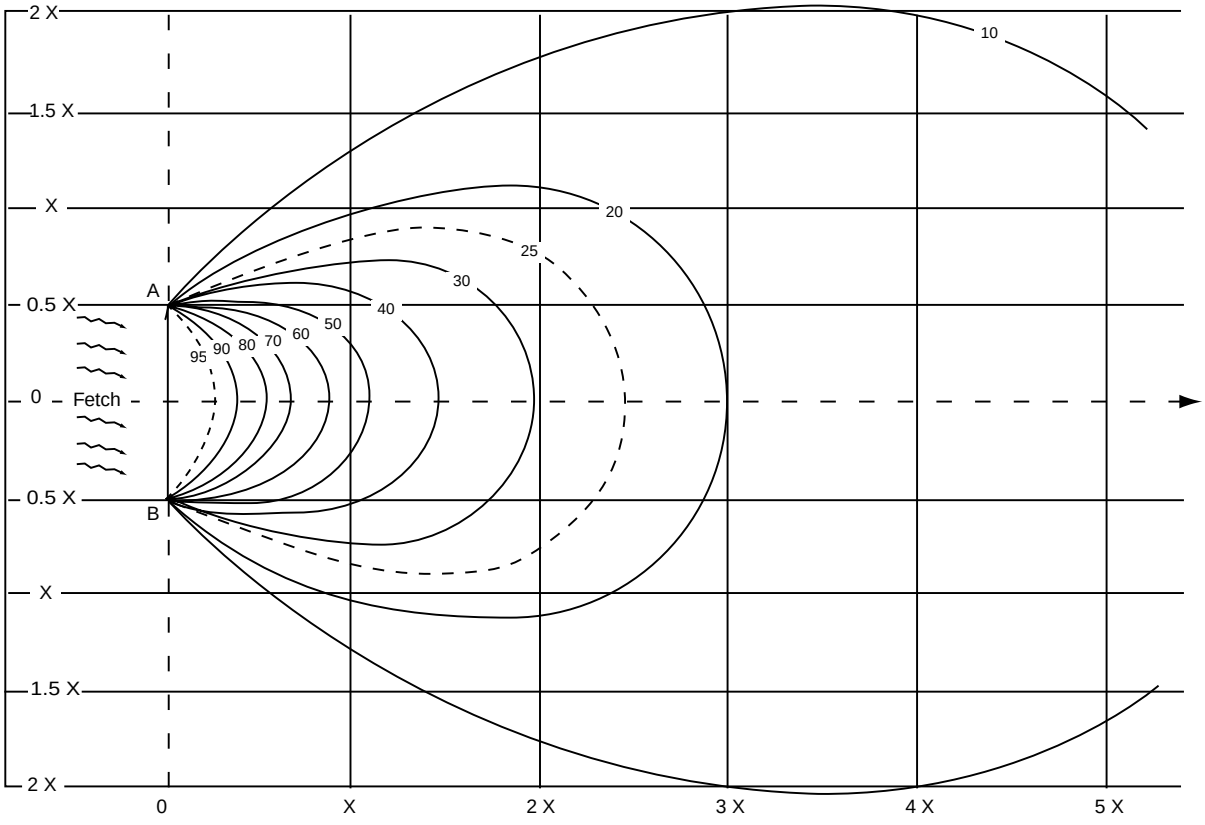

Figure 3.3 — Angular spreading factors (as percentages) for swell energy

small enough that swell can survive over large distances. Some interesting observations of the propagation of swell were made by Snodgrass et al. (1966) when they tracked waves right across the Pacific Ocean from the Southern Ocean south of Australia and New Zealand to the Aleutian Islands off Alaska.

The spectra of swell waves need not be narrow. For points close to large generating areas, faster waves from further back in the generating area may catch up with slower waves from near the front. The result is a relatively broad spectrum. The dimensions of the wave-generating area and the distance from it are therefore also important in the type of swell spectrum which will be observed.

In Chapter 4, more detail will be given on how to determine the spectrum of wind waves and swell and on how to apply the above ideas.

Other considerations in propagating waves are the water depth and currents. It is not too difficult to adapt the advection equation to take account of shoaling and refraction. This is considered in Sections 7.2 and 7.3. For operational modelling purposes, currents have often been ignored. The influence of currents on waves depends on local features of the current field and wave propagation relative to the current direction. Although current modulation of mean parameters may be negligible in deep oceans, and even in shelf seas for ordinary purposes, the modulation of spectral density in the high-frequency range may be significant (see, for instance, Tolman, 1990). Waves in these frequencies may even be blocked or break when they propagate against a strong current, as in an estuary. For general treatment of this subject see Komen et al. (1994). The gain in wave forecast quality by taking account of currents in a forecasting model is not generally considered worth while compared to other factors that increase computing time (e.g. higher grid resolution). Good quality current fields are also rarely available in larger ocean basins.

3.4 Dissipation

Wave energy can be dissipated by three different processes: whitecapping, wave-bottom interaction and surf breaking. Surf breaking only occurs in extremely shallow water where depth and wave heights are of the same order of magnitude (e.g. Battjes and Janssen, 1978). For shelf seas this mechanism is not relevant. A number of mechanisms may be involved in the dissipation of wave energy due to wave-bottom interactions. A review of these mechanisms is given by Shemdin et al. (1978), which includes bottom friction, percolation (water flow in the sand and the sea-bed) and bottom motion (movement of the sea-bed material itself). In Sections 7.6 and 7.7, dissipation in shallow water will be discussed more fully.

The primary mechanism of wave-energy dissipation in deep and open oceans is whitecapping. As waves grow, their steepness increases until a critical point when they break (see Section 1.2.7). This process is highly non-linear. It limits wave growth, with energy being lost into underlying currents. This dissipation depends on the existing energy in the waves and on the wave steepness, and can be written:

$$S_{ds}(f,\theta) = -\psi(E)\,\frac{f^2}{\bar{f}}\,E(f,\theta)\,, \qquad (3.3)$$

where $\psi(E)$ is a property of the integrated spectrum, E. ψ may be formulated as a function of a wave steepness parameter ($\xi = E\bar{f}^4/g^2$, where $\bar{f}$ is the mean frequency). Forms for ψ have been suggested by Hasselmann (1974) and Komen et al. (1984).

There are also the processes of micro-scale breaking and parasitic capillary action through which wave energy is lost. However, there is still much to learn about dissipation and usually no attempt is made to distinguish the dissipative processes. The formulation of S_{ds} still requires research.

Manual wave calculations do not need to pay specific attention to dissipative processes. Generally, the dissipation of wind waves is included implicitly in the overall growth curves used. Swell does suffer a little from dissipative processes, but this is minor. It is observed that swell can travel over large distances. Swell is mostly reduced by dispersion and angular spreading.

3.5 Non-linear interactions

In our introduction we noted that simple sinusoidal waves, or wave components, were linear waves. This is an approximation. The governing equations admit more

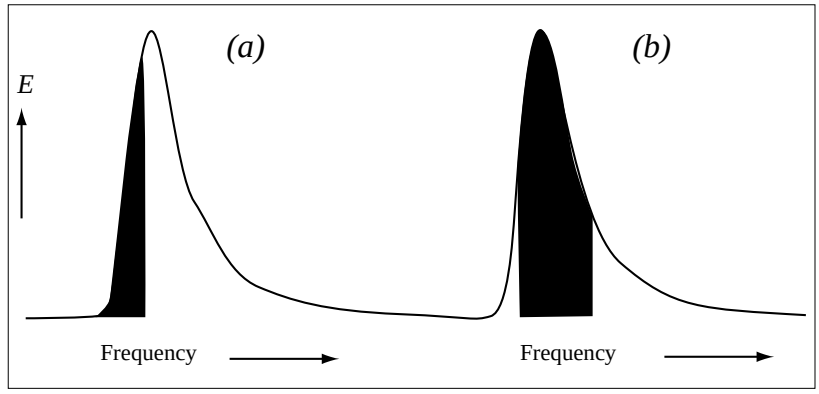

Figure 3.4 — The effect of dispersion on waves leaving a fetch. The spectrum at the fetch front is shown in both (*a*) and (*b*). The first components to arrive at a point far downstream constitute the shaded part of the spectrum in (*a*). Higher frequencies arrive later, by which time some of the fastest waves (lowest frequencies) have passed by as illustrated in (*b*)

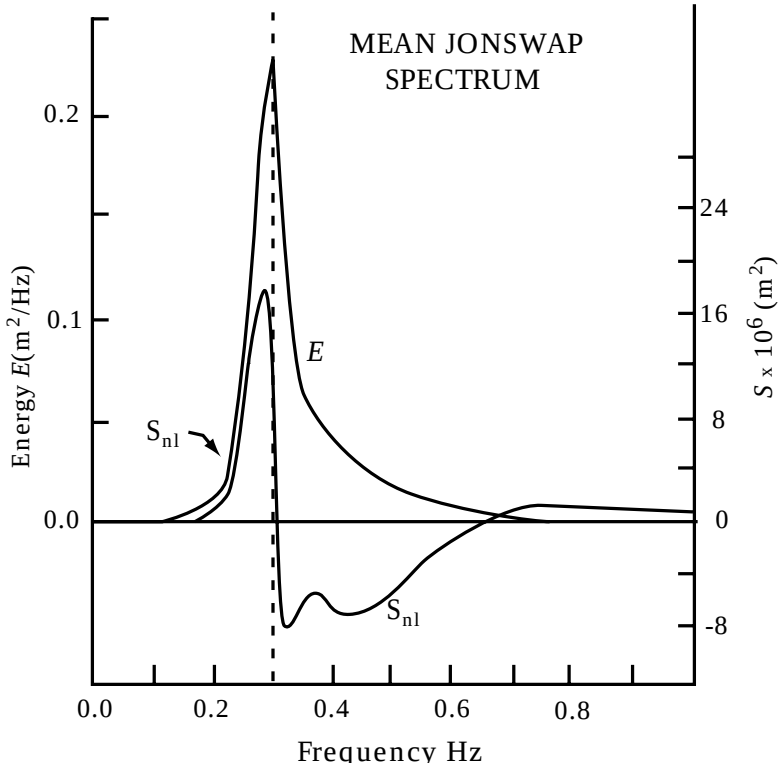

Figure 3.5 — Growth from non-linear interactions (S_{nl}) as a function of frequency for the mean JONSWAP spectrum (E)

detailed analysis. Whilst the theory is restricted by a requirement that the waves do not become too steep, the weakly non-linear interactions have been shown to be very important in the evolution of the wave spectrum.

These weakly non-linear, resonant, wave-wave interactions transfer energy between waves of different frequencies, redistributing the energy within the spectrum in such a way that preserves some characteristics of the spectral shape, i.e. a self-similar shape. The process is conservative, being internal to the wave spectrum and not resulting in any change to the overall energy content in the wave field.

The resonance which allows this transfer between waves can be expressed by imposing the conditions that the frequencies of the interacting waves must sum to zero and likewise the wavenumbers. This first occurs at the third order of a perturbation analysis in wave energy (as shown by Hasselmann, 1962) and the integrals which express these energy transfers are complicated cubic integrals:

$$\begin{aligned} S_{\mathrm{nl}}(f,\theta) = f \iiint \mathrm{d}\boldsymbol{k}_1 \mathrm{d}\boldsymbol{k}_2 \mathrm{d}\boldsymbol{k}_3 \\ \delta(\boldsymbol{k}_1 + \boldsymbol{k}_2 - \boldsymbol{k}_3 - \boldsymbol{k}) \\ \delta(f_1 + f_2 - f_3 - f) \\ \left[n_1 n_2 (n_3 + n) - n_3 n (n_1 + n_2) \right] \\ K(\boldsymbol{k}_1, \boldsymbol{k}_2, \boldsymbol{k}_3, \boldsymbol{k}) . \end{aligned} \qquad (3.4)$$

In this integral, the delta functions, δ, enforce the resonance conditions, the (f_i, $\boldsymbol{k}_i$) for i = 1, 2, 3 are the frequency and wavenumber pairs for the interacting wave components (related as in Equation 1.3), the $n_i = E(f_i,\theta_i)/f_i$, are the wave *action* densities, and the Kernel function, K, gives the magnitude of the energy transfer to the component $\boldsymbol{k}$, (or (f,θ)) from each combination of interacting wave components.

This interactive process is believed to be responsible for the downshift in peak frequency as a wind sea develops. Figure 3.5 illustrates the non-linear transfer function $S_{nl}(f)$ calculated for a wind sea with an energy distribution, $E(f_i,\theta_i)$, given by the mean JONSWAP spectrum (see Section 1.3.9). The positive growth just below the peak frequency leads to this downshift.

Another feature of the non-linear wave-wave interactions is the "overshoot" phenomenon. Near the peak,

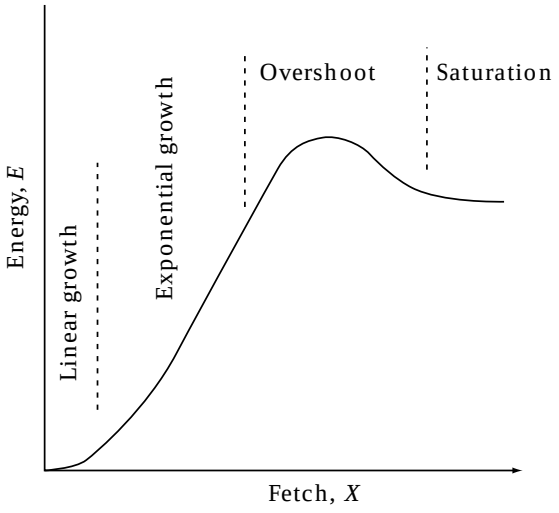

Figure 3.6 — Development of wave energy at a single frequency along an increasing fetch, illustrating the various growth stages

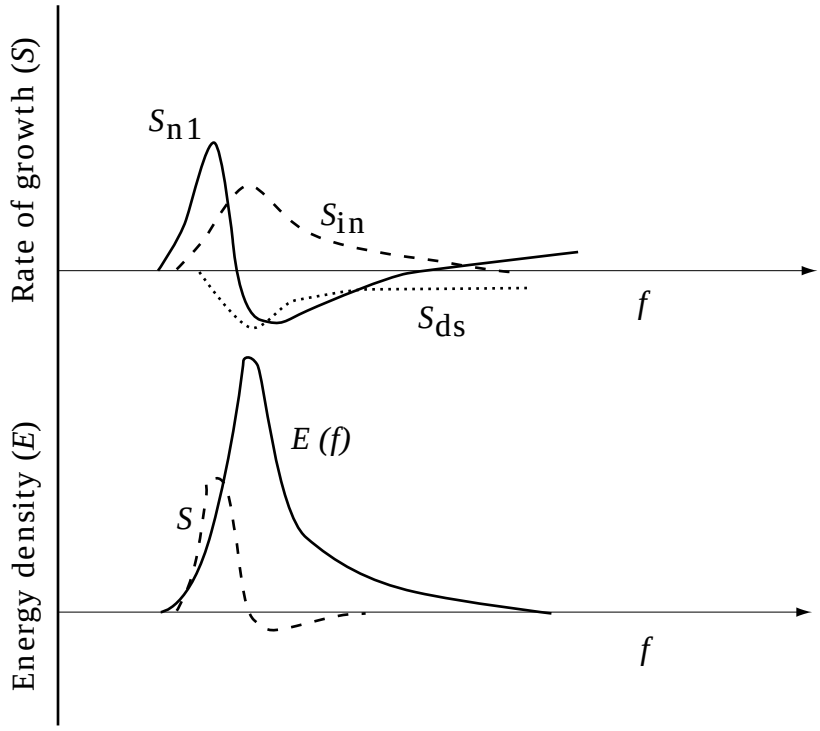

Figure 3.7 — Structure of spectral energy growth. The upper curves show the components S_{nl}, S_{in}, and S_{ds}. The lower curves are the frequency spectrum $E(f)$, and the total growth curve S

growth at a given frequency is dominated by the non-linear wave-wave interaction. As a wind sea develops (or as we move out along a fetch) the peak frequency decreases. A given frequency, f_e, will first be well below a peak frequency, resulting in a small amount of growth from the wind forcing, some non-linear interactions, and a little dissipation. As the peak becomes lower and approaches f_e, the energy at f_e comes under the influence of a large input from non-linear interactions. This can be seen in Figures 3.5 and 3.7 in the large positive region of S or S_{nl} just below the peak. As the peak falls below f_e this input reverses, and an equilibrium is reached (known as the saturation state). Figure 3.6 illustrates the development along a fetch of the energy density at such a given frequency f_e.

Although the non-linear theory can be expressed, as in Equation 3.4, the evaluation is a problem. The integral in Equation 3.4 requires a great deal of computer time, and it is not practical to include it in this form in operational wave models. Some wave models use the similarity of spectral shape, which is a manifestation of this process, to derive an algorithm so that the integral calculation can be bypassed. Having established the total energy in the wind-sea spectrum, these models will force it into a pre-defined spectral shape. Alternatively, it is now possible to use integration techniques and simplifications which allow a reasonable approximation to the integral to be evaluated (see the discrete interaction approximation (DIA) of Hasselmann and Hasselmann, 1981, Hasselmann and Hasselmann, 1985, and Hasselmann et. al., 1985; or the two-scale approximation (TSA) of Resio et al., 1992). These efficient computations of the non-linear transfer integral made it possible to develop third generation wave models which compute the non-linear source term explicitly without a prescribed shape for the wind-sea spectrum.

Resonant weakly non-linear wave-wave interactions are only one facet of the non-linear problem. When the slopes of the waves become steeper, and the non-linearities stronger, modellers are forced to resort to weaker theories and empirical forms to represent processes such as wave breaking. These aspects have been mentioned in Section 3.4.

3.6 General notes on application

The overall source term is $S = S_{in} + S_{ds} + S_{nl}$. Ignoring the directional characteristics (i.e. looking only at the frequency dependence), we can construct a diagram for S such as Figure 3.7. This gives us an idea of the relative importance of the various processes at different frequencies. For example, we can see that the non-linear transfer is the dominant growth agent at frequencies near the spectral peak. Also, for the mid-frequency range (from the peak to about twice the peak frequency) the growth is dominated by the direct input from the atmosphere. The non-linear term relocates this energy mostly to the lower frequency range. The dissipation term, so far as is known, operates primarily on the mid- and high-frequency ranges.

The development of a frequency spectrum along a fetch is illustrated in Figure 3.8 with a set of spectra measured during the JONSWAP experiment. The downshift in peak frequency and the overshoot effect at each frequency are evident.

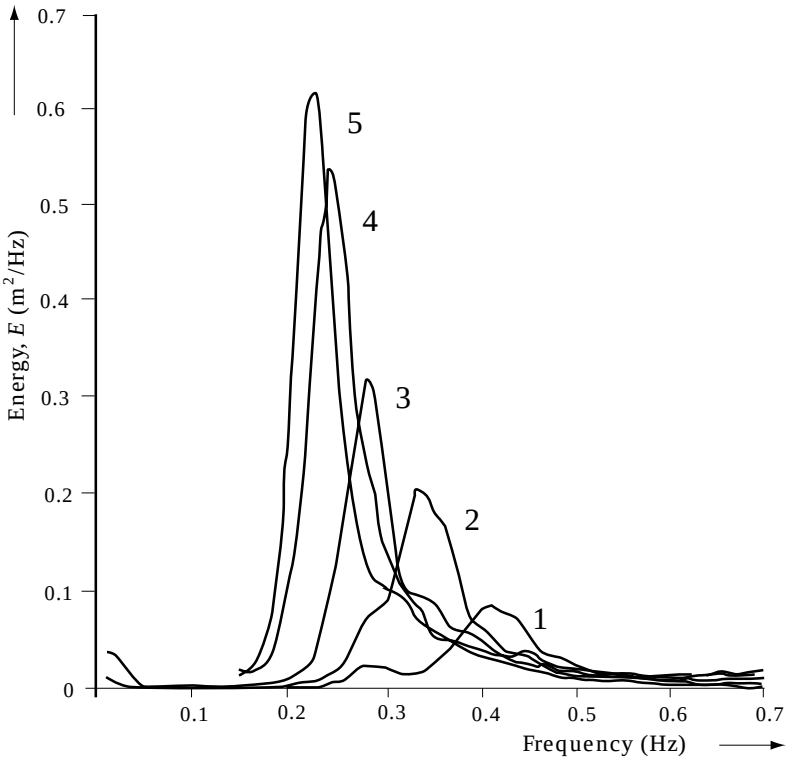

Figure 3.8 —
Growth of a frequency spectrum along a fetch. Spectra 1–5 were measured at distances 9.5, 20, 37, 52, and 80 km, respectively, offshore. The wind is 7 m/s (*after Hasselmann et al., 1973*)

Application of the source terms is not always straightforward. The theoretical-empirical mix in most wave models allows for some "tuning" of the models. This also depends on the grid, the boundary configuration, the type of input winds, the time-step, the influence of depth, computer power available, etc. Manual methods, on the other hand, conform to what may be regarded as fairly universal rules and can usually be applied anywhere without modification.

For manual calculations, the distinction between wind sea and swell is quite real and an essential part of the computation process. For the hybrid parametric models (see Chapter 5) it is necessary, although the problem of interfacing the wind-wave and swell regimes arises. For numerical models which use spectral components for all the calculations (i.e. discrete spectral models) the definition of swell is quite arbitrary. From the spectrum alone there is no hard and fast rule for determining the energy which was generated locally and that which was propagated into the area. This can pose problems when attempting to interpret model estimates in terms of features traditionally understood by the "consumer". Many users are familiar with, and often expect, information in terms of "wind sea" and "swell". One possible algorithm is to calculate the Pierson-Moskowitz spectrum (Section 1.3.9) for fully developed waves at the given local wind speed and, specifying a form for directional spreading (Section 3.3.1), allocate energy in excess of this to a swell spectrum. More sophisticated algorithms will assess a realistic cut-off frequency for the local generation conditions, which may be considerably higher than the the peak frequency from the Pierson-Moskowitz spectrum and hence also designate as swell excess low-frequency wave energy at directions near the wind.

CHAPTER 4

WAVE FORECASTING BY MANUAL METHODS

L. Burroughs: editor

4.1 Introduction

There are many empirical formulae for wave growth which have been devised from large visually observed data sets. There are also formulae, more recently derived, which are based on wave measurements. These formulae make no attempt to separate the physical processes involved. They represent the net wave growth from known properties of the wind field (wind speed and direction, fetch and duration).

There are some inherent differences between visually and instrumentally observed wave heights and periods which affect wave prediction. In general, the eye concentrates on the nearer, steeper waves and so the wave height observed visually approximates the significant wave height ($\bar{H}_{1/3}$), while the visually observed wave periods tend to be shorter than instrumentally observed periods. There are several formulae which have been used to convert visual data to $\bar{H}_{1/3}$ more accurately. For almost all practical meteorological purposes, it is unlikely to be worth the transformation. Operationally useful graphical presentations of such empirical relations have existed since the mid-1940s.

The curves developed by Sverdrup and Munk (1947) and Pierson, Neumann and James (1955) (PNJ) are widely used. These two methods are similar in that the basic equations were deduced by analysing a great number of visual observations by graphical methods using known parameters of wave characteristics. However, they differ fundamentally in the way in which the wave field is specified. The former method describes a wave field by a single wave height and wave period (i.e. $\bar{H}_{1/3}$ and $\bar{T}_{H_{1/3}}$) while the latter describes a wave field in terms of the wave spectrum. The most obvious advantage of the PNJ method is that it allows for a more complete description of the sea surface. Its major disadvantage is the time necessary to make the computations.

A more recent set of curves has been developed by Gröen and Dorrestein (1976) (GD). These curves comprise a variety of formats for calculating wave height and period given the wind speed, fetch length, wind duration, and the effects of refraction and shoaling. These curves differ little from those found in PNJ except that the wave height and period are called the characteristic wave height (H_c) and period (T_c) rather than $\bar{H}_{1/3}$ and $\bar{T}_{\bar{H}_{1/3}}$, and mks units are used rather than feet and knots. Both PNJ and GD are derived from visually assessed data. The only difference between "characteristic" and "significant" parameters (i.e. H_c and $\bar{H}_{1/3}$, and T_c and $\bar{T}_{H_{1/3}}$) is that H_c and T_c are biased slightly high when compared to $\bar{H}_{1/3}$ and $\bar{T}_{H_{1/3}}$, which are assessed from instruments. However, the differences are insignificant for all practical purposes, and H_c and T_c are used throughout this chapter to be consistent with the GD curves.

Figure 4.1 shows the GD curves for deep water. This figure is of the form introduced in Figure 3.1 (Section 3.2) and will be used in wave calculations in this chapter. The PNJ curves are presented for comparison in Annex IV. For example, in Figure 4.1, thick dark lines represent the growth of waves along increasing fetch, which is shown by thin oblique lines. Each thick line corresponds to a constant wind speed. The characteristic wave height, H_c, is obtained from the horizontal lines and the characteristic period T_c from the dotted lines. The vertical lines indicate duration at which that stage of development will be reached. If the duration is limited, the waves will not develop along the thick dark lines beyond that point irrespective of the fetch length.

It should be noted that the curves are nearly horizontal on the right-side of the diagram. This implies that for a given wind speed, the waves stop growing when the duration or fetch is long enough.

Of the formulae which have been devised from measured wave data, the most noteable are from the JONSWAP experiment which was introduced in Chapter 1, Section 1.3.9 (see also Figure 1.17 and Equation 4.1).

In this chapter several manual forecasting examples are presented. Each example is designed to show how to make a forecast for a given set of circumstances and/or requirements. Some empirical working procedures are briefly mentioned in Section 4.2. These procedures have proved their value in actual practice and are alluded to in Sections 4.3 and 4.4. In Section 4.3 examples highlighting the various aspects of computing wind waves are explained. Examples of swell computations are given in Section 4.4. In Sections 4.3 and 4.4 all the examples are related to deep-water conditions. In Chapter 7 shallow-water effects on waves will be discussed, and in Section 4.5 a few examples of manual applications related to shallow (finite-depth) water conditions are presented. Table 4.1 provides a summary of each example given, and indicates the sub-section of Chapter 4 in which it can be found.

The explanations given in this chapter and in Chapter 2 provide, in principle, all the material

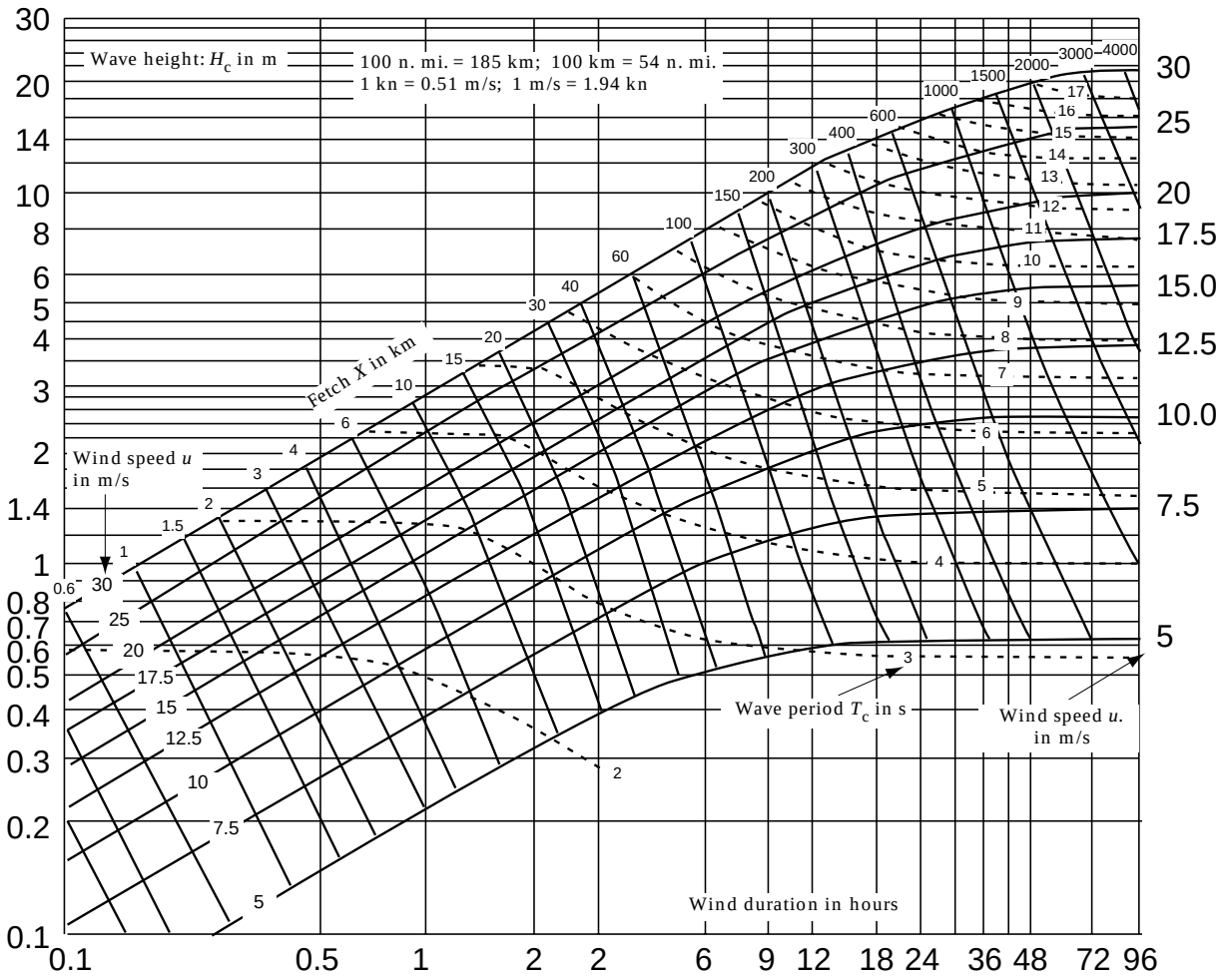

Figure 4.1 — Manual wave forecasting diagram (*from Gröen and Dorrestein, 1976*)

TABLE 4.1

Specific examples of manual forecasting presented in Chapter 4 and associated sub-section number

	Description	***Sub-section No.***
1	Determining sea-state characteristics for a given wind speed and fetch	4.3.1
2	Determining sea state for an increasing wind speed	4.3.2
3	Extrapolating an existing wave field with further development from a constant wind	4.3.3
4	Extrapolating an existing wave field with further development from an increasing wind	4.3.4
5	Computing when swell will arrive, what periods it will have and how these periods will change for 36 h after arrival begins	4.4.1
6	Same as 5, except for a long fetch in the generation area	4.4.2
7	Computing swell characteristics at Casablanca for a storm of nearby origin	4.4.3
8	Estimating the swell heights for the cases described in 5, 6 and 7	4.4.4
9	Determining wave number and shoaling factor for two wave periods and several representative depths	4.5.1.1
10	Finding the shallow water refraction factor and angle, for a given deep water wave angle with the bottom, shallow depth, and wave period	4.5.1.2
11	Finding the refraction factor by Dorrestein's method	4.5.1.3
12	Finding the shallow water height and period for a given wind speed, shallow water depth, and fetch	4.5.2

necessary to forecast waves for a particular location and also to perform a spatial wave analysis (i.e. analyse a wave chart) by manual methods. A great deal of experience is necessary to analyse an entire chart within reasonable time limits, mainly because one has to work with constantly changing wind conditions.

Generally, one starts from known wave and wind conditions, say 12 h earlier, and then computes, using the present analysed wind chart, the corresponding wave chart. In cases of sudden wind changes, the intermediate wind chart from 6 h earlier may also be needed. The forecast wind in the generation area and the forecast movement of the generation area are also necessary to produce the best wave forecast over the next 24 to 36 h.

4.2 Some empirical working procedures

Three empirical procedures are briefly discussed in this section. They are concerned with freshening of the wind at constant direction, changing wind direction, and slackening of the wind. These procedures are useful when time is short for preparing a forecast.

4.2.1 *Freshening of the wind at constant direction*

Freshening wind at constant direction is a frequent occurrence and the procedure described in Section 4.3.4 should be used. For quick calculations: subtract one-quarter of the amount the wind has increased from the new wind speed, and work with the value thus obtained. Example: the wind speed has increased from 10 to 20 kn (1.94 kn = 1 m/s) over the last 12 h; to compute the characteristic wave height, use a wind speed of 17.5 kn over a duration of 12 h. When sharp increases of wind speed occur, it is advisable to perform the calculation in two stages.

4.2.2 *Changing wind direction*

If the direction changes 30° or less, wave heights and periods are computed as if no change had occurred; the wave direction is assumed to be aligned with the new direction. At greater changes, the existing waves are treated as swell, and the newly generated waves are computed with the new wind direction.

4.2.3 *Slackening of the wind*

When the wind speed drops below the value needed to maintain the height of existing waves, the waves turn into swell and should be treated as such. As a first approximation, swell may be reduced in height by 25 per cent per 12 h in the direction of propagation. For instance, swell waves 4 m high will decrease to 3 m in 12 h.

TABLE 4.2

Characteristic parameters of wind waves

H_c (m)	T_c (s)	T_p (s)	$\bar{T}_{H1/3}$ (s)	f_p (s^{-1})	*Range of periods* (s)	H_{max} (m)
5	9	10.3	9.3	0.097	5 –15	10

4.3 Computation of wind waves

4.3.1 *Determining sea-state characteristics for a given wind speed and fetch*

Problem:

Determine the characteristics of the sea state for a wind speed of 15 m/s (about 30 kn), with a fetch of 600 km (about 325 nautical miles (n.mi.)) and after a duration of 36 h.

Solution:

According to the diagram given in Figure 4.1, the fetch is the limiting factor. For a fetch of 600 km, the characteristic wave height (H_c) is 5 m and the characteristic period (T_c) is 9 s.

Other characteristics can be obtained as well. From the JONSWAP spectrum (see Section 1.3.9, Figure 1.17, and Equation 4.1), we can find the peak frequency and period, and from them the range of important wave periods and the period of the highest one-third of the waves (significant wave period, $\bar{T}_{H_{1/3}}$). From $\bar{T}_{H_{1/3}}$ we can derive the highest wave in a 6-h period.

The peak frequency f_p is given by:

$$f_p = 0.148\, H_{m0}{}^{-0.6}\, u^{0.2} \qquad (4.1)$$

where H_{m0} is the model wave height in metres, and u is wind speed in metres per second. The model period is $T_p = 1/f_p$. Assume $H_{m0} \approx H_c = 5$ m, and $u = 15$ m/s, then $f_p = 0.097\ s^{-1}$, and $T_p = 10.3$ s.

To determine $\bar{T}_{H_{1/3}}$, we use Goda's (1978) results in an approximate form:

$$\bar{T}_{H_{1/3}} \approx 0.9\, T_p \ . \qquad (4.2)$$

For our problem, $\bar{T}_{H_{1/3}} \approx 0.9 \times 10.3 = 9.3$ s.

The range of important wave periods can be determined from Figure 1.17, where f (= $1/T$) varies from about 0.7 f_p to about 2.0 f_p. This translates to a range of 5 to 15 s. The maximum energy in the spectrum will be near the period of 10 s.

For a record of wave heights with about 2 000 wave measurements, we can use the following approximation to find the maximum wave height:

$$H_{max} \approx 2.0\, \bar{H}_{1/3} \approx 10 \text{ m}.$$

Table 4.2 presents all these results.

4.3.2 *Determining sea state for an increasing wind speed*

Problem:

An aeroplane has had to ditch at sea 200 km from shore. The closest ship is positioned 600 km from shore. The wind speed over the last 24 h has been steady at 17 m/s.

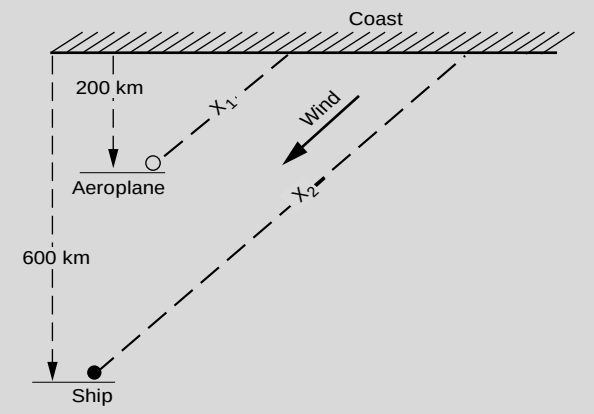

Figure 4.2 — Illustration of the situation in Problem 4.3.2

During the preceding 24 h, it had gradually increased from 13 to 17 m/s. The wind direction remained constant for the entire period and at an angle of 30° from land to sea. Figure 4.2 illustrates the situation.

Forecast the sea conditions for:

- The point at which the aeroplane ditched in order to determine whether a search and rescue seaplane could land and rescue the pilot, or whether the nearest vessel should be dispatched — which would take more time; and
- The position of the ship.

Solution:

The effective fetch for the landing place of the aeroplane is:

$$X_1 = \frac{200}{\sin 30°} = \frac{200}{0.5} = 400 \text{ km}$$

and for the position of the ship is

$$X_2 = \frac{600}{\sin 30°} = \frac{600}{0.5} = 1200 \text{ km}.$$

This is an example of more complicated wind-duration conditions. During the first full 24 h period, the wind increased steadily from 13 to 17 m/s. Recalling Section 4.2.1, we divide the 24 h period into two 12 h periods with the wind increasing from 13 and 15 m/s in the first half and from 15 to 17 m/s in the second. One-quarter of the increase in each period is 0.5 m/s. Subtracting this from 15 m/s and 17 m/s, gives 14.5 m/s and 16.5 m/s, respectively.

TABLE 4.3

Values of wave parameters at the locations of the ditched aeroplane and the ship

	H_c (m)	T_c (s)	u (m/s)	T_p (s)	$\bar{T}_{H1/3}$ (s)	H_{max} (m)
Aeroplane	5.6	9	17	10.8	9.7	11.2
Ship	6.5	10	17	11.8	10.6	13

Use of the diagram in Figure 4.1 shows that, for a wind speed of 14.5 m/s, wind waves reach a height of 3.7 m after 12 h. The same height would be attained after 8 h, at a speed of 16.5 m/s. Therefore, instead of working with a wind speed of 14.5 m/s over the first interval, we work with a wind speed of 16.5 m/s, but an equivalent duration of 8 h. The equivalent duration for the two periods amounts to 8 h + 12 h = 20 h. The diagram shows that, for a duration of 20 h and wind speed of 16.5 m/s, the wave height is 5.3 m.

At the beginning of the second full 24 h period, wave heights are 5.3 m, and the wind speed is 17 m/s and remains constant throughout the period. In order to work with a wind speed of 17 m/s, we determine the equivalent duration necessary to raise waves to a height of 5.3 m. It is 16 h. Thus, the equivalent duration for a 17 m/s wind speed is 16 h + 24 h or 40 h. For these conditions, H_c = 6.5 m and T_c = 10 s.

For these conditions to occur, a minimum fetch of 1 050 km is required. At the position of the nearest ship, there is no fetch limitation, but at the position of the ditched aeroplane there is. From Figure 4.1 we see that for a fetch of 400 km and a wind speed of 17 m/s, H_c = 5.6 m and T_c = 9 s.

Table 4.3 shows the values of other wave parameters which can be computed from u and H_c for both locations.

4.3.3 *Extrapolation of an existing wave field with further development from a constant wind*

Problem:

Figure 4.3 shows a wave field at time t_0. Forecast the characteristics of the sea state at point B at the time t_0 + 12 h, with a constant west wind of 17.5 m/s blowing at and to the west of point B.

Solution:

The starting point for the calculation cannot be at point B because the waves there move away from it. We must look for a starting point upwind at a point where waves have travelled from time t_0 to arrive at B at time t_0 + 12 h.

To estimate how far upwind A should be from B, we pick a point where the wave height is 4 m. From Figure 4.1 we see that waves with H_c = 4 m and u = 17.5 m/s have T_c = 7 s. After 12 h, T_c increases to about 9 s,

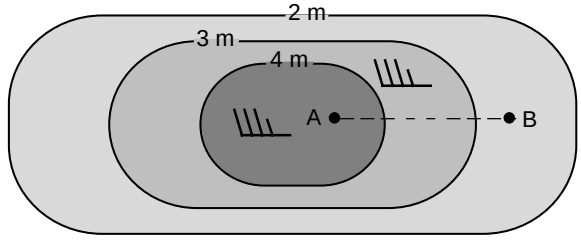

Figure 4.3 — Wave field at time t_0 indicated by lines of equal wave height

TABLE 4.4
Additional wave information for Problem 4.3.3

	H_c (m)	T_c (s)	u (m/s)	T_p (s)	$\bar{T}_{H1/3}$ (s)	H_{max} (m)
Point B	6	9.3	17.5	11.2	10	12

TABLE 4.5
Values of parameters computed from H_c for Problem 4.3.4

	H_c (m)	T_c (s)	u (m/s)	T_p (s)	$\bar{T}_{H1/3}$ (s)	H_{max} (m)
Point B	9.2	10.6	27.5	13.2	11.9	18.4

and the mean period is about 8 s. The wave propagation rate is given by $c = gT_c/2\pi$ and the group velocity is given by $c_g = c/2$ in deep water. Since $g/2\pi = 1.56$ m/s^2 (or 3.03 kn/s) then the group velocity $c_g \approx 0.78\ T_c$ m/s or $\approx 1.5\ T_c$ kn. Waves with $T_c = 8$ s have $c_g \approx 12$ kn and, in 12 h, cover a distance of 144 n.mi., or 2.4° of latitude. Dividing 2.4 by $T_c = 8$ gives 0.3. This example shows that the travel distance over 12 h, expressed in degrees of latitude, is 0.3 T_c. This is an easy formula to use to determine how far upwind to put A.

H_c equals 4.2 m at time t_0 at point A. To produce waves of that height, a wind of 17.5 m/s needs an equivalent duration of 8 h. H_c at point B at t_0 + 12 h can be determined by taking a total duration 8 h + 12 h = 20 h. From Figure 4.1, $H_c = 6$ m and $T_c = 9.3$ s. Table 4.4 gives additional information.

4.3.4 *Extrapolation of an existing wave field with further development from an increasing wind*

Problem:
The situation at t_0 is the same as in Figure 4.3, but now the wind increases from 17.5 m/s at t_0 to 27.5 m/s at t_0 + 12 h over the area which includes the distance AB. Forecast the sea state at Point B.

Solution:
Because the increase in wind speed is so great, divide the time period into two 6 h periods with winds increasing from 17.5 m/s at t_0 to 22.5 m/s, and 22.5 m/s to 27.5 m/s, respectively. Recalling Section 4.2.1, the corresponding speeds used to compute the waves are 21 m/s (21.25) and 26 m/s (26.25).

At t_0, H_c equals 4.2 m. Waves grow to this height with 21 m/s winds after 5 h. Over the first period then the equivalent duration with $u = 21$ m/s is 5 h + 6 h = 11 h. At the end of the interval, $H_c = 6.5$ m.

Waves would reach the 6.5 m height after an equivalent duration of 5.5 h with a wind of 26 m/s. Over the second 6 h period then, we may work with an equivalent duration of 11.5 h and a wind of 26 m/s. Thus, $H_c = 9.2$ m, and $T_c = 10.6$ s (see Table 4.5).

Actually these waves would have passed point B, since the average wave period during the 12 h period in this case was nearly 9 s. Their travel distance would be slightly greater than 2.6° of latitude. This small adjustment to the distance AB would not have influenced the calculations. In routine practice the travel distances are rounded to the nearest half degree of latitude.

4.4 Computation of swell

For most practical applications two different types of situation need to be distinguished:

(*a*) *Swell arriving at the point of observation from a storm at a great distance, i.e. 600 n.mi. or more.* In this case, the dimensions of the wave-generating area of the storm (e.g., tropical cyclone) can be neglected for most swell forecasting purposes, i.e. the storm is regarded as a point source. The important effect to be considered is wave dispersion;

(*b*) *Swell arriving at the point of observation from a nearby storm.* Swell fans out from the points along a storm edge. Because of the proximity of the storm edge, swell may reach the point of observation from a range of points on the storm front. Therefore, apart from wave dispersion, the effect of angular spreading should also be considered.

In swell computations, we are interested in the propagation of wave energy. Therefore, the group velocity of individual wave components, as approximated by representative sinusoidal waves, should be considered. Since large distances are often involved, it is more convenient to measure distances in units of nautical miles (n.mi.) and group velocities in knots (kn). The wave period T is measured in seconds as usual. We then have (as in Section 1.3.2):

$$c_g = \frac{c}{2} = \frac{1}{2}\frac{gT}{2\pi} = \frac{1}{2}3.03T = 1.515T \text{ (kn)}. \quad (4.3)$$

4.4.1 *Distant storms*

In the case of a distant storm (Figure 4.4), the questions to be answered in swell forecasting are:

(*a*) When will the first swell arrive at the point of observation from a given direction?

(*b*) What is the range of wave periods at any given time?

(*c*) Which wavelengths are involved? and, possibly

(*d*) What would the height of the swell be?

The known data to start with are the distance, R_p (n.mi.), from the storm edge to the point of observation, P, the duration, D_p, of wave generation in the direction of P, and the maximum wave period in the storm area.

Because they travel faster, the wave components with the maximum period are the first to arrive at P. Their travel time is:

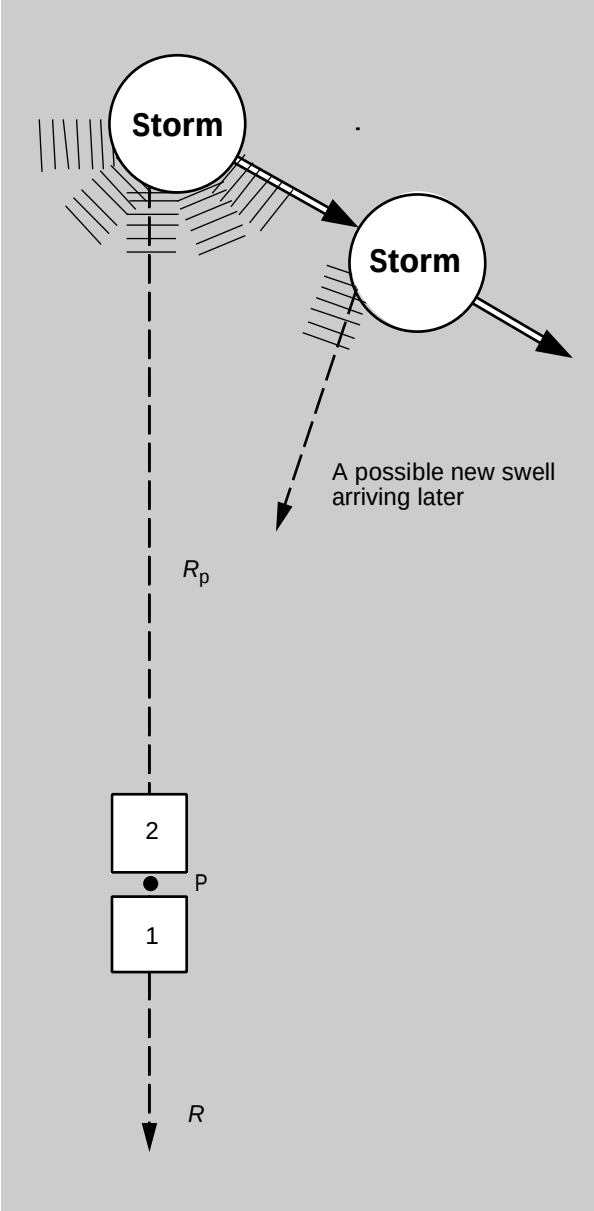

Figure 4.4 — Swell from a distant storm. Waves travelling in the direction of P have been generated over a time period D_p

$$t = \frac{R_p}{c_g} = \frac{R_p}{1.515T} = 0.660\,\frac{R_p}{T}\ \text{(h)}. \qquad (4.4)$$

These components continue to arrive over a period of D_p hours, then they disappear. D_p is determined from weather charts by examining how long a given fetch remained in a given area. In the meantime, slower wave components have arrived and each component is assumed, in the present example, to last for D_p hours. There is a wave component which is so slow that it starts to arrive at the moment when the fastest wave component present is about to disappear (compare boxes 1 and 2 in Figure 4.4). The first wave of the slow component (box 2) with period T_2 has travelled over a time of t hours; the last wave of the fast component (box 1) with period T_1 has started out D_p hours later and has thus travelled over a time of $(t - D_p)$ hours. We have, for the slow component:

$$T_2 = \frac{R_p}{1.515\,t} = 0.660\,\frac{R_p}{t}\ \text{(s)} \qquad (4.5)$$

and, for the fast component:

$$R_p = c_g\left(t - D_p\right) = 1.515\,T_1\left(t - D_p\right)$$

or

$$T_1 = \frac{R_p}{1.515\left(t - D_p\right)} = 0.660\,\frac{R_p}{t - D_p}\text{(s)} \qquad (4.6)$$

(R_p is measured in n.mi.; t and D_p in hours.)

T_1 and T_2 are the limits of all wave periods which can possibly be present at P at a given time of observation. Some periods within this range may actually not be present in the observed wave spectrum; the components could be dissipated during their long travel outside the storm area. It can easily be shown from the above equations that the range of possible wave frequencies is given by:

$$f_1 - f_2 = 1.515\,\frac{D_p}{R_p}\,. \qquad (4.7)$$

This means that the band width (range) of frequencies of wave components, which exist at a given point of observation, is a constant for that point and depends on the duration of wave generation, D_p. The range of frequencies becomes smaller at greater distances from the storm. This result, obtained from a schematic model, is indeed observed. Thus, as the result of wave dispersion, swell attains a more regular appearance at greater travel distances.

Example of swell from a distant storm

Problem:

Waves were generated in the direction *R* for a period of 18 h. The highest wave period generated in the storm was 15 s. Forecast swell for point A at 600 n.mi. and for point B at 1 000 n.mi. from the area of generation. Compute when the first waves arrive and which periods could possibly be present during the subsequent 36 h.

Solution:

At point A, R_p = 600 n.mi.; D_p = 18 h; T_{max} = 15 s.

From Equation 4.4 the first waves arrive at t = 0.660 x 600/15 = 26.4 h after the beginning of the storm. These waves continue for 18 h after they first arrive.

The range of periods $(T_1 - T_2)$ at point A are computed for the 36 h subsequent to the arrival time of the first wave at 6 h intervals beginning with 30 h after the storm as shown in Table 4.6. The range of wavelengths can also be given using the relation $\lambda = 1.56\,T^2$ (m). The wave components with a period of 15 s disappear after t = 44.4 h.

TABLE 4.6

Ranges of swell periods and wavelengths at point A for arrival time after storm beginning

Arrival time (h)	*Periods (s)*	*Wavelengths (m)*
30	15.0–13.2	351–272
36	15.0–11.0	351–189
42	15.0–9.4	351–138
48	13.2–8.2	272–105
54	11.0–7.3	189–83
60	9.4–6.6	138–68
66	8.2–6.0	105–56

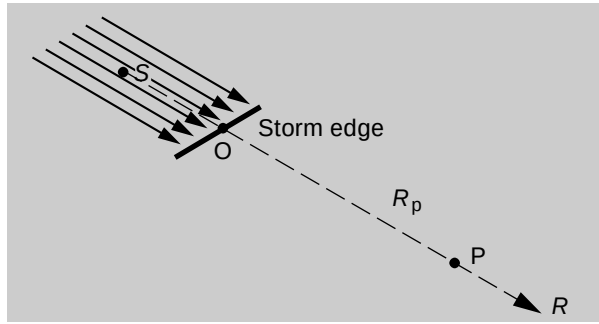

Figure 4.5 — Swell from a quasi-stationary, distant storm, in which the waves travel over a distance R_p, and the generation area has a long fetch

For point B, R_p = 1 000 n.mi.; D_p = 18 h; T_{max} = 15 s.

The first waves arrive 44 h after the beginning of the storm. Table 4.7 shows the same information as Table 4.6, but now for point B, starting at 48 h and ending at 84 h. The wave components with a period of 15 s disappear after t = 62 h.

Rather long forecast times have been given for both points to demonstrate the gradual change of wave periods. In practice, the shorter waves may not be noticeable after two to three days' travel time, and also after displacement of the storm in the case of a tropical cyclone. A cyclone does not, however, generate swell in all directions; this depends on the structure of the wind fields in the cyclone.

4.4.2 *Distant storm with long fetch*

Forecasting the waves from a distant storm with long fetch is a more complicated case, since the distance travelled by individual wave components inside the wave-generating area will generally not be the same for the various components. The longer and larger waves will generally be found in the downwind part of the storm area.

For all practical purposes, one may choose an appropriate mean value for the distance S (see Figure 4.5) and apply a corrected duration D'_p by adding to D_p the time needed by wave components to cover the distance S:

$$D'_p = D_p + \frac{S}{c_{gi}} = D_p + \frac{S}{1.515 T_1} \qquad (4.8)$$

TABLE 4.7

Same as Table 4.6 except at point B

Arrival time (h)	*Periods (s)*	*Wavelengths (m)*
48	15.0–13.8	351–297
54	15.0–12.2	351–232
60	15.0–11.0	351–184
66	13.8–10.0	297–156
72	12.2–9.2	232–132
78	11.0–8.5	189–113
84	10.0–7.9	156–97

in which c_{gi} is the group speed of the component considered. It can be shown that in this case the range of wave frequencies of the swell does not remain constant for a given point P, but increases slightly as the larger components disappear, and the spectrum consists of progressively smaller components.

Example of swell from distant storm with long fetch

Problem:

Referring to Figure 4.5, waves were generated in the direction R. The "mean" generation fetch is 180 n.mi. for waves with periods between 12 and 15 s; R_p = 600 n.mi.; D_p = 18 h. Find the wave conditions at P.

Solution:

The corrected duration for waves with T = 15 s, is D_p = 18 h + (0.660 x 180/15) = 18 h + 8 h = 26 h. This component arrives at P, 26.4 h after the storm as before, but disappears 26 h later. Likewise the corrected duration for generation of waves with T = 12 s is D_p = 27.9 h. The travel time for this component to arrive at point P is t = 0.660 x (600/12) = 33 h. The last waves with T = 12 s pass point P at t = 33 h + 27.9 h = 60.9 h.

The ranges of periods and wavelengths are reflected in Table 4.8.

Comparison of the examples in Sections 4.4.1 and 4.4.2 shows that, in the latter, the wave spectrum remains

TABLE 4.8

Ranges of swell periods and wavelengths at point P for arrival times after the beginning the storm

Arrival time (h)	*Periods (s)*	*Wavelengths (m)*
30	15.0–13.2	351–272
36	15.0–11.0	351–189
42	15.0–9.4	351–138
48	15.0–8.2	351–105
54	14.1–7.3	310–83
60	12.0–6.6	225–68
66	10.4–6.0	169–56

broader for a longer period. Because of the wide range of energetic periods, the swell will also have a less regular appearance.

4.4.3 *Swell arriving at a point of observation from a nearby storm.*

As pointed out in the introduction to Section 4.4, swell, fanning out from different points of a nearby storm edge (less than 600 n.mi.), may reach the observation point. When forecasting swell from a nearby storm, therefore, the effect of angular spreading should be considered in addition to wave dispersion.

For swell estimates:

- The sea state in the fetch area which has influence on the forecast point must be computed;
- The distance from the leading edge of the fetch area to the observation point measured;
- The period of the spectral peak, and the range of wave periods about the peak found;
- The arrival time of the swell at the forecast point determined;
- The range of periods present at different times calculated; and
- The *angular spreading factor and the wave dispersion factor* at each forecast time determined.

The angular spreading can be calculated by using the width of the fetch area and the distance from the fetch area to the forecast point in Figure 3.3 (see also Section 3.3). This factor is a percentage of the energy, so, when applied to a wave height the square root must be taken.

From the JONSWAP results, Hasselman et al. (1976) proposed a relation between sea-surface variance (wave energy) and peak frequency for a wide range of growth stages. Transforming their results into terms of H_{m0} and f_p gives

$$H_{m0} = 0.414\, f_p^{-2}\, (f_p u)^{1/3} . \qquad (4.9)$$

Equation 4.9 together with the JONSWAP spectrum (Figure 1.17) and PNJ can be used to find the wave dispersion factor at each forecast time at the forecast point. Figures 3.4(*a*) and (*b*) illustrate how the wave spectrum disperses over time. This is illustrated in the following example.

Problem:

Figure 4.6 shows the storm that produced waves which we want to forecast at Casablanca. A review of previous weather charts showed that, in the past 24 h, a cold front had been moving eastward. It travelled slowly, but with sufficient speed to prevent any waves from moving out ahead of the fetch. At chart time, the front was slowing down, and a secondary low started to develop. The forecast indicated that, as the secondary low intensified, the wind in the fetch area would change to become a cross-wind from the south. It was also expected that the front would continue its movement, but the westerly winds in the rear would decrease in strength. At chart time the well-developed sea that existed in the fetch area would no longer be sustained by the wind.

The fetch area (hatched area in Figure 4.6) was 480 n.mi. long and 300 n.mi. wide at chart time. The winds in the area were WNW. The distance to Casablanca from the leading edge of the fetch (R_c) is 600 n.mi. Determine all of the swell characteristics at Casablanca and their direction.

Solution:

During the past 24 h, the average wind speed was u = 15 m/s in the fetch area; for that wind H_c = 4.8 m, and T_c = 8.6 s. From Equation 4.1, T_p = 10.1 s, and the range of important wave periods is from 14.4 s down to 5.0 s (2 f_p to 0.7 f_p).

The first waves with a period of 14.4 s will arrive at the coast at

$$t = \frac{0.660 \text{ x } 600}{14.4} = 27.5\,\text{h}$$

after chart time. Also, the waves with a period of 14.4 s cease to arrive at the coast in

$$t = \frac{0.660 \text{ x } (480 + 600)}{14.4} = 49.5\,\text{h} .$$

Since the time to get from the rear of the fetch area for the wave components with T = 14.4 s is less than 24 h, Equations 4.5 and 4.6 are used to determine the range of frequencies at each forecast time at Casablanca. These ranges are shown in Table 4.9.

The angular spreading factor is determined from the ratio of R_c to the fetch width, i.e. 600/300 = 2. For

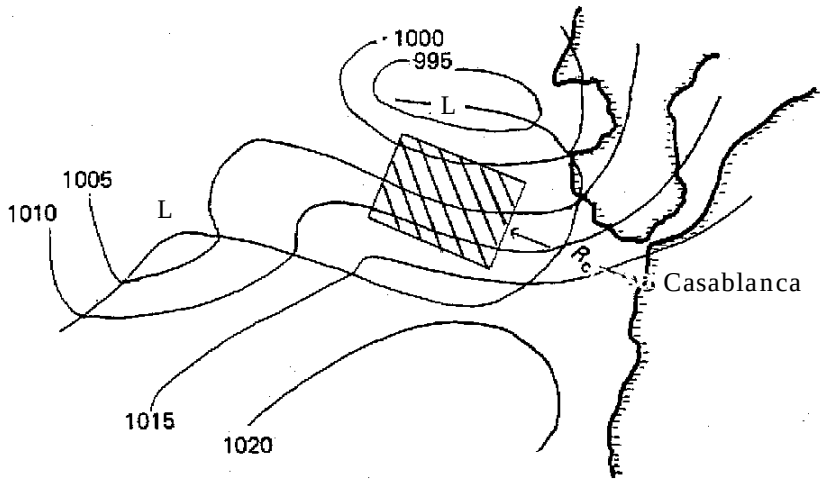

Figure 4.6 — Weather situation over the North Atlantic at t = 0

TABLE 4.9

Forecast of swell periods, wavelengths and heights at Casablanca for various times after the arrival of the longest period waves. H_c and angular spreading and dispersion multipliers are also shown

(The bracketed values in the last two columns are based on the "uniform distribution" approximation.)

Arrival time (h)	*Periods (s)*	*Wave-lengths (m)*	H_c *(m)*	*Angular spreading multiplier*	*Dispersion multiplier*		*Arriving wave heights (m)*	
30	14.4 – 13.2	323 – 272	4.8	0.55	0.35	(0.23)	0.9	(0.6)
36	14.4 – 11.0	323 – 189	4.8	0.55	0.63	(0.41)	1.7	(1.1)
42	14.4 – 9.4	323 – 138	4.8	0.55	0.75	(0.54)	2.0	(1.4)
48	14.4 – 8.2	323 – 105	4.8	0.55	0.90	(0.64)	2.4	(1.7)
54	13.2 – 7.3	272 – 83	4.8	0.55	0.84	(0.70)	2.2	(1.8)
60	11.0 – 6.6	189 – 68	4.8	0.55	0.73	(0.69)	1.9	(1.8)
66	9.4 – 6.0	138 – 56	4.8	0.55	0.62	(0.68)	1.6	(1.8)
72	8.2 – 5.5	105 – 47	4.8	0.55	0.40	(0.68)	1.1	(1.8)

this situation, the angular spreading factor is 30 per cent (from Figure 3.3). This means that the height of swell observed at the shore of Casablanca should be less than $\sqrt{0.30}$ x 4.8 or 2.6 m.

The wave dispersion factor at any given forecast time is the most difficult part of the forecast. A model spectrum must be chosen, and the mathematical integration of the frequency spectrum, $S(f)$, should be carried out for the range of frequencies at each forecast time. In this example, Equation 4.1 is used in conjunction with the JONSWAP spectrum (Figure 1.17) to determine the range of important frequencies corresponding to $f_p = 1/T_p$ = 0.099, i.e. between 0.7 f_p and 2 f_p (1/14.4 = 0.069 Hz and 1/5.04 = 0.199 Hz), and PNJ is used to determine the fraction of energy in given ranges of frequencies (dispersion factor) arriving at any given time at Casablanca.

To determine the energy values, use the distorted co-cumulative spectra for wind speeds 10–44 kn as a function of duration from PNJ (shown in Annex IV). The wind speed is 15 m/s (30 kn). Determine where the upper and lower frequencies intersect the 30 kn curve, and find the E values that intersect with those points. For f = 0.069 Hz, E = 51. For f = 0.199, E = 2.5. The difference is 48.5. To calculate the dispersion factor at 36 h, find the E values for the periods arriving at that time and divide by the total energy, i.e. (51 – 31.5)/48.5 = 0.402. Note that the PNJ curves are used only to find the proportion of energy in the given frequency ranges; for the significant wave height it is preferable to use the GD curves (Figure 4.1).

The wave height is determined by multiplying the square root of the dispersion factor (i.e. the dispersion multiplier) times the square root of the angular spreading factor (angular spreading multiplier) times H_c. For 36 hours this is $\sqrt{0.402}$ x $\sqrt{0.3}$ x 4.8 = 1.7 m.

At t = 48 h a much larger part of the wave spectrum is still present with periods shifted to lower values (wave frequencies to higher values). The dispersion factor is (51 – 12)/48.5 = 0.804, and the wave height is given by $\sqrt{0.804}$ x $\sqrt{0.3}$ x 4.8 = 2.4 m. The various wave heights computed in this way are given in Table 4.9.

A short cut: A rough approximation to the dispersion factor may be obtained by simply assuming that the fraction of the energy we are seeking is dependent only on the proportion of the frequency range we are considering, i.e. the ratio of the frequency range to the total significant frequency range. For this example, the significant frequency range is (0.199 – 0.069) = 0.13 Hz. For the first row in Table 4.9 the frequency range is (0.076 – 0.069) = 0.007 Hz, which leads to a dispersion multiplier of $\sqrt{(0.007/0.13)}$ = 0.23. The appropriate estimates have been entered in Table 4.9 in brackets.

It must be emphasised that this is a rough approximation. It assumes that the energy distribution is uniform across the frequencies, which we know to be wrong (see Figure 1.17). As the worked example in Table 4.9 shows, the errors may be acceptable if a rapid calculation is required, although they are significant. The peak of the storm will inevitably be underestimated and the decay will also characteristically be too gradual. Using these observations some subjective corrections can be developed with experience.

This example has shown the common features of swell development as a function of time: a general increase in wave height at first and, over a long period of time, a more or less constant height as the spectrum reaches its greatest width. Since factors such as internal friction and air resistance have not been taken into account, it is likely that the swell would have died out after about 60 h.

4.4.4 *Further examples*

Problem:

Assuming that swell originates from a small fetch area of hurricane winds in a tropical cyclone, wind waves have a characteristic height of 12 m over a width of

120 n.mi., estimate the swell heights in the cases described in Sections 4.4.1 and 4.4.2 with the experience gained from Section 4.4.3.

Solution 4.4.1:

In Section 4.4.1, the distance to point A is 600 n.mi., or five times the fetch width. From Figure 3.3, the angular spreading factor is about 12 per cent. Thus, the characteristic height of the swell arriving at A should be less than $\sqrt{0.12 \times 12} = 4.2$ m.

We can determine the dispersion factor from the same PNJ graph as before (see Annex IV), but we have to determine an effective wind speed since only the wave height is known. The effective wind speed is determined by following the line for a 15 s period on the PNJ graph to where it intersects the given wave height. We can determine the effective wind speed from the intersection point, in this case 21.5 m/s (43 kn). Then we determine the *E* values, and compute the dispersion factors as in Section 4.3.3. Since the swell spectrum is broadest at 42 h, the wave heights are highest at that time. The dispersion factor is about 0.8 giving a multiplier of about 0.9 which leads to a characteristic wave height of about 3.7 m when angular spreading is included in the computation.

The height is very small at first, when only long waves arrive at A. The wave heights are highest in the period between 40 h and 50 h (see Table 4.6), since the swell spectrum has its greatest width during that period.

The distance to point B equals about eight times the width of the fetch area, which leads to an angular spreading factor of about 6 per cent; therefore the swell heights at point B should be no more than 2.9 m. Considering that the wave dispersion must have progressed further from point A to point B and that the smaller components may have been dissipated on their long journey as a result of internal friction and air resistance, we can compute, from PNJ, wave dispersion factors for each arrival time. The widest part of the spectrum, with the highest heights, passes point B about 60 h after generation. The dispersion factor for this time is about 0.6, so the multiplier is about 0.8; therefore, the characteristic swell height will be about 2.3 m.

Solution 4.4.2:

In Section 4.4.2, the swell spectrum at point A is more complex. There is a range of generation wave periods from 12 to 15 s. There is also a limited fetch (180 n.mi.). The highest characteristic waves possible differ for each of these wave limits.

To determine these wave period limits, we use the distorted co-cumulative spectra for wind speeds 10–44 kn as a function of fetch from PNJ. To ascertain the maximum characteristic wave height for the 15 s waves, we trace the 15 s period line to where it intersects the 180 n.mi. fetch line and read the wave height (4.5 m = 14.8 ft). We also find an effective wind speed for these waves (13 m/s = 26 kn). Likewise we discover these values for the 12 s waves (characteristic wave height = 4.8 m = 15.8 ft, and effective wind speed = 14 m/s = 28 kn). The *E* values (energy proportions) are determined in the same way as before.

By comparing the 15 s and 12 s wave heights after the dispersion factors have been taken into account for each forecast hour, we can show that the waves arriving at 60 h have the greatest characteristic heights. Recall, the angular spreading factor at point A is 12 per cent; this means the highest characteristics possible for these conditions have a height of about 1.7 m. The dispersion factor at 60 h is about 0.82 with the multiplier being about 0.9; thus, the waves arriving at point A at 60 h can have a characteristic height of no more than 1.5 m.

4.5 Manual computation of shallow-water effects

Several kinds of shallow-water effects (shoaling, refraction, diffraction, reflection, and bottom effects) are described elsewhere in this *Guide*. In this section, a few practical methods are described which have been taken from CERC (1977) and Gröen and Dorrestein (1976). In absolute terms, a useful rule of thumb is to disregard the effects of depth greater than about 40 m unless the waves are very long, i.e. if a large portion of the wave energy is in waves with periods greater than 10 s. Distinction is made between:

(*a*) Swell originating from deep water entering a shallow area with variable depth; and

(*b*) Wind waves with limited wave growth in shallow water with constant depth.

More complicated cases with combinations of (*a*) and (*b*) will generally require the use of numerical models.

Section 4.5.1 deals with shoaling and refraction of swell whose steepness is sufficiently small to avoid wave breaking after shoaling and focusing due to refraction. In Section 4.5.2 a diagram is presented for estimating wave heights and periods in water with constant depth.

4.5.1 *Shoaling and refraction of swell in a coastal zone*

In this section, wave decay due to dissipation by bottom friction and wave breaking is neglected. Shoaling and refraction generally occur simultaneously; however, they will be considered separately.

4.5.1.1 *Variation in wave height due to shoaling*

To obtain the shoaling factor, K_s, which represents the change of wave height (H) due to decreasing depth (without refraction), we need to consider the basic rule that energy flux must be conserved. Since energy is related to the square of the wave height (Sections 1.2.4 and 1.3.8) and wave energy travels at the group velocity,

the energy flux is $c_g H^2$. This is a constant. Hence the shoaling factor depends on the ratio between the deep-water group velocity c_{g0} and the group velocity c_g at depth h, and is given by:

$$K_s = \frac{H}{H_0} = \sqrt{\frac{c_{g0}}{c_g}} = \sqrt{\frac{1}{2}\frac{c_0}{c_g}}\,, \qquad (4.10)$$

where c_0 is the phase velocity in deep water ($\sqrt{g/k_0}$), k_0 is the wavenumber in deep water and H_0 is the wave height in deep water. Since the group velocity c_g is given by:

$$c_g = \beta \sqrt{\frac{g}{k}\tanh kh}\,,\ \beta = \frac{1}{2}\left(1 + \frac{2kh}{\sinh 2kh}\right),$$

the shoaling factor can also be expressed as:

$$K_s = 2\beta \sqrt{\tanh kh}^{\,-1/2}\,. \qquad (4.11)$$

The wavenumber $k = 2\pi/\lambda$ at depth h can be approximated as follows:

$$k = k_0 (\tanh kh)^{-1},$$

$$k = k_0 [\tanh (k_0\ h \tanh kh)^{-1}]^{-1} \approx k_0 (\tanh k_0 h)^{-1}\,. \qquad (4.12)$$

Figure 4.7(*a*) shows various curves involved in the transformation of properties of a wave propagating from deep to shallow water. The shoaling factor, K_s, is also shown in this figure. But for the convenience of the user interested in obtaining only the shoaling factor K_s associated with a deep water wave of a given wave-number k_0 (= $2\pi/\lambda_0$), the curve of K_s vs h/λ_0 is presented in Figure 4.7(*b*) in an expanded scale.

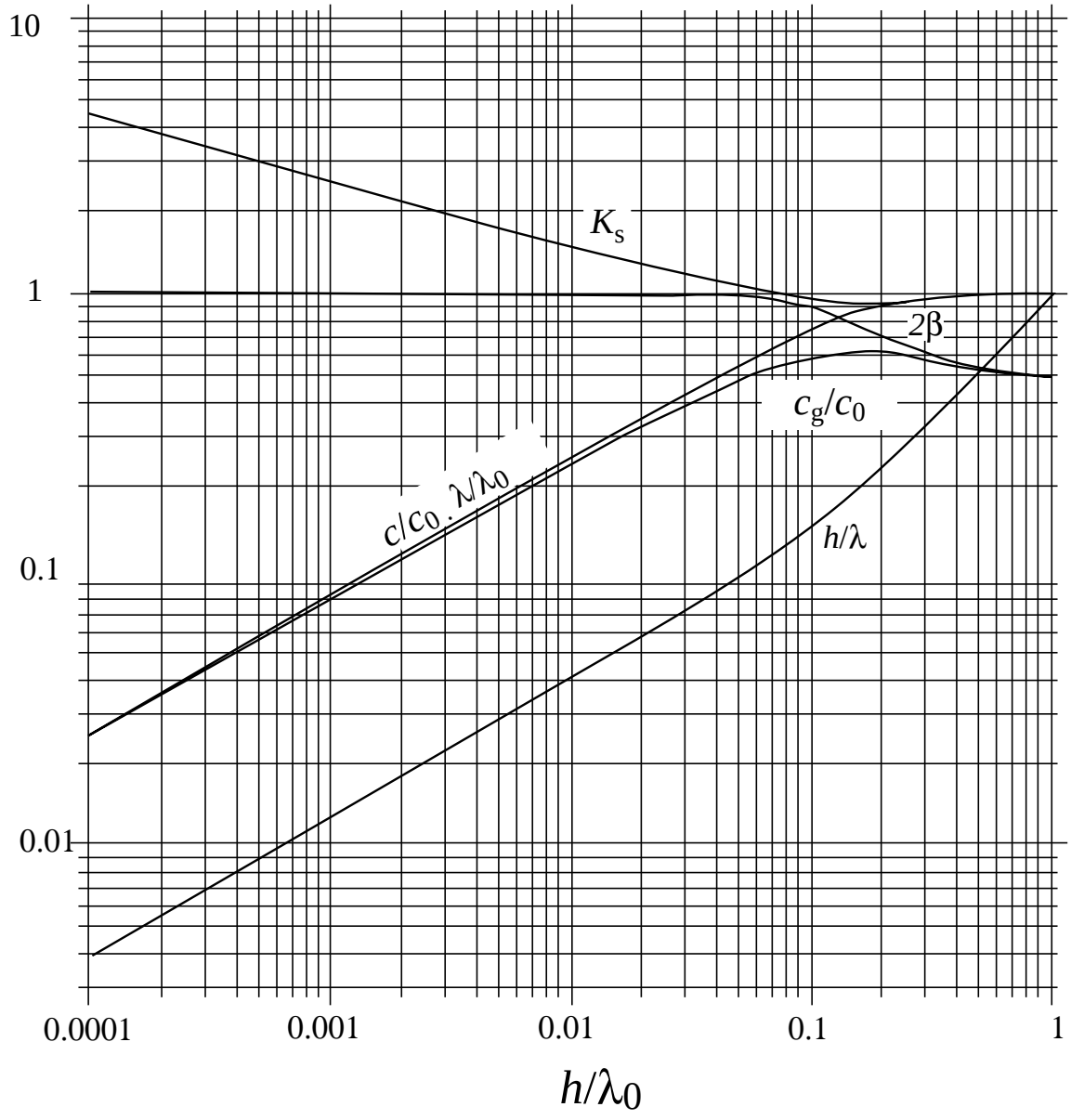

Figure 4.7(*a*) — Illustration of various functions of h/λ_0 (*derived from CERC, 1984*)

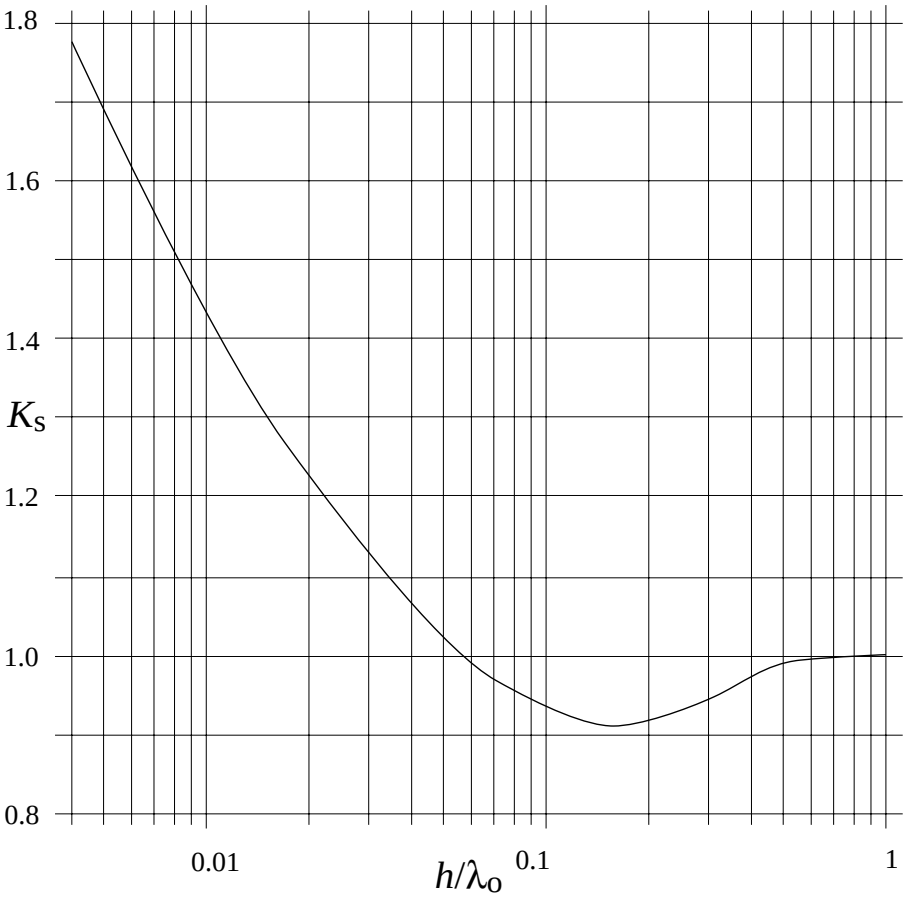

Figure 4.7(*b*) — A graph of shoaling factor K_s versus h/λ_0 (*derived from CERC, 1984*)

Example:

For a deep water wavelength $\lambda_0 = 156$ m and $T_0 = 10$ s, then $k_0 = 0.04$ m^{-1}, and for $T_0 = 15$ s, $k_0 = 0.018$ m^{-1}.

Table 4.10 shows the shoaling factor K_s for a number of shallow depths. It also shows that the height of shoaling waves is reduced at first, but finally increases up to the point of breaking which also depends on the initial wave height in deep water (see also Figures 4.7(*a*) and (*b*)).

4.5.1.2 *Variation of wave height due to refraction*

In the previous example, no refraction was taken into account, which implies propagation of waves perpendicular to parallel bottom depth contours. In natural conditions this will rarely occur. So the angle of incidence with respect to the bottom depth contours usually differs from 90°, which is equivalent to α, the angle between a wave crest and the local isobath, being different from 0°. This leads to variation of the width between wave rays. Using Snell's law,

$$\frac{H}{H_0} = \sqrt{\frac{c_{g0}}{c_g}} \sqrt{\frac{\cos \alpha_0}{\cos \alpha}} .$$

The refraction factor is:

$$K_r = \sqrt{\frac{\cos \alpha_0}{\cos \alpha}} \qquad (4.13)$$

with α_0 the angle between a wave crest and a local isobath in deep water. Figure 4.8, taken from CERC (1984), is based on Equation 4.13. For a given depth and wave period the shallow-water angle of incidence (solid lines) and the refraction factor (broken lines) can be read off easily for a given deep-water angle of incidence α_0. It is valid for straight parallel depth contours only.

Problem:

Given an angle $\alpha_0 = 40°$ between the wave crests in deep water and the depth contours of the sloping bottom, find α and the refraction at $h = 8$ m for $T = 10$ s.

TABLE 4.10

Wavenumber k and shoaling factor K_s for two wave periods, at several depths, h, in metres, using Equations 4.11 and 4.12

h (m)	$T = 10$ s, $k_0 = 0.04$ m^{-1}		$T = 15$ s, $k_0 = 0.018$ m^{-1}	
	k (m^{-1})	K_s	k (m^{-1})	K_s
100	0.040	1.00	0.018	0.94
50	0.041	0.95	0.021	0.92
25	0.046	0.91	0.028	0.98
15	0.055	0.94	0.035	1.06
10	0.065	1.00	0.043	1.15
5	0.090	1.12	0.060	1.33
2	0.142	1.36	0.095	1.64

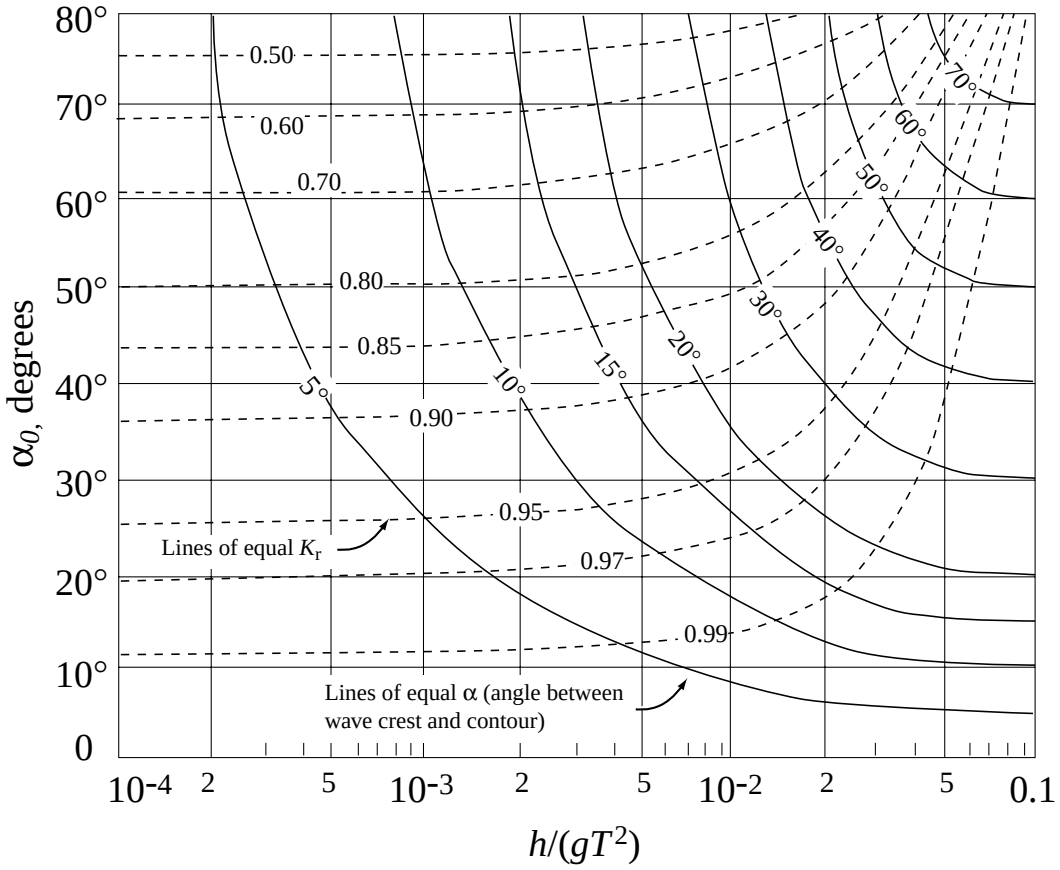

Figure 4.8 — Changes in wave direction and height due to refraction on slopes with straight parallel bottom contours. α_0 is the deep water angle of incidence, measured between the wave crest and the local isobath. The continuous curves are lines of equal incidence for various combinations of period and depth. To estimate the refraction as a wave moves into shallower water, starting from a given α_0 follow a horizontal line from right (deep water) to left. The broken lines are lines of equal refraction factor, K_r (*derived from CERC, 1977*)

Solution:

$h/(gT^2)$ = 8/(9.8 x 100) = 0.0082, and from Figure 4.8 the refraction factor is 0.905, and α = 20°.

4.5.1.3 *Dorrestein's method*

Due to the fact that in reality the bottom depth contours rarely are straight, we generally find sequences of convergence and divergence (see also Section 1.2.6 and Section 7.3). Dorrestein (1960) devised a method for manually determining refraction where bottom contours are not straight. This method requires the construction of a few wave rays from a given point P in shallow water to deep water, including all wave directions that must be taken into account according to a given directional distribution in deep water.

We assume that, in deep water, the angular distribution of wave energy is approximately a uniform distribution in the azimuthal range α'_1 and α'_2. These angles correspond, respectively, to the angles of incidence α_1 and α_2 at point P. Rays must at least be constructed for waves at these outer limits of the distribution. It may be sufficient to assume straight isobaths and use Figure 4.8 to calculate these angles. Then, according to Dorrestein, the refraction factor is:

$$K_r = \sqrt{\frac{c_0}{c} \cdot \frac{\alpha_1 - \alpha_2}{\alpha'_1 - \alpha'_2}} \qquad (4.14)$$

with c_0 and c the phase velocities in deep water and at point P, respectively.

Problem:

As in the example in Section 4.5.1.2, h = 8 m at point P. T = 10 s, so $h/(gT^2)$ = 0.0082. With the help of Figure 4.8, α = 20° for α_0 = 40°. Find K_r by Dorrestein's method.

Solution:

Snell's law gives:

$$\frac{c_0}{c} = \frac{\sin \alpha_0}{\sin \alpha} = \frac{\sin 40°}{\sin 20°} = 1.88 .$$

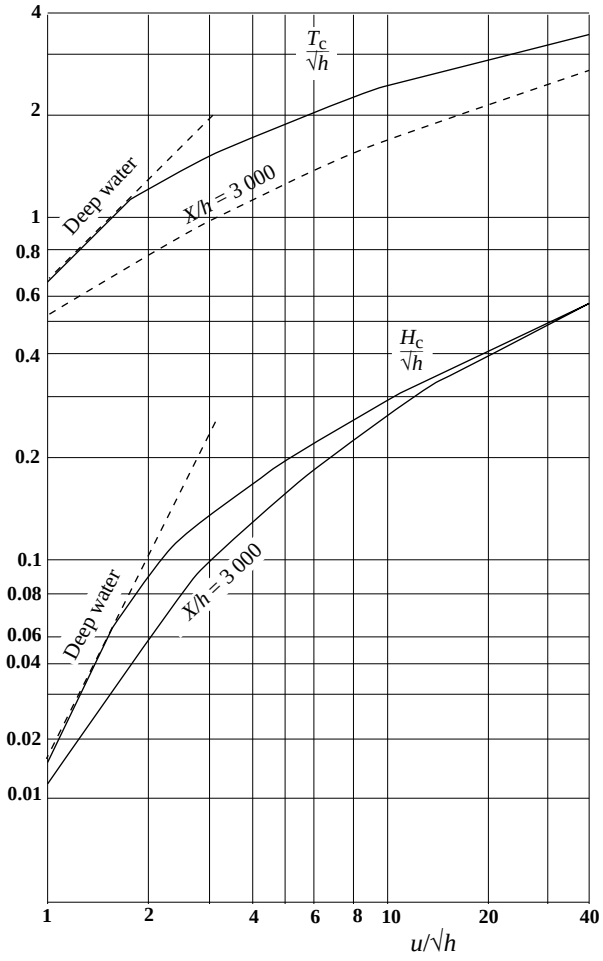

Figure 4.9 — Diagram to estimate characteristic wave heights and period of wind waves in shallow water of constant depth. Solid lines indicate limiting values for sufficiently long fetches. Broken lines indicate conditions with relatively short fetches, specified by X/h = 3 000 (*from Gröen and Dorrestein, 1976*)

In general it is prudent to use a small window $\Delta\alpha = \alpha_1 - \alpha_2$ centered around α (= 20° in this case) in applying the ideal linearly sloping bottom results to obtain the answers to a real case of bottom topography. If we take α_1 = 21° and α_2 = 19°, we find from Figure 4.8, $\alpha_1 \approx 42°$ and $\alpha_2 \approx 37.5°$. Then, Equation 4.14 gives K_r = 0.904.

In general the results for K_r are sensitive to the choice of the spread between α_1 and α_2 (or α'_1 and α'_2).

4.5.2 *Wind waves in shallow water*

In shallow water the bottom topography and composition has a dissipating effect on waves. Here we present a simple manual method for prediction of the characteristic wave height, H_c, and the associated wave period in shallow water with constant depth. To that end, we use Figure 4.9, taken from Gröen and Dorrestein (1976), based on the same deep-water growth curve, but with additional terms for taking the limitation of wave growth by the bottom into account. These are similar to the shallow-water growth curves of CERC (1984), but with somewhat different coefficients.

As in the previous sections of this chapter, we assume that H_c is approximately equal to the significant wave height $\bar{H}_{1/3}$ or H_{m0}, and T_c is approximately equal to the significant wave period $\bar{T}_{H_{1/3}}$ or T_p (see Chapter 1). For the sake of compactness, only ratios are shown: H_c/h and $T_c/\sqrt{h}$, both as a function of $u/\sqrt{h}$. u denotes wind speed at standard level (usually 10 m above water) in m/s. Wave height, H_c, and depth, h, are expressed in m, and wave period, T_c, in s. The solid curves show H_c/h and $T_c/\sqrt{h}$ for sufficiently long fetches, e.g. a X/h ratio much greater than 3 000. Then a sort of balance between wind input and bottom dissipation can be assumed. The effect of limited fetch is shown for X/h = 3 000.

Problem:

Find H_c and T_c for u = 20 m/s, h = 10 m and X = 200 km and 30 km.

Solution:

$u/\sqrt{h} = 20/\sqrt{10} = 6.3$. For X = 200 km, X/h = 200 000/10 = 20 000. From Figure 4.9, we use the solid curves, and H_c/h = 0.23, while $T_c/\sqrt{h}$ = 2.1, or H_c = 0.23 m x 10 = 2.3 m is the maximum characteristic height for the given u and h, and $T_c = 2.1\sqrt{10} = 6.6$ s.

For X = 30 km, X/h = 3 000. Using the curves for X/h = 3 000 in Figure 4.9, H_c/h = 0.2, $T_c/\sqrt{h}$ = 1.5, or H_c = 0.2 x 10 = 2 m, and $T_c = 1.5\sqrt{10} = 4.7$ s.

CHAPTER 5

INTRODUCTION TO NUMERICAL WAVE MODELLING

M. Reistad with A.K. Magnusson: editors

5.1 Introduction

National Meteorological Services in maritime countries have experienced a rapidly growing need for wave forecasts and for wave climatology. In particular the offshore oil industry needs wave data for many purposes: design sea states, fatigue analysis, operational planning and marine operations. Furthermore, consulting companies operating in the maritime sector have an increasing need for wave information in their projects.

To meet this growing requirement for wave information, wave conditions must be estimated over large tracts of ocean at regular intervals, often many times a day. The volume of data and calculations makes computers indispensable. Furthermore, measured wave data are often sparse and not available when and where they are desired. Using wind information and by application of the basic physical principles that are described in Chapter 3, numerical models have been developed to make the required estimates of wave conditions.

In wave modelling, we attempt to organize our theoretical and observational knowledge about waves into a form which can be of practical use to the forecaster, engineer, mariner, or the general public. The most important input to the wave models is the wind at the sea surface and the accuracy of the wave model output is strongly dependent on the quality of the input wind fields. Chapter 2 is devoted to the specification of marine winds.

In the WMO *Handbook on wave analysis and forecasting* (1976), one particular model was described in detail to exemplify the structure and methodology of numerical wave models. Since then new classes of models have appeared and were described in the WMO *Guide to wave analysis and forecasting* (1988). Rather than giving details of one or a few particular models, this chapter will give general descriptions of the three model classes that were defined in the SWAMP project (SWAMP Group, l985). A short description of the "third generation" WAM model developed by an international group of wave modellers is added.

The basic theory of wave physics was introduced in Chapter 3. In this chapter, Section 5.2 gives a brief introduction to the basic concepts of wave modelling. Section 5.3 discusses the wave energy-balance equation. Section 5.4 contains a brief description of some elements of wave modelling. Section 5.5 defines and discusses the most important aspects of the model classes. The practical applications and operational aspects of the numerical wave models are discussed in Chapter 6.

5.2 Basic concepts

The mathematical description of surface waves has a large random element which requires a statistical description. The statistical parameters representing the wave field characterize conditions over a certain time period and spatial extent. Formally, over these scales, we need to assume stationarity (steadiness in time) and spatial homogeneity of the process describing the sea surface. Obviously, no such conditions will hold over the larger scales that characterize wave growth and decay. To model changing waves effectively, these scales (time-step or grid length) must be small enough to resolve the wave evolution, but it must be recognized that in time or space there are always going to be smaller scale events which have to be overlooked.

The most used descriptor of the wave field is the energy-density spectrum in both frequency and direction $E(f,\theta)$, where f is the frequency, and θ the direction of propagation (see Section 1.3.7). This representation is particularly useful because we already know how to interpret what we know about wave physics in terms of the spectral components, $E(f,\theta)$. Each component can be regarded as a sinusoidal wave of which we have a reasonably well-understood theory. From this spectrum, we can deduce most of the parameters expected of an operational wave model, namely: the significant wave height, the frequency spectrum, the peak frequency and secondary frequency maxima, the directional spectrum, the primary wave direction, any secondary wave directions, the zero-crossing period, etc. (see Chapter 1).

Not all models use this representation. Simpler models may be built around direct estimation of the significant wave height, or on the frequency spectrum, with directional characteristics often diagnosed directly from the wind.

There is a reasonable conception of the physical processes which are thought to control wave fields. To be of general use in wave modelling, these processes are described by the response of wave ensembles, i.e. they are translated into terms of useful statistical quantities such as the wave spectrum. Not all the processes are yet fully understood and empirical results are used to varying degrees within wave models. Such representations allow a certain amount of "tuning" of wave models, i.e. model performance can be adjusted by altering empirical constants.

Although models for different purposes may differ slightly, the general format is the same (see Figure 5.1 for a schematic representation).

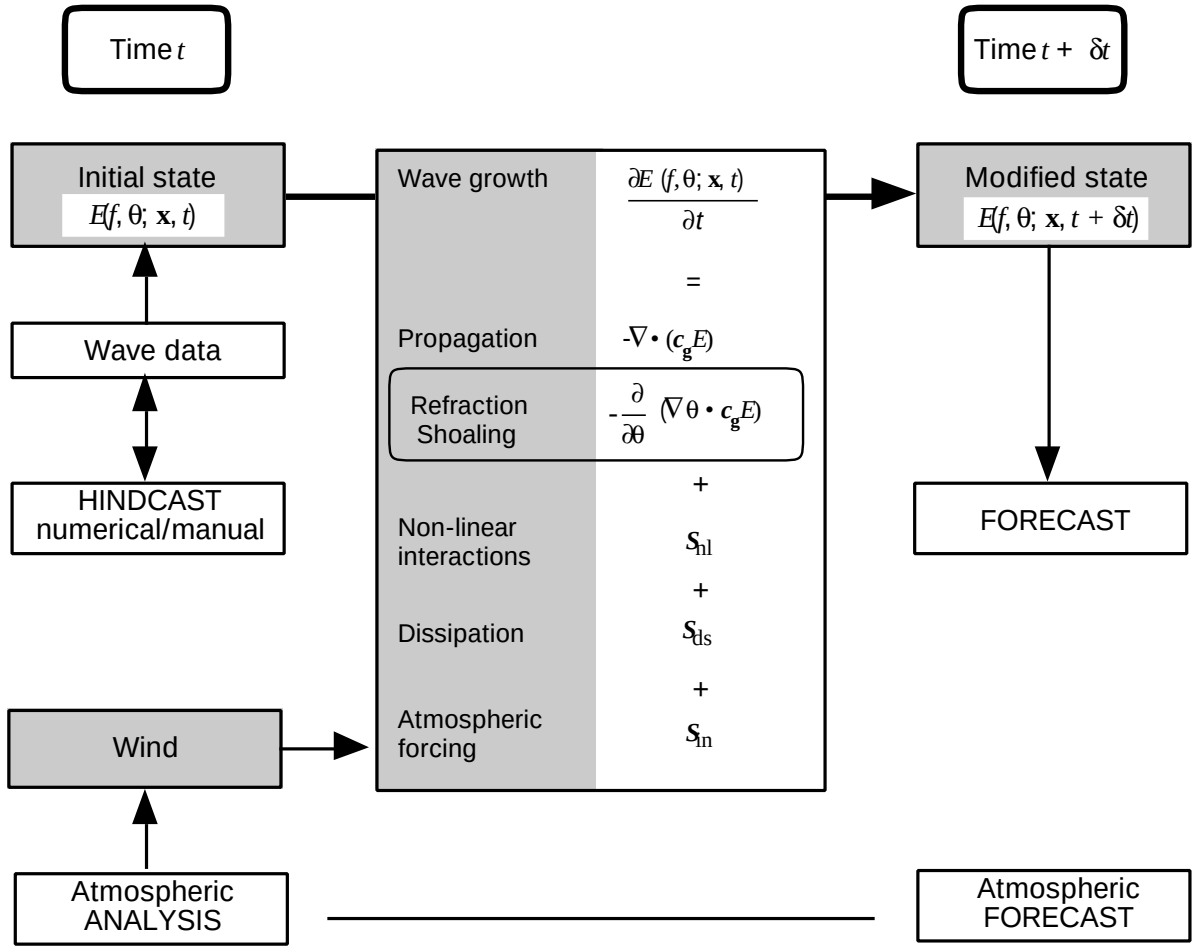

Figure 5.1 — The elements of wave modelling

5.3 The wave energy-balance equation

The concepts described in Chapter 3 are represented in wave models in a variety of ways. The most general formulation for computer models based on the elements in Figure 5.1 involves the spectral energy-balance equation which describes the development of the surface gravity wave field in time and space:

$$\frac{\partial E}{\partial t} + \nabla \bullet \left(\boldsymbol{c}_g E \right) = S = S_{in} + S_{nl} + S_{ds} \qquad (5.1)$$

where:

$E = E(f,\theta,\boldsymbol{x},t)$ is the two-dimensional wave spectrum (surface variance spectrum) depending on frequency, f, and direction of propagation, θ;

$\boldsymbol{c}_g = \boldsymbol{c}_g(f,\theta)$ is the deep-water group velocity;

S is the net source function, consisting of three terms:

- S_{in}: energy input by the wind;
- S_{nl}: non-linear energy transfer by wave-wave interactions; and
- S_{ds}: dissipation.

This form of the equation is valid for deep water with no refraction and no significant currents.

5.4 Elements of wave modelling

The essence of wave modelling is to solve the energy-balance equation written down in Equation 5.1. This first requires the definition of starting values for the wave energy, or initial conditions which in turn requires definition of the source terms on the right hand side of Equation 5.1 and a method for solving changes as time progresses.

5.4.1 *Initial conditions*

It is rare that we have a flat sea to work from, or that we have measurements which completely characterize the sea state at any one time.

For computer models, the usual course of action is to start from a flat sea and “spin up” the model with the winds from a period of several days prior to the period of interest. We then have a hindcast derived for the initial time. For operational models this has to be done

only once, since it is usual to store this hindcast and progressively update it as part of each model run.

In some ocean areas in the northern hemisphere, there is sufficient density of observations to make a direct field analysis of the parameters observed (such as significant wave height or period). Most of the available data are those provided visually from ships; these data are of variable quality (see Chapter 8). Such fields are not wholly satisfactory for the initialization of computer models. Most computer models use spectral representations of the wave field, and it is difficult to reconstruct a full spectral distribution from a height, period and direction. However, the possibility of good quality wave data from satellite-borne sensors with good ocean coverage, has prompted attempts to find methods of assimilating these data into wave models. The first tested methods have been those using significant wave heights measured by radar altimeters on the GEOSAT and ERS-1 satellites. It has been shown that a positive impact on the wave model results can be achieved by assimilating these data into the wave models (e.g. see Lionello et al., 1992, and Breivik and Reistad, 1992). Methods to assimilate spectral information, e.g. wave spectra derived from SAR (Synthetic Aperture Radar) images, are also under development. More details on wave data assimilation projects are given in Section 8.6.

5.4.2 *Wind*

Perhaps the most important element in wave modelling is the motion of the atmosphere above the sea surface. The only input of energy to the sea surface over the time-scales we are considering comes from the wind. Transfer of energy to the wave field is achieved through the surface stress applied by the wind, which varies roughly as the square of the wind speed. Thus, an error in wind specification can lead to a large error in the wave energy and subsequently in parameters such as significant wave height.

The atmosphere has a complex interaction with the wave field, with mean and gust wind speeds, wind profile, atmospheric stability, influence of the waves themselves on the atmospheric boundary layer, etc., all needing consideration. In Chapter 2, the specification of the winds required for wave modelling is discussed.

For a computer model, a wind history or prognosis is given by supplying the wind field at a series of time-steps from an atmospheric model. This takes care of the problem of wind duration. Similarly, considerations of fetch are taken care of both by the wind field specification and by the boundary configuration used in the propagation scheme. The forecaster using manual methods must make his own assessment of fetch and duration.

5.4.3 *Input and dissipation*

The atmospheric boundary layer is not completely independent of the wave field. In fact, the input to the wave field is dominated by a feedback mechanism which depends on the energy in the wave field. The rate at which energy is fed into the wave field is designated by S_{in}.

This wind input term, S_{in}, is generally accepted as having the form:

$$S_{in} = A(f,\theta) + B(f,\theta)\, E(f,\theta) \qquad (5.2)$$

$A(f,\theta)$ is the resonant interaction between waves and turbulent pressure patterns in the air suggested by Phillips (1957), whereas the second term on the right-hand side represents the feedback between growing waves and induced turbulent pressure patterns as suggested by Miles (1957). In most applications, the Miles-type term rapidly exceeds the Phillips-type term.

According to Snyder et al. (1981), the Miles term has the form:

$$B(f,\theta) = \max\left[0, \mathrm{K}_1 \frac{\rho_a}{\rho_w}\left(\mathrm{K}_2 \frac{U_5}{g} f \cos(\theta-\psi) - 1\right) 2\pi f\right] \qquad (5.3)$$

where ρ_a and ρ_w are the densities of air and water, respectively; K_1 and K_2 are constants; ψ is the direction of the wind; and U_5 is the wind speed at 5 m (see also Section 3.2).

Equation 5.3 may be redefined in terms of the friction speed $u_* = \sqrt{(\tau/\rho_a)}$, where τ is the magnitude of the wind shear stress. From a physical point of view, scaling wave growth to u_* would be preferable to scaling with wind speed U_z at level z. Komen et al. (1984) have approximated such a scaling, as illustrated in Equation 3.1, however, lack of wind stress data has precluded rigorous attempts. U_z and u_* do not appear to be linearly related and the drag coefficient, C_d, used to determine τ ($\tau = \rho_a C_d U_z^2$), appears to be an increasing function of U_z (e.g. Wu, l982; Large and Pond, 1981). The scaling is an important part of wave modelling but far from resolved. Note that C_d also depends on z (from U_z) (see for example Equation 2.14). Recent advances with a quasi-linear theory which includes the effects of growing waves on the mean air flow have enabled further refinement of the formulation (Janssen, 1991; Jenkins, 1992; Komen et al., 1994).

Note also that in the case of a fully developed sea, as given by the Pierson-Moskowitz spectrum E_{PM} (see Equation 1.28), it is generally accepted that the dimensionless energy, ε,

$$\varepsilon = \frac{g^2 \int E_{PM}(f)\, df}{u_*^4} = \frac{g^2 E_{total}}{u_*^4}$$

is a universal constant. However, if ε is scaled in terms of U_{10} this saturation limit will vary significantly with wind speed since C_d is a function of U_{10}. Neither Equation 5.3 nor the dependence of C_d on U_z are well documented in strong wind.

The term S_{ds} describes the rate at which energy is lost from the wave field. In deep water, this is mainly through wave breaking (whitecapping). In shallow water

it may also be dissipated through interaction with the sea-bed (bottom friction). More details are given in Sections 3.4 and 7.6.

5.4.4 *Non-linear interactions*

Generally speaking, any strong non-linearities in the wave field and its evolution are accounted for in the dissipation terms. Input and dissipation terms can be regarded as complementary to those linear and weakly non-linear aspects of the wave field which we are able to describe dynamically. Into this category fall the propagation of surface waves and the redistribution of energy within the wave spectrum due to weak, non-linear interactions between wave components, which is designated as a source term, S_{nl}. The non-linear interactions are discussed in Section 3.5.

The effect of the term, S_{nl}, is briefly as follows: in the dominant region of the spectrum near the peak, the wind input is greater than the dissipation. The excess energy is transferred by the non-linear interactions towards higher and lower frequencies. At the higher frequencies the energy is dissipated, whereas the transfer to lower frequencies leads to growth of new wave components on the forward (left) side of the spectrum. This results in migration of the spectral peak towards lower frequencies. The non-linear wave-wave interactions preserve the spectral shape and can be calculated exactly.

The source term S_{nl} can be handled exactly but the requirement on computing power is great. In third generation models, the non-linear interactions between wave components are indeed computed explicitly by use of special integration techniques and with the aid of simplifications introduced by Hasselmann and Hasselmann (1985) and Hasselmann et al. (1985). Even with these simplifications powerful computers are required to produce real-time wave forecasts. Therefore many second generation models are still in operational use. In second generation numerical wave models, the non-linear interaction is parameterized or treated in a simplified way. This may give rise to significant differences between models. A simplified illustration of the three source terms in relation to the wave spectrum is shown in Figure 3.7.

5.4.5 *Propagation*

Wave energy propagates not at the velocity of the waves or wave crests (which is the phase velocity: the speed at which the phase is constant) but at the group velocity (see Section 1.3.2). In wave modelling we are dealing with descriptors such as the energy density and so it is the group velocity which is important.

The propagative effects of water waves are quantified by noting that the local rate of change of energy is equal to the net rate of flow of energy to or from that locality, i.e. the divergence of energy-density flux. The practical problem encountered in computer modelling is to find a numerical scheme for calculating this. In manual models, propagation is only considered outside the generation area and attention is focused on the dispersion and spreading of waves as they propagate.

Propagation affects the growth of waves through the balance between energy leaving a locality and that entering it. In a numerical model it is the propagation of wave energy which enables fetch-limited growth to be modelled. Energy levels over land are zero and so downwind of a coast there is no upstream input of wave energy. Hence energy input from the atmosphere is propagated away, keeping total energy levels near the coast low.

Discrete-grid methods

The energy balance, Equation 5.1, is often solved numerically using finite difference schemes on a discrete grid as exemplified in Figure 5.2. $\Delta \boldsymbol{x}_i$ (i = 1, 2) is the grid spacing in the two horizontal directions. Equation 5.1 may take such a form as:

$$E(\boldsymbol{x}, t+\Delta t) = E(\boldsymbol{x}, t) - \Delta t \sum_{i=1}^{2} \left[\frac{\left(c_{g_i} E\right)_{x_i} - \left(c_{g_i} E\right)_{x_i - \Delta x_i}}{\Delta x_i} \right] + \Delta t\, S(\boldsymbol{x}, t) \quad (5.4)$$

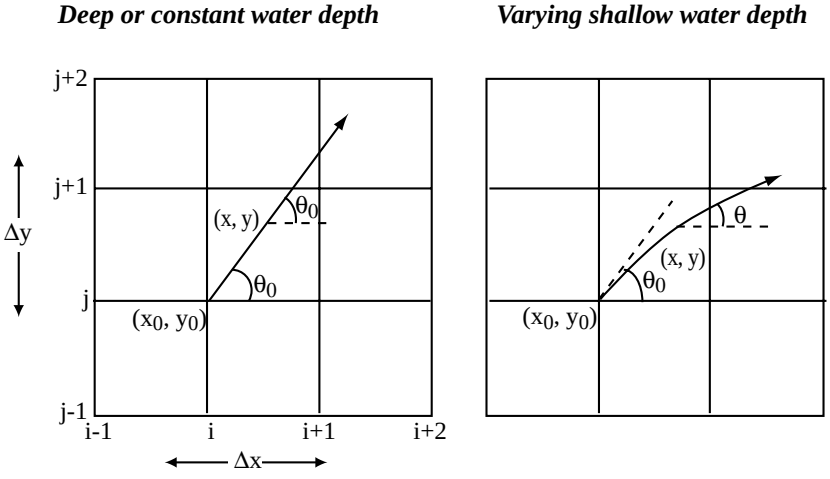

Figure 5.2 — Typical grid for numerical wave models ($\boldsymbol{x}$ stands for $\boldsymbol{x}_1$ and $\boldsymbol{y}$ for $\boldsymbol{x}_2$). In grid-type models the energy in (f,θ) bins is propagated between points according to an equation like Equation 5.4. In ray models the energy is followed along characteristic lines

Frequency	Period	Distance travelled in km	Length of disturbance in km
0.050	20	3630	556
0.067	15	2722	232
0.083	12	2185	333
0.100	10	1815	278
0.167	6	1092	167

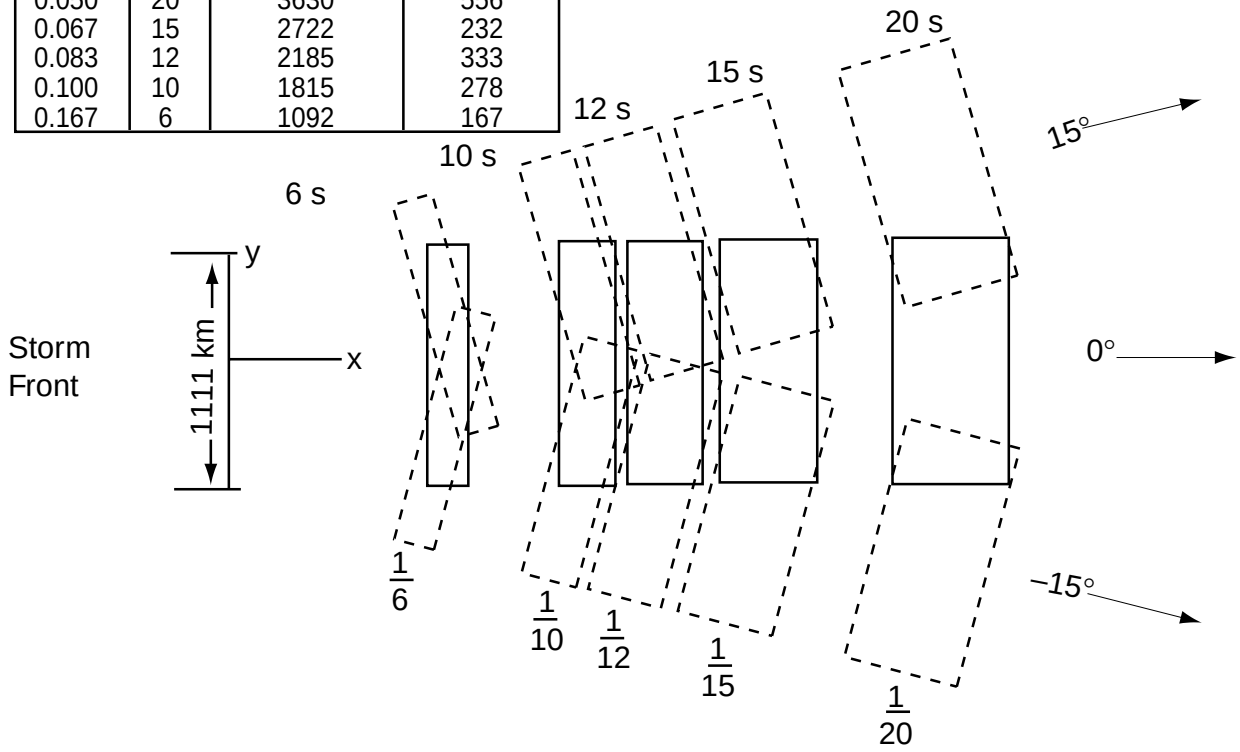

Figure 5.3 — Propagation of discrete spectral components from a storm front. This illustrates the effects of angular spreading and dispersion on the wave energy. The "garden sprinkler" effect resulting from the discretization of the spectrum can be seen

where Δt is the time-step; E and S are functions of wavenumber ($\boldsymbol{k}$), or frequency and direction (f,θ).

Using the spectral representation $E = E(f,\theta)$, we have energy density as an array of frequency direction bins (f,θ). The above approach collects a continuum of wave components travelling at slightly different group velocities into a single frequency bin, i.e. it uses a single frequency and direction to characterize each component. Due to the dispersive character of ocean waves, the area of a bin containing components within (Δf, $\Delta\theta$) should increase with time as the waves propagate away from the origin; the wave energy in this bin will spread out over an arc of width $\Delta\theta$ and stretch out depending on the range of group velocities. In the finite difference approach, all components propagate at the mean group velocity of the bin, so that eventually the components separate as they propagate across the model's ocean. This is called the "sprinkler" effect as it resembles the pattern of droplets from a garden sprinkler. It should be stressed that this is only an artifice of the method of modelling. All discrete-grid models in the inventory suffer from the sprinkler effect (see Figure 5.3), although usually the smoothing effect of continual generation diminishes the potential ill effects, or it is smoothed over as a result of numerical error (numerical diffusion).

There are many finite difference schemes in use: from first-order schemes, which use only adjacent grid points to work out the energy gradient, to fourth-order schemes, which use five consecutive points. The choice of time-step, Δt, depends on the grid spacing, $\Delta \boldsymbol{x}$, as for numerical stability the distance moved in a time-step must be less than one grid space. Typically models use from 20–200 km grid spacings and time-steps of several minutes to several hours.

The discrete-grid models calculate the complete (f,θ) spectrum at all sea points of the grid at each time-step.

Ray tracing methods

An alternative method is to solve the energy balance (Equation 5.1) along characteristics or rays. The time integration is still performed by finite-differencing but the spatial integration is not needed and the sprinkler effect is avoided. However, the number of output points is usually reduced for reasons of computational costs.

For ocean waves there is a dispersion relation, relating the wave frequency to the wavenumber (see Equations 1.3 and 1.3a), of the form:

$$f(\boldsymbol{x},t) = \sigma\left[\boldsymbol{k}(\boldsymbol{x},t),\Psi(\boldsymbol{x},t)\right]. \qquad (5.5)$$

Here, σ is used to denote the particular frequency associated with wavenumber, $\boldsymbol{k}$, and the property of the medium, Ψ, which in this context will be the bottom depth and/or currents. Characteristic curves are then obtained by integration of

$$\frac{\mathrm{d}\boldsymbol{x}}{\mathrm{d}t} = \boldsymbol{c}_{\mathrm{g}} = \frac{\delta\sigma}{\delta\boldsymbol{k}} \qquad (5.6)$$

and in an ocean with steady currents these curves need only be obtained once. Examples including refraction due to bottom topography are shown in Figures 5.2 and 7.1. For more details on ray theory see LeBlond and Mysak (1978).

Thus, starting from the required point of interest, rays or characteristics are calculated to the boundary of the area considered necessary to obtain reliable wave energy at the selected point. Since we are considering the history of a particular wave frequency, our reference frame moves with the component and all we need consider is the source function along the rays, i.e.

$$\frac{\delta E}{\delta t} = S. \qquad (5.7)$$

Rays are calculated according to the required directional resolution at the point of interest; along each ray, Equation 5.7 may be solved either for each frequency separately or for the total energy. In the former approach S_{nl} is not considered at all. In the latter case interactions in frequency domain are included but the directions are uncoupled.

The ray approach has been extensively used in models where wind sea and swell are treated separately. In such cases, swell is propagated along the rays subjected only to frictional damping and geometric spread. Interactions with the wind sea may take place where the peak frequency of the Pierson-Moskowitz spectrum ($\approx 0.13g/U_{10}$) is less than the swell frequency.

5.4.6 *Directional relaxation and wind-sea/swell interaction*

Many of the differences between numerical wave models result from the way in which they cater for the weakly non-linear wave-wave interactions (S_{nl}). The differences are particularly noticeable in the case of non-homogeneous and/or non-stationary wind fields. When the wind direction changes, existing wind sea becomes partly swell and a new wind sea develops. The time evolution of these components results in a relaxation of the wave field towards a new steady state that eventually approaches a fully developed sea in the new wind direction.

Three mechanisms contribute to the directional relaxation:

(*a*) Energy input by the wind to the new wind sea;
(*b*) Attenuation of the swell; and
(*c*) Weak non-linear interactions, resulting in energy transfer from swell to wind sea.

The way these mechanisms are modelled may yield significant deviations between models. The third mechanism appears to be dominant in this respect.

5.4.7 *Depth*

Water depth can considerably affect the properties of waves and how we model them. We know that waves feel the sea-bed and are changed significantly by it at depths less than about one-quarter of the deep-water wavelength (see also Section 1.2.5). In a sea with a wide spectrum, the longer waves may be influenced by the depth without much effect on the short waves.

One major effect of depth is on the propagation characteristics. Waves are slowed down and, if the sea-bed is not flat, may be refracted. Also, the non-linear interactions tend to be enhanced and, of course, there are more dissipative processes involved through interaction with the sea-bed. The framework we are describing for wave modelling is broad enough in its concept to be able to cope with depth-related effects without drastic alterations to the form of the model outlined in Figure 5.1. In Chapter 7 the effect of shallow water will be discussed in more detail.

5.4.8 *Effects of boundaries, coastlines and islands*

With the exception of global models, most existing wave models have an open ocean boundary. Wave energy may then enter the modelled area. The best solution is to obtain boundary data from a model operating over a larger area, e.g. a global model. If there is no knowledge of the wave energy entering the model area, a possible boundary condition is to let the energy be zero at the boundaries at all times. Another solution may be to specify zero flux of energy through the boundary. In either case it will be difficult to get a true representation of distantly generated swell. The area should therefore be sufficiently large to catch all significant swell that affects the region of interest.

In operational models, with grid resolution in the range 25–400 km, it is difficult to get a true representation of coastlines and islands. A coarse resolution will strongly affect the shadowing effects of islands and capes. To obtain a faithful representation of the sea state near such a feature we need to take special precautions. One solution may be to use a finer grid for certain areas, a so-called "nested" model, where results from the coarse grid are used as boundary input to the fine grid. It may also be necessary to increase the directional resolution so as to model limited depth and shadowing effects better. Another way may be to evaluate the effects of the topographic feature for affected wave directions at a certain number of grid points and tabulate these as "fudge factors" in the model.

5.5 Model classes

Wave models compute the wave spectrum by numerical integration of Equation 5.1 over a geographical region.

The models may differ in several respects, e.g.: the representation of the spectrum, the assumed forms of S_{in} and S_{ds}, the representation of S_{nl} and whether the integration is carried out in natural characteristic coordinates along individual rays or in terms of a discretized advection operator in a grid-point system common to all wave components.

The most difficult term to model is the non-linear source term, S_{nl}, and it is in its specification that the differences between the categories are to be found.

In the energy-balance Equation 5.1, the interactive term S_{nl} couples the components. Models based on discrete spectral components with a non-linear term which is formulated in terms of several (if not all) components are called *coupled discrete* (CD) models. In such models estimates of all components are needed just to be able to compute the evolution of any one component.

Computations for these models are often time consuming, and some modellers prefer to dispense with the coupling term, and include the weak non-linear interactions implicitly in their formulation for $S_{in} + S_{ds}$. Such models are *decoupled propagation* (DP) models. Each component can then be calculated independently. Advanced models in this class may include a simple parametric form for S_{nl}, but they are nevertheless distinguished by the pre-eminence of S_{in} and S_{ds} in the source term.

The third type of model uses the evidence that spectra of growing seas are shaped by the non-linear interactions to conform to a self-similar spectrum (e.g. JONSWAP — see Section 1.3.9). The spectral shape is characterized by some small number of parameters and the energy-balance equation can then be written in these terms. This gives an evolution equation for each of a small number of parameters rather than one for each of a large number of components. However, this parametric representation is only valid for the self-similar form of the wind-sea spectrum, and waves outside the generating area (swell) require special treatment. This is usually achieved by interfacing the parametric model for wind sea with a decoupled propagation model for "swell" through a set of algorithms by which wind-sea energy and swell energy are interchanged, hence the naming of this class as *coupled hybrid* (CH) models.

Table 6.2 in Chapter 6 gives details and references for a variety of numerical wave models. A thorough description and discussion of the model classes can be found in SWAMP Group (1985).

5.5.1 *Decoupled propagation (DP) models*

Models of this class generally represent the wave spectrum as a two-dimensional discretized array of frequency-direction cells in which each cell or component propagates at its appropriate group velocity along its own ray path. The components are grown according to a source function of the form

$$S = A + B\,E(f,\theta)\ .$$

As non-linear energy transfer is basically neglected, the factors A and B are usually empirically determined.

Each component is grown independently of all the other components up to a saturation limit, which is also independent of the other spectral components and is represented by a universal equilibrium distribution. If non-linear coupling is considered at all, it is parameterized in a simple way, e.g. by one or two spectral parameters. The saturation limit may be given by the energy of a fully developed sea, often represented by the Pierson-Moskowitz spectrum (see Section 1.3.9). Let the fully developed sea spectrum be given by E_∞. A modification of S_{in} may then appear as

$$S = \frac{\delta E}{\delta t} = \left[A\sqrt{1-\left(\frac{E}{E_\infty}\right)^2} + BE\right]\left[1-\left(\frac{E}{E_\infty}\right)^2\right]$$

(Pierson et al., 1966; Lazanoff and Stevenson, 1975), or

$$S = \frac{\delta E}{\delta t} = (A + BE)\left(1-\frac{E}{E_\infty}\right)^2$$

(Ewing, 1971). It is also possible to use the Phillips' saturation range,

$$E_\infty = \frac{\alpha g^2}{(2\pi)^4}\ f^{-5}$$

as the saturation limit (Cavaleri and Rizzoli, 1981).

The introduction of a saturation limit also works as an implicit representation of wave-energy dissipation, except for dissipation due to bottom friction and dissipation of swell. None of these effects is specific to DP models and may vary from model to model.

For strictly decoupled models, and for only weakly coupled models, the differential time and space scales dt and ds are related through the group velocity c_g for a wave component, ds = c_gdt. From this it follows that for DP models the laws for fetch-limited waves under uniform stationary wind conditions are immediately translated into the corresponding duration-limited growth laws by replacing the fetch, X, with $c_g t$ for each wave component.

Another feature of DP models that can be traced to the decoupling of wave components is that the spectrum generally develops a finer structure both in frequency and direction than coupled models, which continually redistribute energy and smooth the spectrum.

5.5.2 *Coupled hybrid (CH) models*

The independent evolution of individual wave components is effectively prevented by the non-linear energy transfer. Unless the wind field is strongly non-uniform, the non-linear transfer is sufficiently rapid relative to advection and other source functions that a

quasi-equilibrium spectral distribution is established. The distributions appear to be of the same shape for a wide variety of generation conditions and differ only with respect to the energy and frequency scales. The quasi-self-similarity was confirmed theoretically by Hasselmann et al. (1973 and 1976).

Further, a universal relationship appears to exist between the non-dimensional total energy and frequency parameters, ε and ν, respectively. The non-dimensional scalings incorporate g and some wind-speed measure, e.g. the wind speed at 10 m, U_{10}, or the friction speed, u_*. Hence $\varepsilon = E\,g^2/u^4$, and $\nu_p = f_p g/u$, where $u = U_{10}$ or u_*, and E is the total energy (from the integrated spectrum).

Since the evolution of the developing wind-sea spectrum is so strongly controlled by the shape stabilizing non-linear transfer, it appears reasonable to express the growth of the wind-sea spectrum in terms of one or a few parameters, for example ε, the non-dimensional wave energy. In such a one-parameter, first-order representation, all other non-dimensional variables (e.g. ν_p, the non-dimensional peak frequency) are uniquely determined, and hence diagnosed.

Thus, in one extreme the parametric model may prognose as few as one parameter (e.g. the total spectral energy), the wind-sea spectrum being diagnosed from that. For such a model the evolution equation is obtained by integrating Equation 5.1 over all frequencies and directions:

$$\frac{\delta E}{\delta t} + \nabla \bullet \left(\bar{\boldsymbol{c}}_{\mathbf{g}} E \right) = S_E$$

in which $\bar{\boldsymbol{c}}_{\mathbf{g}}$ is the effective propagation velocity of the total energy

$$\bar{\boldsymbol{c}}_{\mathbf{g}} = \frac{\int \boldsymbol{c}_{\mathbf{g}} E(f,\theta)\, df\, d\theta}{\int E(f,\theta)}$$

and S_E is the projection of the net source function S onto the parameter E

$$S_E = \int S(f,\theta)\, df\, d\theta$$

$\bar{\boldsymbol{c}}_{\mathbf{g}}$ is uniquely determined in terms of E by a prescribed spectral shape and S_E must be described as a function of E and U_{10} or u_*. This function is usually determined empirically.

If additional parameters are introduced, e.g. the peak frequency, f_p, the Phillips' parameter, α, or the mean propagation direction, $\bar{\theta}$, the growth of the wind-sea spectrum is expressed by a small set of coupled transport equations, one for each parameter. A general method for projecting the transport equation in the complete (f,θ) representation on to an approximate parameter space representation is given in Hasselmann et al. (1976).

In slowly varying and weakly non-uniform wind, parametric wave models appear to give qualitatively the same results. The more parameters used, the more varied are the spectral shapes obtained and, in particular, if the mean wave direction, $\bar{\theta}$, is used, directional lag effects become noticeable in rapidly turning winds.

The fetch-duration relation for a parametric wave model will differ from that of a DP model in that a mean propagation speed takes the place of the group speed for each frequency band, i.e.

$$\boldsymbol{X} = \mathrm{A}\bar{c}_{\mathrm{g}} t\,,$$

where: $\boldsymbol{X}$ = the fetch, t = duration and A is a constant (typically A = 2/3). Thus, it is not possible to tune the two types of model for both fetch- and duration-limited cases.

Once the non-linear energy transfer ceases to dominate the evolution of the wave spectrum, the parametric representation breaks down. This is the case for the low-frequency part of the wave spectrum that is no longer actively generated by the wind, i.e. the swell part. The evolution of swell is controlled primarily by advection and perhaps some weak damping. It is therefore represented in parametric wave models in the framework of discrete decoupled propagation. The combination of a parametric wind-sea model and a decoupled propagation swell model is termed a coupled hybrid model.

CH models may be expected to encounter problems when sea and swell interact. Typical transition regimes arise:

- In decreasing wind speed or when the wind direction turns, in which cases wind sea is transformed to swell;
- When swell enters areas where the wind speed is sufficiently high that the Pierson-Moskowitz peak frequency $f_p = 0.13g/U_{10}$ is lower than the swell frequency, in which case the swell suddenly comes into the active wave growth regime.

These transitions are modelled very simply in CH models. For turning winds it is common that the wind sea loses some energy to swell. The loss may be a continuous function of the rate of change of wind direction or take place only when the change is above a certain angle.

When the wind decreases, the CH models generally transfer frequency bands that travel faster than the wind to swell. Some models also transfer the energy that exceeds the appropriate value for fully developed wind sea into swell.

Swell may be reabsorbed as wind sea when the wind increases and the wind-sea peak frequency becomes equal to or less than the swell frequency. Some CH models only allow reabsorption if the angle between wind-sea and swell propagation directions fulfil certain criteria.

Some models allow swell to propagate unaffected by local winds to destination points. Interaction takes place only at the destinations. If wind sea exceeds swell at a point, the swell is completely destroyed. Thus, the reabsorption of swell into wind sea is non-conservative.

CH models generally use characteristics or rays to propagate swell.

The CH class may include many semi-manual methods. The parametric approach allows empirical relationships for the evolution of spectral parameters to be used. These may often be evaluated without the assistance of a computer, as may the characteristics of the swell.

5.5.3 *Coupled discrete (CD) models*

The problem of swell/wind sea interaction in CH models may be circumvented by retaining the discrete spectral representation for the entire spectrum and introducing non-linear energy transfers. In the models in operational use today these interactions are parameterized in different ways. The number of parameters are, however, often limited, creating a mismatch between the degrees of freedom used in the description of the spectrum (say for example 24 directions and 15 frequencies) and the degrees of freedom in the representation of the non-linear transfer (e.g. 10 parameters).

In CD models a source function of the Miles type, $S_{in} = B.E$ is very common, as in DP models. However, the factor B is strongly exaggerated in the DP models to compensate for the lack of explicit S_{nl}. A Phillips' forcing term may also be included so that $S_{in} = A + B.E$, but the value of A is usually significant only in the initial spin-up of the model.

The difference between present CH and CD models may not be as distinct as the classification suggests. In CD models the non-linear transfer is sometimes modelled by a limited set of parameters. The main difference can be found in the number of degrees of freedom. It should also be noted that the CD models usually parameterize the high-frequency part of the spectrum.

The non-linear source term, S_{nl}, may be introduced in the form of simple redistribution of energy according to a parameterized spectral shape, e.g. the JONSWAP spectrum. Another solution can be to parameterize S_{nl} in a similar way to the spectrum. This approach is generally limited by the fact that each spectral form will lead to different forms of S_{nl}. This problem may be avoided by using an S_{nl} parameterized for a limited number of selected spectral shapes. The shape most resembling the actual spectrum is chosen. Further approaches include quite sophisticated calculations of S_{nl}, such as the discrete interaction approximation of Hasselmann and Hasselmann (1985) and the two-scale approximation of Resio et al. (1992), and the near exact calculations which result from numerical integration of Equation 3.4.

The individual treatment of growth for each frequency-direction band in CD models provides a certain inertia in the directional distribution. This allows the mean wind-sea direction to lag the wind direction and makes the models more sensitive to lateral limitations of the wind field or asymmetric boundary condition. The CD models also develop more directional fine structure in the spectra than CH models.

5.5.4 *Third generation models*

A classification of wave models into first, second and third generation wave models is also used, which takes into account the method of handling the non-linear source term S_{nl}:

- First generation models do not have an explicit S_{nl} term. Non-linear energy transfers are implicitly expressed through the S_{in} and S_{ds} terms;
- Second generation models handle the S_{nl} term by parametric methods, for example by applying a reference spectrum (for example the JONSWAP or the Pierson-Moskowitz spectrum) to reorganize the energy (after wave growth and dissipation) over the frequencies;
- Third generation models calculate the non-linear energy transfers explicitly, although it is necessary to make both analytic and numerical approximations to expedite the calculations.

Results from many of the operational first and second generation models were intercompared in the SWAMP (1985) study. Although the first and second generation wave models can be calibrated to give reasonable results in most wind situations, the intercomparison study identified a number of shortcomings, particularly in extreme wind and wave situations for which reliable wave forecasts are most important. The differences between the models were most pronounced when the models were driven by identical wind fields from a hurricane. The models gave maximum significant wave heights in the range from 8 to 25 m.

As a consequence of the variable results from the SWAMP study, and with the advent of more powerful computers, scientists began to develop a new, third generation of wave models which explicitly calculated each of the identified mechanisms in wave evolution. One such group was the international group known as the WAM (Wave Modelling) Group.

The main difference between the second and third generation wave models is that in the latter the wave energy-balance equation is solved without constraints on the shape of the wave spectrum; this is achieved by attempting to make an accurate calculation of the S_{nl} term. As mentioned in Section 3.5 a simplified integration technique to compute the non-linear source term, S_{nl}, was developed by Klaus Hasselmann at the Max Planck Institute in Hamburg. Resio et al. (1992) has also derived a new method for exact computation of this term. The efficient computation of the non-linear source term together with more powerful computers made it possible to develop third generation spectral wave prediction models (e.g. the WAM model, WAMDI Group, 1988).

Third generation wave models are similar in structure, representing the state-of-the-art knowledge of the physics of the wave evolution. For the WAM model the wind input term, S_{in}, for the initial formulation was adopted from Snyder et al. (1981) with a u_* scaling

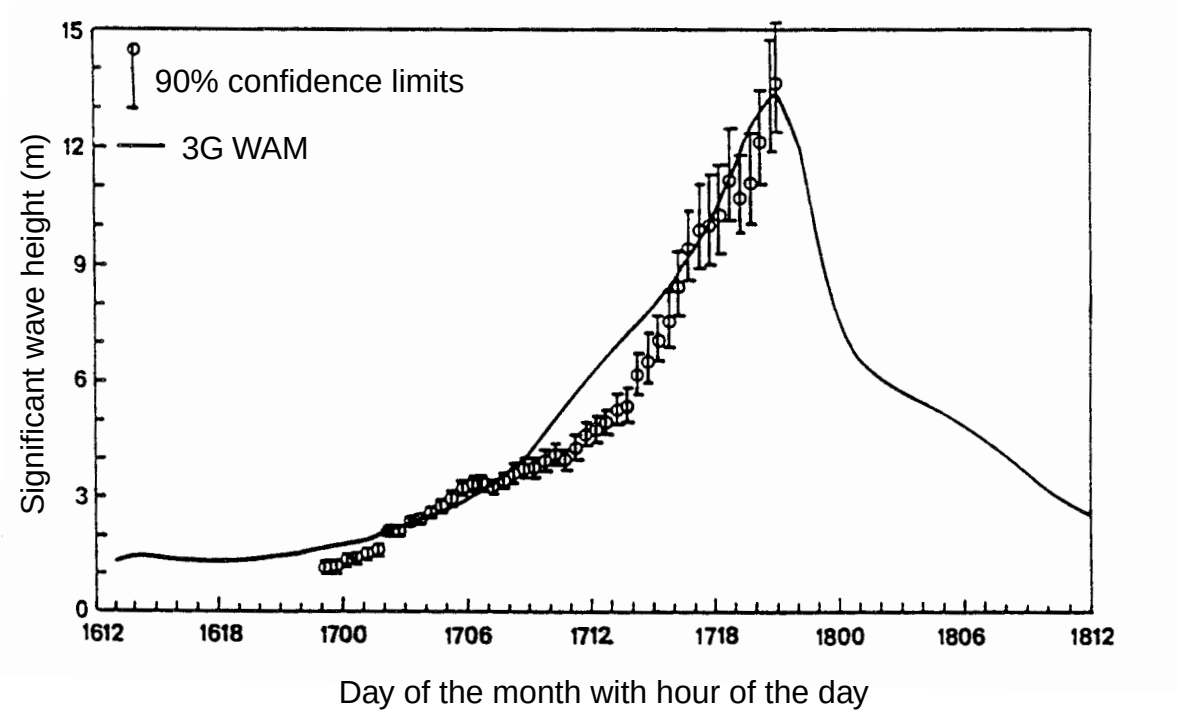

Figure 5.4 — A comparison of calculated and observed wave heights during Hurricane Camille (1969). At the height of the storm the wave sensor failed (*WAMDI Group, 1988*)

instead of U_5 (see Section 3.2). This has been superseded by a new quasi-linear formulation by Janssen (1991) (see also Komen et al., 1994) which includes the effect of the growing waves on the mean flow. The dissipation source function, S_{ds}, corresponds to the form proposed by Komen et al. (1984), in which the dissipation has been tuned to reproduce the observed fetch-limited wave growth and to eventually generate the fully developed Pierson-Moskowitz spectrum. The non-linear wave interactions, S_{nl}, are calculated using the discrete interaction approximation of Hasselmann et al. (1985). The model can be used both as a deep water and a shallow water model. Details are described by the WAMDI Group (1988) and a comprehensive description of the model, its physical basis, its formulation and its various applications are given in Komen et al. (1994).

Other models may differ in the propagation schemes used, in the method for calculating the non-linear source term, S_{nl}, and in the manner in which they deal with shallow water effects and the influence of ocean currents on wave evolution.

The WAM model has shown good results in extreme wind and wave conditions. Figure 5.4 shows a comparison between observed significant wave heights and significant wave heights from the WAM model during Hurricane Camille, which occurred in the Gulf of Mexico in 1969. The grid spacing was a 1/4° in latitude and longitude. The comparison shows a good performance of the model in a complicated turning wind situation.

The WAM model is run operationally at the European Centre for Medium-range Weather Forecasts (ECMWF) on a global grid with 1.5° resolution. It is also run operationally at a number of other weather services including the National Weather Service (USA) and the Australian Bureau of Meteorology. Further, it may be run at higher resolution as a nested regional model, and once again a number of national Meteorological Services have adopted it in this mode (see also Table 6.2 in Chapter 6). It has also been used in wave data assimilation studies using data from satellites (e.g. Lionello et al., 1992).

CHAPTER 6

OPERATIONAL WAVE MODELS

M. Khandekar: editor

6.1 Introductory remarks

Since the pioneering development of wave forecasting relations by Sverdrup and Munk (1947), operational wave analysis and forecasting has reached quite a sophisticated level. An introduction to modern numerical wave models has been provided in Chapter 5. National Meteorological Services of many maritime countries now operationally use numerical wave models which provide detailed sea-state information at given locations. Often this information is modelled in the form of two-dimensional (frequency-direction) spectra. The two-dimensional spectrum, which is the basic output of all spectral wave models, is not by itself of great operational interest; however, many wave products which can be derived from this spectrum are of varying operational utility depending upon the type of coastal and offshore activity. An example of a schematic representation of a two-dimensional spectrum is given in Figure 6.1. The spectra were generated by the Canadian Spectral Ocean Wave Model (CSOWM), developed by the Atmospheric Environment Service (AES) of Canada. The four spectra shown refer to four overpass times of the satellite ERS-1 during the wave spectra validation field experiment conducted on the Grand Banks of Newfoundland in the Canadian Atlantic from 10 to 25 November 1991. The wind-sea regions of the wave field are the elongated energy maxima located opposite to the wind direction and around the wind-sea frequency of about 0.15 Hz. The wave energy maxima outside of the wind-sea region are the swells generated by the model during the two-week period of the field experiment (for additional details, see Khandekar et al., 1994).

Significant wave height may be regarded as the most useful sea-state parameter. As defined earlier (in Section 1.3.3), the significant wave height describes the sea state in a statistical sense and is therefore of universal interest to most offshore and coastal activities. The significant wave height can be easily calculated from the two-dimensional spectrum, using a simple formula. Besides significant wave height, two other parameters, which are of operational interest, are the peak period (or,

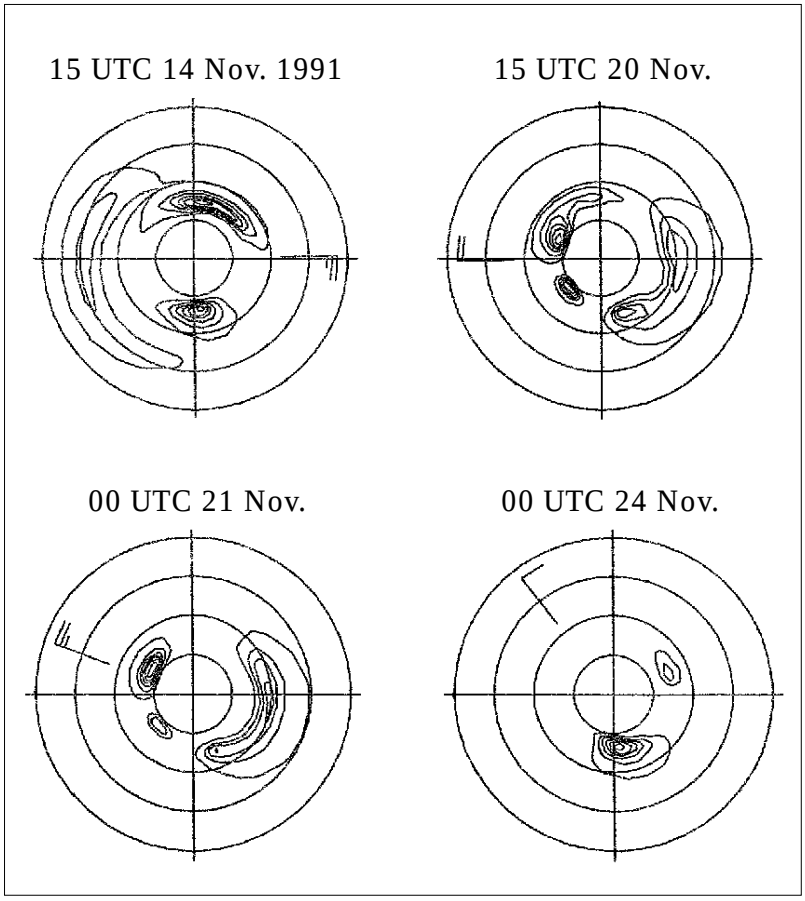

Figure 6.1 —
Normalized wave directional spectra generated by the AES CSOWM at a grid point location in the Canadian Atlantic. The spectra are presented in polar plots with concentric circles representing frequencies, linearly increasing from 0.075 Hz (inner circle) to 0.30 Hz (outer circle). The isopleths of wave energy are in normalized units of m^2/Hz/rad and are shown in the direction to which waves are travelling in relative units from 0.05 to 0.95. Model generated wind speed and direction are also shown (*from Khandekar et al., 1994*)

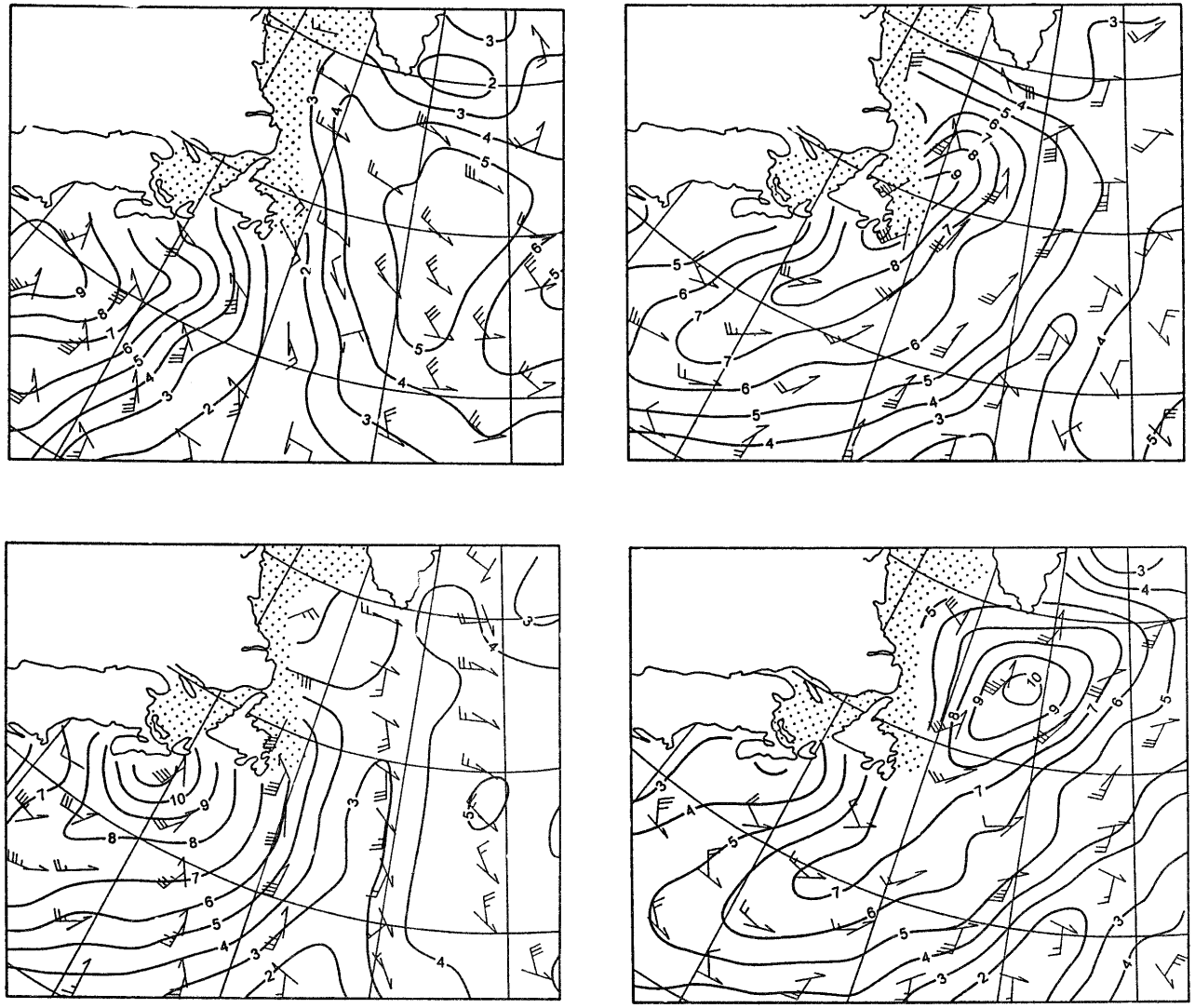

Figure 6.2 — A simplified output from the AES CSOWM in the form of a four-panel chart of significant wave height contours. The wave parameters are usually plotted according to a wave plot model shown below. Only the wind parameters and swell directions are displayed here. The panels show: the diagnostic (0-hour) wave height chart for 14 March 1993, 12 UTC (*top left*), the 12-hour forecast valid for 15 March, 00 UTC (*bottom left*), the 24-hour forecast valid for 15 March, 12 UTC (*top right*), and the 36-hour forecast valid for 16 March, 00 UTC (*bottom right*) (*courtesy CMC, Canada; after Khandekar and Swail, 1995*)

Full plotting scheme

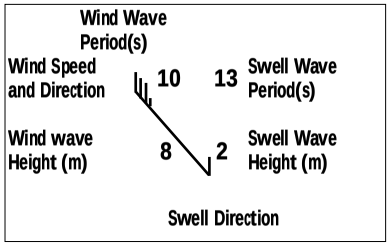

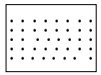

Ice valid 14 March 1993, 00 UTC

in some applications, the zero up/downcrossing period) and the direction in which waves are moving. It should be noted that the convention of wave direction from wave models varies (i.e. "from which" direction or "to which" direction), whereas measured data are invariably presented as the direction "from which" waves travel, consistent with the meteorological convention for wind direction.

The parameters for significant height, peak period and direction can be further separated into their wind-sea and swell components giving a total of six additional wave parameters of operational interest. For the sake of completeness, these six wave parameters are often accompanied by three related atmospheric parameters, namely surface pressure, wind speed and wind direction. Either all, or a selected few of these nine parameters can be suitably plotted on a map and disseminated to users. The algorithms for separating wave trains may be quite simple (see Section 3.6) or they may fully partition the spectrum into the wind sea and primary and secondary swell features (Gerling, 1992). In this case for each feature integral parameters for the significant wave height, mean period and mean direction are computed.

6.2 Wave charts

A map (or chart) showing spatial distribution of a selected number of wind and wave parameters is called a wave chart. For efficient transmission, a wave chart should be simple and uncluttered. Almost all wave charts show isopleths of significant wave height suitably labelled and a few additional parameters like peak period, wave direction, etc. The chart may provide sea-state information in a diagnostic (analysed) or in a prognostic (forecast) form.

Examples of typical output from operational centres

The AES operational wave model CSOWM is run twice daily at the Canadian Meteorological Center (CMC) in Montreal and is driven by 10 m level winds generated by the CMC regional weather prediction model. Figure 6.2 provides an example of a four-panel wave chart showing wave fields at analysis time (zero-hour forecast) plus forecast fields out to 12, 24 and 36 hours, respectively. The wave height contours refer to the total wave height, H, which is defined as:

$$H^2 = H_{wi}^2 + H_{sw}^2 \qquad (6.1)$$

In Equation 6.1, H_{wi} and H_{sw} are wind-wave and swell-wave heights, respectively. The wave charts cover the north-west Atlantic region extending from the Canadian Atlantic provinces to about 20°W and refer to the "storm of the century" in mid-March 1993 when significant wave heights of 15 m and higher were recorded in the Scotian Shelf region. A similar four-panel chart covering the Canadian Pacific extending from the west coast of Canada out to about the International Date Line is generated by the Pacific version of the CSOWM, which is also run twice a day at the CMC.

Wave charts prepared and disseminated by other national Services typically include wave height contours and a few other selected parameters. For example:

- The GSOWM (Global Spectral Ocean Wave Model of the US Navy), which was run operationally at the Fleet Numerical Meteorology and Oceanography Center in Monterey, California, until May 1994 (when it was replaced by an implementation of the WAM model, see Section 5.5.4), produced wave charts depicting contours of significant wave height and primary wave direction by arrows (see Clancy et al., 1986);
- The National Oceanographic and Atmospheric Administration (NOAA) in Washington, D.C. (USA) has been running a second generation deep-water global spectral wave model since 1985; the main output from the NOAA Ocean Wave (NOW) model is a wave chart depicting contours of significant wave height and arrows showing primary wave direction. In addition to the global wave model, NOAA also operates a regional wave model for the Gulf of Mexico, which is also a second generation spectral wave model but with shallow-water physics included. A typical output from the regional model is given in Figure 6.3;
- The Japan Meteorological Agency (JMA) in Tokyo has been operating a second generation coupled discrete spectral wave model (Uji, 1984) for the north-west Pacific and a hybrid model for the coastal regions of Japan. A typical output from the coupled discrete model is the wave chart in Figure 6.4.

  In addition, directional wave spectrum output charts for selected locations in the north-west Pacific and in the seas adjacent to Japan are prepared and disseminated — see Figure 6.5 which shows two-dimensional spectra at 12 selected locations near Japan. The wave spectra are displayed in polar diagrams. Such detailed spectral information at selected locations can be very useful for offshore exploration and related activities.

For a general discussion on the various types (classes) of wave models see Section 5.5.

6.3 Coded wave products

Measured wave data (perhaps from a Waverider buoy or a directional wave buoy) can be reported or disseminated using a code called WAVEOB. This code is constructed to allow for wave parameters and one-dimensional or two-dimensional spectral information.

For a one-dimensional spectrum (perhaps measured by a heave sensor), the report consists of a maximum spectral density value followed by ratios of individual spectral densities to the maximum value. For a two-dimensional spectrum, the report consists of directional wave functions in the form of mean and principal wave directions together with first and second normalized polar Fourier coefficients.

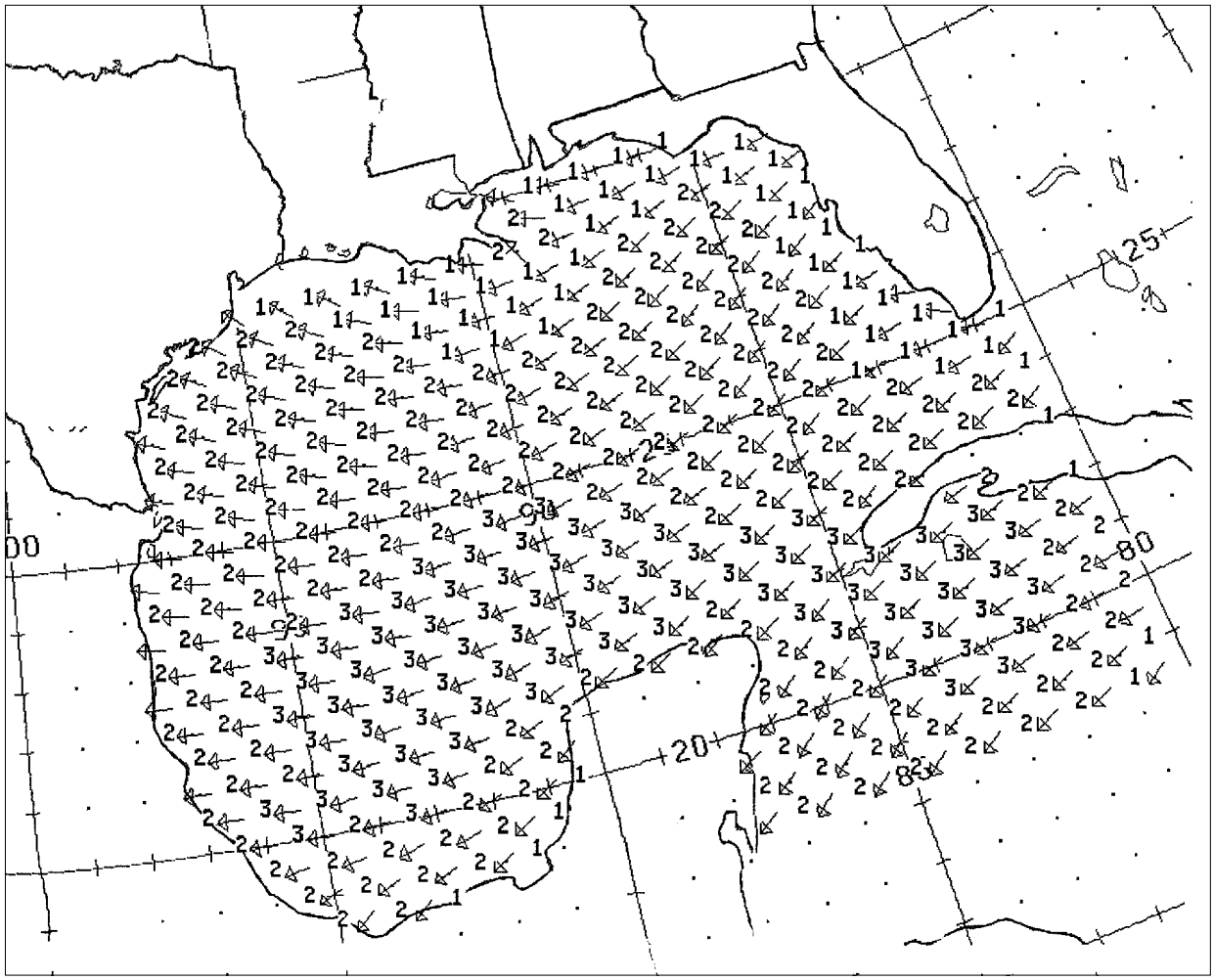

Figure 6.3 — A sample output (12-h forecast, valid 12 UTC, 13 September 1992) from the regional Gulf of Mexico shallow-water wave model operated by NOAA. The chart shows wave height values (in feet) and primary wave directions plotted at alternate grid points of the model (*source: D. B. Rao, Marine Products Branch, NOAA*)

In addition to the spectral information, the WAVEOB code includes reports of derived wave parameters like significant wave height, spectral peak period, etc. The details of various sections of the WAVEOB code can be found in Annex II and in the WMO *Manual on codes* (WMO-No. 306, code form FM 65-IX; WMO, 1995). A binary format for reporting these data is also available, namely BUFR (code form FM 94-X Ext.). This code has been used experimentally for several years to transmit ERS-1 satellite data over the Global Telecommunication System.

For reporting wave model forecast products in a gridded format, the approved code is called GRID (FM 47-IX Ext.) (see WMO-No. 306) in which the location of a grid point is reported first, followed by other information as defined above. A binary version, called GRIB, is now widely used.

6.4 Verification of wave models

With ocean wave models being used in operational mode, appropriate verification of a wave model against observed wind and wave data is necessary and important. The performance of a wave model must be continually assessed to determine its strengths and weaknesses so that it can be improved through adjustment or modifications. It is also necessary to develop sufficient confidence in the model products for operational use.

There are a number of levels of model testing and verification. In wave model development a number of idealized test cases are usually modelled. The basic output of spectral wave models is the two-dimensional wave spectrum and a suitable test would be to use the model to simulate the evolution of a wave spectrum with fetch or duration for stationary uniform wind fields. Data from field experiments, such as the JONSWAP experiment (see Section 1.3.9), can be used to assess the model's performance.

Ideally, a model would be verified by comparisons with measured directional wave spectra. However, such measurements are relatively uncommon and there are problems with interpreting the results of comparisons of individual directional wave spectra. For example, in rapidly changing conditions, such as in storms, small errors in the prediction of the time of the storm peak can

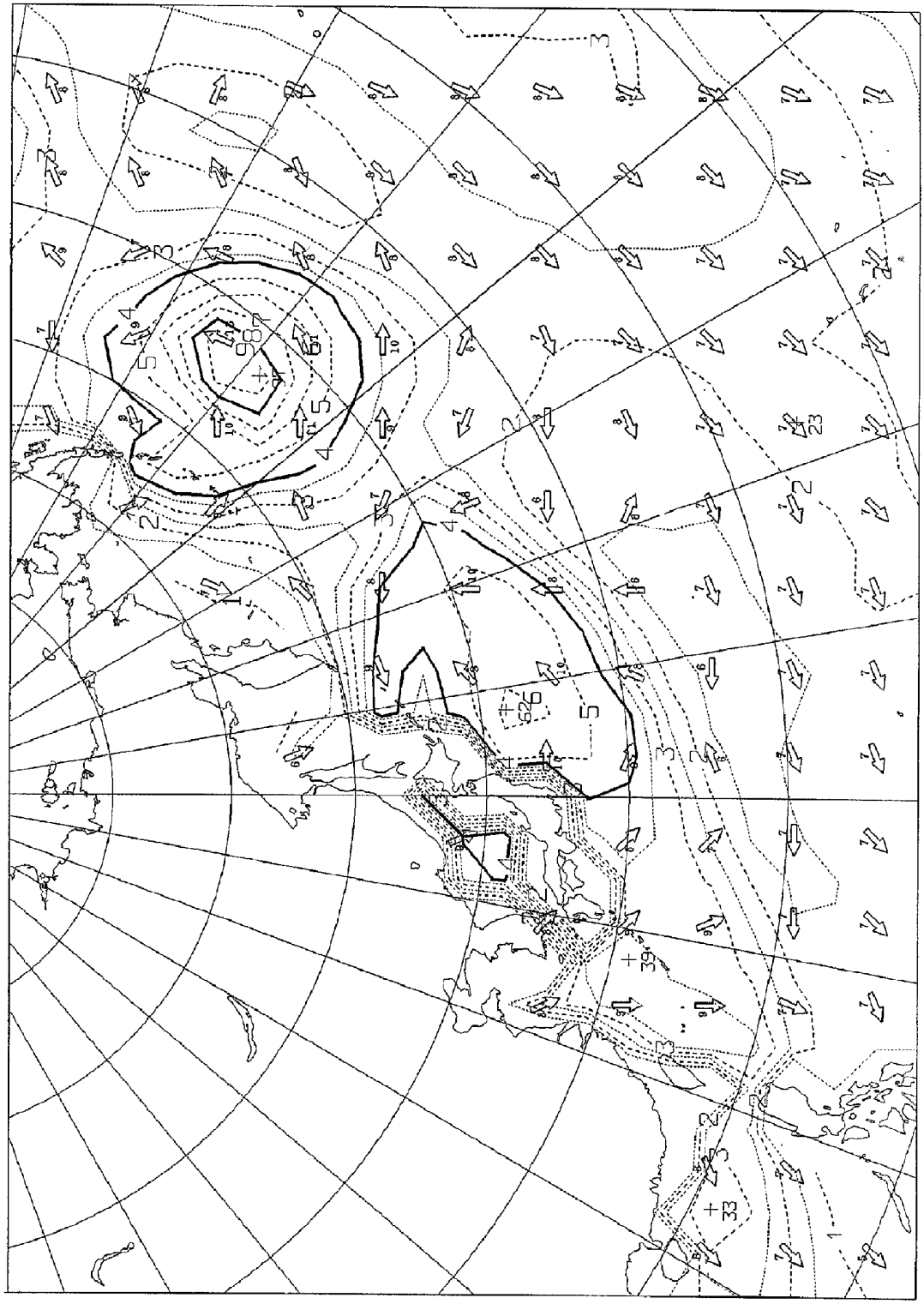

Figure 6.4 — A sample wave height chart from the wave model MRI-II operated by JMA. The chart shows contours of significant wave heights with thick solid lines for every 4 m, dashed lines for every metre and dotted lines for every half metre. Prevailing wind-wave directions are shown by arrows, while representative wave periods are shown by a small numeral attached to the arrow (*source: Tadashi Asoh, JMA*)

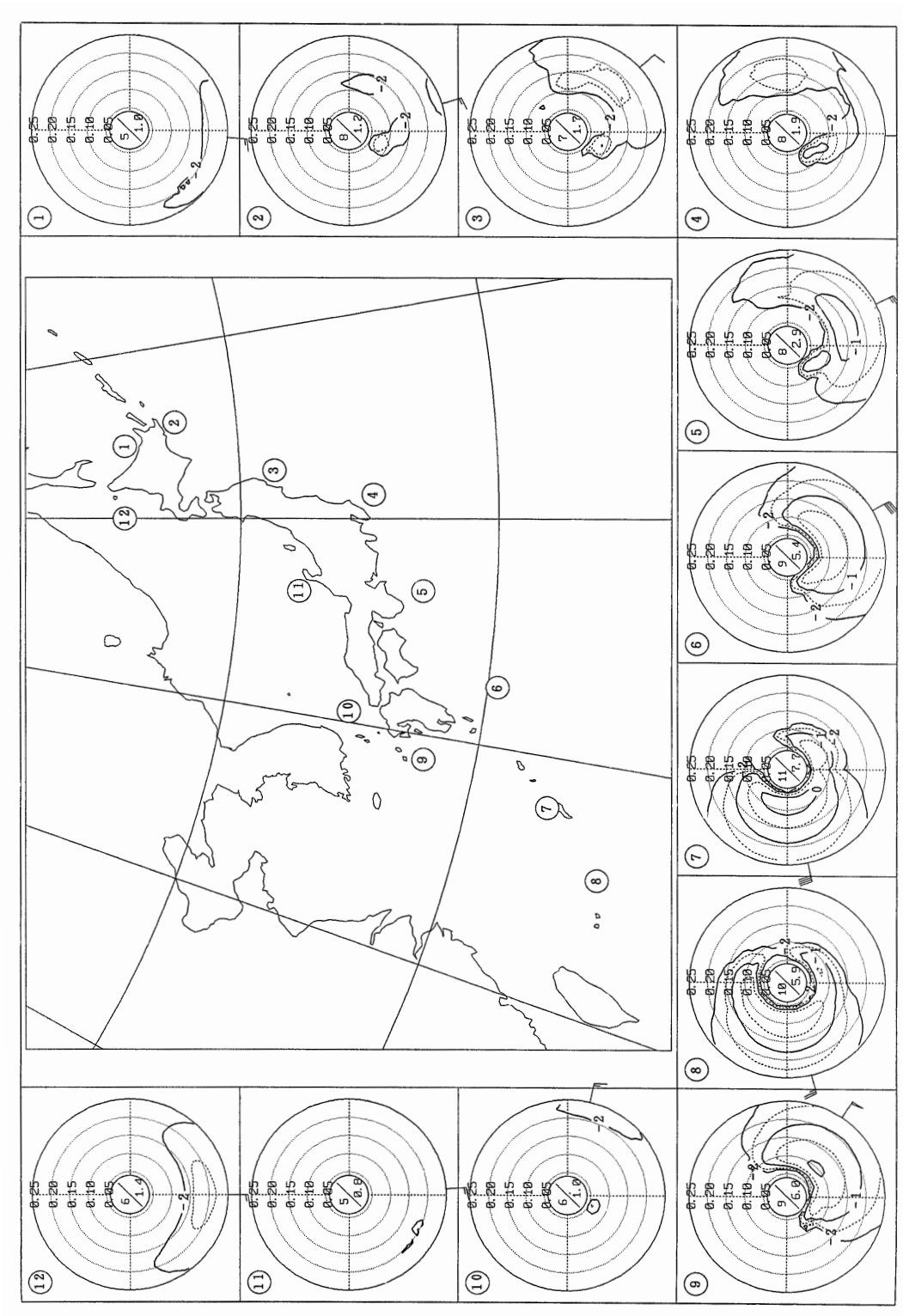

Figure 6.5 — Wave directional spectra at 12 selected locations in the seas adjacent to Japan for the 24-hour forecast valid at 00 UTC, 27 September 1991. The directional spectra are presented in polar plots with concentric circles representing wave frequencies (in Hz) and isopleths of spectral energy in units of m^2/Hz/rad. Isopleths are labelled by order of magnitude (–1 means 10^{-1} m^2/Hz/rad) and indicate the direction from which waves are coming. Also depicted on the perimeters are the wind speed and direction at each location. The values of peak period (s) and significant wave height (m) are shown at the centre of each spectrum plot (*source: Tadashi Asoh, JMA*)

give large differences in the comparisons. Further, it must be remembered that *in situ* measurements are only estimates and individual spectral components may have quite large uncertainty due to high sampling variability in the estimates.

For these reasons, model validation studies are usually performed in a statistical sense using all available data, and are based on comparisons of derived parameters. A common approach is to perform a regression analysis on a set of important parameters such as H_s, $\overline{T}_z$ (or T_p) and, if directional wave data are available, the mean direction (for different frequency bands). In addition, it may be useful to compare mean wave spectra or cumulative distributions (of, for example, H_s) for simultaneous model results and measurements. Since the wind field that drives the model is intimately related to the model wave field, most evaluation studies also include verification of wind speed and direction.

An important requirement for evaluation of a wave model is the availability of reliable sea-state measurements and related weather data. Most of the evaluation studies reported in the last 15 years have used buoy data for wind and wave measurements and have occasionally used analysed weather maps for additional wind information. A few earlier studies (e.g. Feldhausen et al., 1973) have used visual ship reports for wave height to make a qualitative evaluation of several wave hindcasting procedures. More recently, satellite altimeter data have been used to validate wave model results. For example, Romeiser (1993) validated the global WAM model (WAMDI Group, 1988; Komen et al., 1994) for a one-year period using global data from the GEOSAT altimeter.

Most verification studies have attempted to calculate several statistical parameters and analysed the magnitude and variation of these parameters to determine the skill of a wave model. Among the parameters that are most commonly used are:

- The mean error (ME) or bias;
- The root-mean-square error (RMSE);
- The Scatter Index (SI) defined as the ratio of RMSE to the mean observed value of the parameter; and
- r, the sample linear correlation coefficient between the model and the observed value.

A few studies have considered other statistical measures to evaluate wave model performance such as the slope of the regression line between model and observed values or the intercept of the regression line on the y axis. The four parameters as listed above are the best indicators of the performance of a wave model.

Verification of operational wave models at national Services of many countries is an ongoing activity. At most Services, the initial verification of a wave model is performed during the implementation phase and the verification statistics are updated periodically so as to monitor the model's performance. Table 6.1 shows the performance of a few wave models which are presently in operational use at various national (international) organizations in different parts of the world. The table presents verification statistics for wind speed, wave height and peak period (where available) in terms of four statistics, namely: ME, RMSE, SI and r as defined above. The table includes a variety of models developed over the last twenty years, ranging from first generation (1G) to the recent third generation (3G) models (see Section 5.5 for a discussion of model classifications).

Verification statistics for many more models have been summarized elsewhere by Khandekar (1989). Based on these statistics, it may be concluded that a first-generation wave model driven by winds obtained from a weather prediction model can provide wave height simulations with an RMS error of about 1.0 m and a scatter index of around 35 per cent. The second- and third-generation wave models, driven by winds from operational weather prediction models, can provide wave height simulations with RMS errors of about 0.5 m and scatter indices of about 25 per cent. The third-generation WAM model (see Section 5.5.4), which has run operationally since early 1992 at the European Centre for Medium-Range Weather Forecasts (ECMWF) in the United Kingdom, generates wave height values with RMS errors ranging from 0.4 m to 0.7 m in different parts of world oceans, while the bias (or mean error) ranges from 0.05 m to 0.2 m. Since these statistics were generated further improvements have been made both to the determination of wind fields and the wave models themselves, so it is expected that the results of the verifications will also be continually improving.

A sample wave height plot generated by the US Navy's GSOWM at a buoy location in the Gulf of Alaska is shown in Figure 6.6. The figure shows wave height variation in the Gulf of Alaska as measured by the buoy and as modelled by the GSOWM. The GSOWM was driven by winds from the GSCLI (Global Surface Contact Layer Interface) boundary-layer model. The figure also shows wave height variation simulated by the WAM model, which was configured to run on a 1° x 1° grid and was driven by surface wind stress fields generated by the Navy Operational Global Atmospheric Prediction System (NOGAPS). Also shown along with the wave plots are wind and wave error statistics covering the one-month period from 20 February to 20 March 1992. The GSOWM has a high bias of about 1 m in its wave height simulation on the US west coast. This bias is due to the model's tendency to retain excess low-frequency energy from swell waves which often travel from the central Pacific to the US west coast.

Figure 6.7 shows the verification of the global wave height field generated by the WAM model at ECMWF against wave heights measured by the radar altimeter aboard the satellite ERS-1 (see Section 8.5.2). The altimeter wave heights plotted along the sub-satellite tracks cover a six-hour window centred around the time for which the model wave height field is valid. In general, the model wave heights show an excellent agreement with

TABLE 6.1

Performance of operational wave models (the statistics quoted in the last columns are defined in the text)

Model	*Organization*	*Location of buoys*	*Verifying data and verification period*	*Wind/wave parameter*	*Verification statistics — analysis (0-hour forecast unless otherwise indicated)*				
					ME	RMSE	SI	*r*	N*
CSOWM	Environment Canada	NW Atlantic	10 buoys on US/Canadian east coast (May–July 1990)	Wind speed (m/s)	1.7	3.2	59	0.68	871
				Wave height (m)	0.19	0.56	42	0.80	974
				Peak period (s)	–1.0	2.4	32	0.30	918
		NE Pacific	12 buoys on US/Canadian west coast (May–July 1990)	Wind speed	0.0	2.4	41	0.67	575
				Wave height	–0.18	0.55	31	0.81	629
				Peak period	–1.4	3.8	42	0.12	630
GSOWM	US Navy	US east coast	US/Canada east coast buoys (20 February–20 March 1992)	Wind speed	–0.1	3.0	37	0.72	967
				Wave height	0.31	0.86	41	0.83	1016
		US west coast	US/Canada west coast buoys (20 February–20 March 1992)	Wind speed	–1.2	3.1	55	0.54	644
				Wave height	0.95	1.16	56	0.58	710
		Hawaii	Buoys around Hawaiian Islands (20 February–20 March 1992)	Wind speed	–1.3	1.7	23	0.92	203
				Wave height	0.09	0.63	23	0.59	209
		NW Pacific	Buoys around Japan (20 February–20 March 1992)	Wind speed	–0.4	2.6	37	0.76	158
				Wave height	0.25	0.67	39	0.77	160
MRI-II	Japan Meteorological Agency	NW Pacific	Buoys around Japan (entire year 1991)	Wave height (24-hour forecast)	0.05	0.58	34	0.83	–
Coastal wave model (hybrid)		Coastal Japan	11 buoys off the coast of Japan (entire year 1991)	Wave height (24-hour forecast)	–0.06	0.46	39	0.82	–
WAM	European Centre for Medium-Range Weather Forecasts (ECMWF)	NW Atlantic	US/Canada east coast buoys (August 1992)	Wind speed	0.06	2.0	42	0.64	434
				Wave height	–0.06	0.36	34	0.73	549
		NE Pacific	US/Canada west coast buoys (August 1992)	Wind speed	–0.01	1.5	23	0.89	369
				Wave height	0.16	0.40	20	0.88	371
		Hawaii	Buoys around Hawaiian Islands (August 1992)	Wind speed	–0.42	1.5	20	0.46	351
				Wave height	0.0	0.35	17	0.50	352
		NW Pacific	Buoys around Japan (August 1992)	Wind speed	–0.78	2.6	34	0.86	204
				Wave height	–0.08	0.68	31	0.88	194

* Number of data points

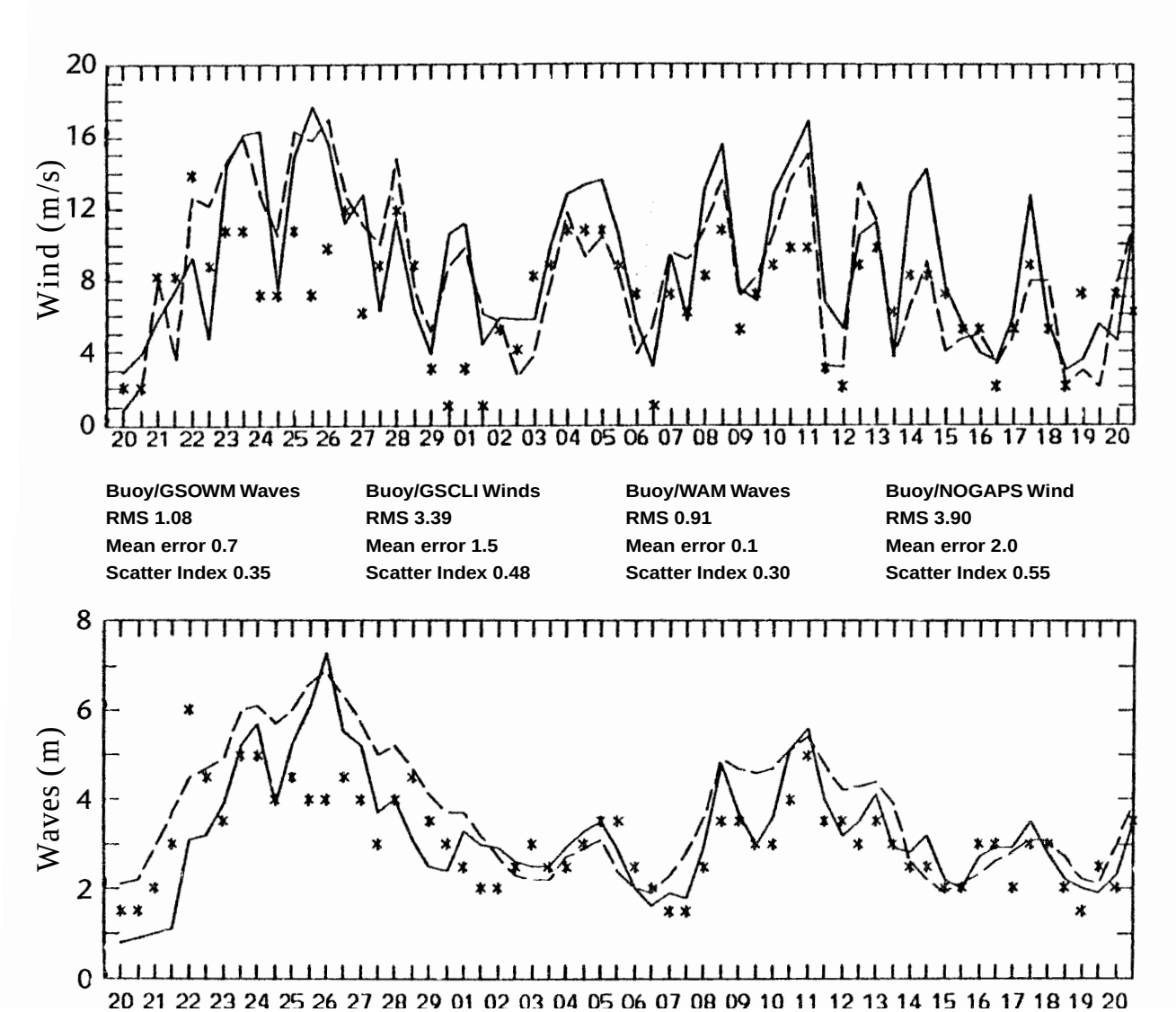

Figure 6.6 — Wind and wave verification at a buoy location (lat. 50°54'N, long. 135°48'W) in the Gulf of Alaska. The plot shows wind speed and significant wave height values for the period 20 February to 20 March 1992 as measured by the buoy (∗ ∗ ∗) and as simulated by the wave models GSOWM (– – –) and WAM (——). Also shown are wind and wave verification statistics for GSOWM and WAM (*source: Paul Wittman, Fleet Numerical Oceanography Centre, Monterey, USA*)

altimeter wave heights. The WAM model wave height field is compared daily against the altimeter fast delivery product from the ERS-1 which is received in real time. (Note that care should be taken in using altimeter data provided by the space agencies, as H_s may be significantly biased and require correction. Further, the bias for data from a particular instrument may change as algorithms change, and it may differ from one originating source to another.)

A list of wave models operated by various national Meteorological (and Oceanographic) Services is given in Table 6.2. Most of these wave models are verified routinely against available wind and wave data. Besides these wave models, there are other wave models which have been developed and are being used either experimentally or operationally by other organizations like universities, private companies, etc. Additional information on these wave models and their verification programmes is available elsewhere (see WMO, 1985, 1991, 1994(*a*)).

6.5 Wave model hindcasts

A wave model in operational use will usually be forced by forecast winds to produce wave forecasts. However, the model may also be driven by analysed winds pertaining to past events, such as the passage of hurricanes (tropical cyclones) or rapid cyclogenesis over the sea. In such cases the wave field generated by the wave model is called the hindcast wave field. Wave hindcasting is a non-real-time application of numerical wave models which has become an important marine application in many national weather services.

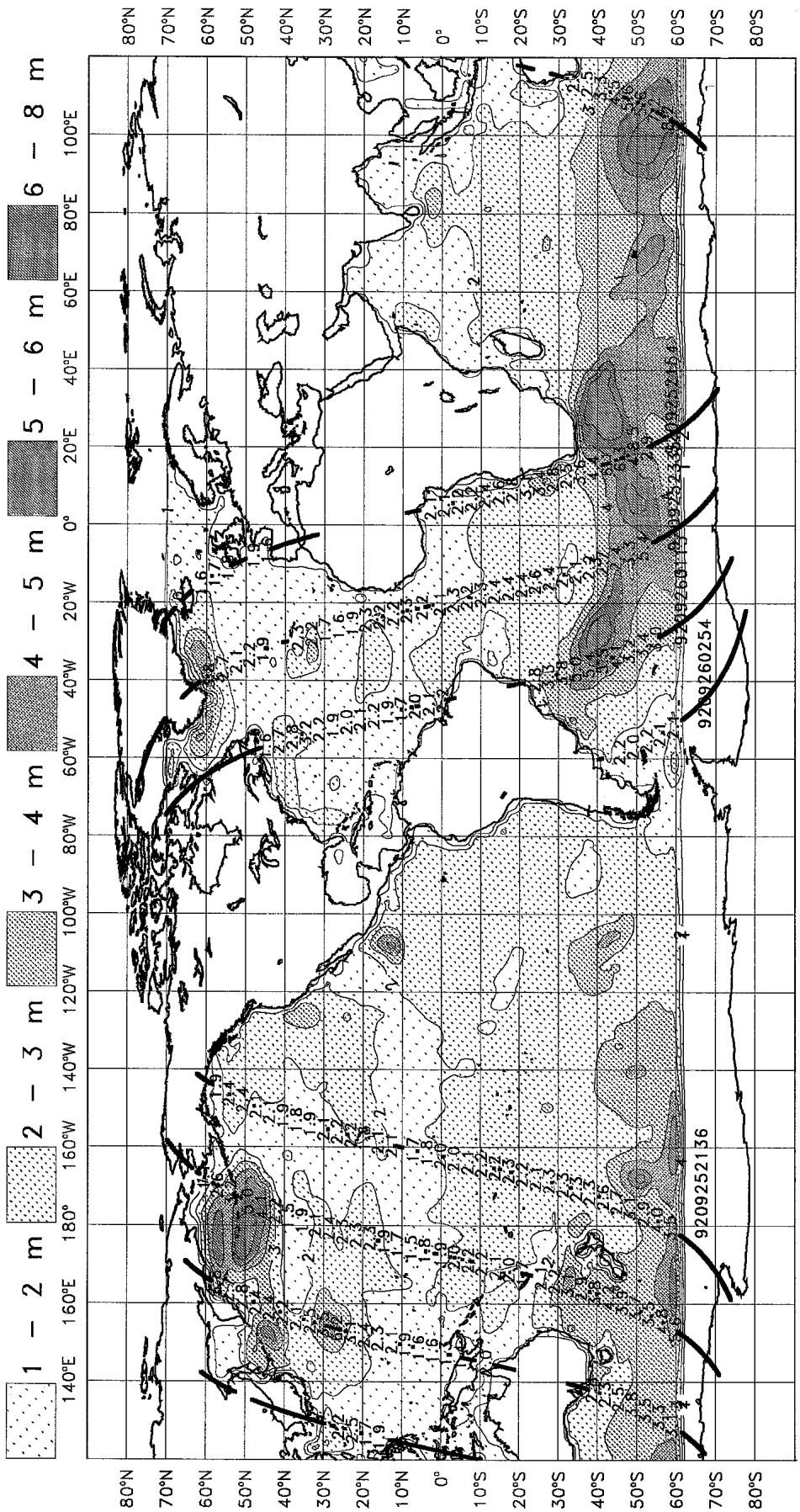

Figure 6.7 — Verification of global wave height field generated by the WAM model against wave heights measured by the radar altimeter aboard the satellite ERS-1 (radar altimeter wave heights from 25 September, 21 UTC, to 26 September 1992, 03 UTC; model field 26 September 1992, 00 UTC) (*source: A. Guillaume, while at ECMWF, UK*)

TABLE 6.2

Numerical wave models operated by national Meteorological Services

Country	*Name of model*	*Area*	*Grid*	*Type of model*	*Products*	*Source of wind information*
AUSTRALIA	WAM	Global	3° x 3° lat./long.	Deep water, coupled spectral	Forecasts (+12 to +48 h), significant wave, swell and wind-sea height, period, direction	Australian global NWP model, GASP
	WAM	Australian region 80°E–180°, 0°–60°S	1° x 1° lat./long.		Forecasts (+12 to +36 h)	Australian regional NWP model RASP
CANADA	Canadian Spectral Ocean Wave Model (CSOWM)	North Atlantic	Coarse mesh (1.08° long.) transverse Mercator	Deep water, 1st generation spectral	4-panel charts (t + 0, 12, 24, 36) plots of swell height and period, wind-wave height and period, surface wind speed and direction, contours of significant wave height	Regional Finite Element (RFE) model surface wind applicable at 10 m level
	CSOWM	North Pacific	Coarse mesh (1.08° long.) transverse Mercator	Deep water, 1st generation spectral	4-panel charts (t + 0, 12, 24, 36) plots of swell height and period, wind-wave height and period, surface wind speed and direction, contours of significant wave height	Global spectral model 1 000 hPa winds
EUROPE (EU)	WAM	Global	1.5° x 1.5° lat./long.	Deep/shallow water modes, coupled spectral	2-D spectra, significant wave height, mean direction, peak period of 1-D spectra, mean wave period. T+0 to T+120 at 6-h intervals; T+132 to T+240 at 12-h intervals. Outputs coded into FM 92-X Ext. GRIB	Surface winds (10 m) from ECMWF analyses and forecasts
	WAM	Baltic and Mediterranean	0.25° x 0.25° lat./long.		Same as global model except for T+0 to T+120 at 6-h intervals	
FRANCE	VAGMED	Western Mediterranean Sea	35 km polar stereographic at 60°N	Deep water, coupled discrete model	Forecast every 3 h up to 48 h. Maps of wave height contours with swell and wind-sea directions. Directional spectra (telex). Archive of analysed 2-D spectra and of forecast height fields	Wind fields from the fine mesh model PERIDOT
	VAGATLA	North Atlantic	150 km polar stereographic at 60°N	Deep water, coupled discrete model, 2nd generation	Forecasts every 6 h up to 48 h. Maps of wave height contours with swell and wind-sea directions. Directional spectra (telex). Archive of analysed 2-D spectra and of forecast height fields	Wind fields from EMERAUDE model
GERMANY	Deutscher Wetterdienst	Atlantic, north of 15°N		Deep water, coupled hybrid	Prognoses for 6 h, then at 12-h intervals to 96 h run twice daily, verification only	BKF model, 950 hPa level, diagnostically interpolated for about 20 m above sea
	AMT für Wehrgeophysik	North-east Atlantic, southern Norwegian Sea, North Sea	50 km	Continental shelf of North Sea, coupled hybrid	(1) Maps of wave and swell direction for south Norwegian Sea and North Sea – 24 h prognoses (2) Wind direction and velocity, significant wave height, swell height, wave period, swell period – 24 h hindcast and forecast for nine geographic positions	Reduced wind components of geopotential fields at 1 000 hPa from meteorological forecast model 7-LPE

TABLE 6.2 (cont.)

Country	*Name of model*	*Area*	*Grid*	*Type of model*	*Products*	*Source of wind information*
GREECE	Mediterranean model	Central and eastern Mediterranean Sea	100 km polar stereographic	Deep water, decoupled propagation	Daily wave forecasts for 6-h intervals to 48 h (radio-facsimile broadcasts)	Operational atmospheric numerical model of the ECMWF at 1 000 hPa
HONG KONG	MRI-II	5°–35°N, 105°–135°E	2.5° x 2.5° Mercator	Deep water, coupled discrete	Hindcast and 24- and 48-h forecasts of significant waves and swell at grid points every 12 h, charts	*Hindcast*: 2.5° winds – objective analysis of 6-h wind observations and incorporation of tropical cyclone wind model *Forecast*: Prognostic surface wind fields from NWP model
	HK coast	Coastal waters around Hong Kong	4.4 x 4.4 km	Shallow water SMB model with swells from deep water model output	6-, 12-, 18- and 24-h forecasts of significant wave height and swells every 12 h, charts	Surface winds at selected coastal stations in Hong Kong
INDIA	Sverdrup-Munk Bretschneider	Indian seas		Deep water, simple SMB model	Wave forecasts	
IRELAND	Adapted NOWAMO (Norway)	North Atlantic		Hybrid	12-h sea, swell and combined wave heights	
JAPAN	MRI-II	Western North Pacific	381 km 36 x 27	Deep water, spectral model, coupled discrete	Fax chart of analysis and 24-h forecast, daily	Surface winds from numerical weather prediction model
	MRI-II	Seas adjacent to Japan	127 km 37 x 31	Deep water, spectral model, coupled discrete	Fax chart of 24-, 36- and 48-h forecast, twice a day	Surface winds from numerical weather prediction model
	Coastal wave model	Coastal waters of Japan	10 km inshore of 100 km	Hybrid of significant wave and spectral model	Fax chart of 24-, 36-, and 48-h forecast, twice a day	Surface winds from numerical weather prediction model
MALAYSIA	GONO	Equator to 18°N, 110°–118°E	2° x 2° Mercator	Deep and shallow coupled hybrid	Analysis and forecast of 6-h intervals for pre-selected points	*Analysis*: Grid point wind from subjectively analysed charts *Forecast*: Persistence
NETHERLANDS	GONO	North Sea and Norwegian Sea	75 km Cartesian stereographic	Deep and shallow, coupled hybrid	Analysis and 6-, 12-, 18-, 24-h forecasts of wind-sea charts every 6 h	Numerical atmospheric 4-layer baroclinic model based on air pressure analysis
NEW ZEALAND	–	South-west Pacific (including Tasman Sea and Southern Ocean)	Polar stereographic 40 x 30 Cartesian 190 km at 60°S	Deep water, coupled spectral	Daily wave combined height contours, primary and secondary direction arrows, analysis and 24-, 48-h prognoses. Swell also at 24 h	Regional 10-layer primitive equation NWP model coupled to surface winds with 2-layer diagnostic boundary layer model
NORWAY	WINCH	North Sea, Norwegian Sea, Barents Sea, northern parts of north-eastern Atlantic	75 km polar stereographic	Deep water, coupled discrete, 2nd generation	Forecast charts of wave parameters at 6-h intervals, time series and wave spectra for selected points	10 m winds from Norwegian Meteorological Institute (DNMI) limited area model run up to +48 h. Also 10 m winds from ECMWF to +168 h

TABLE 6.2 (cont.)

Country	*Name of model*	*Area*	*Grid*	*Type of model*	*Products*	*Source of wind information*
SAUDI ARABIA	Advective singular wave model	5°N, 45°E; 20°N, 70°E; 30°N, 30°E; 43°N, 55°W; Red Sea and Arabian Gulf	28.1 km	Shallow water, advective singular	Charts of significant wave height and period at 6-h intervals	From numerical analysis model – a numerical sea breeze simulation is used near coast and a gradient wind modified from friction is computed
SWEDEN	NORSWAM	North Sea	100 km	Deep water, coupled hybrid	Wave forecast	
UNITED KINGDOM	European model	North Atlantic, east of 14°W; 30°45'N–66°45'N including Mediterranean and Black Seas	0.25° lat. x 0.4° long.	To 200 m depth with 2 m resolution, coupled discrete	12-h hindcast and 36-h forecasts of wind sea and swell sea (height, direction and period), also significant wave height. Fields output on charts or for selected grid points as meteograms or by printer. Tabulated results of coastal areas	Forecast winds from lowest level of operational, fine mesh, limited area numerical weather prediction models, every hour
	Global model	Global oceans	1.25° lat. x 0.8333° long.	Deep water, coupled discrete	12-h hindcasts and 120-h forecasts of wind sea and swell sea (height, direction and period), also significant wave height. Fields output on charts for local use or in digitally-coded bulletins (GRID or GRIB) on GTS	Forecast winds from lowest level of operational, coarse-mesh, global numerical weather prediction model, every two hours
USA	NOAA/WAM	Global	2.5° x 2.5° lat./long.	Deep water, coupled spectral	Significant wave height charts for T+12, T+24, T+48 and T+72. Charts of direction of peak energy for Atlantic and Pacific, and period of peak energy for Pacific. Alpha-numeric bulletins of wave spectra, special charts for Gulf of Alaska, Hawaii and Puerto Rico regions	Lowest layer winds corrected to 10 m height from the operational Medium Range Forecast (MRF) model
	GWAM	Global	1° x 1° lat./long.	Deep water, coupled spectral	Significant wave height, sea height, swell height, max. wave height, mean wave direction, sea direction, swell direction, mean period, sea period, swell period, whitecap coverage, T+0 to T+144	Surface winds stress for Navy Operational Global Atmospheric Prediction System (NOGAPS)
	IOWAM	Indian Ocean	0.25° x 0.25° lat./long.	Shallow water, coupled spectral, nested in GWAM	As above, T+0 to T+48	Navy Operational Regional Atmospheric Prediction System (NORAPS)
	MEDWAM	Mediterranean Sea	0.25° x 0.25° lat./long.	Shallow water, coupled spectral	As above, T+0 to T+72	NORAPS
	KORWAM	Korean area	0.2° x 0.2° lat./long.	Shallow water, coupled spectral, nested in GWAM	As above, T+0 to T+36	NORAPS

The purpose of a wave hindcast is to generate wave data that will help describe the temporal and spatial distribution of important wave parameters. The existing network of wave observing buoys is very limited and quite expensive to maintain. Consequently, a meaningful wave climatology describing temporal and spatial distribution of wave parameters cannot be developed solely from the buoy data. An operational wave model can be used in a hindcast mode to create a valuable database over historical time periods for which very limited wave information may be available. A reliable and an extensive database can help develop a variety of wave products which can be used in design studies for harbours, coastal structures, offshore structures such as oil-drilling platforms and in planning many other socio-economic activities such as fishing, offshore development, etc.

Several wave models, including some of those listed in Table 6.2, have been used in the hindcast mode to create wave databases and related wave climatologies. Among the well-known studies reported in last 15 years are the following:

(*a*) A 20-year wind and wave climatology for about 1 600 ocean points in the northern hemisphere based on the US Navy's wave model SOWM (US Navy, 1983);

(*b*) A wave hindcast study for the north Atlantic Ocean by the Waterways Experiment Station of the US Army Corps of Engineers (Corson et al., 1981); and

(*c*) A 30-year hindcast study for the Norwegian Sea, the North Sea and the Barents Sea using a version of the wave model SAIL, initiated by the Norwegian Meteorological Institute (Eide, Reistad and Guddal, 1985).

In Chapter 9, Table 9.3 gives a more extensive list of databases generated from wave model hindcasts.

In recent years, wave hindcasting efforts have been extended to simulate wave fields associated with intense storms that particularly affect certain regions of the world. Among the regions that are frequently affected by such storms are the North Sea and adjacent north European countries, the north-west Atlantic and the east coast of Canada, the north-east Pacific region along the US-Canadian west coast, the Gulf of Mexico and the Bay of Bengal in the north Indian Ocean. Several meteorological studies initiated in Canada, Europe and the USA have developed historical catalogues of these intense storms and the associated weather patterns. Two recent studies have simulated wind and wave conditions associated with these historical storm events in order to develop extreme wind and wave statistics. One of the studies is the North European Storm Studies (NESS) reported by Francis (1987) and the other is Environment Canada's study on wind-wave hindcast extremes for the east coast of Canada (Canadian Climate Center, 1991). A similar study for the storms in the north-east Pacific is in progress at Environment Canada and is expected to be completed shortly. More details on wave climatology and its applications will be found in Chapter 9.

6.6 New developments

Until 1991 most operational wave models were purely diagnostic, both in forecast and hindcast modes. That is, they used wind fields as the only input from which to diagnose wave conditions from these winds. These models are initialized with similarly diagnosed wave hindcasts. Wave data had been too sparse to consider objective analyses in the same sense as those performed for initializing atmospheric models. However, widespread wave and wind data from satellites have become a reality and there are opportunities for enhancing the wave modelling cycle with the injection of such data.

One of the goals of the WAM Group (see Komen et al., 1994) was to develop data assimilation techniques so that wave and wind data, especially those from satellites, could be routinely used in wave modelling. An algorithm was developed to incorporate ERS-1 altimeter wind and wave data (see Section 8.5.2), and the ECMWF model was modified to use ERS-1 scatterometer (see Sections 2.2.4 and 8.5.4) data. Further, some techniques for retrieving wind information from scatterometers use wave model output. Similar efforts have been made at several other institutes, including the UK Meteorological Office in Bracknell, Environment Canada in Downsview, Ontario, the Australian Bureau of Meteorology in Melbourne, the Norwegian Meteorological Institute in Oslo, and the US Navy's Fleet Numerical Meteorology and Oceanography Center, in Monterey, California. A list of projects is provided in Chapter 8, Table 8.1. It is expected that in the next few years, satellite wind and wave data will be assimilated routinely in increasing numbers of operational wave models.

CHAPTER 7

WAVES IN SHALLOW WATER

L. Holthuijsen: editor

7.1 Introduction

The evolution of waves in deep water, as treated in Chapter 3, is dominated by wind and by propagation along straight lines (or great circles on the globe). When waves approach the coast, they are affected by the bottom, currents and, very close to shore, also by obstacles, such as headlands, breakwaters, etc., the effects of which usually dominate — surpassing the effects of the local wind — and the resulting wave propagation is no longer along straight lines.

When approaching the continental shelf from the ocean the initial effects of the bottom on the waves are not dramatic. In fact, they will hardly be noticeable until the waves reach a depth of less than about 100 m (or rather, when the depth is about one-quarter of the wavelength). The first effect is that the forward speed of the waves is reduced. This generally leads to a slight turning of the wave direction (refraction) and to a shortening of the wavelength (shoaling) which in turn may lead to a slight increase or decrease in wave height. Wind generation may be enhanced somewhat as the ratio of wind speed over wave speed increases when the waves slow down. However, this is generally masked by energy loss due to bottom friction. These effects will be relatively mild in the intermediate depths of around 100 m but they will accumulate so that, if nothing else happens, they will become noticeable as the distances increase.

When the waves approach the coast from intermediate water depth and enter shallow water of 25 m or less, bottom effects are generally so strong (refraction and dissipation) that they dominate any wind generation. The above effects of refraction and shoaling will intensify and energy loss due to bottom friction will increase. All this suggests that the wave height tends to decrease but propagation effects may focus energy in certain regions, resulting in higher rather than lower waves. However, the same propagation effects may also defocus wave energy, resulting in lower waves. In short, the waves may vary considerably as they approach the coast.

In the near-shore zone, obstacles in the shape of headlands, small islands, rocks and reefs and breakwaters are fairly common. These obviously interrupt the propagation of waves and sheltered areas are thus created. The sheltering is not perfect. Waves will penetrate such areas from the sides. This is due to the short-crestedness of the waves and also due to refraction which is generally strong in near-shore regions. When the sheltering is very effective (e.g. behind breakwaters) waves will also turn into these sheltered regions by radiation from the areas with higher waves (diffraction). When finally the waves reach the coast, all shallow water effects intensify further with the waves ending up in the surf zone or crashing against rocks or reefs.

Very often near the coast the currents become appreciable (more than 1 m/s, say). These currents may be generated by tides or by the discharge from rivers entering the sea. In these cases the currents may affect waves in roughly the same sense as the bottom (i.e. shoaling, refraction, diffraction, wave breaking). Indeed, waves themselves may generate currents and sea-level changes. This is due to the fact that the loss of energy from the waves creates a force on the ambient water mass, particularly in the breaker zone near a beach where long-shore currents and rip-currents may thus be generated.

7.2 Shoaling

Shoaling is the effect of the bottom on waves propagating into shallower water without changing direction. Generally this results in higher waves and is best demonstrated when the wave crests are parallel with the bottom contours as described below.

When waves enter shallow water, both the phase velocity (the velocity of the wave profile) and the group velocity (the velocity of wave energy propagation) change. This is obvious from the linear wave theory for a sinusoidal wave with small amplitude (see also Section 1.2.5):

$$c_{\text{phase}} = \frac{\omega}{k} = \sqrt{\frac{g}{k}\tanh(kh)} \qquad (7.1)$$

with wavenumber $k = 2\pi/\lambda$ (with λ as wavelength), frequency $\omega = 2\pi/T$ (with T as wave period), local depth, h, and gravitational acceleration, g. These waves are called "dispersive" as their phase speed depends on the frequency. The propagation speed of the wave energy (group speed c_g) is $c_g = \beta c_{\text{phase}}$ with $\beta = {}^1/_2 + kh/\sinh(2kh)$. For very shallow water (depth less than $\lambda/25$) both the phase speed and the group speed reduce to $c_{\text{phase}} = c_g = \sqrt{(gh)}$, independent of frequency. These waves are therefore called "non-dispersive".

The change in wave height due to shoaling (without refraction) can be readily obtained from an energy balance. In the absence of wave dissipation, the total *transport* of wave energy is not affected, so that the rate of change along the path of the wave is zero (stationary conditions):

$$\frac{\mathrm{d}}{\mathrm{d}s}\left(c_g E\right) = 0, \qquad (7.2)$$

where c_gE is the energy flux per unit crest length (energy $E = \rho_w g H^2/8$, for wave height H) and s is the coordinate

in the direction of wave propagation. Any decrease in c_g is therefore accompanied by a corresponding increase in wave height (and vice versa, any increase in c_g by a decrease in wave height). This is readily illustrated with a wave perpendicular to a straight coast. Its wave height can be determined from this conservation of energy transport (i.e. assuming no dissipation), with:

$$H_2 = \sqrt{\frac{c_{g,1}}{c_{g,2}}} \cdot H_1, \qquad (7.3)$$

where H is the wave height and the subscripts 1 and 2 refer to any two different locations along the (straight) path of the wave.

The inclusion of shoaling in an Eulerian discrete spectral wave model as described in Section 5.3 is relatively simple. Only the determination of $c_{g,x}$ and $c_{g,y}$ in Equation 5.4 needs to be adapted as described above by $c_g = \beta c_{phase}$.

7.3 Refraction

In addition to changing the wave height, the change in phase velocity will turn the wave direction (when the crests are not parallel to the bottom contours). This is readily illustrated with a long-crested harmonic wave approaching a straight coastline at an angle. In this case the crest of the wave is infinitely long in deep water. When the crest enters shallow water, its velocity is reduced, in the first instance at the shallow water part of the crest (see Figure 7.1), which will therefore slow down, whereas the deeper part of the crest retains (more or less) its speed. This results in a turning of the crest towards shallow water (the deep water part keeps running whereas the shallow water part delays). In the final situation, when the wave runs up the beach, the wave crest is parallel to the beach irrespective of its deep water direction.

In the situation considered here of long-crested, harmonic waves approaching a straight beach (with straight bottom contours), the direction of the wave is governed by the well-known Snell's law, by which, along the wave ray (the orthogonal to the wave crests):

$$\frac{\sin\theta}{c_{phase}} = \text{constant}. \qquad (7.4)$$

The angle θ is taken between the ray and the normal to the depth contour. At two different locations, with subscripts 1 and 2, the wave direction can then be readily determined from $\sin\theta_1/c_{phase,1} = \sin\theta_2/c_{phase,2}$. When c_{phase} approaches zero (at the beach), the angle θ approaches zero and the crest is parallel with the beach.

Again, the change in wave height can be readily obtained from an energy balance. In the absence of dissipation, the energy transport between two wave rays is not affected (note the addition of "between two wave rays" compared with the shoaling case of Section 7.2 in which crests are parallel to the bottom contours). This means that the energy transport between two adjacent wave rays Δb is constant (stationary conditions):

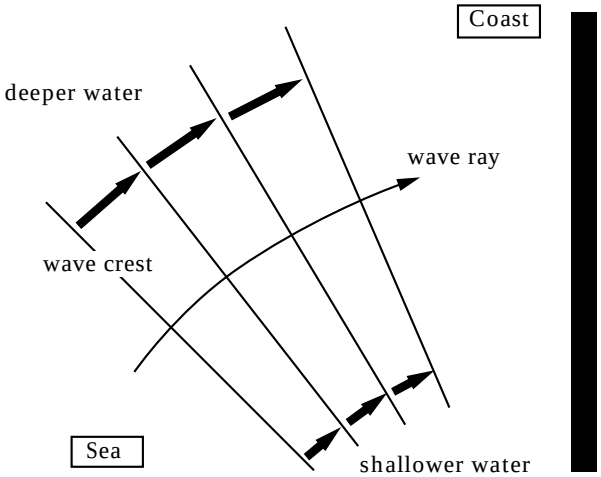

Figure 7.1 — Waves turning towards shallow water due to variations in phase speed along the crest (refraction)

$$\frac{\mathrm{d}\left(c_g E \cdot \Delta b\right)}{\mathrm{d}s} = 0. \qquad (7.5)$$

An increase in the distance between the orthogonals is therefore accompanied by a corresponding decrease in wave height.

In the situation considered here the change in wave ray separation can be readily obtained from Snell's law: $\Delta b_1/\Delta b_2 = \cos\theta_1/\cos\theta_2$. It follows then from the energy transport being constant that

$$H_2 = \sqrt{\frac{\cos\theta_1}{\cos\theta_2}} \cdot \sqrt{\frac{c_{g,1}}{c_{g,2}}} \cdot H_1. \qquad (7.6)$$

When the waves approach the coast at normal incidence the crests are parallel to the bottom contours. No refraction occurs and the wave rays remain straight (at right angles with the straight depth contours) so that the ratio $\cos\theta_1/\cos\theta_2$ is equal to 1. The change in wave height is then entirely due to the change in group velocity as in the case of shoaling described above (Section 7.2). The extra ratio $\sqrt{(\cos\theta_1/\cos\theta_2)}$ therefore represents the effect of refraction on the wave height.

In situations where the coast is not straight, the wave rays are computed with a generalization of Snell's law which says that the rate of turning of the wave direction depends on the rate of change of the phase speed along the crest (due to depth variation):

$$\frac{\mathrm{d}\theta}{\mathrm{d}s} = -\frac{1}{c}\frac{\partial c}{\partial n}, \qquad (7.7)$$

where s is the distance along the wave ray and n is the distance along the wave crest. Manual methods to obtain a wave ray by integrating this wave ray equation have been developed (e.g. CERC, 1973) but computers have mostly taken over the task. In this traditional approach one usually calculates refraction effects with a set of initially parallel wave rays which propagate from a deep

water boundary into shallow water. The changes in wave direction thus obtained may focus energy in areas where the rays converge, or defocus energy in areas where the rays diverge. An example of a ray pattern in an area of non-uniform depth is given in Figure 7.2.

From the energy balance (Equation 7.5) between two adjacent wave rays, it is relatively simple to estimate the wave height. If no generation or dissipation occurs the wave height at a location 2 is computed from the wave height at a location 1 with the energy balance between two adjacent wave rays:

$$H_2 = \sqrt{\frac{\Delta b_1}{\Delta b_2}} \cdot \sqrt{\frac{c_{g,1}}{c_{g,2}}} \cdot H_1, \qquad (7.8)$$

where the ray separations and the group speeds are Δb_1, Δb_2, and $c_{g,1}$, $c_{g,2}$, respectively.

In areas with a very smooth bathometry, the approach based on the local ray separation generally presents no problem. However, in the case of an irregular bathometry, the ray pattern may become chaotic (see Figure 7.2 for example). In such cases a straightforward transformation of local ray separation into local wave heights, if at all possible, yields highly erratic values. Quite often adjacent rays will cross and fundamental problems arise. The ray separation becomes zero and the wave height would be infinite (as diffraction effects are ignored, see Section 7.4). A continuous line of such crossing points (a caustic) can be created in classical academic examples. A spatial averaging technique to smooth such erratic results has been proposed by Bouws and Battjes (1982). An alternative ray method which avoids the problem of crossing wave rays is to backtrack

(*a*)

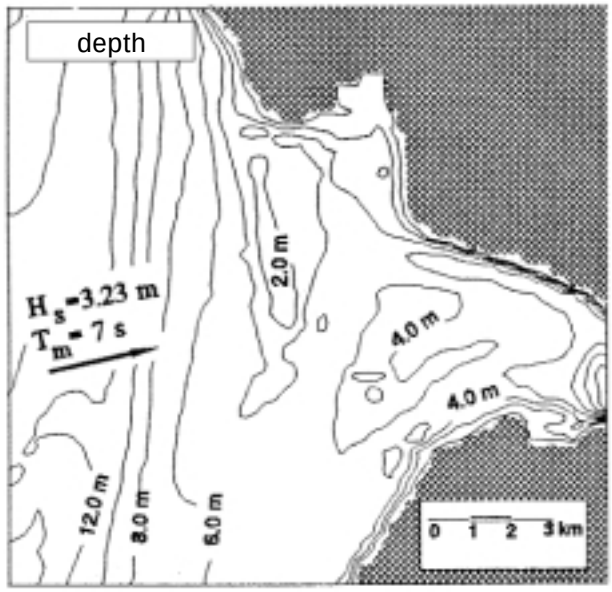

(*b*)

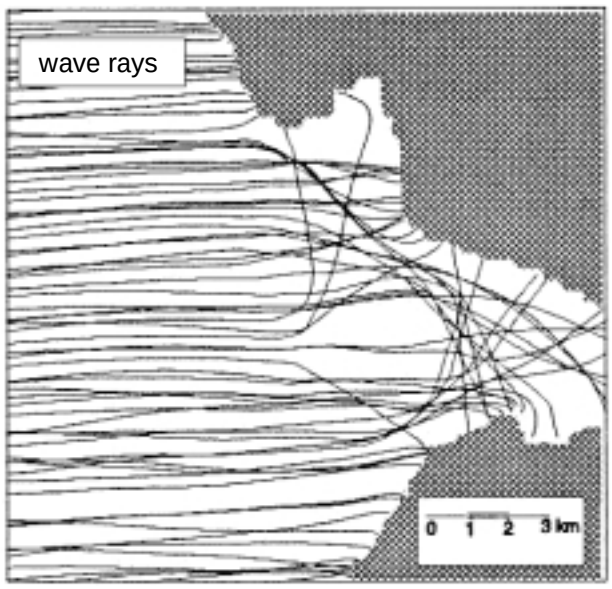

(*c*)

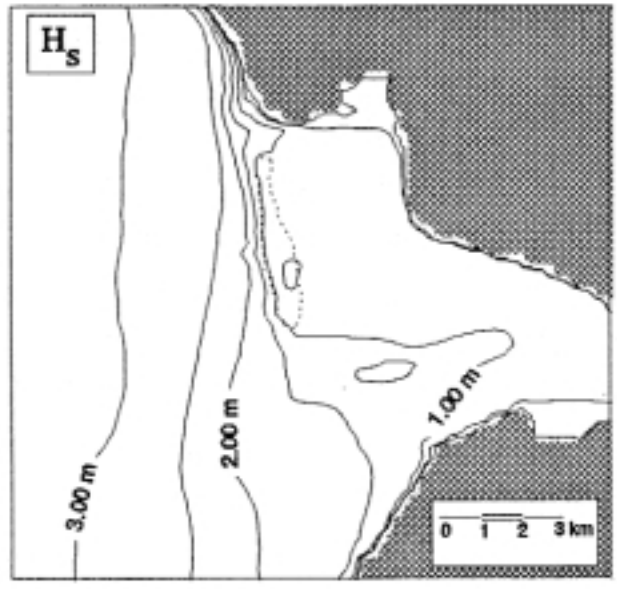

Figure 7.2 —
(*a*) The bathometry of the Haringvliet branch of the Rhine estuary (the Netherlands), (*b*) The wave ray pattern for the indicated harmonic wave entering the Haringvliet, and (*c*) The significant wave height computed with the shallow water spectral wave model SWAN (no triad interactions; Ris et al., 1994) (*courtesy Delft University of Technology*)

the rays from a given location in shallow water to deeper water in a fan of directions. The corresponding relationship between the shallow water direction of the ray and its deep water direction provides the wave height estimate in shallow water (Dorrestein, 1960). This technique avoids the caustic problem by an inherent smoothing over spectral directions.

With either of the above techniques it is relatively simple to calculate the change in wave height for a harmonic wave. A proper calculation for a random, short-crested sea then proceeds with the combination of many such harmonic waves and the inclusion of wave generation and dissipation. The spectrum of such a discrete spectral model is more conveniently formulated in wavenumber (***k***) space. This has the advantage that the energy density, moving along a wave ray with the group velocity, is constant (Dorrestein, 1960). Generation and dissipation can be added as sources so that the energy balance moving along the wave ray with the group velocity c_g is (for stationary and non-stationary conditions):

$$\frac{\mathrm{d}E(\boldsymbol{k})}{\mathrm{d}t} = S(\boldsymbol{k},u,h)\ . \qquad (7.9)$$

This is exploited in the shallow water model of Cavaleri and Rizzoli (1981). However, non-linear effects such as bottom friction and non-linear wave-wave interactions are not readily included in such a Lagrangian technique. An alternative is the Eulerian approach where it is relatively simple to include these effects. This technique is fairly conventional in deep water, as described in Section 5.3. However, in shallow water the propagation of waves needs to be supplemented with refraction. The inclusion of refraction in an Eulerian discrete spectral model is conceptually not trivial. In the above wave ray approach, a curving wave ray implies that the direction of wave propagation changes while travelling along the ray. In other words, the energy transport continuously changes direction while travelling towards the coast. This can be conceived as the energy travelling through the geographic area and (simultaneously) from one direction to another. The speed of directional change c_θ, while travelling along the wave ray with the group velocity, is obtained from the above generalized Snell's law:

$$c_\theta = -\frac{c_g}{c}\frac{\partial c}{\partial n}. \qquad (7.10)$$

To include refraction in the Eulerian model, propagation through geographic x — and y — space (accounting for rectilinear propagation with shoaling) is supplemented with propagation through directional space:

$$\frac{\partial E(\omega,\theta)}{\partial t} + \frac{\partial\left[c_x E(\omega,\theta)\right]}{\partial x} + \frac{\partial\left[c_y E(\omega,\theta)\right]}{\partial y} + \frac{\partial\left[c_\theta E(\omega,\theta)\right]}{\partial \theta} = S(\omega,\theta,u,h). \qquad (7.11)$$

In addition to the above propagation adaptations, the source term in the energy balance requires some adaptations in shallow water too. The deep water expressions of wind generation, whitecapping and quadruplet wave-wave interactions need to be adapted to account for the depth dependence of the phase speed of the waves (WAMDI Group, 1988; Komen et al., 1994) and some physical processes need to be added. The most important of these are bottom friction (e.g. Shemdin et al., 1980), bottom induced wave breaking (e.g. Battjes and Janssen, 1978) and triad wave-wave interactions (e.g. Madsen and Sorensen, 1993). When such adaptations are implemented, the above example of a confused wave ray pattern becomes quite manageable (Figure 7.2).

7.4 Diffraction

The above representation of wave propagation is based on the assumption that locally (i.e., within a small region of a few wavelengths) the individual wave components behave as if the wave field is constant. This is usually a good approximation in the open sea. However, near the coast, that is not always the case. Across the edges of sheltered areas (i.e. across the "shadow" line behind obstacles such as islands, headlands, rocks, reefs and breakwaters), rapid changes in wave height occur and the assumption of a locally constant wave field no longer holds. Such large variations may also occur in the absence of obstacles. For instance, the cumulative effects of refraction in areas with irregular bathometry may also cause locally large variations.

In the open sea, diffraction effects are usually ignored, even if caustics occur. This is usually permissible because the randomness and short-crestedness of the waves will spatially mix any caustics all over the geographic area thus diffusing the diffraction effects. This is also true for many situations near the coast, even behind obstacles (Booij et al., 1992).

However, close behind obstacles (i.e. within a few wavelengths) the randomness and short-crestedness of the waves do not dominate. Moreover, swell is fairly regular and long-crested, so the short-crestedness and the randomness are less effective in diffusing diffraction effects. The need for including diffraction in wave models is therefore limited to small regions behind obstacles and to swell-type conditions and mostly concerns the wave field inside sheltered areas such as behind breakwaters and inside harbours (see, for example, Figure 7.3).

For harmonic, unidirectional incident waves, a variety of diffraction models is available. The most illustrative model is due to Sommerfeld (1896) who computed the penetration of unidirectional harmonic waves into the area behind a semi-infinite screen in a constant medium (see also Chapter 5 of Mei, 1989). Translated to water waves, this means that the water depth should be constant and the screen is interpreted as a narrow breakwater (less than a wavelength in width). Sommerfeld considers both incoming waves and

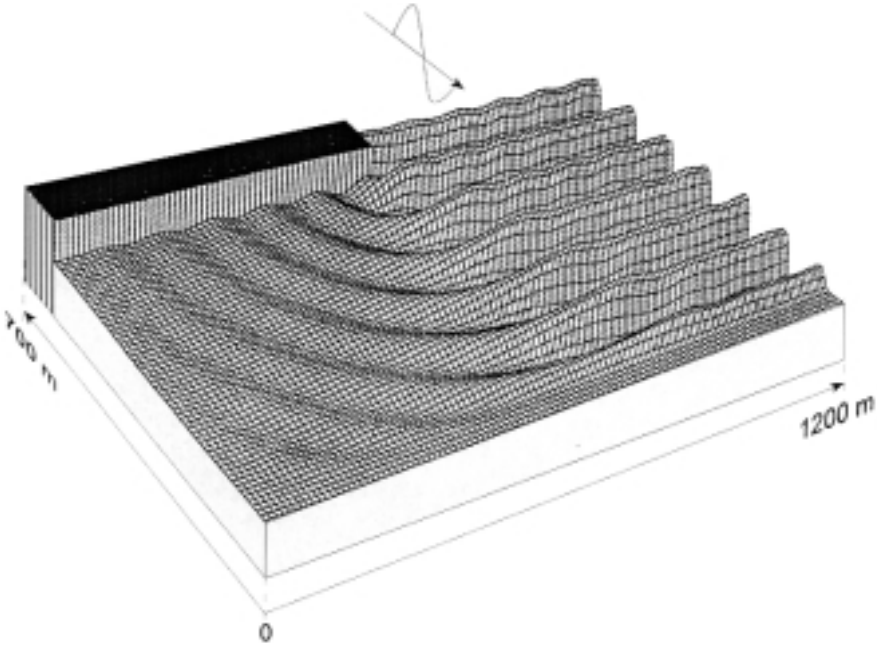

Figure 7.3 — The diffraction of a harmonic wave behind a breakwater (*courtesy Danish Hydraulic Institute*)

reflected waves, although the latter are usually negligible. In that case the technique can be readily illustrated with Huygens' principle. Each point on a crest is the source of a new wave on the down-wave side. If the waves are undisturbed, the next down-wave crest can be constructed from the point sources on the seaward crest. When the wave propagation is interrupted by an obstacle, the down-wave crests are constructed only from those seaward point sources that *can* radiate beyond the obstacle (along straight lines). This technique of reconstructing diffraction has been transferred into a graphical technique (the Cornu spiral, Lacombe, 1965). Graphs for standard situations are available to use for rough estimates (e.g. CERC, 1973; Wiegel, 1964).

A joint theory for refraction and diffraction (for cases with an uneven sea-bed) is available in the mild-slope equation of Berkhoff (1972). The key assumption for mild slope is that depth variations are gradual but horizontal variations in wave characteristics may be rapid, as in refraction (see for example, Section 3.5 of Mei, 1989). The Berkhoff equation is a generalization of the Helmholtz equation which is the basis of the above Sommerfeld solution. However, the computational demands are rather severe in terms of computer capacity and an approach based on the full mild-slope equation is of practical use only for small areas with dimensions of a few wavelengths (Booij et al., 1992).

The mild-slope equation includes the effects of wave reflections (e.g. from steep bottom slopes and obstacles). For waves that approach a coast with mild slopes, the reflection may often be neglected, usually implying that only the wave height variations along the wave crest are relevant (and not the variations in the wave direction). This provides a computational option (the parabolic approach) in which the solution is obtained simultaneously for all points along a line more or less aligned with the wave crests. The solution then moves down-wave through a succession of such lines. This approach saves considerable computer capacity, so it is suitable for substantially larger areas than the full mild-slope equation. It has been implemented in numerical models in which also the effects of currents, wind and dissipation due to bottom friction and bottom induced breaking have been included (Vogel et al., 1988).

The mild-slope equation, and its parabolic simplification, is expressed in terms of wave height variations. It has not been formulated in terms of energy density and, until such a formulation is developed, diffraction cannot be incorporated into the spectral energy-balance equation.

A somewhat more general approach than the mild-slope equation is provided by the Boussinesq equation (e.g. Abbott et al., 1978). The basic assumption of a harmonic wave is not required and the random motion of the sea surface can be reproduced with high accuracy (e.g. Schäffer et al., 1992) except for plunging breakers. However, this approach has the same limitations as the mild-slope equation (suitable only for small areas) and it too is not suitable for solving the spectral energy balance.

7.5 Wave growth in shallow waters

In situations with moderate variations in the wave field (therefore at some distance from the coast, or in the idealized case of a constant wind blowing perpendicularly off a long, straight coast over water with uniform depth), the frequency spectrum of the waves seems to have a universal shape in shallow water in the same sense as it seems to have in deep water (where the Pierson-Moskowitz and the JONSWAP spectra have been proposed, see Section 1.3.9). The assumption of a k^{-3} spectral tail in the wavenumber spectrum (Phillips, 1958) leads, in deep water, to the corresponding f^{-5} tail in the Pierson-Moskowitz and JONSWAP spectra. The same assumption in shallow water leads to another shape of the frequency tail, as the dispersion relationship is

different. For very shallow water the result is an f^{-3} frequency tail. This assumption has lead Bouws et al. (1985) to propose a universal shape of the spectrum in shallow water that is very similar to the JONSWAP spectrum in deep water (with the f^{-5} tail replaced with the transformed k^{-3} tail). It is called the TMA spectrum.

The evolution of the significant wave height and the significant wave period in the described idealized situation is parameterized from observations in deep and shallow water with the following formulations:

$$H^* = A\tanh\left(\kappa_3 h^{*m_3}\right)\tanh\left[\frac{\kappa_1 X^{*m_1}}{\tanh\left(\kappa_4 h^{*m_4}\right)}\right]$$

$$T^* = 2\pi B\tanh\left(\kappa_4 h^{*m_4}\right)\tanh\left[\frac{\kappa_2 X^{*m_2}}{\tanh\left(\kappa_4 h^{*m_4}\right)}\right], \quad (7.12)$$

where dimensionless parameters for significant wave height, H^*, significant wave period, T^*, fetch, X^*, and depth, h^*, are, respectively: $H^* = gH_s/u^2$, $T^* = gT_s/u$, $X^* = gX/u^2$, $h^* = gh/u^2$ (fetch is the distance to the upwind shore). The values of the coefficients have been estimated by many investigators. Those of CERC (1973) are:

$A = 0.283$	$B = 1.2$		
$\kappa_1 = 0.0125$	$\kappa_2 = 0.077$	$\kappa_3 = 0.520$	$\kappa_4 = 0.833$
$m_1 = 0.42$	$m_2 = 0.25$	$m_3 = 0.75$	$m_4 = 0.375$

Corresponding growth curves are plotted in Figure 7.4.

7.6 Bottom friction

The bottom may induce wave energy dissipation in various ways, e.g., friction, percolation (water penetrating the bottom) wave induced bottom motion and breaking (see below). Outside the surf zone, bottom friction is usually the most relevant. It is essentially nothing but the effort of the waves to maintain a turbulent boundary layer just above the bottom.

Several formulations have been suggested for the bottom friction. A fairly simple expression, in terms of the energy balance, is due to Hasselmann et al. (1973) in the JONSWAP project:

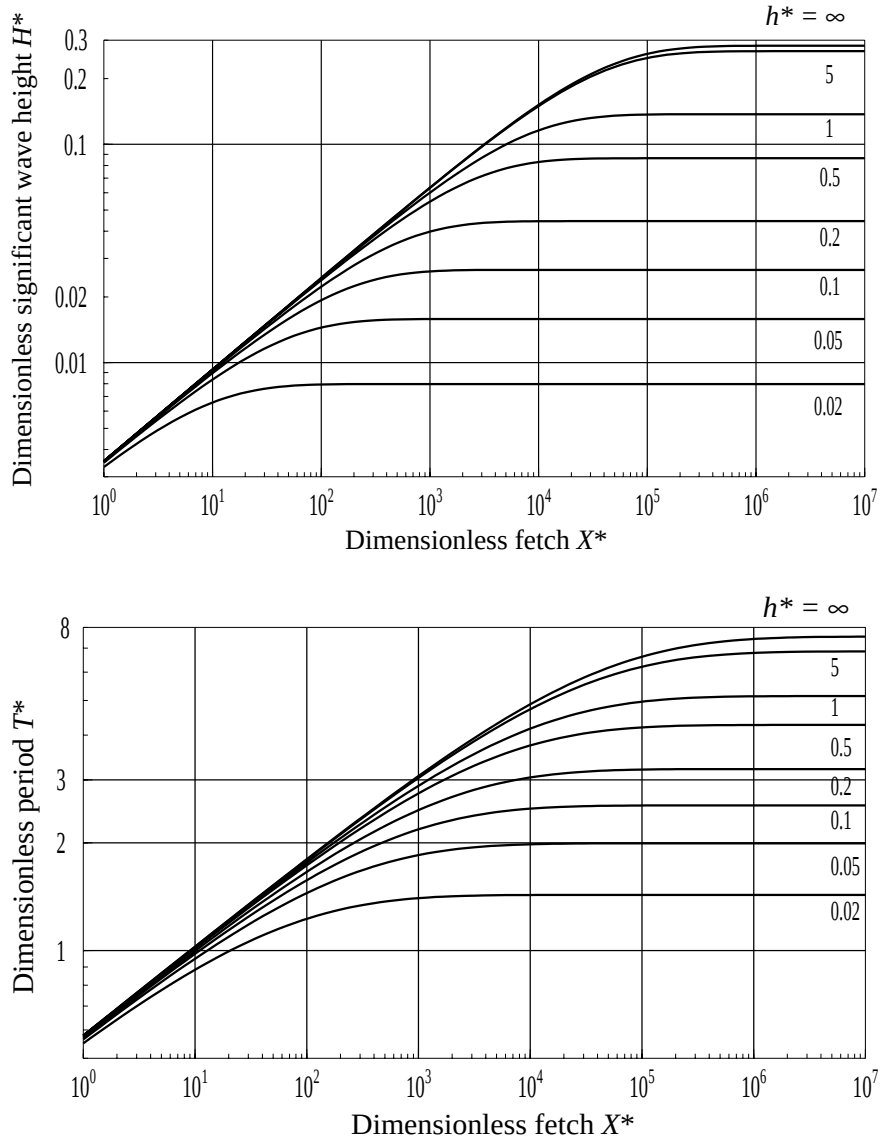

Figure 7.4 — Shallow water growth curves for dimensionless significant wave height (upper) and period (lower) as functions of fetch, plotted for a range of depths

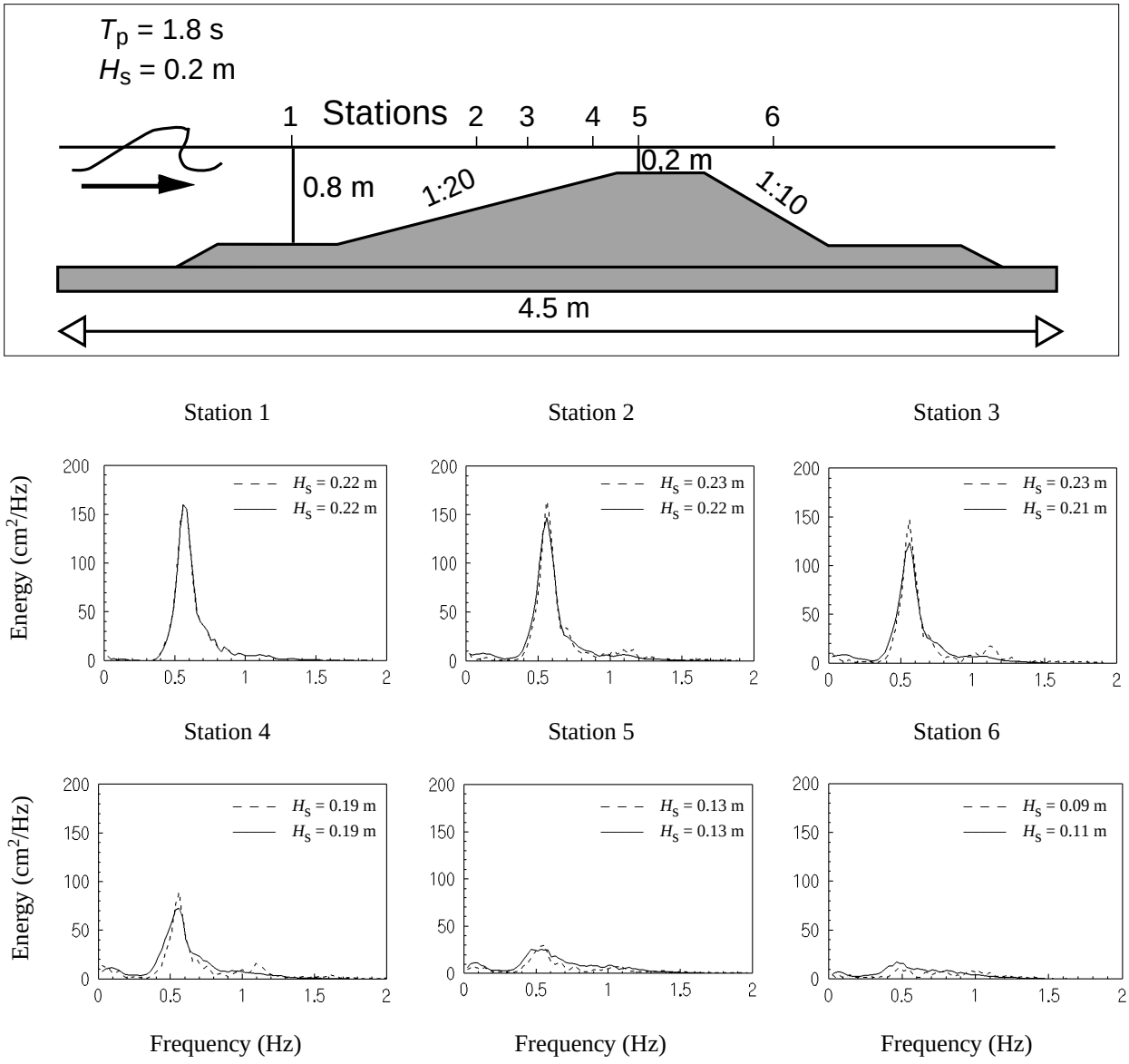

Figure 7.5 — Comparison of spectral observations and computations of wave breaking over a bar in laboratory conditions. Solid lines indicate the computations and dashed lines the experiment (Battjes et al., 1993) (courtesy: *Delft University of Technology*)

$$S_{\text{bottom}}(\omega,\theta) = -\Gamma \frac{\omega^2}{g^2 \sinh kh} E(\omega,\theta), \quad (7.13)$$

where Γ is an empirically determined coefficient. Tolman (1994) shows that this expression is very similar in its effects to more complex expressions that have been proposed.

7.7 Wave breaking in the surf zone

When a wave progresses into very shallow water (with depth of the order of the wave height), the upper part of the wave tends to increase its speed relative to the lower part. At some point the crest attains a speed sufficiently high to overtake the preceding trough. The face of the wave becomes unstable and water from the crest "falls" along the forward face of the wave (*spilling*). In extreme cases the crest falls freely into the trough (*plunging*). In all cases a high-velocity jet of water is at some point injected into the area preceding the crest. This jet creates a submerged whirl and in severe breaking it forces the water up again to generate another wave (often seen as a continuation of the breaking wave). This wave may break again, resulting in an intermittent character of the breaker (Jansen, 1986).

Recent investigations have shown that the overall effect of very shallow water on the wave spectrum can be described with two processes: bottom induced breaking and triad interaction. The latter is the non-linear interaction between three wave components rather than four as in deep water where it is represented by the quadruplet interactions of Section 3.4.

The breaking of the waves is of course very visible in the white water generated in the surf zone. It appears to be possible to model this by treating each breaker as a bore with a height equal to the wave height. The

dissipation in such a bore can be determined analytically and, by assuming a certain random distribution of the wave heights in the surf zone, the total rate of dissipation can be estimated. This model (e.g. Battjes and Janssen, 1978) has been very successful in predicting the decrease of the significant wave height in the surf zone.

The effect of triad interactions is not as obvious but, when wave records are analysed to show the spectral evolution of the waves in the surf zone, it turns out that, in the case of mild breaking, a second (high-frequency) peak evolves in the spectrum. In that case the waves transport energy to higher frequencies with little associated dissipation. This second peak is not necessarily the second harmonic of the peak frequency. In cases with more severe breaking, the transport to higher frequencies seems to be balanced by dissipation at those frequencies as no second peak evolves (while the low frequency part of the spectrum continues to decay). In either case numerical experiments have shown that these effects can be obtained by assuming that the dissipation is proportional to the spectral energy density itself.

The evolution of the waves in the surf zone is extremely non-linear and the notion of a spectral model may seem far-fetched. However, Battjes et al. (1993) have shown that a spectral triad model (Madsen and Sorensen, 1993), supplemented with the dissipation model of Battjes and Janssen (1978) and the assumption that the dissipation is proportional to the energy density, does produce excellent results in laboratory conditions, even in high-intensity breaking conditions (Figure 7.5). The source term for breaking in the spectral energy balance, based on Battjes and Janssen (1978), is then:

$$S_{\text{breaking}}(\omega,\theta) = -\alpha \frac{Q_b \,\overline{\omega}\, H_m^{\,2}}{8\pi} \frac{E(\omega,\theta)}{E_{\text{total}}}, \quad (7.14)$$

in which α is an empirical coefficient of the order one, $\overline{\omega}$ is the mean wave frequency, Q_b is the fraction of breaking waves determined with

$$\frac{1-Q_b}{\ln Q_b} = -8\frac{E_{\text{total}}}{H_m^{\,2}}, \quad (7.15)$$

H_m is the maximum possible wave height (determined as a fixed fraction of the local depth) and E_{total} is the total wave energy.

The triad interactions indicated above have not (yet) been cast in a formulation that can be used in a spectral energy balance. Abreu et al. (1992) have made an attempt for the non-dispersive part of the spectrum. Another more general spectral formulation is due to Madsen and Sorensen (1993) but it requires phase information.

7.8 Currents, set-up and set-down

Waves propagate energy and momentum towards the coast and the processes of refraction, diffraction, generation and dissipation cause a horizontal variation in this transport. This variation is obvious in the variation of the significant wave height. The corresponding variation in momentum transport is less obvious. Its main manifestations are gradients in the mean sea surface and the generation of wave-driven currents. In deep water these effects are usually not noticeable, but in shallow water the effects are larger, particularly in the surf zone. This notion of spatially varying momentum transport in a wave field (called "radiation stress"; strictly speaking, restricted to the horizontal transport of horizontal momentum) has been introduced by Longuet-Higgins and Stewart (1962) with related pioneering work by Dorrestein (1962).

To introduce the subject, consider a normally incident harmonic wave propagating towards a beach with straight and parallel depth contours. In this case the waves induce only a gradient in the mean sea surface (i.e. no currents):

$$\frac{\mathrm{d}\overline{\eta}}{\mathrm{d}x} = -\frac{1}{\rho_w g\left(h+\overline{\eta}\right)} \frac{\mathrm{d}\,M_{xx}}{\mathrm{d}x}, \quad (7.16)$$

where h is the still-water depth, $\overline{\eta}$ is the mean surface elevation above still-water level and M_{xx} is the shoreward transport (i.e. in x-direction) of the shoreward component of horizontal momentum:

$$M_{xx} = (2\,\beta - 0.5)\,E\,, \quad (7.17)$$

where $E = \rho_w g H^2/8$ and $\beta = {}^1/_2 + kh/\sinh(2kh)$.

Outside the surf zone the momentum transport tends to increase slightly with decreasing depth (due to shoaling). The result is a slight lowering of the mean water level (set-down). Inside the surf zone the dissipation is strong and the momentum transport decreases rapidly with decreasing depth, causing the mean sea surface to slope upward towards the shore (set-up). The maximum set-up (near the water line) is typically 15– 20 per cent of the incident RMS wave height, H_{rms}.

In general waves cause not only a shoreward transport of shoreward momentum M_{xx} but also a shoreward transport of long-shore momentum M_{xy}. Energy dissipation in the surf zone causes a shoreward decrease of M_{xy} which manifests itself as input of long-shore momentum into the mean flow. That input may be interpreted as a force that drives a long-shore current. For a numerical model and observations, reference is made to Visser (1984). In arbitrary situations the wave-induced set-up and currents can be calculated with a two-dimensional current model driven by the wave-induced radiation stress gradients (e.g. Dingemans et al., 1986).

CHAPTER 8

WAVE DATA: OBSERVED, MEASURED AND HINDCAST

J. Ewing with D. Carter: editors

8.1 Introduction

Wave data are often required by meteorologists for real-time operational use and also for climatological purposes. This chapter discusses the three types of wave data that are available, namely, observed, measured and hindcast. Sections 8.2 and 8.3 deal with visual wave data. Section 8.4 is a brief description of instruments for wave measurement and includes a discussion of the measurement of wave direction. Section 8.5 contains a review of remotely-sensed data which are becoming of increasing importance in real-time and climatological applications. These new data sources have made possible the assimilation of real data into wave modelling procedures, and an introduction to this subject is given in Section 8.6. The analysis of measured data records is briefly considered in Section 8.7 and some of the repositories for wave data are indicated in Section 8.8.

8.2 Differences between visual and instrumental data

Although the simplest method to characterize waves is to make visual observations of height and period, this produces data which are not necessarily compatible with those from instrumental measurements.

It is generally accepted that visual observations of wave height tend to approximate to the significant wave height (see definitions in Section 1.3.3). Although there are several formulae which have been used to convert visual data to significant wave height more accurately, for almost all practical meteorological purposes it is unlikely to be worth the transformation.

Visually observed wave periods are much less reliable than instrumentally observed ones, as the eye tends to concentrate on the nearer and steeper short-period waves, thereby ignoring the longer-period and more gently sloping waves, even though the latter may be of greater height and energy. This can be seen by examination of joint probability plots (scatter diagrams) of visually observed wave period and height. In many of these the reported wave period is so short that the steepness (height to length ratio) is very much higher than is physically possible for water waves. It is almost certainly the wave period which is in error, not the height.

8.3 Visual observations

Waves are generally described as either sea (wind sea) or swell; in this context, sea refers to the waves produced by the local wind at the time of observation, whereas swell refers either to waves which have arrived from elsewhere or were generated locally but which have subsequently been changed by the wind.

Useful visual observations of wave heights can be made at sea from ships. Visual observations from land is meaningful only at the observation site because the waves change dramatically over the last few hundred metres as they approach the shore, and the observer is too far away from the unmodified waves to assess their characteristics. Shore-based observations normally apply only to that particular location and although relevant to a study of local climatology they are rarely meaningful for any other meteorological purpose.

Mariners, by the very nature of their work, can be regarded as trained observers. The observation of waves is part of their daily routine, and a knowledge of changes in sea and swell is vitally important for them, since such changes affect the motion of the ship (pitching, rolling and heaving) and can be the cause of late arrivals and structural damage.

The observer on a ship can usually distinguish more than one wave train, make an estimate of the height and period of each train and give the directions of wave travel. Waves travelling in the same direction as the wind are reported as sea; all other trains are, by definition, swell (although mariners often refer to well-developed seas in long fetches, such as in the “trade winds”, as swell). To a coastal observer, waves usually appear to approach almost normal to the shore because of refraction.

8.3.1 *Methods of visual observation*

Visual observations should include measurement or estimation of the following characteristics of the wave motion of the sea surface in respect of each distinguishable system of waves, i.e. sea and swell:

(*a*) Height in metres;
(*b*) Period in seconds;
(*c*) Direction *from which* the waves *come*.

There may be several different trains of swell waves. Where swell comes from the same direction as the sea, it may sometimes be necessary to combine the two and report them as sea. The following methods of observing characteristics of separate wave systems should be used as a guide.

Figure 8.1 is a typical record drawn by a wave recorder and is representative of waves observed on the sea (see also Figures 1.14 and 1.15). However, it cannot indicate that there are two or more wave trains or give any information on direction. It shows the height of the

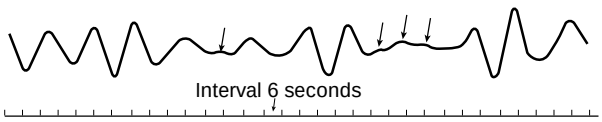

Figure 8.1 — Example of a wave record. In an analysis the waves marked with arrows are ignored

sea surface above a fixed point plotted against time, i.e. it represents the up-and-down movement of a floating body on the sea surface as it is seen by the observer, and is included to illustrate the main difficulty in visually observing height and period — the irregularity of the waves. The pattern shown is typical of the sea surface, because waves invariably travel in irregular groups of perhaps five to 20 waves with relatively calm areas in between groups.

It is essential that the observer should note the height and period of the higher waves in the centre of each group; the flat and badly formed waves (marked with arrows) in the area between the groups must be entirely omitted. The analysis should therefore include:

- Height and period: that is the mean height and period of about 15–20 well-formed waves from the centres of the groups; of course all these waves cannot be consecutive;
- Wave direction: the direction *from which* the waves *come* should be noted, and reported to the nearest 10° on the scale 01–36, as for wind direction. For example, waves arriving from the west (270°) should be reported as direction 27. Where more than one wave train is clearly identifiable, the direction as well as an observed height and period should be reported for each such train.

The observer must bear in mind that *only good estimates are to be reported*. Rough guesses will have little value, and can even be worse than no estimate at all. The quality of observations must have priority over their quantity. If only two, or even one, of the three elements (height, period, direction) can be measured, or really well estimated (e.g. at night), the other element(s) could be omitted and the report would still be of value.

When different wave trains — for example sea and swell or several swells — are merged, the heights do not combine linearly. Wave energy is related to the square of the wave height and it is the energy which is additive. Consequently, when two or more wave trains are combined, the resultant height is determined from the square root of the sum of the squares of the separate trains:

$$H_{\text{combined}} = \sqrt{H_{\text{sea}}^2 + H_{\text{swell}}^2}\ . \qquad (8.1)$$

More than one swell train can be combined if necessary.

The following possible systematic errors in the observation of waves should be borne in mind by an observer:

(*a*) Waves running against a current are steeper and usually higher than when in still water, while they are lower when running with the current. Observers may not necessarily be aware of this in a given case;

(*b*) Refraction effects due to bottom topography in shallow water may also cause an increase or decrease in wave height;

(*c*) Waves observed from a large ship seem smaller than those same waves observed from a small ship.

8.3.1.1 *Observations from merchant ships*

A traditional source of wave information has been from so-called ships of opportunity. Given the lack of surface-based measurements of waves on the open ocean, the coverage offered by merchant shipping has been utilized in the WMO Voluntary Observing Ship (VOS) Programme. The participating ships report weather information including visual observations of waves. The guidelines for making these observations are set down in the WMO *Guide to meteorological instruments and methods of observation* (WMO, 1996, see Part II, Chapter 4).

HEIGHT

With some experience, fairly reliable estimates of height can be made. To estimate heights of waves which have relatively short lengths with respect to the length of the ship, the observer should take up a position as low down in the ship as possible, preferably amidships, where the pitching is least violent, and on the side of the ship from which the waves are coming. Observations should be made during the intervals, which occur every now and then, when the rolling of the ship temporarily ceases.

In the case of waves longer than the ship, the preceding method fails because the ship as a whole rises over the wave. Under these circumstances, the best results are obtained when the observer moves up or down in the ship until, when the ship is in the wave trough, the oncoming waves appear just level with the horizon. The wave height is then equal to the height of the eye of the observer above the level of the water beneath him. By far the most difficult case is that in which the wave height is small and the wavelength exceeds the length of the ship. The best estimate of height can be obtained by going as near to the water as possible, but even then the observation can only be approximate.

An observer on a ship can often distinguish waves coming from more than one direction. Wave characteristics from each direction must be reported separately; only the waves under the influence of the local wind (i.e. of the same direction as the local wind) are termed sea, the others are, by definition, swell and should be reported as such. Sometimes it is possible to distinguish more than one swell train, and each such wave train should be reported separately as swell.

PERIOD AND DIRECTION

Period and direction can be reported as outlined in Section 8.3.1. The period of waves can often be estimated by watching a patch of foam or other floating

matter and timing the intervals between successive crests passing by. It is necessary to do this for a number of waves, as many as is convenient and preferably at least ten, to form a good average value.

8.3.1.2 *Observations from coastal stations*

HEIGHT AND PERIOD

At coastal stations, it is important to observe the height and period of waves at a spot where they are not deformed either by the wave being in very shallow water (i.e. of a depth only a low multiple of the wave height), or by the phenomenon of reflection. This means that the spot chosen for observations should be well outside the breaker zone; not on a shoal or in an area where there is a steep bottom gradient, nor in the immediate vicinity of a jetty or steep rocks which could reflect waves back on to the observation point. The observation point should be fully exposed to seaward, i.e. not sheltered by headlands or shoals.

Observations are generally more accurate if a fixed vertical staff with some form of graduated markings can be used to judge the height of passing waves. Observing an object on the surface, such as a floating buoy, may also improve estimation.

If the observations are to be of use for wave research it is important that:

(*a*) They should always be taken at the same place, so that correction for refraction, etc. can be applied later;

(*b*) The exact mean depth of water at the place and time of observation should be known, so that corrections for change of height with depth can be applied later.

It is worth repeating here that, as for observations from ships, only the well-developed waves in the centres of the groups should be chosen for observation. The flat and badly formed waves between the groups should be entirely omitted, both from height and period observations. The mean height and period of at least 20 waves, chosen as above and hence not necessarily consecutive, should be noted.

DIRECTION

Coastal observations of wave direction are only meaningful at that particular location. If the user does not realize that the data were obtained at a site where shallow water has a major effect, i.e. refraction, his interpretation of the report could be erroneous. This problem is described more extensively in Chapters 1 and 7 (see also Figures 1.6, 1.7 and 1.8 which illustrate some effects in the coastal zone).

8.4 Instruments for wave measurements

Many different techniques are used for the measurement of sea waves. There is no universal instrument suitable for all wave measurements. An instrument used at one location may be entirely inappropriate at another position. Furthermore, the type of instrument to be deployed depends on the application for which the wave data is required. For example, the design of breakwaters at the coast depends on the properties of the longer waves or swell while the motions of small ships are influenced by short, steep seas. Care must therefore be taken in the choice of instrument. Finally, the chosen instrument must be capable of being readily deployed and have a good prospect of giving a high return of wave data for climatological purposes over at least one year.

8.4.1 ***Types of instrument***

Wave measurement techniques can be grouped into three categories:

(*a*) Measurements from below the sea surface;

(*b*) Measurements at the sea surface;

(*c*) Measurements from above the sea surface.

8.4.1.1 *Wave measurements from below the surface*

Systems to measure waves from below the surface have an advantage in that they are not as vulnerable to damage as systems on the surface. However, there are problems in bringing the data ashore as cable is expensive and can be damaged. An alternative technique is to transmit the information by radio from a buoy moored nearby.

Pressure transducers are most often used in shallow water (< 15 m) but have also been mounted below the surface on offshore platforms in deep water. Here the change in pressure at the sensor is a measure of wave height. A pressure spectrum at the measurement depth can be derived from the pressure signal using spectral analysis. The measured pressures must be corrected for hydrodynamic attenuation with depth. For this purpose linear wave theory (see Section 1.2) is used (although there is evidence that the correction it gives is too small). One-dimensional wave spectra and associated parameters such as significant wave height can then be calculated. The attenuation has the effect of filtering out the shorter wavelengths, but for most practical applications the loss of high frequency wave information is not a disadvantage. However, if the water depth is greater than about 10–15 m, the attenuation affects too much of the frequency range and the correction factors become very large, diminishing the value of the data.

Inverted echo sounders on the sea-bed can also be used in shallow water. The travel time of the narrow beam of sound is directly related to wave elevation and gives a measurement without depth attenuation. In severe seas, however, the sound beam is scattered by bubbles from breaking waves making the measurements unreliable.

8.4.1.2 *Wave measurements at the sea surface*

In shallow water, where a platform or structure is available, it is possible to obtain wave measurements at the sea surface by using resistance or capacitance wave staffs. The wave elevation is then directly related to the

change in resistance or capacity of the wave staff. Wave staffs can however be easily damaged by floating objects and are subject to fouling by marine growth.

In deep water, surface-following wave buoys are used. In these systems, the vertical acceleration is measured by means of an accelerometer mounted on a gyroscope (or partially stabilized platform). Wave height can then be inferred from the measured acceleration by standard methods. (Since vertical acceleration is the double time differential of the surface elevation, the essence of the processing is a double time integration of the acceleration.) The buoys are carefully moored so that their motions are not greatly influenced by the mooring. The most widely used system of this type is the Datawell "Waverider". Data can be recorded internally on board the buoy and transmitted to a nearby shore station or, over larger distances, transmitted by satellite.

A Shipborne Wave Recorder (SBWR) has been developed to obtain wave information from measurements of the motion of a stationary vessel or lightship. In these systems pressure recorders mounted below the surface in the hull on both sides of the ship give measurements of the waves relative to the ship. Accelerometers in the ship measure the vertical motion of the vessel. After calibration, the sum of the signals from the pressure sensors and the accelerometers give an estimate of the motion of the sea surface, from which the wave height and period are derived. The SBWR is a robust system which is not as vulnerable as a buoy and is also able to give wave information in extreme sea conditions, although the measurement accuracy is generally not quite as good as a Waverider buoy.

For more information on analysis of such data see Section 8.7.

8.4.1.3 *Measurements from above, but near, the surface*

Waves can be measured from above the surface by downward-pointing laser, infra-red, radar or acoustic instruments if a suitable platform is available. However, some offshore platforms can significantly modify the wave field by refraction, diffraction and sheltering. Care must be taken in siting the instruments to minimize these effects. For "jacket" type structures, a rough guide is that the measurement "footprint" on the sea surface should be located more than ten leg-radii away from the platform leg. Advantages with this type of instrument are that they are non-intrusive (that is, they do not disturb the flow), and can be easily mounted and maintained.

Comprehensive intercomparisons between these same instruments and buoys have shown that for significant wave height, maximum wave height and various wave periods, there is no detectable difference (Allender et al., 1989). However, in recent years, much interest has been shown by the offshore industry in accurately specifying the observed asymmetry of high waves, since this affects the design of offshore structures. The extreme crest height (distance from mean water level to the wave crest) turns out to be significantly greater than half the maximum wave height (Barstow, 1995; Vartdal et al., 1989). Generally, downlooking instruments seem to measure higher crests than buoys do, but the reasons for this are not yet resolved.

Commonly used instruments of the downlooking, non-intrusive type include the EMI and Schwartz lasers and Saab and Marex (Plessey) radar. The radar instruments generally measure over a larger footprint on the ocean surface, but are less able to measure high frequency (short) waves.

The subject of remote sensing from large distances is discussed in Section 8.5.

8.4.2 ***Wave direction***

Various methods are available for measuring the directional wave spectra at sea, on offshore installations and at the coast. The most common systems for routine data collection are various types of wave buoy (Section 8.4.2.1) which are still the major source of data in deep water, away from offshore platforms. Satellite synthetic aperture radar (SAR) measurements (see Section 8.5.5) show some promise, but the data are collected along the satellite orbit and are therefore only sporadically available at any fixed location.

If a platform is available several other options are possible including direct sub-surface measurements and remote sensing (Sections 8.4.2.2, 8.4.2.3 and 8.5.3).

8.4.2.1 *Directional buoys*

At present the most commonly used directional wave measuring system is Datawell's Directional Waverider. This buoy measures the acceleration (doubly integrated to give displacement) in the vertical and two horizontal directions. Time series data over typically 30 minutes are then analysed on board the buoy to compute directional wave spectra using similar techniques to the heave/pitch/roll buoy. The latter measures the vertical acceleration and two components of the surface slope. The Directional Waverider buoy has been available since 1989 and various intercomparison studies have since been made against conventional heave/pitch/roll buoys and platform instruments (O'Reilly et al., 1995; Barstow and Kollstad, 1991). The consensus is that, at least in deep water, the Directional Waverider provides more accurate estimates of the directional wave spectrum than conventional buoys.

A comprehensive intercomparison of commercially available heave/pitch/roll buoys and platform-based directional wave systems was carried out in the mid-1980s (Allender et al., 1989). However, only one of these systems remains on the market today, Seatex's Wavescan buoy (which also includes a meteorological station). Datawell's Wavec is still apparently available but has largely been superseded by the Directional Waverider. An alternative to the Wavescan is Oceanor's Seawatch buoy, a multi-sensor marine environmental monitoring buoy which can incorporate

a Directional Waverider (Barstow et al., 1994(*a*)), and of which there are about 25–30 operational worldwide. In the USA, NOAA operates a number of directional buoys in its extensive measurement network, including large 6–20 m heave/pitch/roll buoys and a smaller 3 m system operated closer to the coast. The large buoys from which the UKOOA (United Kingdom Offshore Operators Association) acquired directional wave data also used the heave/pitch/roll system. For further information on systems presently in use refer to Hamilton (1990, presently under revision) and WMO (1985, 1991, 1994(*a*)). For more on analysis of these data see Section 8.7.2.

8.4.2.2 *Arrays of wave recorders*

Arrays of recorders can provide directional detail and have been used in several oceanographic and engineering studies. The degree of directional resolution depends on the number of wave recorders and their spacing. The types of instruments which can be used include wave staffs (Donelan et al., 1985) and pressure transducers (O'Reilly et al., 1995). Wave directional information collected from such systems are usually site specific as the recorded waves are influenced by refraction and dissipation in shallow water. The arrays can be either mounted on an offshore platform or bottom mounted in shallow water if the depth does not exceed 10–15 m. Similarly, pressure transducer arrays on offshore platforms should not be located deeper than 10–15 m below the surface because of depth attenuation of the surface wave signature.

8.4.2.3 *Current meters*

Ultrasonic or electromagnetic current meters which measure the two horizontal components of wave orbital velocity in conjunction with a pressure recorder or wave staff can provide useful directional information. These systems are usually deployed in shallow water but can also be mounted on offshore platforms, provided the influence of the platform is not too great. These systems are directly analogous to the Directional Waverider or pitch/roll buoy system discussed in Section 8.4.2.1. Perhaps the most well-known, self-contained instrument of this type is the "S4" current meter. Also commonly used is the "UCM-40" current meter.

8.5 Remote sensing from large distances

In general, conventional wave recorders measure the displacement with respect to time of the water surface at a fixed point. Remote-sensing techniques (E. D. R. Shearman, 1983) are not able to measure in this way. Instead they interrogate an area or footprint which, in the case of satellite-borne sensors, has typical dimensions of several kilometres (except synthetic aperture radar, which can have a footprint of a few tens of metres) and report some measure of the average wave conditions over the whole area. Surface-based radars also can have a range resolution of a few metres, smaller than the wavelengths of the gravity waves being measured, although the footprint is still broad in azimuth. In consequence, low-resolution sensors are rarely used for coastal or shallow water sites, because the wave field there can vary considerably over distances of much less than one kilometre. The strength of remote sensing is that equipment can usually be kept in a safe place well away from the ravages of the sea and be readily accessible for maintenance and testing.

The satellite is the most spectacular mounting for a sea-wave sensor. It is an extremely powerful tool and can obtain vast quantities of oceanic wave data worldwide.

Wave measurements made using remote sensing generally use active microwave sensors (radar), which send out electromagnetic waves. Deductions about wave conditions are made from the return signal. Before considering individual sensors, some features of the interaction between electromagnetic waves and the sea surface will be discussed.

8.5.1 *Active sensing of the ocean surface with electromagnetic waves*

If we consider a radar sending energy directly down towards a level, glassy, calm sea surface, the energy will be reflected from a small region directly below the radar as if from a mirror. If now the surface is perturbed by waves, a number of specular reflections (glints) will arise from facets within the radar beam and perpendicular to it — essentially from horizontal facets for a narrow beam radar (see Figure 8.2).

Now consider a radio beam pointing obliquely at the sea surface at a grazing angle Δ as in Figure 8.3. If the sea wavelength, λ_s, is scaled to the radar wavelength, λ_r, as shown, backscattered echoes returning to the radar from successive crests will all be in phase and reinforced. The condition for this "Bragg resonant scatter" is:

$$\lambda_s \cos\Delta = \frac{\lambda_r}{2}. \qquad (8.2)$$

In the real sea, there will be a mix of many wavelengths and wave directions, and the Bragg resonance mechanism will select only those waves approaching or

Figure 8.2 — A radar altimeter normally incident on a rough sea, illustrating the different path lengths for energy reflected from facets (*from Tucker, 1991*)

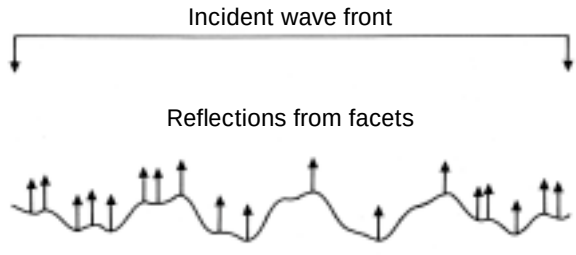

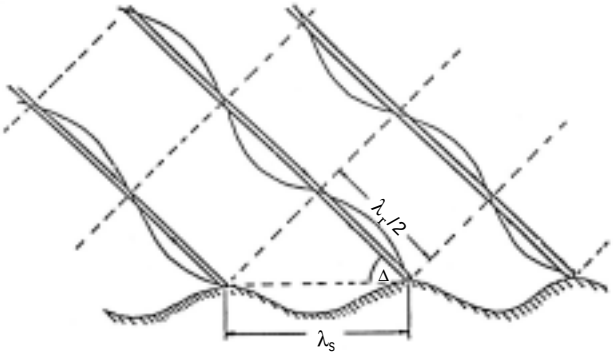

Figure 8.3 — Bragg diffraction of radio waves from a sinusoidal sea-wave. Conditions for constructively interfering backscatter from successive crests (*after E. D. R. Shearman, 1983*)

receding from the radar and of the correct wavelength. For a microwave radar these would be ripples of a few centimetres. However, the mechanisms illustrated in Figure 8.4 ensure that the longer waves influence (modulate) the ripples, by:

(*a*) "Straining" (stretching and compressing the ripples by the orbital motion of the long waves), accompanied by velocity modulation;

(*b*) Tilting the surface on which the ripples move and so modifying the Bragg resonance condition through Δ in Equation 8.2; and

(*c*) Hydrodynamic interaction, which concentrates on the leading edge of long waves, or through the perturbed wind flow over the long-wave crests, both of which produce a roughness modulation.

A radar observing backscatter from short waves by these mechanisms sees exhibited, in the spatial variation of backscatter intensity and in the Doppler spectrum, a representation of the long waves.

Figure 8.4 — Mechanisms of spatial modulation by long gravity waves of radar scattering from capillary waves (*a*) Straining and velocity modulation of short wind waves by longer wind waves and swell; (*b*) Tilt modulation; and (*c*) Roughness modulation (*after E. D. R. Shearman, 1983*)

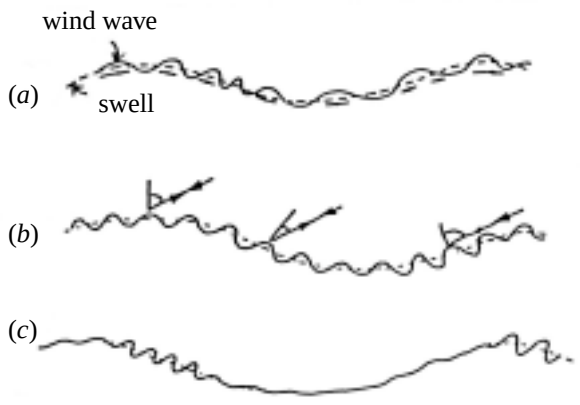

8.5.2 *Radar altimeter*

The higher the waves then, as indicated in Figure 8.2, the greater the time between the arrivals of returns from the crests and from the troughs of the waves, and the more spread out is the return pulse. From our knowledge of the statistics of the sea surface, this stretching of the shape of the return pulse can be related quantitatively to the variance of the sea surface, and hence to the significant wave height H_{m0} (using the spectral definition — see Section 1.3.8). Satellite altimeters usually have a pulse rate of 1 000 Hz; estimates of H_{m0} are derived on board and values averaged over one second are transmitted. Theoretically, there should be no need to calibrate these values, but in practice it has been found necessary to do so, comparing them with buoy measurements (Carter et al., 1992).

Radar altimeters give near-global coverage and hence provide wave height data for almost anywhere on the world's oceans, including areas where data were previously very scarce. Four long-term satellite altimeter missions have so far made global measurements. These are GEOSAT (1985–89), ERS-1 (1991–), ERS-2 (launched April 1995) and Topex/Poseidon (1992–). Raw data from each of these missions can be obtained from the responsible space agencies. Fast delivery data from the ERS satellites are also available in near-real time (see also Section 6.4). Note that these data can be significantly biased compared to reference buoy data and should therefore be corrected before use. From these data world maps of significant wave height can be produced, see, for example, Chelton et al. (1981), and Challenor et al. (1990) and the example in Figure 8.5. In addition, specialized products are available from a number of commercial companies (e.g. Oceanor in Norway, Satellite Observing Systems in the UK).

The strength of the return pulse is also dependent upon the statistics of the sea surface which are affected by the wind speed over the surface. So there is a relationship between the strength of the return pulse and the wind speed, but this relationship is complex and not fully understood. In general the stronger the wind, the lower the strength of the return. Various algorithms have been derived from observations which give estimates of wind speed at 10 m above the sea surface from the strength of the altimeter return, but further work needs to be done to determine which is the most accurate, see, for example, Witter and Chelton (1991) and the recent studies based on the Topex/Poseidon data (Freilich and Challenor, 1994; Lefevre et al., 1994).

8.5.3 *Oblique platform-mounted sensors*

An interesting sensor for measurements at fixed sites, using the phenomena shown in Figure 8.4 to measure wave characteristics, is the Norwegian MIROS microwave wave radar (Grønlie et al., 1984), which uses an oblique 6 GHz (5 cm wavelength) beam and a radar range resolution of 7.5 m. The velocity of ripples is

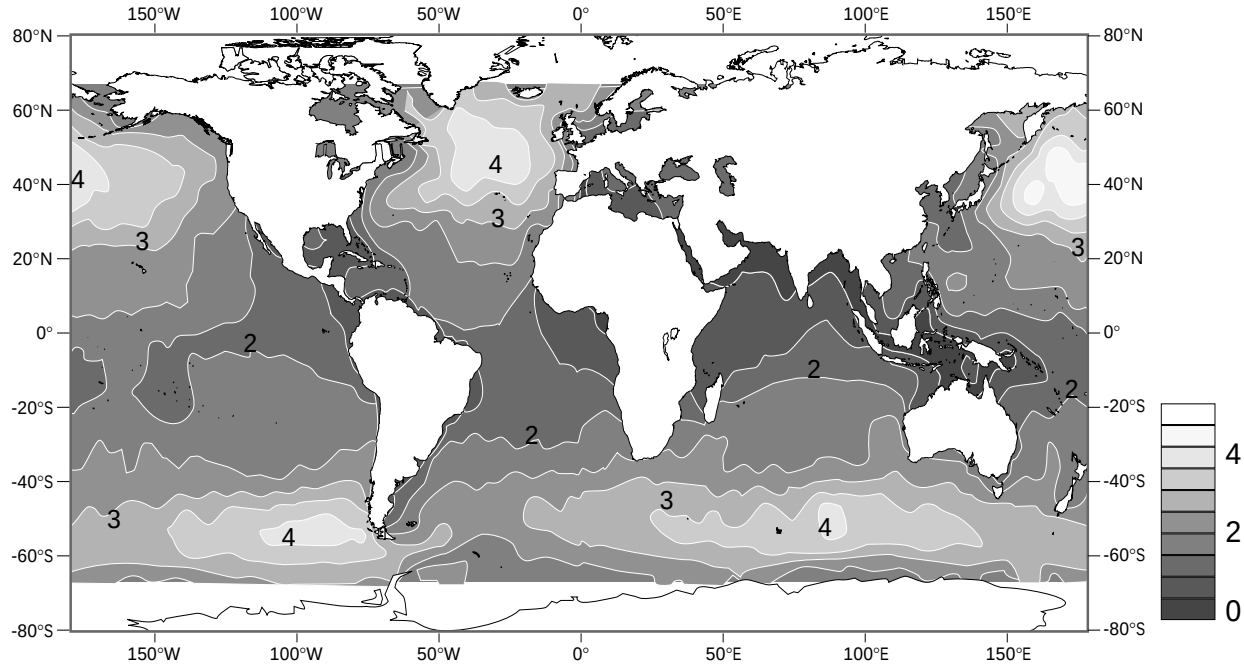

Figure 8.5 — Mean significant wave height (in metres) for the period January–March 1996 from the Topex altimeter (*courtesy D. Cotton, Southampton Oceanography Centre*)

small compared with that of the long wavelength of interest, so that the radial velocity measured by the radar Doppler shift is dominantly due to the orbital motion of the long waves. By analysis of the fluctuation of the observed Doppler shift, the spectrum of the waves travelling along the radar beam is deduced. Directional wave spectrum measurements are achieved by making measurements in 6 different directions (using a steerable beam) for a claimed wave-height range 0.1–40 m and period 3–90 s.

8.5.4 *The satellite scatterometer*

The satellite-borne scatterometer (Jones et al., 1982) is another oblique-looking radar sensor. The total echo power from its radar beam footprint is used to estimate wind speed, and the relative return power from different look directions gives an estimate of the wind direction, because the small-scale roughness of the sea surface, seen by the radar, is modulated by the longer wind waves. Calibration is achieved by comparison with near-surface wind measurements. The scatterometer does not give information about the waves, except for the direction of the wind waves, but its estimates of wind velocity and hence estimates of wind stress on the sea surface are proving to be very useful inputs to wave models, particularly in the Southern Ocean where few conventional measurements are made.

8.5.5 *Synthetic aperture radar (SAR)*

Practical aircraft and satellite-borne antennas have beam widths too large to permit wave imaging. In the synthetic aperture technique, successive radar observations are made as the aircraft or satellite travels horizontally. Subsequent optical or digital processing produces narrow focused beams and high-grade imaging of the longer waves, as evidenced by the variation of the radar-echo intensity ("radar brightness") produced by the mechanisms shown in Figure 8.4. Figure 8.6(*a*) shows an example from SEASAT of wave imagery and Figure 8.6(*b*) shows a wave directional spectrum (with 180° ambiguity) achieved by analysis of an image. Figure 8.7 shows a high resolution scene in north-western Spain taken from the ERS-1 SAR.

SAR has the advantage of being a broad-swath instrument, with swath width and resolution of about 100 km and 25 m, respectively. However, the physical processes underlying its imaging of waves are complex and still not universally agreed. The main difficulty in interpreting the images of ocean waves is that the sea surface is not at rest, as assumed by the synthetic processor, and the orbital velocities of the longer waves, which transport the ripples responsible for backscattering the radar waves, are around 1 m/s. This results in a highly non-linear effect which can lead to a complete loss of information on waves travelling in the along-track direction. Moreover, waves of length less than about 100 m travelling in any direction are not imaged by the SAR — because of smearing and decrease in the signal-to-clutter ratio.

Thus SAR is more likely to provide useful data in the open ocean rather than in enclosed seas such as the North Sea where wavelengths tend to be less than 100 m, but even in mid-ocean the waves can sometimes be so short that the SAR will fail to "see" them.

Given the directional wave spectrum, it is then possible to obtain a good estimate of the spectrum from

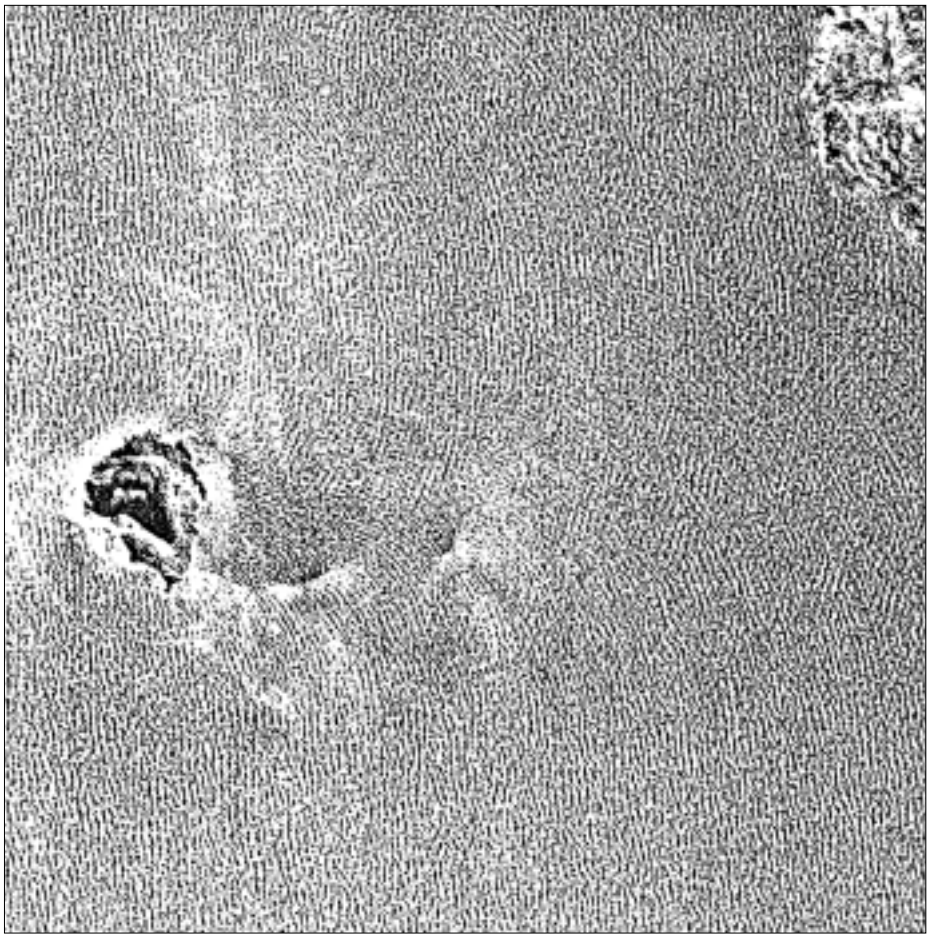

Figure 8.6(*a*) (*left*) — SEASAT SAR image of the wave field between the Islands of Foula and Shetland (*ESA photograph, processed at the Royal Aircraft Establishment, United Kingdom*)

Figure 8.6(*b*) (*below*) — Examples of directional wave-energy spectrum derived by digital processing of SEASAT synthetic aperture radar data. The five levels of greyness indicate spectral amplitude, while the distance from the centre represents wavenumber ($2\pi/\lambda$). The circles are identified in wavelength. A 200 m swell system is shown coming from ESE and broader spread 100 m waves coming from ENE. The analysis has an 180° ambiguity (*after Beale, 1981*)

the SAR image. Our problem is to go the other way: to derive the directional wave spectrum given the SAR image. Research has shown that if a global wave model is run to provide an initial estimate of the wave spectrum, then the difference between the observed SAR spectrum and that estimated from the model spectrum can be used to correct the model spectrum and hence to improve the wave model output (Hasselmann et al., 1991).

A practical problem with SAR, which tends to inhibit its use, is the vast quantity of data it produces (108 bits per second) and the consequent cost of processing and acquiring the data. Moreover, these data cannot be stored on board the satellite, so SAR data can only be obtained when the satellite is in sight of a ground receiving station. An exception to this is the ERS-1 which obtains a small SAR image, with a footprint of 5 x 5 km, every 200 km. These "wave vignettes" can be stored on board and transmitted later to ground.

8.5.6 *Microwave radiometry*

As well as reflecting incident radio waves, the sea radiates thermal radio noise as a function of its temperature and emissivity; this radiation can be detected by a microwave radiometer (analogous to an astronomer's radio telescope). The emissivity varies with surface roughness, amount of foam and, to a small extent, with salinity. Thus the signal received at the antenna is mainly

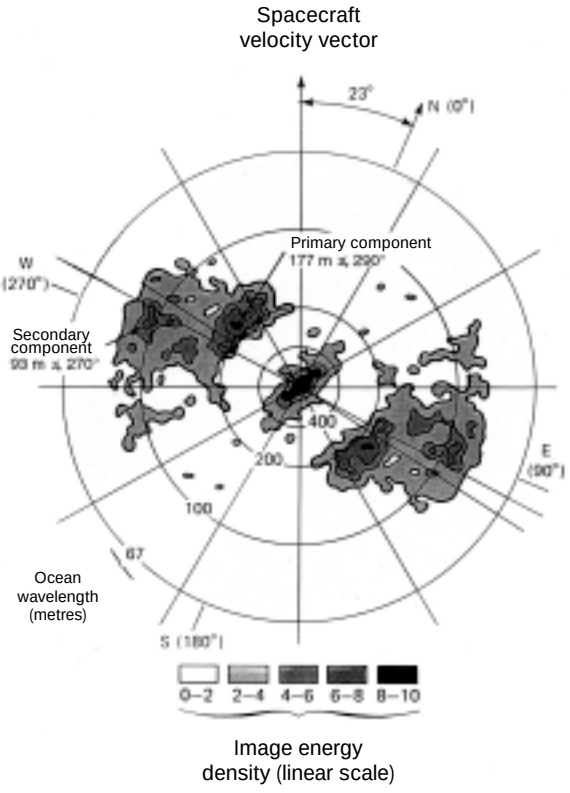

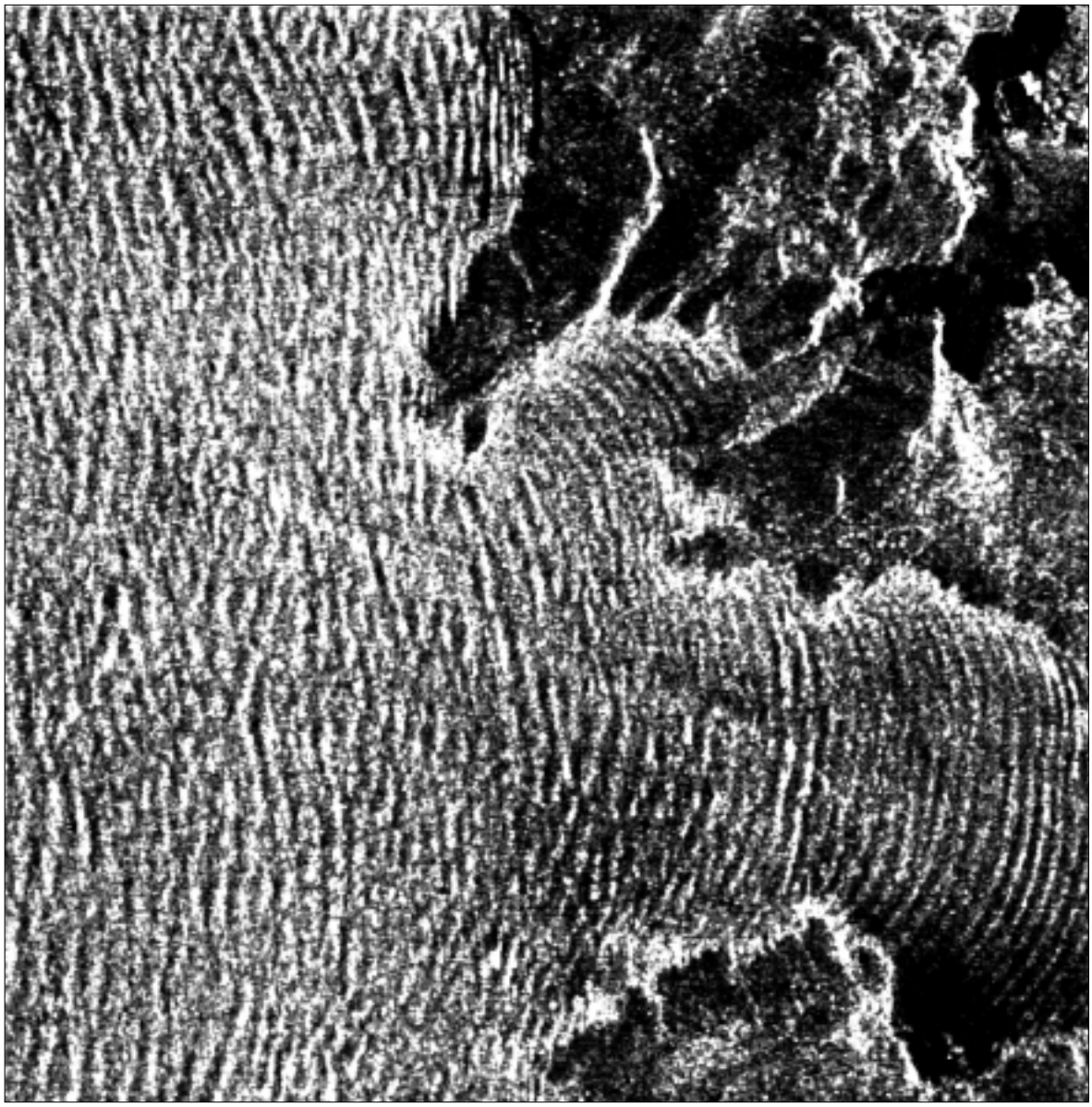

Figure 8.7 — ERS-1 SAR sub-scene acquired on 17 January 1993 by the ESA station in Fucino, Italy. The image shows the entrance to the Ria de Betanzos (Bay of La Coruña), north-western Spain. The image represents an area of 12.8 x 12.8 km. An east-southeast swell (i.e. travelling from west-northwest) enters the bay and the waves are diffracted as they travel through the narrower opening of the bay. However, waves do not enter the very narrow northern Ria de El Ferrol. The inner part remains wind and wave sheltered and therefore dark. As the waves get closer to the shore their length becomes shorter, as can be observed near the coast to the north. The long linear feature through the middle of the image is probably linked to a strong current shear, not usually visible in such a sea state (*image copyright: ESA; J. Lichtenegger, ERS Utilisation Section, ESA/ESRIN, Frascati*)

a combination of sea-surface temperature and wind effects, modified by atmospheric absorption and emission due to water vapour and cloud liquid water. Since the sensitivity to each of these parameters is frequency dependent, a multichannel radiometer can be used to separate them.

The sea-surface temperature data complement infra-red values in that they can be obtained through cloud, though with less accuracy and poorer spatial resolution. Wind speed can be derived over a broader swath than from the present satellite scatterometer, but no estimate of wind direction is obtained.

8.5.7 *Ground-wave and sky-wave HF radar*

HF radar (employing the high frequency band, 3–30 MHz, wavelength 100–10 m), is of value because it is capable of measuring wave parameters from a ground station to ranges far beyond the horizon, utilizing the Doppler spectrum of the sea echo (E. D. R. Shearman 1983, Barrick and Gower 1986, Wyatt and Holden, 1994).

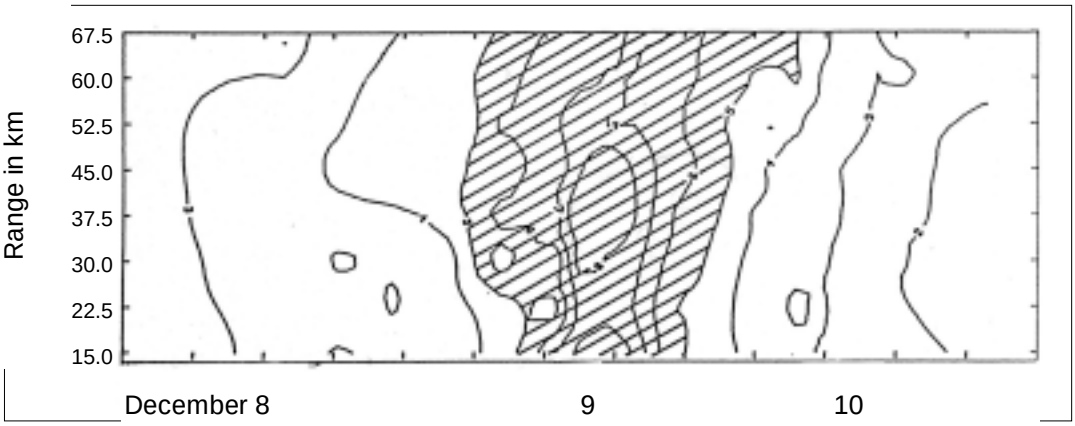

Figure 8.8 — Time history of significant wave height vs range, as measured by HF ground-wave radar (*after Wyatt et al., 1985*)

Ground-wave radars use vertically polarized radio waves in the HF band and must be located on a sea coast, island, platform or ship. Coverage of 0–200 km in range is achievable. The potential for continuous sea-state monitoring is shown in Figure 8.8. Recent work indicates that two stations some distance apart can triangulate on particular sea areas and can yield maps of directional spectra with a one-hour update.

Sky-wave radars are large installations, but can be located well back from the sea coast as they employ radio waves travelling by way of the ionosphere. Coverage extends from 900 to 3 000 km. Surface wind direction measurement is readily achieved, but ionospheric variability limits wave-height measurement (Barrick and Gower, 1986).

8.5.8 *Comparison of remote-sensing methods*

Platform-based microwave sensors fulfil a useful role for point measurement in environments where buoys are a hazard. HF ground-wave radars promise to provide maps of spatial-temporal wave spectra (if necessary, at hourly intervals), up to 200 km from the coast. Sky-wave radars extend coverage to oceanic areas, particularly for tracking fronts and hurricanes, but suffer ionospheric limitations (Georges and Harlan, 1994).

Satellite altimeters, scatterometers and radiometers provide worldwide coverage of wave height and surface wind for modest telemetry and processing overheads. Data close to coastlines can be suspect, either due to land in the sensor footprint or to a delay in the sensor switching from land to ocean mode as the satellite ground track moves from land to sea. Spatial and temporal coverage of the Earth is constrained by the satellite orbit. The satellite usually has an exact repeat cycle of between three and 35 days. The spacing between tracks is inversely proportional to the repeat cycle — from about 900 km (three-day cycle) to 80 km (35-day cycle) at the Equator. Satellite data are therefore particularly suitable for long-term wave climate studies, but they can also be incorporated, with other observations, into numerical forecast models or used for validating hindcast data.

Satellite synthetic aperture radars require expensive real-time telemetry and off-line processing. Difficulty is experienced in imaging waves travelling parallel to the satellite track and waves travelling in any direction if the wavelength is less than about 100 m. But research indicates that SAR data can be used with wave models to give improved estimates of directional wave spectra.

8.6 Wave data in numerical models

Wave models are being increasingly used, not only for predicting wave conditions a few hours or days ahead, but also for deriving wave climate statistics (see Section 9.6.2 *et seq.*). Wave data are needed to validate the models, and they have recently (since 1992) also been used in model initializations.

The assimilation of wave data into a model, re-initializing the model at each time step, can improve its performance, and considerable activity is under way to develop techniques for doing this. Satellite data, with their global coverage, are especially useful. Table 8.1 lists countries at present carrying out research into the assimilation of satellite data into wave models, and indicates those which are using the data in their operational wave models.

Data from the satellite altimeter are most readily and widely available, but the only wave parameter it measures is significant wave height. How best to incorporate this one value into a model's directional wave spectrum has been addressed in several studies and workable solutions found (see, for example, Thomas, 1988).

8.7 Analysis of wave records

Nowadays, most wave data are collected digitally for subsequent computer analysis. Data are commonly either transmitted from the measurement site by radio link or by satellite (e.g. via ARGOS), or recorded locally (e.g. on board a buoy). A number of systems are available for real-time presentation of data in the form of time series plots or statistical presentations. In addition to providing information suitable for operations, such systems also give an immediate indication of the correct functioning of the system. Traditionally, however, analysis was carried out by a manual technique based on analogue chart records (see also Section 1.3).

TABLE 8.1
On-going projects on the assimilation of remotely sensed data in ocean wave models
(R = Research project; O = Operational project (with starting date in brackets). Collated from responses to a WMO survey of Member states)

Members/ organizations	*Project status*	*Data*	*Data origin*	*Investigators*
Australia	R O R R/O	SAR Altimeter Scatterometer HF sky-wave radar	ERS-1 Jindalee	I. Jones G. Warren R. Seaman T. Keenan
Canada	R/O (1994)	SAR (wave mode)	Radarsat ERS-1/ERS-2	L. Wilson M. L. Khandekar R. Lalbeharry
ECMWF	R/O (1993)	SAR Altimeter	ERS-1 (Fast delivery products)	A. Guillaume
France	R	Altimeter	ERS-1 Topex-Poseidon	J. M. Lefèvre
Germany	R	SAR Altimeter	GEOSAT ERS-1	S. Hasselmann
Netherlands	R/O (1992)	Altimeter	ERS-1	G. Burgers V. Makin
Japan	R	SAR Scatterometer Altimeter Microwave-radiometer	GEOSAT ERS-1 Topex-Poseidon	H. Kawamura
New Zealand	R	Scatterometer Altimeter	GEOSAT ERS-1	A. Laing
Norway	R O	Altimeter SAR	ERS-1	M. Reistad
United Kingdom	R/O (1992)	Altimeter	ERS-1 (Fast delivery products)	S. Foreman
USA	R/O (1993)	SAR Scatterometer Altimeter	ERS-1	D. Esteva W. Gemmill

8.7.1 *Digital analysis of wave records*

Wave measurements are analysed over, typically, a 20- to 35-minute record with values of wave elevation sampled every 0.5–2 seconds. Measurements are then taken either continuously (for operational monitoring) or three-hourly for long-term data collection, although continuous measurements are becoming more standard. A preferred oil-industry standard for the measurement and analysis of wave data has been given by Tucker (1993).

The most commonly used wave analysis nowadays estimates the (directional) wave spectra (Section 1.3.7) using Fast Fourier Transform techniques and hence computes a standard set of wave parameters (e.g. H_{m0}, T_{m02}).

In the case of directional wave measurements, two additional parameters are commonly analysed and stored for future use. These are the mean wave direction, θ_1, the directional spread, σ, at each frequency of the wave spectrum (see, for example, Ewing, 1986) and associated directional wave parameters such as the wave direction at the spectral peak period. Full directional wave analysis in real time is also commonly available from commercial wave measuring systems.

8.7.2 *Manual analysis of chart records*

A rapid analysis of a 10-minute chart record, similar to that illustrated in Figure 8.1 (or Figure 1.14), can be made in the following widely-used manner. This was originally presented by Tucker in 1961, and is more widely available in Draper (1963) and interpreted by Draper (1966) for practical application.

Measure the height of the highest crest above the mean (undisturbed) water level, label this *A*. Measure the height of the second highest crest, *B*. Similarly, measure the depths of the lowest, *C*, and second lowest, *D*, troughs:

$$A + C = H_1 \qquad B + D = H_2.$$

The simplest estimate of the significant wave height (the average value of the height of the highest one-third of all the waves) is calculated from:

$$H_s = 0.625\, H_1 .$$

A second estimate can be obtained from:

$$H_s = 0.69\, H_2 .$$

The two results can be combined by taking the average.

The relationships between H_s, H_1 and H_2 depend slightly on the number of upcrossing waves. These expressions are for 100 waves or for a 10-minute record if $\overline{T}_z = 6$ s. See Tucker (1991) for further details.

8.8 Sources of wave data

We discuss the three types of wave data in turn.

8.8.1 *Visual observations*

Much of the visual wave information is derived from the observations made by WMO-recruited Voluntary Observing Ships under the WMO/VOS Programme. Many of the observations are reported in real time as part of the routine meteorological reports which are circulated internationally on the Global Telecommunication System. These reports use the WMO SHIP code (see the *Manual on codes*, WMO, 1995). The observations are also logged and conveyed through the Port Meteorological Officers to central repositories.

The National Oceanographic and Meteorological Services of many nations have such information on visual observations of waves (and winds) and can be approached in the first instance for data on observations in their own regions. The largest collections of worldwide visual observations are however maintained in the USA and the UK with information available from the following:

- National Climatic Data Centre/World Data Centre A – Meteorology,
  Federal Building, Asheville, NC 28801, USA.
- UK Meteorological Office, Marine Consultancy Service,
  Johnson House, Meteorological Office, London Road, Bracknell, Berkshire RG12 2SY, UK

An atlas, *Global wave statistics* was produced by British Maritime Technology, Ltd., in conjunction with the UK Meteorological Office, in 1986 (Hogben et al., 1986). This publication gives the annual and seasonal statistics of waves for 104 sea areas worldwide. A recent extension of the atlas has been made to include detailed information in European waters. See Hogben (1990) for further details. A PC version of the atlas is also available.

8.8.2 *Measured wave data*

In the 1970s, the Intergovernmental Oceanographic Commission (IOC) of UNESCO established a centre with the responsibility of identifying and cataloguing locations at which instrumental wave data had been obtained. A catalogue was published from time to time during the 1980s containing a summary of the data and its location. Until recently this service was provided by the UK through the British Oceanographic Data Centre (formerly the MIAS Data Banking Service). However, at present there is no centre responsible for maintaining and updating this information.

To facilitate reporting, exchange and archiving of measured wave data, WMO has developed the WAVEOB code. This enables a uniform format for wave spectra and is sufficiently flexible to cater for a variety of both directional and non-directional spectra. The details of this code are given in Annex II.

8.8.3 *Hindcast wave data*

Hindcast wave data from numerical wave models are produced operationally and archived by many major meteorological services. These centres should be first approached for wave data in their regions. Modelled data are also produced for special case studies by public and private organizations.

Chapter 9 of this Guide includes a useful catalogue of hindcast climatologies available at the present time (Section 9.6.2).

8.8.4 *Satellite wave data*

Satellite wave data with global coverage are now available from various sources. In raw form, data can be obtained from the space agencies. These data require considerable treatment before they can be used. Various national space agencies have, however, funded the work required to make these data more readily available. High-level altimeter wave data (sorted, quality controlled and corrected) can be provided from the GEOSAT, Topex/Poseidon and ERS-1 missions by the following institutions:

- OCEANOR, Pir-Senteret, N7005 Trondheim, Norway
  Fax: +47 73 52 50 33
  (Data also available on a PC MS-Windows application, World Wave Atlas)
- Satellite Observing Systems, 15 Church St, Godalming, Surrey GU7 1EL, United Kingdom
  Fax: +44 1483 428 691
  On the world wide web:
  http://www.satobsys.co.uk
- MeteoMer, Quartier des Barestes – RN7
  83480 Puget-sur-Agens, France
  Fax: +33 94 45 68 23

The GEOSAT data have also been presented in accessible form both as hard copy and on interactive CD-ROM in the *Atlas of oceans: wind and wave climate* by Young and Holland (1996).

CHAPTER 9

WAVE CLIMATE STATISTICS

D. Carter with V. Swail: editors

9.1 Introduction

Chapter 8 described methods of measuring waves and explained how to analyse the results to obtain estimates of values describing the sea state, such as the significant wave height. These estimates are usually obtained from records made routinely over 15–35 minutes at three-hour intervals. This chapter describes ways of analysing and presenting the results from such records collected over many months or years in order to give a description of the wave climate at the recording location. Other record lengths or intervals may be used; for example, measurements are sometimes made at hourly intervals. Some of the results may vary with the recording interval and it is advisable always to specify this interval when giving wave climate statistics.

This chapter first describes the relevant sea-state parameters and defines the term "return value" which is widely used to specify extreme environmental values for designing structures such as offshore oil platforms and sea defences. Methods of plotting wave data and statistical analyses of the data to illustrate the wave climate are briefly explained, together with the use of these plots to check for possible errors in the data. Various methods which have been developed over the years to estimate 50- and 100-year return values of wave heights are then outlined. Some publications recommended for further reading — in addition to the references cited — are listed and the chapter concludes with a section on wave climatologies and a description of the process of wave hindcasting (Section 9.6). Annex III to this *Guide* contains formulae for the statistical distributions used in this chapter.

9.2 Definitions

9.2.1 *Sea-state parameters*

The two parameters most widely used to describe sea state are the significant wave height, $\overline{H}_{1/3}$, and the mean zero-upcrossing or zero-downcrossing wave period, $\overline{T}_z$, or their spectral equivalents H_{m0} and T_{m02} defined in Section 1.3.8. The notations H_s and $\overline{T}_z$ are used throughout this chapter to represent both pairs of parameters — since the methods described are applicable to both.

High waves are often of particular importance, and another sea-state parameter which is commonly used is the height of the highest wave most likely to occur during a three-hour interval, $H_{max,3h}$. Its value may be estimated from H_s and $\overline{T}_z$ (see Section 1.3.6) assuming these values remain constant for three hours. $H_{max,3h}$ varies only slowly with $\overline{T}_z$ and is about 1.9 H_s. In recent years the height of the maximum wave crest (relative to mean water level) has been of great interest, particularly to the oil industry (interested readers can find more details in Barstow, 1995).

There are numerous measures of ocean wave period, but $\overline{T}_z$, which was originally chosen because it could readily be estimated from an analogue wave trace, remains the most popular for many applications.

9.2.2 *Return value of wave height*

Designers of structures which have to stand for many years need an estimate of the severest conditions likely to be experienced. The usual parameter chosen to describe such conditions is either the 50- or the 100-year return value of wave height, where the N-year return value is defined as that which is exceeded on average once every N years.

This definition assumes that wave climate will remain unchanged over 50 or 100 years, which is most unlikely. An alternative definition is the height with a probability of two or one per cent, respectively, of being exceeded by the highest wave during one year. This is equivalent to the above definition, except it does not allow for the very small probability that the rare 50- or 100-year event might occur more than once during a year.

Return value is a statistical parameter, and the engineer in his design has to allow for the possibility of a wave greater than say the 100-year return value, or even of several such waves, occurring within a few years. Nevertheless, the concept of return value as a design criterion has proved useful (but see, for example, Borgman, 1963, on risk analysis). The wave height specified for the return value can be either H_s or $H_{max,3h}$, or even the height of an individual wave. Much of the effort given to wave climate studies in recent years has concentrated upon methods for estimating return values of these parameters — see Section 9.4. Sometimes, the return value of wave crest elevation is also required in order to specify, for example, the base height of an oil platform. (Elevation is measured from mean sea level; wave height is measured from crest to trough — see Section 1.2.1.) Note that the maximum crest height is not half of H_{max}, as would be the case for a sinusoidal wave, because extreme waves tend to be quite asymmetric with typical values of crest to total wave height of around 0.6.

9.3

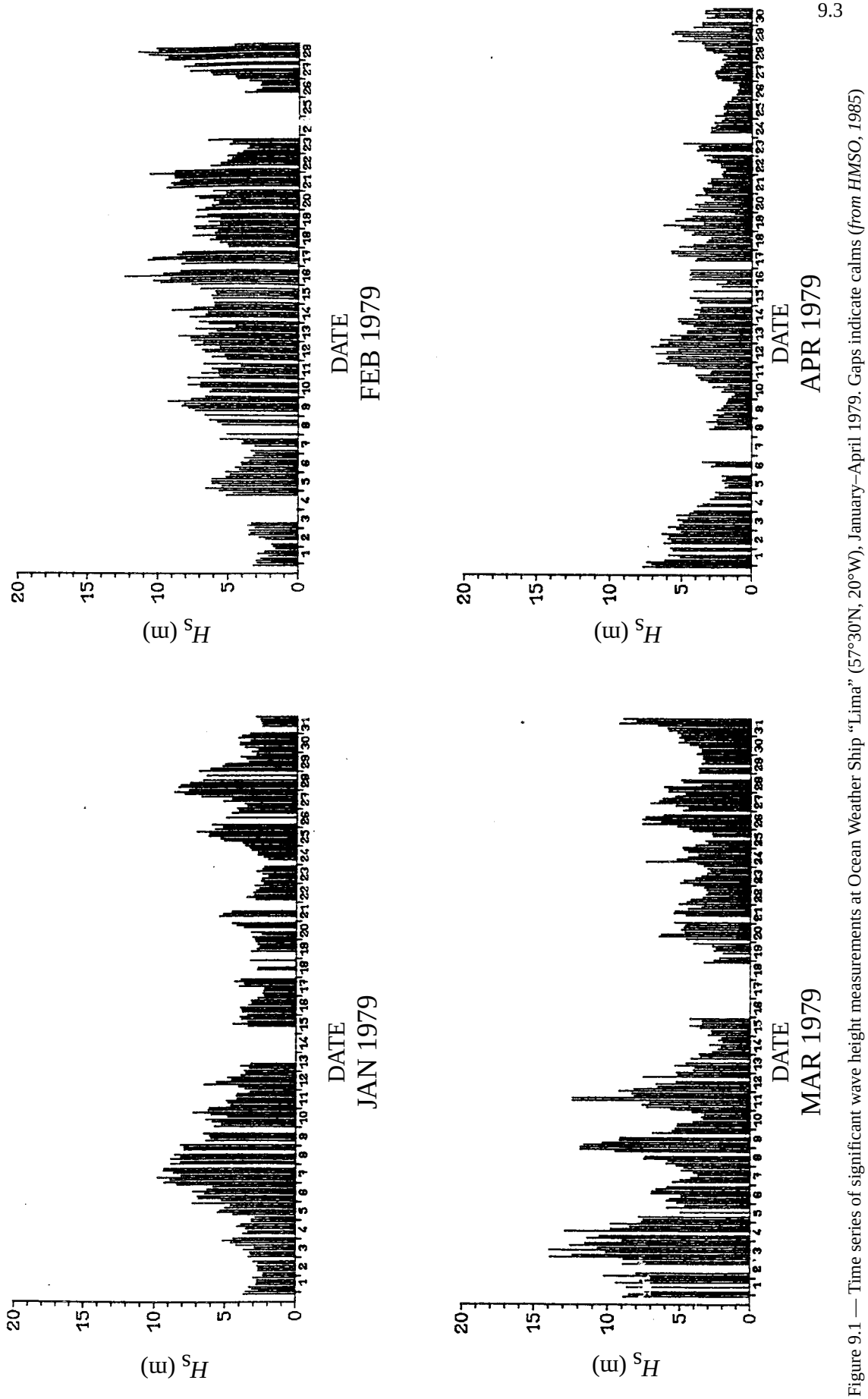

Figure 9.1 — Time series of significant wave height measurements at Ocean Weather Ship "Lima" (57°30'N, 20°W), January–April 1979. Gaps indicate calms (*from HMSO, 1985*)

Presentation of data and wave climate statistics

9.3.1 *Plot of the data*

Having obtained a data set of wave parameters over, say, a year, it is important to plot the results to obtain an overall view of the range of values, the presence of any gaps in the data and any outliers suggesting errors in the data, etc. Figure 9.1 shows an example, in the form of a "comb" plot, which provides a good visual impact.

9.3.2 *Plotting statistical distributions of individual parameters*

Estimates from the data set of the parameter's probability distribution can be obtained by plotting a histogram. Given, for example, $\overline{T}_z$ measurements for a year (2 920 values if a recording interval of three hours is used), then a count of the number of measurements $\overline{T}_z$ in, say, 0.5-s bins (i.e. 0.0–0.5 s, 0.5–1.0 s, ...) is made and estimates of the probability of a value in each bin is obtained by dividing the total in the bin by 2 920. Such a plot, as shown in Figure 9.2, is called a histogram. The bin size can, of course, be varied to suit the range of data — one giving a plot covering 5–15 bins is probably most informative. Note that a histogram or comb plot of the spectral peak period, T_p, may give additional information to a $\overline{T}_z$ plot. Over large expanses of the world's oceans long swells commonly coincide with shorter wind seas, leading to wave spectra which are bimodal (double-peaked form). Over a long measurement series the histogram distribution may also be bimodal.

Wave height data may also be presented in a histogram, but it is more usual to give an estimate of the cumulative probability distribution, i.e. the probability that the wave height from a randomly chosen member of the data set will be less than some specified height. Estimates are obtained by adding the bin totals for increasingly high values and dividing these totals by the number of data values. Sometimes, to emphasize the occurrence of high waves, the probability of waves greater than the specified height is plotted — see Figure 9.3.

9.3.3 *Plotting the joint distribution of height and period*

A particularly useful way of presenting wave climate data, combining both height and period data in one figure, is an estimate from the data of the joint distribution of H_s and $\overline{T}_z$ (often called the joint frequency table or scatter table). Data are counted into bins specified by height and period and the totals divided by the grand total of the data to give an estimate of the probability of occurrence. In practice — see for example Figure 9.4 — the estimates are usually multiplied by 1 000, thus expressing the probability in parts per thousand (‰), and rounded to the nearest whole number, but with a special notation to indicate the bins with so few values that they would be lost by rounding.

It is sometimes more convenient for further analysis to plot the actual bin totals. In any case, the grand total should be given with the scatter plot together with the number of calms recorded. It is also useful to draw on the scatter plot lines of equal significant steepness ($2\pi H_s/g\overline{T}_z^2$ — see Section 1.3.5). The line representing a significant steepness of one-tenth is particularly useful, since this seems in practice to be about the maximum value found in measurements from open waters. Any records indicating steeper waves should therefore be checked for possible errors.

9.3.4 *Checks on the data sets*

As mentioned above, the various plots of the data and the estimates from the data of probability distributions

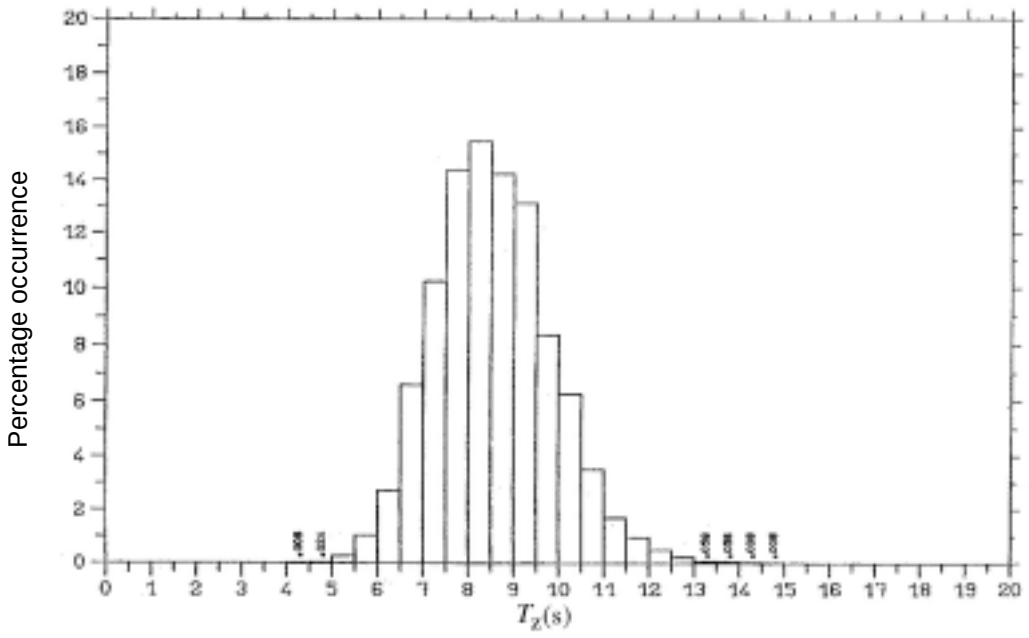

Figure 9.2 — Histogram of zero-upcrossing period measurements (12 520 valid observations, including six calms), at three-hour intervals at OWS "Lima", December 1975 to November 1981 (*from HMSO, 1985*)

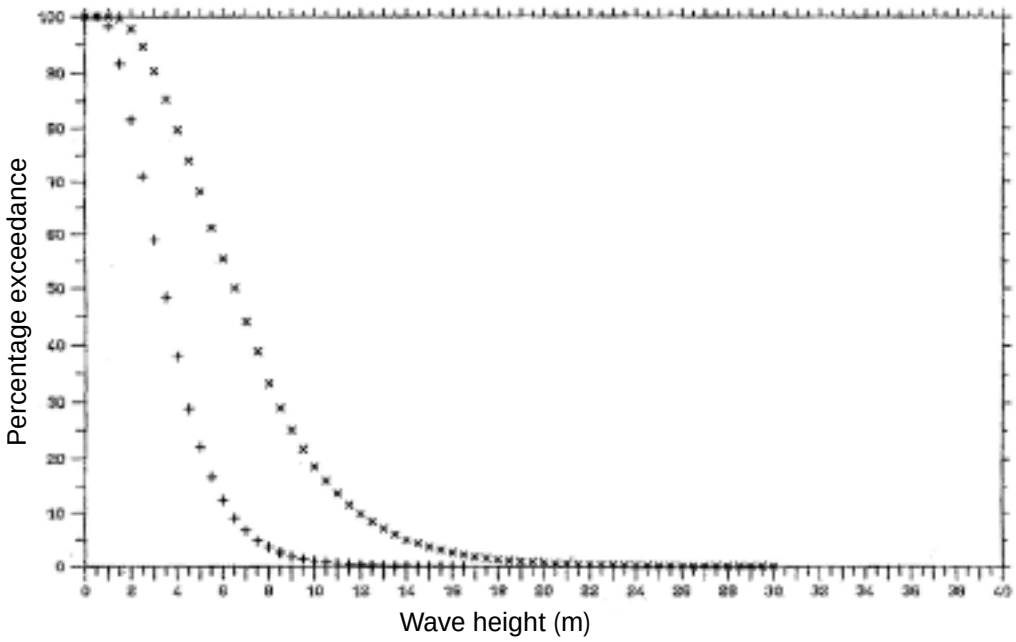

Figure 9.3 — Percentage exceedance of significant wave height, H_s, and the most likely highest wave in three hours, $H_{max,3h}$, from measurements (12 520 valid observations, including six calms), at three-hour intervals at OWS "Lima", December 1975 to November 1981 (x x = $H_{max,3h}$; + + = H_s) (*from HMSO, 1985*)

provide useful indications of possible errors in the data. Of course, no data should be totally discarded simply because they do not meet some criteria without further investigation.

Before progressing, it is important to examine the results so far to see whether to analyse the entire data set as a whole or whether to divide it in any way to separate values arising from different physical realizations. It is most important when analysing data from sites affected by tropical storms to separate out those caused by such storms — see Section 9.4.3. The occurrence of mixed distributions has occasionally been reported from some sites. For example, Resio (1978) found that wave heights off Cape Hatteras, North Carolina, hindcast from storm winds could be better explained by fitting different distributions depending upon the storm tracks.

In most parts of the world there is a marked seasonal variation in wave conditions. In higher latitudes, for example, generally much higher waves occur in the winter than in the summer and Dattatri (1973) reports higher waves off the west coast of India during

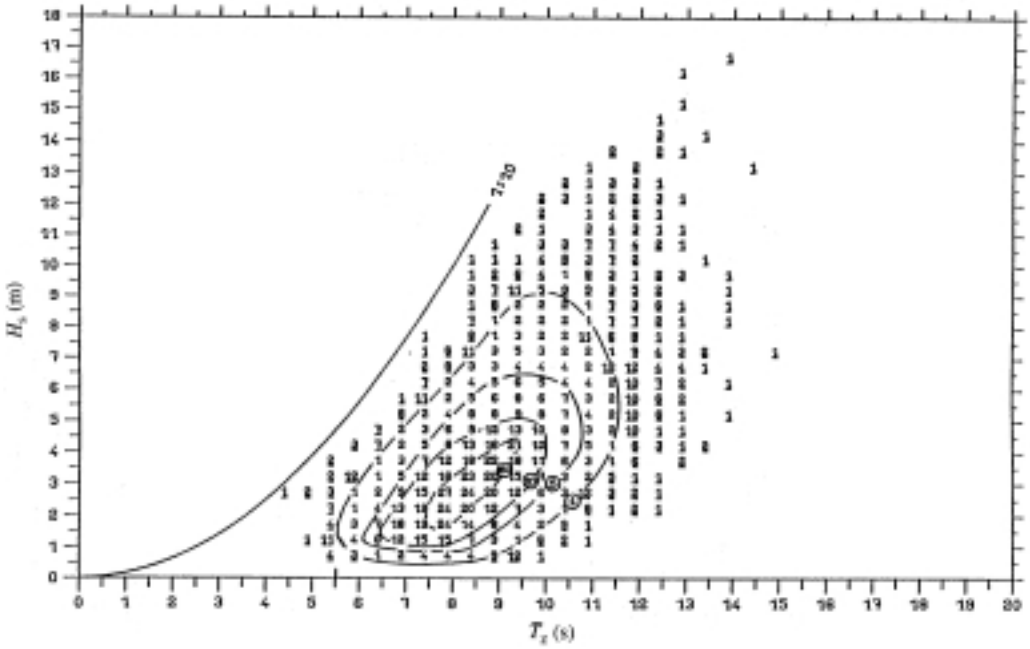

Figure 9.4 — Joint distribution (scatter plot) of significant wave height, H_s, and zero-upcrossing period, $\bar{T}_z$, from measurements (12 520 valid observations, including six calms), at three-hour intervals at OWS "Lima", December 1975 to November 1981 (Key: n – parts per thousand (PPT), n – number of occurrences (< 1 PPT) (*from HMSO, 1985*)

the monsoon season of June to September than at other times of the year. It would be preferable if this seasonal cycle (or intra-annual variation) could be removed before further statistical analysis, but wave data records are generally too short for this to be done satisfactorily (because of the large inter-annual variation superimposed upon the intra-annual cycle) and the data are usually analysed as a whole — although distribution plots for each season are often produced (see, for example, Jardine and Latham (1981) and Smith (1984)). The seasonal cycle, which is of fixed length, does not present quite the same problem as that of tropical storms which occur with random frequency from year to year.

When analysing data with a marked seasonal cycle, it is essential to check that the number of data values from each season is proportional to its length. Clearly, analysis of, say, 18 months' data would give a poor indication of the wave climate for any site with a marked intra-annual cycle unless this was taken into account. However, even when given complete years of data, it is still necessary to check that any gaps are uniformly spread and that, for example, there are not more gaps during the winter months.

It is difficult to make wave measurements — the sea is often a hostile environment for electronic equipment as well as for man — and long series of wave data often contain gaps. Providing these occur at random, they can generally be allowed for in the statistical analysis. Stanton (1984), however, found that gaps in measurements made by a Waverider buoy in the North Atlantic off Scotland appeared particularly in high-sea states, which poses considerable problems for the statistician (see Stanton (1984) for further details). The active avoidance by merchant ships of heavy weather could also bias visual wave data statistics.

Seasonal cycles are not the only ones to be borne in mind. Some sites can be routinely affected by a marked sea or land breeze. Elsewhere, the state of the tide can significantly affect the sea state — either by wave-current interaction or, if the site is partially protected, by the restricted water depth over nearby sandbanks. These are largely diurnal or semi-diurnal cycles and hence are of particular importance if the data set has only one or two records per day.

9.4 Estimating return values of wave height

In this section we first discuss how to estimate the 50-year return value of significant wave height from wave records at sites unaffected by tropical storms. The methods are applicable not only to data sets of significant wave height, $\bar{H}_{1/3}$, but also to data sets of the spectral estimate, H_{m0}. The notation H_{s50} will be used for the 50-year return value of either. The same methods can also be applied to other data sets — such as $H_{max,3h}$ — and to obtain other return values such as the 100-year value, H_{s100}.

Then we consider the estimation of the 50-year return value of individual wave height and, finally, briefly comment upon estimates of return values in areas affected by tropical storms. The methods can also be used to analyse "hindcast" wave heights (estimated from observed wind fields using wave models described in Chapter 6). See Section 9.6.2 for further details.

9.4.1 *Return value of significant wave height excluding tropical storms*

9.4.1.1 *Introduction*

The method usually employed to estimate the 50-year return value of significant wave height is to fit some specified probability distribution to the few years' data and to extrapolate to a probability of occurrence of once in 50 years. This method is commonly used for measured *in situ* data and, recently, has been successfully applied to satellite altimeter data (Carter, 1993; Barstow, 1995). Sometimes, the distribution is fitted only to the higher values observed in the data (i.e. the "upper tail" of the distribution is fitted).

An alternative method, given considerably longer data sets of at least five years, is that of "extreme value analysis", fitting, for example, the highest value observed each year to an extreme value distribution. So, if ten years of data are available — i.e. 29 220 estimates of H_s if recorded at three-hour intervals and allowing for leap years — only ten values would be used to fit the extreme-value distribution, which illustrates why long series of data are required for this method. (The advantage of the method is explained below.) It is widely used in meteorology, hydrology, and in sea-level analysis in which records covering 20–30 years are not uncommon. There are rarely sufficient data for it to be used for wave analysis, but it has been applied, for example, to the Norwegian hindcast data set (Bjerke and Torsethaugen, 1989) which covers 30 years.

F(.) will be used to represent a cumulative probability distribution i.e.:

$$\mathrm{F}(x) = \mathrm{Prob}\,(X < x)\,, \qquad (9.1)$$

where X is the random variable under consideration.

In our case, the random variable is H_s which is strictly positive so

$$\mathrm{F}(0) = \mathrm{Prob}\,(H_s < 0) = 0. \qquad (9.2)$$

Assuming a recording interval of three hours, so that there are on average 2 922 values of H_s each year, the probability of not exceeding the 50-year return value H_{s50} is given by

$$\mathrm{F}\left(H_{s50}\right) = 1 - \frac{1}{50 \times 2\,922} \approx 0.9999932. \qquad (9.3)$$

It is important to note that the value of $\mathrm{F}(H_{s50})$ depends upon the recording interval. If 12-hour data are being analysed, then:

TABLE 9.1

Distributions for wave height

1	Log-normal	Two-parameter distribution — widely used at one time but found often to be a poor fit, for example to wave data in UK waters. (Possibly a good fit if the seasonal cycle could be removed.)
2	Weibull	Sometimes gives a good fit — particularly if the three-parameter version is used (also often fitted to wind speeds) — more often fitted only to the upper-tail.
3	Extreme value distributions	The Fisher-Tippett Type I (FT-I) distribution often seems to give a good fit to three-hourly data from the North Atlantic and North Sea. The FT-III is bounded above so should be more appropriate in shallow water but there is no good evidence for this. (The FT-I and FT-III give probabilities of $H_s < 0$, but when fitted to wave data the probabilities are found to be extremely small.)

$$\mathrm{F}(H_{s50}) = 1 - \frac{1}{50 \times 365.25 \times 2} \approx 0.9999726. \quad (9.4)$$

Therefore, to estimate H_{s50} we have to select:
(*a*) The distribution to fit; and
(*b*) The method of fitting.

9.4.1.2 *The choice of distribution*

The choice of distribution to fit all the data is open, providing that F(0) = 0. There is no theoretical justification for any particular distribution. This is an enormous weakness in the method, particularly since considerable extrapolation is involved. In practice, various distributions, from among those which have been used with some success over the years, are tried and the one giving the best visual fit is accepted. These distributions, which are defined in Annex III, are listed with comments in Table 9.1.

The choice of distribution to fit the observed maxima is limited by the theory of extreme values (see, for example, Fisher and Tippett, 1928; Gumbel, 1958; and Galambos, 1978) which shows that the distribution of maxima of m values are asymptotic with increasing m to one of three forms (FT-I, II and III)*. These can all be expressed in one three-parameter distribution: the generalized extreme value distribution (Jenkinson, 1955). This theoretical result is a great help in the analysis of environmental data, such as winds and waves for which the distributions are not known, and explains the frequent application of extreme value analysis when sufficient data are available. As usual, the theory contains some assumptions and restrictions, but in practice they do not appear to impose any serious limitations. The assumption that the data are identically distributed is invalid if there is an annual cycle. Carter and Challenor (1981(*a*)) suggest reducing the cycle's effect by analysing monthly maxima separately, but this has not been generally accepted, partly because it involves a reduction by a factor of 12 in the number of observations from which each maximum is obtained and, hence, concern that the asymptotic distribution might not be appropriate. Estimates of either or both the seasonal or directional variation of extreme values (e.g. what is the N-year H_{m0} for northerly waves) may be possible, but suffer from decreased confidence due to shorter data sets. This may result in higher return values in certain directions or months than the all-data analysis.

The choice of distribution to fit the upper tail is in general limited to those given in Table 9.1. Theory gives asymptotic distributions for the upper tails of any distribution, analogous to the extreme value theory. For example, distributions whose maxima are distributed FT-I have an upper tail asymptotic to a negative exponential distribution (Pickands, 1975). However, in practice, there is the problem of determining where the upper tail commences — which determines the proximity to the asymptote — and the theory has not proved useful, to date, for analysing wave data.

Sometimes, instead of analysing all values above some threshold, a "peaks-over-threshold" analysis is carried out, analysing only the peak values between successive crossings of the threshold. Usually the upcrossings of the threshold are assumed to be from a Poisson process and the peak values either from a negative exponential distribution or from a generalized Pareto distribution (see NERC, 1975; Smith, 1984).

9.4.1.3 *The method of fitting the chosen distribution*

The method of fitting the chosen distribution often involves the use of probability paper. Alternatives include the methods of moments and of maximum likelihood.

Probability paper is graph paper with non-linear scales on the probability and height axes. The scales are chosen so that if the data came from the selected distribution then the cumulative distribution plot, such as shown in Figure 9.3, should be distorted to lie along a straight line. For example, if the selected distribution is FT-I given by

$$\mathrm{F}(h) = \exp\left\{-\exp\left[\frac{-(h-A)}{B}\right]\right\} \quad (9.5)$$

then taking logarithms and rearranging gives

$$h = A + B\,[-\log_e(-\log_e \mathrm{F})]. \quad (9.6)$$

So, a plot of h against $-\log_e(-\log_e \mathrm{F})$ should give a straight line with intercept A and slope B. (Note in this

* Figure 9.5 shows an example of FT-I scaling: the cumulative FT-I distribution appears then as a straight line.

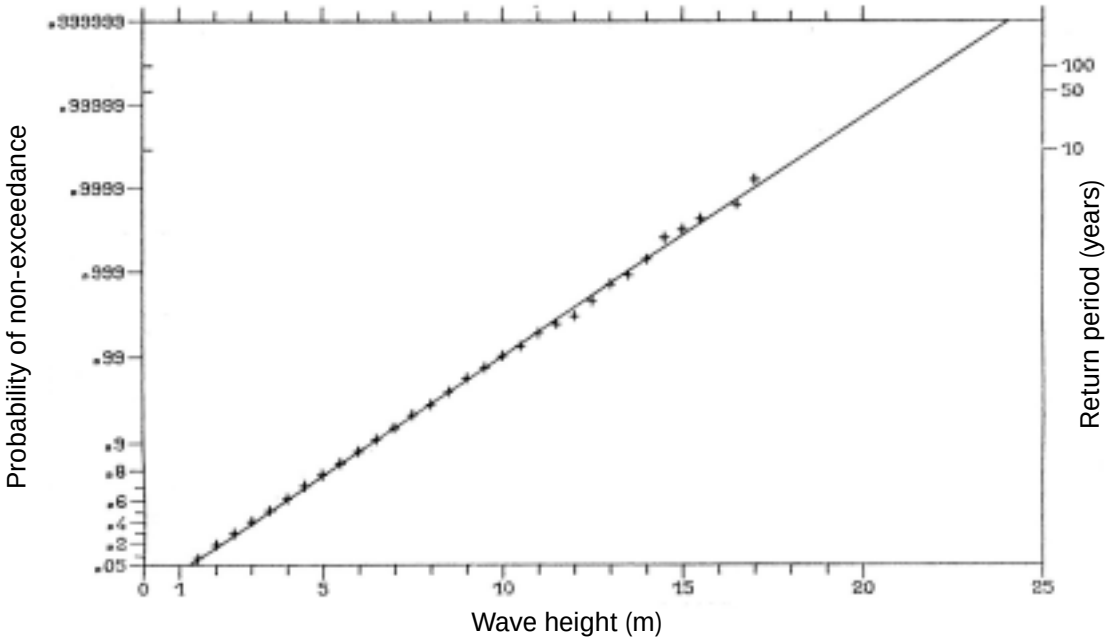

Figure 9.5 — Cumulative probability distribution of significant wave height, H_s, from measurements (12 520 valid observations), at three-hour intervals at OWS "Lima", December 1975 to November 1981 on FT-I plotting paper (*from HMSO, 1985*)

case that the height axis remains linear.) Figure 9.5 shows such an example.

Probability paper can be constructed for many distributions — including those given in Table 9.1, but there are some notable omissions (e.g. the gamma distribution).

In practice, plotting the data raises difficulties. If cumulative values are plotted at, say, 0.5 m intervals as in Figure 9.5, then besides any non-linear grouping effect, the highest few plotted points are determined by considerably fewer observations than those with lower wave heights, a point can even be plotted for a bin which contains no data. Alternatively, a point can be plotted for each observation by ordering the n observations and then plotting the r^{th} highest at, say, the expected probability of the r^{th} highest of n from the specified distribution. Determining this probability is not a trivial problem and it is often approximated by r/(n + 1) — which is correct for a uniform distribution U(0,1). See Carter and Challenor (1981(*b*)) for further details.

The distribution is then fitted by putting a straight line through the plotted values, either by eye or by least squares. Sometimes, if the values are obviously not co-linear, the line to extrapolate for H_{s50} is obtained by fitting only the higher plotted values. The visual fit can be highly subjective and it is advisable to obtain independent corroboration. Least-squares is not strictly correct since the errors are not normally distributed; cumulative plots should employ weighted least squares, but it is often felt that, in estimating H_{s50}, the higher measurements should have extra weight.

This method is immediately applicable to distributions with two parameters, such as the FT-I. It is extended to fit three-parameter distributions by plotting the data over a range of values of the third parameter to see which value gives the best fit to a straight line (either by eye or by minimizing the residual variance or by maximizing the correlation coefficient). For example, the three-parameter Weibull distribution is given by:

$$\begin{aligned} \mathrm{F}(h) &= 1-\exp\left[-\left(\frac{h-A}{B}\right)^{C}\right] \quad h \geq A \\ &= 0 \qquad\qquad\qquad\qquad\quad h < A \end{aligned} \tag{9.7}$$

where: $B, C > 0$, i.e.:

$$\log_e(h-A) = \frac{1}{C}\log_e\left[-\log_e(1-\mathrm{F})\right] + \log_e B. \tag{9.8}$$

Therefore, A is chosen by trial at, say, 0.5 m intervals so that a plot of $\log_e(x - A)$ versus $\log_e[-\log_e(1 - F)]$ is nearest to a straight line, the slope of which is $1/C$ and the intercept is $\log_e B$.

The method of moments is an analytic rather than geometric method of estimating the parameters of a distribution. (So it avoids any problem of plotting positions.) It is based upon the simple idea that, since the moments of the distribution (mean, variance, skewness, etc.) depend upon the parameter values, estimates of these values can be obtained using estimates from the data of the mean, etc. An example will make this clear: for the FT-I distribution, specified in Equation 9.5, the mean and variance are given by:

$$\begin{aligned} \text{mean} &= A + \gamma B \\ \text{variance} &= \pi^2 \frac{B^2}{6} \end{aligned} \tag{9.9}$$

where: γ = Euler's constant ≈ 0.5772, and π^2 = $(3.14159)^2 \approx 9.8696$.

For a data set h_i (i = 1, ... n), the estimates of population mean and variance, $\bar{h}$ and s^2, are given by:

$$\bar{h} = \frac{1}{n}\sum_i h_i$$
$$s^2 = \frac{1}{n-1}\sum_i \left(h_i - \bar{h}\right)^2 . \qquad (9.10)$$

The moments estimators of A and B, $\tilde{A}$ and $\tilde{B}$, are obtained from Equations 9.9 and 9.10, which give:

$$\tilde{A} = \bar{h} - \gamma\tilde{B}$$
$$\tilde{B} \approx \sqrt{6}\,\frac{s}{\pi}. \qquad (9.11)$$

If the individual h_i are not available, then the mean and variance can be estimated from grouped data given in a histogram or a scatter plot.

The two-parameter log-normal distribution is readily fitted by this method (see Johnson and Kotz, 1970, for further details). The three-parameter Weibull distribution can also be fitted by moments, the third parameter being estimated by comparing the theoretical and estimated skewness (Johnson and Kotz, l970, p. 257). In theory, the FT-III could also be fitted by moments but, in practice, it does not appear to be done.

The method of maximum likelihood consists of finding values for the distribution parameters, such as A and B in the FT-I (Equation 9.5), which maximize the likelihood that the observed data come from this distribution. This is probably the most widely used method of estimation in statistics because it generally gives statistically optimal estimates for large samples, but the method is often numerically difficult and time-consuming, even if a computer is available. For example, for FT-I, the maximum likelihood estimates, $\hat{A}$ and $\hat{B}$, are given by:

$$\hat{A} = -\hat{B}\log_e\left[\frac{1}{n}\sum_i \exp\left(\frac{-h_i}{\hat{B}}\right)\right]$$
$$\hat{B} = \frac{1}{n}\sum_i h_i - \frac{\sum_i h_i \exp\frac{-h_i}{\hat{B}}}{\sum_i \exp\frac{-h_i}{\hat{B}}}. \qquad (9.12)$$

These equations have to be solved numerically.

The two-parameter log-normal and the two-parameter Weibull are readily fitted by maximum likelihood — also requiring numerical solution of equations — but problems can arise when used for the three-parameter Weibull (and the three-parameter log-normal). (See Johnson and Kotz, 1970, for details.)

Both the method of moments and the maximum likelihood method assume data are statistically independent and identically distributed. Neither assumption applies to wave data but the methods appear to be robust and to give useful results. To meet more nearly the requirement for independent data, it might be preferable to fit data recorded at, say, 24-hour intervals — thus obtaining separate estimates from all the midnight values, another from all the 03.00 values, etc. — but this is not usually done in practice. The considerable annual cycle in wave height found in many parts of the world means that the data are often not identically distributed. As already mentioned in Section 9.4.1.2, it would be more satisfactory to remove this cycle before carrying out any statistical analysis but this is rarely attempted.

9.4.1.4 *Estimating the associated value of $\bar{T}_z$*

An estimate of the zero-downcrossing or zero-upcrossing wave period, $\bar{T}_z$, at the time when the significant wave height has an extreme value, such as H_{s50}, is obtained by assuming a specific value for significant wave steepness. Often, a value of one-eighteenth is used, so that $\bar{T}_z$ is obtained from:

$$\frac{2\pi H_{s50}}{g\bar{T}_z^2} = \frac{1}{18},$$

i.e., using metres and seconds:

$$\bar{T}_z \approx 3.4\sqrt{H_{s50}}\,.$$

Measurements indicate that one-eighteenth is appropriate for open ocean sites, but larger values of about one-fourteenth apply at sites where waves are fetch-limited. In practice, a value is often obtained by a visual inspection and extrapolation of the $H_s - \bar{T}_z$ scatter plot. These rather crude estimates of $\bar{T}_z$ are often sufficient, but if the exact value of $\bar{T}_z$ is important — for instance if a structure being designed is sensitive to small changes in $\bar{T}_z$ — then a range of values should be specified. For example, ISSC (1979) recommends a range from approximately $2.6\sqrt{H_{s50}}$ to $3.9\sqrt{H_{s50}}$, where H_{s50} is in metres. (The precise recommendation is in terms not of $\bar{T}_z$ but of the period corresponding to the spectral peak frequency, which is given as approximately 1.41 $\bar{T}_z$.)

9.4.2 ***Return value of individual wave height***

A value for the highest individual wave which might occur is often obtained from the probability distribution of the maximum individual wave height during the time (about 3–6 hours) for which the return value of significant wave height prevails. The mode — the most likely value — of this distribution is generally quoted but other values such as its mean may be used (see Sections 1.3.6 and 9.4.1.4 for the required $\bar{T}_z$). Alternatively, a data set may be obtained, consisting of the most likely highest wave corresponding to each measurement of significant wave height, and a return value estimated from this data set.

Both methods are based upon the assumption that the highest individual wave, H_{max}, occurs during the time of highest significant wave height. This is not strictly correct. H_{max} will most probably occur during this time but might occur by chance during a time of lower significant wave height. Values for the maximum

individual wave height derived using this assumption are, therefore, likely to be too low. On the other hand, the usual method of estimating the highest individual wave height (assuming a narrow band sea with crest to trough height equal to twice the crest elevation) over-estimates this height. Errors from these two incorrect assumptions tend to cancel out. For further details see Hogben and Carter (1992).

Battjes (1972) gives a method, modified by Tucker (1989), which avoids this assumption. Battjes derives numerically the distribution of individual wave heights from the $H_s - \overline{T}_z$ scatter plot, assuming that, for a specified significant wave height, the individual waves have a Rayleigh distribution (Equation 1.16). The number of individual waves during the year with this significant wave height is obtained from the $\overline{T}_z$ distribution in the scatter plot; summation gives the total number of waves in the year. Extrapolation of the distribution of individual wave heights to a probability of the one wave in the total number in N years — using Weibull probability paper — gives the N-year return value of individual wave height. See Battjes (1972) or Tucker (1989, 1991) for details.

9.4.3 *Return value of wave height in tropical storms*

The methods so far described for estimating return values, such as H_{s50} from a set of measurements, assume that all the measurements in the set and all the estimated extreme values come from the same probability distribution, with the implication that they are generated by the same physical processes. In particular, we have assumed that very severe storms, which give rise to extreme values, are essentially the same as other storms, merely more violent examples. This assumption is obviously invalid in parts of the world where extreme waves are invariably associated with tropical storms. The analysis of wave records from a site in such areas, using the methods outlined in this chapter, may well describe the general wave climate at the site but sensible estimates of extreme conditions will not be obtained.

Unfortunately, without this assumption, it is not possible to estimate long-term extremes using only a few years' measurements from one site because the relevant data are insufficient. We might expect between five and 15 tropical storms in an area such as the Caribbean or the South China Sea during a year, but some might pass too far from the site to make any impact on the local wave conditions. Severe storms are rare. For example, Ward et al. (1978) estimate that only 48 severe hurricanes — the only ones to "affect extreme wave statistics significantly" — occurred in the Gulf of Mexico between 1900 and 1974.

Estimates of return values of wave heights in areas where extremes are dominated by tropical storms may be obtained by analysing storm data from the whole area and by constructing a mathematical model to give the probability distribution of significant wave height. The model usually consists of three basic parts:

(*a*) The probability that a storm will occur in the area (a Poisson distribution is assumed with an average interval estimated from historical records);
(*b*) The probability that a storm centre will pass within a specified distance of a site (a uniform distribution is assumed over the area or part of it determined from historical track records);
(*c*) The probability of the significant wave height exceeding a particular value given a tropical storm passing at a specified distance (from analysis of wave data throughout the area or hindcast wind/wave model results).

Parts (*a*), (*b*) and (*c*) can be put together to give the probability distribution of maximum significant wave height at any site but (*c*) may require modification to include fetch-limited constraints.

Further details are given, for example, in Ward et al. (1978) and Spillane and Dexter (1976). For estimating the height of the highest individual wave in a tropical storm, see Borgman (1973).

9.5 Further reading

Stanton (1984) applies many of the procedures and methods discussed in this chapter to a set of wave data obtained off north-west Scotland with a clear exposition of the methods. Chapter 4 of Carter et al. (1986) expands somewhat on many of the topics covered here and gives further references, see also Goda (1979), which includes a detailed comparison of the various expressions used for wave period. Mathieson et al. (1994) recently published the findings of an IAHR working group on this subject.

Information on fitting distributions can be found, besides that given in Johnson and Kotz (1970), in NERC (1975). A comparison of fitting methods for the FT-I is described in Carter and Challenor (1983) and an application of maximum likelihood to fit environmental data to a generalized extreme-value distribution is given in Challenor and Carter (1983).

Methods of estimating return wave height and further information on fitting distributions are described by Borgman and Resio (1982), by Isaacson and Mackenzie (1981), on pages 529–544 in Sarpkaya and Isaacson (1981), and by Carter and Challenor (1981(*b*)) which includes a summary of some plotting options for use on probability paper.

9.6 Wave climatologies

Knowledge of the wave climatology for a specific location, a region or an entire ocean basin is important for a wide range of activities including:

(*a*) Design, planning and operability studies for harbours, coastal structures including fish farms, offshore structures such as oil platforms, and vessels;
(*b*) Coastal erosion and sediment transport;
(*c*) Environmental studies, e.g. the fate of, and clean-up procedures for, oil spills;
(*d*) Wave energy estimation;

(*e*) Insurance inquiries, damage or loss of property at sea.

The type of wave climate analysis required depends on the particular application, but includes the following:

(*a*) Long-return-period wave heights (e.g. 100 years), associated periods and directions at sites of interest and over regions;
(*b*) Percentage frequency of wave heights or wave periods by wave direction;
(*c*) Exceedance analyses for wave height and wave period;
(*d*) Persistence analysis for wave heights (or wave periods) greater (or less) than selected thresholds;
(*e*) Joint distribution of significant wave height and wave period;
(*f*) Time series plots of wave heights and wave periods;
(*g*) Relationships between significant wave height and maximum wave height and crest height.

In order to produce many of these statistical analyses a long-time series of wave data at one or more locations is required.

The information used to produce wave climatologies comes primarily from two sources: (*a*) wave measurements and observations, (*b*) wave hindcasts. Each of these will be discussed in more detail in the following paragraphs.

9.6.1 *Climatologies from wave measurements and observations*

For climatological purposes wave data has traditionally been derived from two major sources: (*a*) visual observations from vessels participating in the Voluntary Observing Ships scheme; (*b*) measurements from buoys and ships. Wave data has also in recent years become available from satellite sensors and marine radar, but the frequency of observation, length of record and data quality have until recently limited their routine use in climatology studies. Some investigations into the use of satellite radar altimeter measurements to estimate significant wave height distributions and extreme values have been carried out (Carter et al., 1994). Figure 8.5 (from D. Cotton, Southampton Oceanography Centre) shows the global mean significant wave height distribution from January to March 1996 derived from Topex data. Carter et al. (1991) analysed the global variations in monthly mean wave heights using one year of GEOSAT data. At present, significant wave height data are available globally from GEOSAT (1986–89), Topex/Poseidon (1992–), ERS-1 (1991–) and ERS-2 (launched April 1995), see, for example, Young and Holland (1996), in which detailed climatologies of the world's oceans are derived from GEOSAT data. Already these data are giving us high-quality wave climate information of particular value in

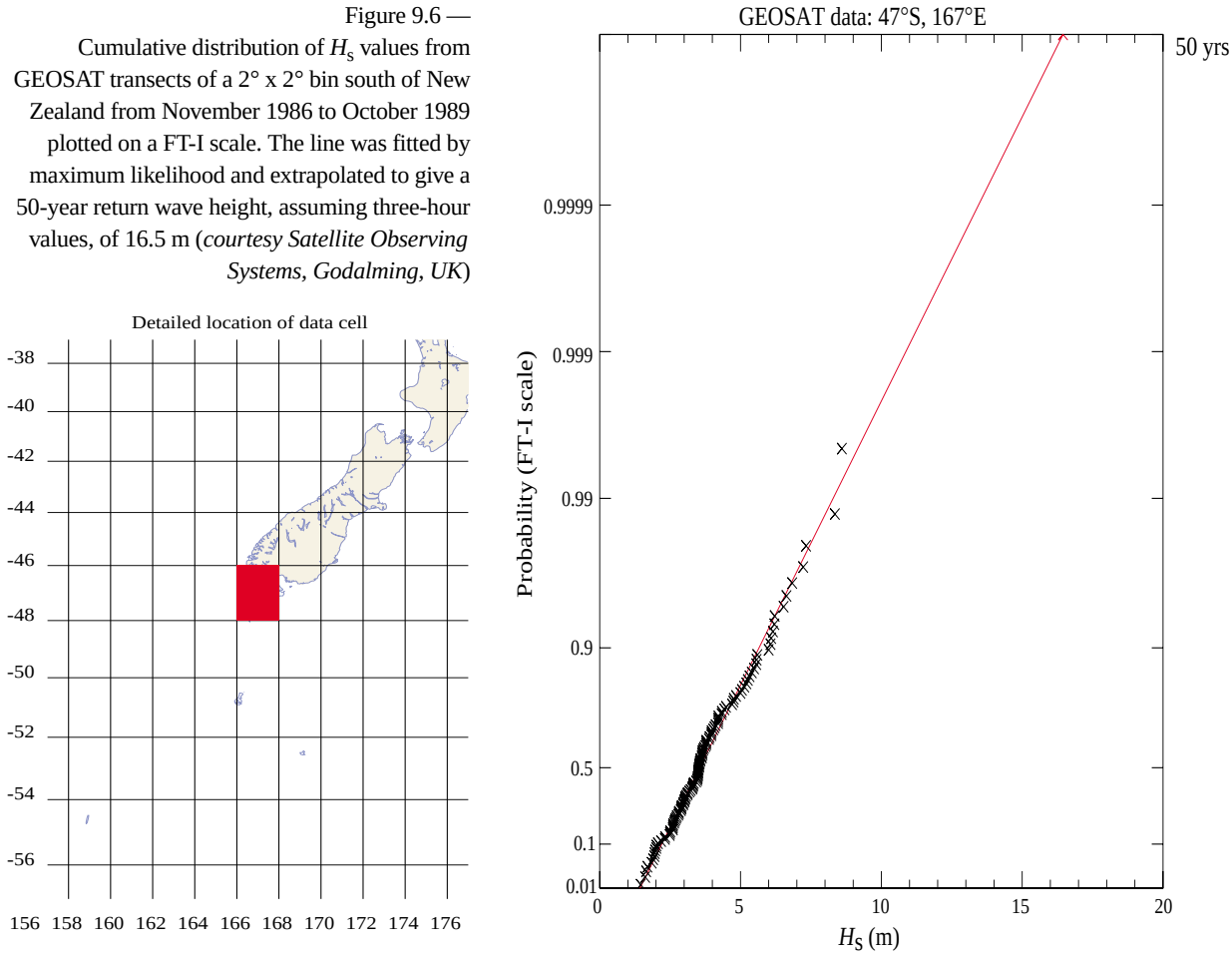

Figure 9.6 — Cumulative distribution of H_s values from GEOSAT transects of a 2° x 2° bin south of New Zealand from November 1986 to October 1989 plotted on a FT-I scale. The line was fitted by maximum likelihood and extrapolated to give a 50-year return wave height, assuming three-hour values, of 16.5 m (*courtesy Satellite Observing Systems, Godalming, UK*)

remote, data-sparse areas. However, these data are also valuable in giving supplementary information in data-rich areas on the spatial variability, in extending measured series in time and for investigating their temporal representativeness for long-term conditions. A review of applications of satellite data is given in Barstow et al. (1994 (*b*)). As further years of data from GEOSAT and later satellites, such as ERS-1 and Topex-Poseidon, become available, such analyses will provide invaluable information on wave climate. Papers on estimating extreme values from altimeter data have been published by Tournardre and Ezraty (1990), Carter (1993) and Barstow (1995). Figure 9.6 shows an estimate of wave height in an area 46°–48°S, 166°–168°E based on three years of GEOSAT data, with an estimated 50-year return value of 16.5 m. The method used and other figures of the wave climate around New Zealand are given in Carter et al. (1994). In addition, it is soon expected that SAR data will become more important.

A list of available databases composed of visual observations and measurements of waves is shown in Table 9.2. A detailed description of wave observations and measurements is given in Chapter 8.

While the data measured by buoys is considered to be of excellent quality, its utility for wave climatology is severely limited. Wave data collection is expensive and logistically difficult. As a result, there are often insufficient data to adequately define the wave climatology over a region, or for deriving with confidence any climate statistic which requires a long-time series (e.g. extremal analysis). Directional wave data from buoys are not yet common but have increased considerably in the last decade. Buoy data *can* be used for some operability studies, as long as due consideration is given to ensuring that the period of instrumental record is representative of the longer term climate. Buoy data are usually inappropriate for extremal analysis due to short record lengths. Buoy data *are* particularly useful for validating (or calibrating) numerical models and remote sensing algorithms.

Shipborne Wave Recorders are more robust than wave buoys and, fitted in Ocean Weather Ships and moored Light Vessels since the 1960s, have provided several years of data at a few locations (see, for example, Figure 9.5). Shipborne Wave Recorder data, as well as visual estimates, have been used to investigate an apparent upward trend in average wave heights in parts of the North Atlantic by one to two per cent per year over the last few decades (Neu, 1984; Carter and Draper, 1988; Bacon and Carter, 1991). It is likely that long-term monitoring of wave climate trends can now be carried out by satellite altimeters provided that the data are validated and corrections applied to make data from different satellites comparable.

Visual wave observations from ships have associated problems of quality and consistency (Laing, 1985) which reduce their utility for climatology. In addition, the fact that most observations are from *transient* ships makes their use for time-series type applications of climate virtually impossible. Ship data are most useful for climatological purposes when treated as an ensemble for regional descriptive climate applications such as "downtime" estimates for offshore operations. Transient ship data are inappropriate for extremal or time-series analysis.

In practice, wave climate studies usually use data from a combination of sources for specifying offshore conditions, and employ shallow water modelling if the site of interest is near the coast.

9.6.2 *Wave hindcasts*

There is no doubt that hindcasts are playing an increasing role in marine climatology. Most recent wave climatologies, especially regional climatologies, are based on hindcast data. The same applies to design criteria produced by offshore oil and gas exploration and production companies, and the regulatory authorities in many countries around the world. The reason is simple: the costs involved in implementing a measuring programme, especially on a regional basis, and the period spent waiting for a reasonable amount of data to be collected, are unacceptable. Therefore, given the demonstrated ability of the present generation of spectral ocean wave models, the timeliness and relatively lower cost of hindcast data becomes quite attractive. The 2nd (Canadian Climate Center, 1989) and 3rd (Canadian Climate Center, 1992 (*a*)) International Workshops on Wave Hindcasting and Forecasting identified no fewer than 12 separate recently-completed regional hindcasts around the world. A number of other such studies are also under way.

The quality of hindcast data (or at least confidence in it) can be improved by validating the results against available *in situ* measurements or satellite altimeter H_s data (for instance, this is currently being carried out in a European Union project, WERATLAS, in which a wave energy resource atlas is being constructed based on ECMWF's WAM model archive and validated by buoy data and altimeter data, Pontes et al., 1995).

Hindcasts can be classified into two basic categories: continuous hindcasts and discrete storm hindcasts; a third possibility arises as a hybrid of the two. The features of each type are described briefly in the following paragraphs.

9.6.2.1 *Continuous hindcasts*

Continuous hindcasts are usually the most useful form of hindcast data, representing a long-term, uniform distribution in space and time of wind and wave information. The time spacing is typically six or 12 hours. The database is then suitable for all manner of statistical analysis, including frequency analysis and persistence, at a single location or over a region. If the period of the hindcast is sufficiently long, the database can also be used for extremal analysis to long-return periods. The major drawback to continuous hindcasts is the time and expense involved in their production. The generation of up to 20 years of data at six-hour intervals requires an enormous amount of effort, especially if it involves the

TABLE 9.2

Available databases of long-term records of visual observations and measurements

Country	*Source of observations*	*Area covered*	*Time spanned*	*Parameters available*
CANADA	Visual observations from Voluntary Observing Ship scheme vessels over whole globe; OWS Papa observations; light vessel observations	Global, but primarily Canadian waters	Late 19th century to present	Wind speed and direction; wave and swell height, period, direction; air and sea temperature, humidity, visibility, cloud amount and type, atmospheric pressure
	Moored buoys – Waverider, WAVEC, NOMAD, 3 m discus	Canadian offshore areas (Atlantic, Pacific, Arctic)	Waverider: 1972 to present NOMAD, discus: 1987 to present	Wind speed and direction (5 m), (NOMAD and discus only); significant wave height, peak period, direction; 1-D spectra; 2-D spectra (WAVEC only)
HONG KONG	Visual wave observations; visual and measured wind observations	0°–26°N, 100°–120°E	1971 to 1980	Wind speed and direction; wave height, period, direction; *Marine climatological summary charts for the South China Sea 1971–80*
INDIA	Visual wave observations; visual and measured wind observations	Indian Ocean: north of 15°S, between 20° and 100°E		Wave height and period; *Marine climatological summaries*
IRELAND	Visual observations from Voluntary Observing Ship scheme vessels	48°–59°N, 3°–16°W	1854 to present	Wind speed and direction; wave height, period, direction; air and sea temperature, humidity, visibility, cloud amount and type, atmospheric pressure
	Beaufort scale wind estimates from light vessels	5 vessels in area bounded by 51°30'–53°12'N, 5°30'–8°12'W	Variable, from June 1939 to February 1982	Beaufort wind estimates twice daily
	Observations from lighthouse stations	6 stations in area bounded by 51°24'–53°18'N, 5°54'–9°54'W	Variable, from September 1985 to present	Wind speed and direction; sea state, weather, cloud cover, visibility, air pressure, air temperature at 0600, 0900, 1100, 1400, 1700, 2300 hours civil time
	Wind measurements from anemometer at 65 m ASL; wave measurements from Baylor wave staff type D19595, air temperature from platinum resistance thermometer in Stevenson screen on helideck of Marathon Gas Platform	51°22'N, 7°57'W	1 August 1979 to 2 February 1990	Wind speed and direction; air temperature, sea temperature; significant wave height, maximum wave height, wave period and mean water level
ISRAEL	Visual observations		20 years	Wind, wave, sea temperature
ITALY	Datawell Waverider buoys, recording 10 minutes every 3 hours	15 locations in area bounded by 36°54'–45°42'N, 8°30'–18°E	Variable, from 1974 to 1991	All relevant sea state parameters
JAPAN	Visual wave observations, visual and measured wind observations	North Pacific Ocean	1964 to 1973	Wind speed and direction; wave height, period and direction; *Papers of Ship Research Institute, Supplement No. 3, March 1980*

TABLE 9.2 (cont.)

Country	*Source of observations*	*Area covered*	*Time spanned*	*Parameters available*
JAPAN (cont.)	Visual wave observations, visual and measured wind observations	North Pacific Ocean	1961 to present	Wind speed and direction; wave height, period and direction; *Marine climatological summaries*
NEW ZEALAND	Waverider buoy, Maui 'A'	39°30'S, 173°20'E	1977 to 1988	Wave spectra (f)
NORWAY	Moored buoy data, including directional data ship-borne recorder (OWS Mike, from 1949) vertical lasers, microwave radar coastal stations (visual)	15 buoy and ship locations bounded by 56°30'–72°N, 2°–30°E	Variable: late 1949 to present	Meteorological parameters (including wind), waves
SOUTH PACIFIC	Waverider	Rarotonga, Cook Is.	July 87 – Jan. 91	)
	Waverider	Tongatapu, Tonga Is.	May 87 – July 92	)
	Directional Waverider		June – Aug. 92	)
	Waverider	Efate, Vanuatu	Nov. 90 – Feb. 93	)
	Directional Waverider		Nov. 92 – Feb. 93	) Wave height, period and energy
	Waverider	Funafuti, Tuvalu	May 90 – April 92	) *Olsen et al.* (*1991*)
	Waverider	Western Samoa	Sept. 89 – July 92	)
	Directional Waverider		March – June 93	)
	Waverider	Kadavu, Fiji	Jan. 91 – Oct. 93	)
	Directional Waverider		April – July 94	)
UNITED KINGDOM	Visual observations from Voluntary Observing Ship scheme vessels over whole globe; SBWR observations at standard OWS locations and light vessels around UK	Global	Late 19th century to present	Wind speed and direction; wave and swell height, period, direction; air and sea temperature, humidity, visibility, cloud amount and type, atmospheric pressure; *R. Shearman (1983)*
USA	Visual observations from Voluntary Observing Ship scheme vessels over whole globe; OWS observations at standard locations	Global	1854 to present	Wind speed and direction; wave and swell height, period, direction; air and sea temperature, humidity, visibility, cloud amount and type, atmospheric pressure; *Slutz et al. (1985)*
	Moored buoys	US coastline (Atlantic, Pacific, Gulf of Mexico)	1972 to present	Wind speed and direction; wave height, period, and direction; 1-D and some 2-D wave spectra; *Climate Summaries for NDBC Buoys and Stations, Update No. 1, 1990, NDBC, NOAA*

quality control and re-analysis of historical information necessary to produce a high-quality database (particularly of the winds needed to drive the hindcast wave model).

One approach, which has been adopted in order to minimize the costs associated with continuous hindcasts, is to archive the analysis portion of operational wave analysis and forecast programmes. This is a very cost-effective means of producing a continuous database, being a by-product of an existing operational programme. The disadvantages are that the operational time constraints mean that not all available data are included in the analysis, that time-consuming techniques such as kinematic analysis cannot be performed, that the use of backward as well as forward continuity in the development of weather patterns is not possible, and that it will take N years of operation to produce an N-year database. There is also a danger that such archives may suggest "climate change" that is not real but is a result of changes in the characteristics of the models used. Nevertheless, this approach represents a viable way to develop a continuous database of wave information, albeit of lesser quality. Attention also needs to be given to the temporal homogeneity of the model data, especially when different procedures to estimate ocean winds are used at different times.

9.6.2.2 *Storm hindcasts*

In order to perform the extremal analysis necessary for establishing design criteria for offshore operations, it is necessary to have wave information for a period of at least 20 years. In fact, recent experience suggests that even 20 years may not be sufficient to produce stable estimates of long return period wave heights. The cost associated with producing a continuous hindcast for more than 20 years is prohibitive in most instances. As a result, an approach has been adopted in many countries whereby a selection of the top-ranked wave-producing storms over a period of 30 or more years is hindcast, with the wave heights analysed using peak-over-threshold techniques (see Section 9.4.1.2).

This approach has several advantages, not least of which is that the cost is a fraction of that for a continuous hindcast. Storms hindcast are typically of about five days duration, so for a sample of 50 storms in a period of 30 years, for example, the total hindcast period would be 250 days. Another major advantage is that the storms can be hindcast in considerably more detail, with full re-analysis of each storm, including kinematic analysis, and forward and backward continuity. All available data can be used in the analysis, including those data abstracted from ships' logs as well as that originally obtained from the Global Telecommunication System (GTS). There is no doubt that this approach produces the highest quality data of any hindcast procedure for the storm periods selected.

On the negative side, the database produced, while suitable for extremal analysis, is inappropriate for any analysis which requires a time series of data at one or more locations (such as persistence analysis). It also cannot give any information on frequency distributions of waves, since only the extreme conditions are analysed. One additional drawback is that one cannot remove lingering doubts that the storms selected for the detailed hindcasts are the most severe wave-producing storms, since these must usually be selected in the absence of direct wave measurements, by proxy criteria such as the time history of pressure gradients over wave-generating areas.

9.6.2.3 *Hybrid hindcasts*

Hybrid hindcasts are being used increasingly to try to combine the best features of the continuous and storm hindcasts. They start from a continuous hindcast produced as described above, and are then augmented by hindcasts of the most severe storms and of periods where the verification against measurements shows that the continuous hindcast has produced significant errors. The periods from the storm hindcast then replace the archive in the continuous hindcast. This approach has been used effectively in the Gulf of Mexico and off the west coast of Canada. It is relatively cost effective, and continued correction to the continuous hindcast can be made depending on available resources. The database produced is suitable for all types of statistical analysis, including extremal analysis if the hindcast period is sufficiently long.

9.6.3 ***Hindcast procedure***

The following paragraphs describe a wave hindcast storm procedure. Most aspects of the hindcast procedure, other than storm selection, are the same whether the continuous or storm approach is selected. If the hindcast is produced using the analysis cycle of an operational wave forecast programme, most of the decisions on model domain, input wind fields, etc. will have been made; the only remaining decision will involve the archiving process. A detailed description of the steps involved in a storm hindcast are given in the WMO *Guide to the applications of marine climatology* (WMO, 1994(*b*)).

The application of the hindcast method includes the following main steps:

(1) Given the point or area where hindcast wave data are required, decide the area necessary to be included to represent the wave conditions in the region of interest (to catch distantly generated swells, etc.).

(2) Select the time span for the hindcast; previous experience with the historical marine meteorological databases supports selection of storms from about the past 30 years. The database for earlier periods is much less extensive and wind fields may not be specified as accurately. Therefore, the historical period which should generally considered extends from about the mid-1950s to the present.

For a storm hindcast, select the most severe wave-producing storms over the time span, using wave and wind data where available, and archived analyses of surface pressure.

(3) Choose a suitable wave model, such as one of those listed in Table 6.2; the grid spacing and time step should be appropriate for the application.

(4) Specify surface wind fields on discrete grids for the time span selected (or for each selected historical storm).

(5) Execute the numerical hindcast of the time history of the sea state on a grid of points representing the basin, for the time span (or for each storm).

(6) Archive input wind fields and hindcast wave parameters and spectra at a large number of sites for each model time step.

9.6.4 *Wind field analysis*

The most crucial point is the production of the wind fields. Data are sparse over the oceans and it is difficult to find grid data of a sufficiently fine resolution farther back than the early 1970s. An example of a procedure may be to:

(1) Procure all available surface data from ships, buoys, synoptic and climatic stations, drilling vessels, Ocean Weather Stations, satellite data and sea ice cover data (where appropriate).

(2) Digitize historical surface pressure analyses (after re-analysis using the available data if necessary), or acquire digital gridded fields of sea-level pressure or wind speed and direction.

(3) Apply a planetary boundary-layer model to the isobaric analysis to approximate the near-surface wind field (e.g. Cardone, 1969).

(4) Construct streamlines and isotachs using all synoptic observations of wind speed and direction from ships and land stations, using forward and backward continuity which defines the movements of storm centres and fronts and other significant features of the surface wind field.

(5) Extract kinematic winds (speed and direction) from the streamline/isotach analyses on the defined grid; where kinematic analysis is performed over part of the grid only, the kinematic winds replace the winds derived from the planetary boundary-layer model, with blending along the boundaries of the kinematic area.

The kinematic winds are by far the most accurate and least biased winds, primarily because the method allows a thorough re-analysis of the evolution of the wind fields. Kinematic analysis also allows the wind fields to represent effects not well modelled by pressure-wind transformation techniques, such as inertial accelerations associated with large spatial and temporal variations in surface pressure gradients and deformation in surface winds near and downstream of coasts.

(6) Define the resulting wind fields at a specific level.

Some modellers have adopted the simple concept of the "effective neutral" wind speed introduced by Cardone (1969) to describe the effects of thermal stratification in the marine boundary layer on wave generation. The effective neutral wind speed is simply the wind which would produce the same surface stress at the sea surface in a neutrally stratified boundary layer as the wind speed in a boundary layer of a given stratification. Calculation of the effective wind at a reference elevation from measured or modelled winds and air-sea temperature differences requires a model of the marine surface boundary wind profile which incorporates a stability dependence and a surface roughness law.

A boundary-layer model is set up to provide the effective neutral wind speed, for example at 10 m. Reports of wind speed from ships and rigs equipped with anemometers are then transformed into the effective neutral 10 m values (see Dobson, 1982; Shearman and Zelenko, 1989), using a file of anemometer heights of ships in the merchant fleet. For ships which use estimated wind speeds, values are adjusted according to the scientific Beaufort scale (see Chapter 2, Table 2.2). A revised table of wind speed equivalents is used to retrieve the 10 m wind speed and then correct for stability.

If winds must be interpolated in time for input to the wave model, the recommended algorithm is linear interpolation in time of zonal and meridional wind components to compute wind direction, and interpolation of the fourth power of wind speed, because wave energy scales with this quantity. This scheme has been found to provide sufficient resolution in wind fields encompassing extra-tropical cyclones off the east coast of North America.

9.6.5 *Archiving of wind and wave fields*

The fields archived depend on the user's needs and should be as comprehensive as possible. For example, for a full spectral wave model it would be useful to archive the following hindcast gridded wind and wave fields at each model grid point:

- Wind speed in m/s (e.g. effective neutral 10 m winds);
- Wind direction in degrees (meteorological notation);
- Wind stress or friction velocity ($\boldsymbol{u}_*$);
- Significant wave height (H_s) in metres and tenths of metres;
- Peak period (T_p) or significant period in seconds and tenths of seconds;
- Vector mean direction, or spectral peak direction in degrees;
- Directional (2-D) spectral variance in m^2.

9.6.6 *Verification of wave hindcasts*

The validation of hindcasts against measurements using comparisons reveal the skill achievable in the hindcasts. Time series plots, error statistics and correlation should

TABLE 9.3

Hindcast wave databases

Country	*Model used*	*Grid and time step*	*Verification*	*Area covered*	*Time spanned*	*Parameters available*
ARGENTINA	DSA V deep water decoupled model; *Rivero et al. (1974)*	Orthodromic grid, spacing 90 n.mi. Time step: 3 hours		Within box defined by 28°S, 48°W; 27°S, 26°W; 57°S, 70°W; 55°S, 15°W	1976 to present	Significant wave height, peak period, peak direction; *Rivero et al. (1978)*
CANADA	ODGP 1-G deep water spectral wave model; 15 frequencies by 24 directions; *Cardone et al. (1976)*	Lat./long. nested grid; spacing 1.25° x 2.5° in coarse mesh, 0.625° x 1.25° in fine mesh near coasts Time step: 2 hours	Unbiased for wind speed and significant wave height; scatter index 0.14	East and west coasts of Canada	1957–1990; 70 discrete storm periods on east coast, 51 on west coast	Wind speed and direction (20 m), significant wave height, peak period, vector mean direction, at all grid points every 2 h; 2-D spectra every 6 h at 118 points; *Canadian Climate Center (1991, 1992 (b))*
	ODGP 1-G deep water spectral wave model; 15 frequencies by 24 directions; *Cardone et al. (1976)*	Wind input on lat./long. grid; spacing 1° x 3°; waves on transverse Mercator, spacing 37.3 km Time step: 1 hour	Unbiased for wind speed and significant wave height; scatter index 0.13	69°–76°N; 120°–162°W (Canadian Beaufort Sea)	1970–1990; 45 discrete storm periods	Wind speed and direction (20 m), significant wave height, peak period, vector mean direction, at all grid points every hour; 2-D spectra every 6 h at 51 points; *MacLaren Plansearch Ltd. and Oceanweather, Inc. (1992)*
	ODGP 1-G deep water spectral wave model; 15 frequencies by 24 directions; *Cardone et al. (1976)*	Lat./long. nested grid; spacing 1.25 x 2.5 in coarse mesh, 0.625 x 1.25 in fine mesh near coasts Time step: 2 hours	Unbiased for wind speed and significant wave height; scatter index 0.30 for Atlantic	North Atlantic and North Pacific Oceans	1 October 1983 – 30 September 1986 for North Atlantic; 1 January 1987 – 31 December 1989 for North Pacific	Wind speed and direction (20 m), significant wave height, peak period, vector mean direction, at all grid points every 2 h; 2-D spectra every 6 hours at 54 points; *Eid et al. (1989)*
GREECE	Deep water model, decoupled propagation; *Hellenic National Meteorological Service Reports No. 14, 15*	Polar stereographic grid, spacing 100 km Time step: 6 hours		Eastern Mediterranean Sea		No parameters in database at present
IRELAND	Irish Meteorological Service model, adapted NOWAMO; sea model plus swell model	23 x 23 grid, spacing 150 km Time step: 3 hours		7 locations between 48°–55°N and 8°–14°W	September 1984 to present	Significant wave height, period and direction
JAPAN	MRI-II coupled discrete wave model; *Uji (1984)*	Grid spacing 300 km Time step: 6 hours wind input 20 m wind derived from 1 000 hPa winds from ECMWF global NWP model		North Pacific Ocean	1980–1989	Wave height, period and direction *Ship and Ocean Foundation (1990, 1991)*

TABLE 9.3 (cont.)

Country	*Model used*	*Grid and time step*	*Verification*	*Area covered*	*Time spanned*	*Parameters available*
NEW ZEALAND	NIWA 2-G coupled spectral model; 15 frequencies by 18 directions	Polar stereographic grid; spacing 190 km at 60°S Time step: 2 hours	Scatter index for H_S 0.29 compared to GEOSAT, 0.24 compared to Waverider	Seas within 800 km of New Zealand	1980–1989 (in progress)	Wind speed and direction, full spectra at all grid points in sub-grid around New Zealand
NORWAY	WINCH wave model	Grid spacing 75 km Time step: 2 hours		North Sea, Norwegian Sea, Barents Sea	1955–1994	Wind speed and direction, significant wave height, peak period, peak direction every 6 h
UNITED KINGDOM	Deep water, 2-G wave model; *Golding (1983)*	Lat./long. grid, spacing 1.5° x 1.875° Time step: 1 hour development, variable advection time step		Global	1 October 1986 – 11 June 1991; new archive started 12 June 1991 with higher resolution	Wind speed and direction, significant wave height, 1-D energy spectra, mean wave direction for each frequency.
	Shallow water, 2-G wave model; *Golding (1983)*	Lat./long. grid, spacing 0.25° x 0.4° Time step: 1 hour development, variable advection time step		30°30'–66°45'N; 14°4'W–35°56'E	1 October 1986 – 11 June 1991; new archive started 12 June 1991 with higher resolution	Wind speed and direction, significant wave height, 1-D energy spectra, mean wave direction for each frequency, depth
USA	US Navy Spectral Ocean Wave Model (SOWM); 15 frequencies by 24 directions; *Pierson (1982)*			Northern hemisphere	1956–1975: Atlantic 1964–1977: Pacific 1975–1985: Mediterranean Sea	Wind speed and direction, 2-D wave spectra; *US Navy Hindcast Spectral Ocean Wave Model climatic atlas (1983, 1985, 1990)*
	US Navy Global Spectral Ocean Wave Model (GSOWM); 15 frequencies by 24 directions; *NCDC Tape Reference Manual*	Grid spacing 2.5°		Global	1985–1994	Wind speed and direction, 2-D wave spectra; *NCDC Tape Deck 9782*
	Deep plus shallow water 2-G wave model; *Brooks and Corson (1984)*			US coastline (Atlantic, Pacific, Gulf of Mexico)	1956–1975	Surface pressure fields, wind speed and direction, 2-D wave spectra; *Wave information studies of the US coastline, Waterways Experiment Station, Vicksburg, MS,* USA

be computed; the bias, RMS (root-mean-square) error and scatter index (ratio of RMS error to mean measured value) are particularly useful as measures of performance. Continuous hindcasts typically show scatter indices for significant wave height in the range of 0.25–0.30, while for peak-to-peak comparisons of storm hindcasts they are often in the range of 0.12–0.16.

In addition, it is useful to construct 1-D spectral plots of the respective observed and modelled spectra, e.g. at peak wave height or within three hours. For continuous wave measurements, an appropriate moving average should be used on the recorded data (e.g. 6 or 7 point moving average). It is instructive to represent the data with error bars indicating appropriate confidence limits (for instance 95 per cent). See, for example, Figure 5.4, where the 90 per cent confidence limits are shown.

If 2-D spectral measurements are available, they should be used to evaluate the model predicted values.

9.6.7 ***Extremal analysis***

From the wave hindcast model, the following quantities are available at all points and at each time step:

- H_s — significant wave height;
- T_p — spectral peak period;
- θ_d — vector mean wave direction;
- W_s — average wind speed;
- W_d — wind direction.

The objective of the extreme analysis is to describe extremes at all contiguous grid locations for the following variables:

- H_s versus annual exceedance probability or inverse return period;
- W_s versus annual exceedance probability;
- H_m (maximum individual wave height) versus annual exceedance probability.

Techniques for extremal analysis of these quantities are described in preceding sections.

9.6.7.1 *Extreme wave/crest height distribution*

For the points at which a detailed extremal analysis is performed, the maximum individual wave height may be estimated in each storm from the hindcast zeroth and first spectral moments following Borgman's (1973) integral expression, which accounts for storm build-up and decay. The integral may be computed for two assumed maximum individual wave height distributions:

(*a*) Rayleigh (as adapted by Cartwright and Longuet-Higgins, 1956);

(*b*) Forristall (1978).

The same approach may be used to estimate the maximum crest height at a site in a storm using the empirical crest-height distribution of Haring and Heideman (1978). The median of the resulting distributions of H_m, H_c may be taken as the characteristic maximum single values in a storm. The mean ratios of H_m/H_s and H_c/H_s should be calculated and used to develop a mean ratio to provide extremes of H_m and H_c from fields of extreme H_s.

9.6.7.2 *Presentation of extremes*

Fields of extremes of H_s, H_m, W_s should be tabulated and displayed as field plots (contour plots if necessary) of numerical values.

Results of detailed extremal analysis at selected grid locations should be presented in tabular form for each analysed point and in graphical form. The graphical display of extrapolations shall include the fitted line, the confidence limits on the fit and the fitted points.

9.6.8 ***Available hindcast databases***

Several hindcast databases have been created covering a wide range of ocean basins. Most of these are continuous hindcasts, a few are storm hindcasts. There are no hybrid hindcast databases presently available. A list of available hindcast databases, with their characteristics, is shown in Table 9.3. These databases cover periods of three years or longer (continuous) or 40 storms or more (storm). It is not possible to include the many other hindcasts, related to short periods for verification purposes or to studies of particular events, in this publication.

ANNEX I

ABBREVIATIONS AND KEY TO SYMBOLS

(Preferable units are shown with alternatives in brackets)

Abbreviation/ Symbol	***Definition***
a	Wave amplitude — m (ft)
ASCE	American Society of Civil Engineers
Δb	Distance between two wave rays
CERC	Coastal Engineering Research Center (US)
c; c_{phase}	Phase speed; the speed of propagation of a wave — m/s (kn)
c_g; $\boldsymbol{c_g}$	Group speed, velocity. The speed (velocity) of propagation of a wave group — m/s (kn)
$\overline{\boldsymbol{c}}_{\mathbf{g}}$	Effective group velocity for total energy — m/s (kn)
c_θ	Speed of directional change — rad/s (deg/s)
C_d; C_{10}	Drag coefficient; drag coefficient at the 10 m level.
CD	Coupled discrete — model class
CH	Coupled hybrid — model class
CMC	Canadian Meteorological Center
deg	Measure of angle, degree
D_p	Duration of wave generation — h
DNMI	The Norwegian Meteorological Institute
DP	Decoupled propagation — model class
e, exp	Exponential constant ≅ 2.71828
E, E_{total}	Wave energy (variance) per unit area — m² per area
E_∞	Energy of fully developed wave field — m² per area
$E(f)$	Wave spectral energy density as a function of frequency — m²/Hz
$E(f,\theta)$	Wave spectral energy density as function of frequency and direction — m²/Hz/rad
$E[\ ]$	Expected value of variable in brackets
ECMWF	European Centre for Medium-range Weather Forecasts
ESA	European Space Agency
f	Wave frequency — Hz
	Coriolis parameter — s
$\overline{f}$	Mean wave frequency — Hz
f_p	Wave frequency corresponding to the peak of the spectrum — Hz
ft	Unit of length, foot
FFT	Fast-Fourier transform
F(H)	Probability of not exceeding the wave height H
FNMOC	Fleet Numerical Meteorology and Oceanography Centre (USA)
FT	Fisher-Tippett distribution
g	Acceleration due to gravity — m/s²
$\boldsymbol{G}$, (u_g, v_g); G	Geostrophic wind velocity; speed — m/s (kn)
GD	Groen and Dorrestein
$\boldsymbol{Gr}$; Gr	Gradient wind velocity; speed — m/s (kn)
GTS	Global Telecommunications System
h	Unit of time, hour
h	Water depth — m

Abbreviation/ Symbol	*Definition*
h_b	Breaking depth; water depth at which a wave of given height breaks — m
hPa	hectoPascal — unit of pressure
H	High pressure centre
H	Wave height — m (ft)
$\bar{H}$	Average wave height in a record — m (ft)
H_b	Breaker wave height — m (ft)
H_c	Characteristic wave height (average height of the larger well-formed waves, observed visually) — m (ft)
$H_{combined}$	Wave height for total wave field — m (ft)
H_{max}, H_m, $H_{max,3h}$	Maximum wave height for specified period of time — m (ft)
H_{m0}	Wave height derived from energy spectrum, approximately equal to $\bar{H}_{1/3}$; $H_{m0} = 4\ m_0^{1/2}$ — m (ft)
H_{rms}	Root-mean-square wave height = $(8\ E/\rho_w g)^{1/2}$ — m (ft)
H_s	Significant wave height = H_{m0} or $\bar{H}_{1/3}$, according to specification — m (ft)
H_{sN}, H_{s50}	N-year, 50-year return value of H_s — m (ft)
H_{sea}	Wind wave height — m (ft)
H_{swell}	Swell height — m (ft)
H_z	Zero-crossing wave height (the vertical distance between the highest and lowest value of the wave record between two zero-downcrossings or upcrossings)
$\bar{H}_{1/n}$	The average height of the 1/n highest waves — m (ft)
$\bar{H}_{1/3}$	Significant wave height: average of the 1/3 highest waves in a record (approximates to the characteristic wave height) — m (ft)
Hz	Hertz, measure of frequency = 1 cycle per second — s^{-1}
HF	High Frequency
HMSO	Her Majesty's Stationary Office (UK)
$\boldsymbol{I}$, (u_i, v_i)	Isallobaric wind vector
IAHR	International Association for Hydraulic Research (Delft, Netherlands)
J	Wave power — kW/m (of wavefront)
JMA	Japan Meteorological Agency
JONSWAP	Joint North Sea Wave Proj ect
k; $\boldsymbol{k}$	Wavenumber ($2\pi/\lambda$); vector wavenumber — m^{-1}
km	Unit of length, kilometre
kn	Unit of speed, knot (1.94 kn = 1 m/s)
kW	Unit of power, kilowatt
K	Mixing coefficient
K_r	Refraction factor
K_s	Shoaling factor
KNMI	Royal Netherlands Meteorological Institute
L	Low pressure centre
L	Monin-Obukhov mixing length — m
m	Unit of length, metre
mks	Metric system of units based on the metre, kilogram and second as the units of length, mass and time; it forms the basis of the International System of Units (SI)
m_n	The n-th order moment of the wave spectrum
m_0	Moment of zero order; represents the integral of a wave spectrum
m/s	Unit of speed, metre per second
ME	Mean error

Abbreviation/ Symbol	*Definition*
MOS	Model output statistics
n	A given number of waves, years, etc.
$n(f,\theta)$	Wave action density
n	Spatial variable normal to direction of travel
n.mi.	Unit of distance, nautical mile (one second of arc of latitude)
N	A given number (of waves, years, etc.)
NDBC	National Data Buoy Center (USA)
NMC	National Meteorological Centre
NMS	National Meteorological Service
NOAA	National Oceanic and Atmospheric Administration (USA)
p	Atmospheric pressure — hPa
PM	Pierson-Moskovitz
PNJ	Pierson, Neumann and James (wave forecasting method)
Q(H)	Probability of exceeding the wave height H
Q_p	Spectral peakedness parameter
Q_b	Fraction of breaking waves
r	Sample correlation (see also ρ)
	Radius of curvature of an isobar
rad	Unit of plane angle, radian (1 radian = 57.296 deg)
R_p	Range or distance to point "p" from storm front — m, km (n.mi.)
RMS	Root-mean-square
RMSE	Root-mean-square error
s	Unit of time, second
s	Spatial variable in direction of motion
s	Standard deviation of a distribution
$S(f)$; $S(\omega)$	Wave-spectral (variance) density as function of frequency; as a function of angular frequency $S(\omega) = S(f)/(2\pi)$
S	Energy-balance equation: combined source terms
S_{in}	Energy-balance equation: input source term
S_{ds}	Energy-balance equation: dissipation source term
S_{nl}	Energy-balance equation: non-linear interaction source term
S_{bottom}	Energy-balance equation: bottom friction term
$S_{breaking}$	Energy-balance equation: wave breaking in surf zone
SAR	Synthetic Aperture Radar
SBWR	Shipborne Wave Recorder
SI	Scatter index (ratio of rmse to mean)
SSM/I	Special Sensor Microwave/Imager
SWAMP	Sea Wave Modelling Project
t	Time variable — s, h
T	Wave period — s
	Temperature
T_c	Characteristic wave period — s (average period of the larger well-formed waves, observed visually)
$\overline{T}_{H_{1/n}}$	Average period of the 1/n highest waves — s
$\overline{T}_{H_{1/3}}$	Significant wave period: average period of 1/3 highest waves — s
T_{m01}	A mean period corresponding to inverse of mean frequency = m_0/m_1, — s
T_{m02}	A wave period from spectral moments = $(m_0/m_2)^{1/2}$; approximates $\overline{T}_z$ — s

Abbreviation/ Symbol	***Definition***
T_{m-10}	Energy wave period = m_{-1}/m_0, — s
T_p	Peak period: wave period at the peak of the spectrum (modal period) — s
T_s	Significant or peak period according to specification
$\overline{T}_z$	Average zero-crossing wave period in a record
u; $\boldsymbol{u}$	Wind speed; wind velocity — m/s, (kn)
U_{10}	Wind speed at the 10 m level — m/s, (kn)
U_z	Wind speed level z — m/s, (kn)
u_*; $\boldsymbol{u}_*$	Friction speed / velocity = $(\tau/\rho_a)^{1/2}$
(u_g, v_g), $\boldsymbol{G}$; G	Geostrophic wind velocity; speed — m/s, (kn)
(u_i, v_i), $\boldsymbol{I}$	Isallobaric wind velocity
UKMO	United Kingdom Meteorological Office
UTC	Universal Time Coordinates
VOS	Voluntary Observing Ships
WAM	WAve Model (a specific third generation wave model)
WAVEOB	Code for interchange of wave observations
X	Fetch length — km (n.mi.)
x; $\boldsymbol{x}$	Space variable; space vector
y	Space variable
z	Height variable
z_0	Roughness length
α	Scaling (Phillips') parameter in model spectrum (= 0.0081 in Pierson-Moskowitz spectrum)
	Angle between wave front (crest) and isobath
	Charnock's constant
γ	Peak-enhancement parameter in JONSWAP spectrum
ε	Spectral width parameter
	Dimensionless wave energy
$\eta(x,t)$	Elevation of water surface at position x and time t
$\overline{\eta}$	Mean water surface elevation
θ	Direction of wave propagation
θ_d	Vector mean wave direction
κ	von Karman constant (≅ 0 41)
λ, λ_s	Wavelength, wavelength of sea — m
λ_r	Radar wavelength
ν	Non-dimensional frequency
π	A constant; ≅ 3.14159
ρ	Correlation coeffficient (r = sample correlation coefficient)
ρ; ρ_w; ρ_a	Density; density of water; density of air
σ	Wave frequency associated with a (current modified) wavenumber
ξ	Wave steepness (various definitions, see text)
ω	Angular frequency = $2\pi f$
τ	Mean stress magnitude
ϕ	Phase of a sinusoidal wave
ψ	Stability function for atmospheric boundary layer
	Wind direction

ANNEX II

FM-65 IX WAVEOB
REPORT OF SPECTRAL WAVE INFORMATION FROM A SEA STATION OR FROM A REMOTE PLATFORM (AIRCRAFT OR SATELLITE)

C O D E F O R M :

SECTION 0 $M_iM_iM_jM_j$ { D . . . . D / or / $A_1b_wn_bn_bn_b$ / or / $I_1I_2I_2$// } ** YYMMJ GGgg/ { IIiii* / or / $Q_cL_aL_aL_aL_a$ $L_oL_oL_oL_oL_o$** }

$00I_aI_mI_p$ 1hhhh $2H_sH_sH_sH_s$ $3P_pP_pP_pP_p$ $(4H_mH_mH_mH_m)$ $(5P_aP_aP_aP_a)$ $(6H_{se}H_{se}H_{se}H_{se})$ $(7P_{sp}P_{sp}P_{sp}P_{sp})$ $(8P_{sa}P_{sa}P_{sa}P_{sa})$ $(9d_dd_dd_sd_s)$

SECTION 1 $(111B_TB_T$ SSSS/ D´D´D´D´/ BB/// $1f_1f_1f_1x$ $1f_df_df_dx$ . . . . . BB/// $nf_nf_nf_nx$ $nf_df_df_dx)$

SECTION 2 (2222x $C_mC_mC_mn_mn_m$ $1c_1c_1c_2c_2$ $3c_3c_3c_4c_4$ . . . . . $n–1c_{n–1}c_{n–1}c_nc_n$ (or nc_nc_n//))

SECTION 3 (3333x $C_{sm}C_{sm}C_{sm}n_{sm}n_{sm}$ $1c_{s1}c_{s1}c_{s2}c_{s2}$ $3c_{s3}c_{s3}c_{s4}c_{s4}$ . . . . . $n–1c_{sn–1}c_{sn–1}c_{sn}c_{sn}$ (or $nc_{sn}c_{sn}$//))

SECTION 4 (4444 $1d_{a1}d_{a1}d_{a2}d_{a2}$ $1r_1r_1r_2r_2$ $2d_{a1}d_{a1}d_{a2}d_{a2}$ $2r_1r_1r_2r_2$ . . . . . $nd_{a1}d_{a1}d_{a2}d_{a2}$ $nr_1r_1r_2r_2)$

SECTION 5 (5555I_b $1A_1A_1A_1x$ $(1d_1d_1d_sd_s)$ $2A_2A_2A_2x$ $(2d_2d_2d_sd_s)$ . . . . . $nA_nA_nA_nx$ $(nd_nd_nd_sd_s))$

N O T E S :

(1) WAVEOB is the name of the code for reporting spectral wave data from a sea station, or from an aircraft or satellite platform.

(2) A WAVEOB report is identified by $M_iM_iM_jM_j$ = MMXX.

(3) The code form is divided into six sections (Sections 1 to 5 are optional):

Section number	*Symbolic figure group*	*Contents*
0	—	Data for reporting identification (type, buoy identifier, date, time, location), indication of frequency or wave number, method of calculation, type of station, water depth, significant wave height and spectral peak period, or wave length, and optional wave parameters
1	111	Sampling interval and duration (or length) of record, and description of measurement system bands

* Included in a fixed sea station report only.
** Included in a sea station or remote platform report only.

Section number	*Symbolic figure group*	*Contents*
2	2222	Maximum non-directional spectral density from heave sensor, and ratios of individual spectral densities to the maximum value
3	3333	Maximum non-directional spectral density from slope sensor, and ratios of individual spectral densities to the maximum value
4	4444	Directional wave functions. Mean and principle wave directions and first and second normalized polar Fourier coefficients, for bands described in Section 1
5	5555	Directional or non-directional spectral estimates by frequency or wave number, as indicated, and direction with directional spread

R E G U L A T I O N S :

65.1 General

65.1.1 The code name WAVEOB shall not be included in the report.

65.1.2 ***Use of groups***

$M_iM_iM_jM_j$ { D . . . . D / or / $A_1b_wn_bn_bn_b$ / or / $I_1I_2I_2$// } ** YYMMJ GGgg/ { IIiii* / or / $Q_cL_aL_aL_aL_a$ $L_oL_oL_oL_oL_o$** }

NOTE: See Regulation 18.2.3, Notes (1), (2) and (3)***.

65.1.2.1 Each individual WAVEOB report, whether or not included in a bulletin of such reports, shall contain as the first group the identification group $M_iM_iM_jM_j$.

65.1.2.2 A sea station shall be indicated by either the group D . . . . D or $A_1b_wn_bn_bn_b$. The position of a sea station shall be indicated by the groups $Q_cL_aL_aL_aL_a$ $L_oL_oL_oL_oL_o$. A satellite shall be indicated by the group $I_1I_2I_2$// and an aircraft shall report ///// for $I_1I_2I_2$//. A fixed sea station (other than an ocean weather station and a moored buoy), which is considered by the Member operating it to be in the same category as a land station, shall report its identification and position by means of the group IIiii.

NOTE: Data may be transmitted from a sea station or from a remote platform (aircraft or satellite).

65.1.2.3 In a report from a sea station (including an ocean weather station and a moored buoy), the latitude and longitude shall be encoded with the actual location of the station. In a satellite or aircraft report, the latitude and longitude shall indicate the (approximate) centre of the area observed.

65.1.3 ***Use of Sections 0 and 1***

65.1.3.1 The first three data groups in Section 0, after the location, shall contain indicators showing if data are expressed as frequency or wave number, the method of calculation of data and type of platform, data on the water depth in metres, significant wave height in centimetres (or tenths of a metre) and spectral peak period in tenths of a second or spectral peak wave length in metres. Optional groups, when included, shall contain data on the maximum wave height, average wave period or average wave length, estimate of significant wave height from slope

---

* Included in a fixed sea station report only.

** Included in a sea station or remote platform report only.

*** Notes to Regulation 18.2.3:

(1) A_1b_w normally corresponds to the maritime zone in which the buoy was deployed. The WMO Secretariat allocates to Members, who request and indicate the maritime zone(s) of interest, a block or blocks of serial numbers ($n_bn_bn_b$) to be used by their environmental buoy stations.

(2) The Member concerned registers with the WMO Secretariat the serial numbers actually assigned to individual stations together with their geographical positions of deployment.

(3) The Secretariat informs all concerned of the allocation of serial numbers and registrations made by individual Members.

sensors, spectral peak wave period or peak wave length derived from slope sensors, average wave period or average wave length derived from slope sensors, and dominant wave direction and directional spread.

65.1.3.2 When used, Section 1 shall contain the section identifier, the total number of bands described in the section, the sampling interval (in tenths of a second or in metres), the duration in seconds of record of the wave or the length in tens of metres, the number (BB) of bands described in the next two groups, the first centre frequency (Hz) or first centre wave number (metres)$^{-1}$, and the increment added to obtain the next centre frequency (Hz) or the next centre wave number (metres)$^{-1}$ and their associated exponents.

NOTE: In deriving the value of the first centre frequency or wave number and increment from the groups $nf_nf_nf_n$x $nf_df_df_d$x, decimal points are assumed at the left of the numeric values. For example, for centre frequency, the groups 13004 11004 would be interpreted as a first centre frequency of 0.300 x 10^{-1} Hz and an increment of 0.100 x 10^{-1} Hz. (The maximum spectral density value $C_mC_mC_m$ in Section 2, or $C_{sm}C_{sm}C_{sm}$ in Section 3, is coded in a similar fashion.)

65.1.3.3 Except when BB = 00, the two groups for the first centre frequency or first centre wave number, and the increment added to obtain the next centre frequency or the next centre wave number (each time preceded by BB) shall be repeated (n) times as required to describe band distribution.

NOTE: If sets of data groups are greater than 9, the group identifier (n) for the tenth set will be 0, the group identifier for the eleventh will be 1, etc.

65.1.3.4 BB shall be encoded BB = 00 when no increments are given and the following (n) groups are actual centre frequencies or actual centre wave numbers.

NOTE: The note under Regulation 65.1.3.3 applies if data groups are greater than 9.

65.1.4 ***Use of Sections 2 and 3***

65.1.4.1 When used, Section 2 shall contain the section identifier, an exponent associated with the first data group on the maximum value for non-directional spectra ($C_mC_mC_m$) in m^2 Hz^{-1} for frequencies or m^3 for wave numbers from wave heave sensors, given as a 3-digit number. The band number (n_mn_m) in which the maximum value for non-directional spectra occurs shall be included in the same group as the value. Subsequent groups shall contain ratios of individual spectra to the maximum (c_1c_1 to c_nc_n) as a percentage (00–99), with 00 meaning either zero or 100 per cent.

NOTES:

(1) See note under Regulation 65.1.3.2.

(2) Confusion between a zero ratio and the maximum ratio (100 per cent) should not arise since the band number (n_mn_m) for the maximum has already been identified.

65.1.4.2 Each group containing ratios shall begin with an odd number representing the unit value of the first band in the group. Thus, the number 1 shall identify values for the first and second or eleventh and twelfth or twenty-first and twenty-second, etc., bands. The last group shall contain two ratios for even numbers of bands and one ratio for odd numbers of bands. In the case of odd numbers of bands, the last two characters in the group shall be encoded as //.

65.1.4.3 When used, Section 3 shall contain the section identifier, and non-directional spectral data derived from wave slope sensors, analogous to Section 2. Regulations 65.1.4.1, with the exception of the section identifier, and 65.1.4.2 shall apply.

65.1.5 ***Use of Section 4***

When used, Section 4 shall contain the section identifier and pairs of data groups of mean direction and principal direction from which waves are coming for the band indicated, relative to true north, in units of 4 degrees, and the first and second normalized polar co-ordinates derived from Fourier coefficients. The pairs of groups shall be repeated (n) times as required to describe the total number of bands given in Section 1.

NOTES:

(1) The note under Regulation 65.1.3.3 applies if pairs of data groups are greater than 9.

(2) The mean direction and principal direction from which waves are coming will range from 00 (actual value 358° to less than 2°) to 89 (actual value from 354° to less than 358°). A value of 99 indicates the energy for the band is below a given threshold.

(3) Placing $d_{a1}d_{a1}$ and $d_{a2}d_{a2}$ for each band in the same group, with r_1r_1 and r_2r_2 for the same band in the next group, allows a quick visual check of the state of the sea.

(4) If $d_{a1}d_{a1} \approx d_{a2}d_{a2}$ and $r_1r_1 > r_2r_2$, there is a single wave train in the direction given by the common value of $d_{a1}d_{a1}$ and $d_{a2}d_{a2}$.

(5) If the coded value of $| d_{a1}d_{a1} - d_{a2}d_{a2} | > 2$ and $r_1r_1 < r_2r_2$, a confused sea exists and no simple assumption can be made about the direction of the wave energy.

65.1.6 ***Use of Section 5***

When used, this section shall contain the section identifier, an indicator (I_b) indicating whether the section includes directional or non-directional data, pairs of data groups of spectral estimates of the first to the n^{th} frequencies or wave numbers and the direction from which waves are coming in units of 4 degrees for spectral estimates (1) to (n) and their directional spread in whole degrees.

NOTES:

(1) When non-directional spectra are transmitted, the group containing direction and directional spread may be omitted.

(2) Complete directional spectra may be coded by repeating as many duplets as needed to define the entire spectrum. A partial directional spectrum may be coded by selecting the largest spectral estimate for any one frequency or wave number band over all directions and coding this for each frequency or wave number band. Secondary peaks may not be coded unless the full directional spectrum is transmitted.

(3) For non-directional frequency spectra, the spectral estimates are in m^2 Hz^{-1}. For non-directional wave number spectra, the spectral estimates are in m^3. For a complete directional frequency spectrum, spectral estimates are in m^2 Hz^{-1} $radian^{-1}$. For a complete directional wave number spectrum, the spectral estimates are in m^4. For incomplete directional spectra, whether in frequency or wave number, the units of the spectral estimates should be m^2 Hz^{-1} or m^3. That is, the total integrated energy within a frequency band is given rather than just that of the peak. If the spectral estimate is less than 0.100×10^{-5}, the value of 0 must be used. The exception to this occurs when all subsequent estimates at higher frequencies are also 0, in which case only the zero immediately after the last non-zero spectral estimate need be included; all others need not be coded.

(4) There may be cases when spectral estimates are given in integrated units, such as m^2, and it is necessary to convert these to the units of the code. This is done by calculating the bandwidth at a frequency by determining the frequency difference between midpoints on either side of the frequency in question. The integrated spectral estimate is then divided by this computed bandwidth.

SPECIFICATIONS OF SYMBOLIC LETTERS USED IN WAVEOB (and not already defined)

A_1 WMO Regional Association area in which buoy, drilling rig or oil- or gas-production platform has been deployed (1 – Region I; 2 – Region II, etc.). (Code table 0161)
(FM 13, FM 18, FM 22, FM 63, FM 64, FM 65)

$A_1A_1A_1$
$A_2A_2A_2$
. . .
$A_nA_nA_n$

Spectral estimates of the first to n^{th} frequencies (or wave numbers if so indicated).
(FM 65)

(1) The use of frequency or wave number is indicated by symbolic letter I_a.

BB Number of bands described by the next two groups, except that BB = 00 indicates each of the following groups represents only a centre frequency or wave number.
(FM 65)

B_TB_T Total number of bands described.
(FM 65)

b_w Sub-area belonging to the area indicated by A_1. (Code table 0161)
(FM 13, FM 18, FM 22, FM 63, FM 64, FM 65)

$C_mC_mC_m$ Maximum non-directional spectral density derived from heave sensors, in m^2 Hz^{-1} for frequencies and m^3 for wave numbers.
(FM 65)

$C_{sm}C_{sm}C_{sm}$ Maximum non-directional spectral density derived from slope sensors, in m^2 Hz^{-1} for frequencies and m^3 for wave numbers.
(FM 65)

$c_{s1}c_{s1}$
$c_{s2}c_{s2}$
. . .
$c_{sn}c_{sn}$

The ratio of the spectral density derived from slope sensors for a given band, to the maximum spectral density given by $C_{sm}C_{sm}C_{sm}$.
(FM 65)

(1) A coded value of 00 may indicate either zero, or that the band contains the maximum spectral density. Since the band containing the maximum value will have been identified, it will be obvious which meaning should be assigned.

c_1c_1
c_2c_2
. . .
c_nc_n

The ratio of the spectral density derived from heave sensors for a given band, to the maximum spectral density given by $C_mC_mC_m$.
(FM 65)

(1) See Note (1) under $c_{s1}c_{s1}$, $c_{s2}c_{s2}$, . . . $c_{sn}c_{sn}$.

D´D´D´D´ Duration of record of wave, in seconds, or length of record of wave, in tens of metres.
(FM 65)

(1) The use of frequency or wave number is indicated by symbolic letter I_a.

D . . . . D Ship's call sign consisting of three or more alphanumeric characters.
(FM 13, FM 20, FM 33, FM 36, FM 62, FM 63, FM 64, FM 65, FM 85)

$d_{a1}d_{a1}$ Mean direction, in units of 4 degrees, from which waves are coming for the band indicated, relative to true north. (Code table 0880)
(FM 65)

(1) A value of 99 indicates the energy for that band is below a given threshold.

$d_{a2}d_{a2}$ Principal direction, in units of 4 degrees, from which waves are coming for the band indicated, relative to true north. (Code table 0880)
(FM 65)

(1) See Note (1) under $d_{a1}d_{a1}$.

d_dd_d True direction, in units of 4 degrees, from which dominant wave is coming. (Code table 0880)
(FM 65)

d_sd_s Directional spread, in whole degrees, of the dominant wave.
(FM 65)

(1) The value of the directional spread is normally less than one radian (about 57°).

d_1d_1
d_2d_2
. . .
d_nd_n

True direction, in units of 4 degrees, from which waves are coming. (Code table 0880)
(FM 65)

$f_df_df_d$ The increment to be added to the previous centre frequency or previous centre wave number, to obtain the next centre frequency (Hz) or the next centre wave number (m^{-1}), in the series, the exponent being given by symbolic letter x.
(FM 65)

$f_1f_1f_1$
$f_2f_2f_2$
. . .
$f_nf_nf_n$

The first centre frequency (Hz) in a series, or the first centre wave number (m^{-1}), the exponent being given by symbolic letter x.
(FM 65)

GGgg Time of observation, in hours and minutes UTC.
(FM 12, FM 13, FM 14, FM 15, FM 16, FM 18, FM 22, FM 35, FM 36, FM 37, FM 38, FM 42, FM 62, FM 63, FM 64, FM 65, FM 67, FM 88)

$H_mH_mH_mH_m$ Maximum wave height, in centimetres.
(FM 65)

(1) In the event wave height can only be reported in tenths of a metre, the final digit in the group shall be encoded as /.

$H_sH_sH_sH_s$ Significant wave height, in centimetres.
(FM 65)

(1) See Note (1) under $H_mH_mH_mH_m$.

$H_{se}H_{se}H_{se}H_{se}$ Estimate of significant wave height from slope sensors, in centimetres.
(FM 65)

(1) See Note (1) under $H_mH_mH_mH_m$.

hhhh Water depth, in metres.
(FM 65)

I_a Indicator for frequency or wave number. (Code table 1731)
(FM 65)

I_b Indicator for directional or non-directional spectral wave data. (Code table 1732)
(FM 65)

I_m Indicator for method of calculation of spectral data. (Code table 1744)
(FM 65)

I_p Indicator for type of platform. (Code table 1747)
(FM 65)

I_1 Name of country or international agency which operates the satellite. (Code table 1761)
(FM 65, FM 86, FM 87, FM 88)

II Block number.
(FM 12, FM 20, FM 22, FM 32, FM 35, FM 39, FM 57, FM 65, FM 71, FM 75, FM 81, FM 83, FM 85)

(1) The block numbers define the area in which the reporting station is situated. They are allocated to one country or a part of it or more countries in the same Region. The list of block numbers for all countries is given in Volume A of publication WMO–No. 9.

I_2I_2 Indicator figure for satellite name (supplied by operator I_1).
(FM 65, FM 86, FM 87, FM 88)

(1) Even deciles for geostationary satellites.

(2) Odd deciles for polar-orbiting satellites.

iii Station number.
(FM 12, FM 20, FM 22, FM 32, FM 35, FM 39, FM 57, FM 65, FM 71, FM 75, FM 81, FM 83, FM 85)

(1) See Section D of this volume. (Editorial note: WMO-No. 306, Volume I.1, Part A)

J Units digit of the year (UTC), i.e. 1974 = 4.
(FM 18, FM 62, FM 63, FM 64, FM 65, FM 88)

$L_aL_aL_aL_a$ Latitude, in degrees and minutes.
(FM 22, FM 42, FM 44, FM 57, FM 62, FM 63, FM 64, FM 65)

$L_oL_oL_oL_oL_o$ Longitude, in degrees and minutes.
(FM 22, FM 42, FM 44, FM 57, FM 62, FM 63, FM 64, FM 65)

MM Month of the year (UTC), i.e. 01 = January; 02 = February, etc.
(FM 18, FM 22, FM 39, FM 40, FM 47, FM 49, FM 57, FM 62, FM 63, FM 64, FM 65, FM 71, FM 72, FM 73, FM 75, FM 76, FM 88)

M_iM_i Identification letters of the report. (Code table 2582)
(FM 12, FM 13, FM 14, FM 20, FM 32, FM 33, FM 34, FM 35, FM 36, FM 37, FM 38, FM 39, FM 40, FM 41, FM 62, FM 63, FM 64, FM 65, FM 67, FM 85, FM 86, FM 87, FM 88)

M_jM_j Identification letters of the part of the report or the version of the code form. (Code table 2582)
(FM 12, FM 13, FM 14, FM 20, FM 32, FM 33, FM 34, FM 35, FM 36, FM 37, FM 38, FM 39, FM 40, FM 41, FM 62, FM 63, FM 64, FM 65, FM 67, FM 85, FM 86, FM 87, FM 88)

n_mn_m Number of the band in which the maximum non-directional spectral density determined by heave sensors lies.
(FM 65)

$n_{sm}n_{sm}$ Number of the band in which the maximum non-directional spectral density determined by slope sensors lies.
(FM 65)

$n_bn_bn_b$ Type and serial number of buoy.
(FM 13, FM 18, FM 22, FM 63, FM 64, FM 65)

$P_aP_aP_aP_a$ Average wave period, in tenths of a second, or average wave length, in metres.
(FM 65)

$P_pP_pP_pP_p$ Spectral peak period derived from heave sensors, in tenths of a second, or spectral peak wave length, in metres.
(FM 65)

$P_{sa}P_{sa}P_{sa}P_{sa}$ Average period derived from slope sensors, in tenths of a second, or average wave length, in metres.
(FM 65)

$P_{sp}P_{sp}P_{sp}P_{sp}$ Spectral peak period derived from slope sensors, in tenths of a second, or spectral peak wave length, in metres.
(FM 65)

Q_c Quadrant of the globe. (Code table 3333)
(FM 13, FM 14, FM 18, FM 20, FM 33, FM 34, FM 36, FM 37, FM 38, FM 40, FM 41, FM 44, FM 47, FM 62, FM 63, FM 64, FM 65, FM 72, FM 76, FM 85)

r_1r_1 First normalized polar coordinate derived from Fourier coefficients.
(FM 65)

r_2r_2 Second normalized polar coordinate derived from Fourier coefficients.
(FM 65)

SSSS Sampling interval (in tenths of a second or in metres).
(FM 65)

x Exponent for spectral wave data. (Code table 4800)
(FM 65)

YY Day of the month (UTC), with 01 indicating the first day, 02 the second day, etc.:

(*a*) On which the actual time of observation falls;
(FM 12, FM 13, FM 14, FM 15, FM 16, FM 18, FM 20, FM 32, FM 33, FM 34, FM 35, FM 36, FM 37, FM 38, FM 39, FM 40, FM 41, FM 42, FM 62, FM 63, FM 64, FM 65, FM 67, FM 85, FM 86, FM 87, FM 88)

WAVEOB CODE TABLES

0161

A_1 ***WMO Regional Association area in which buoy, drilling rig or oil- or gas-production platform has been deployed*** **(1 – Region I; 2 – Region II, etc.)**

b_w ***Sub-area belonging to the area indicated by*** **A_1**

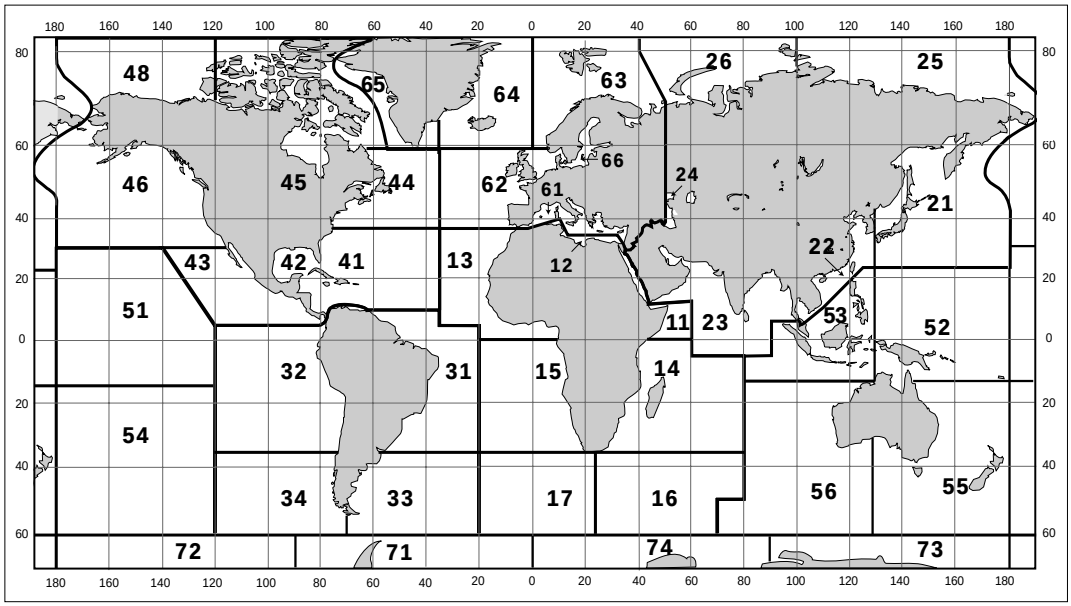

0880

$d_{a1}d_{a1}$ ***Mean direction, in units of 4 degrees, from which waves are coming for the band indicated, relative to true north***

$d_{a2}d_{a2}$ ***Principal direction, in units of 4 degrees, from which waves are coming for the band indicated, relative to true north***

d_dd_d ***True direction, in units of 4 degrees, from which the dominant wave is coming***

d_1d_1
d_2d_2
. . .
d_nd_n ***True direction, in units of 4 degrees, from which waves are coming***

Code figure		Code figure	
00	358° to less than 2°	.	
01	2° to less than 6°	89	354° to less than 358°
02	6° to less than 10°	90–98	Not used
.		99	Ratio of the spectral density for the band to the maximum is less than 0.005
.			

1731

I_a ***Indicator for frequency or wave number***

Code figure		Code figure	
0	Frequency (Hz)	1	Wave number (m^{-1})

1732

I_b ***Indicator for directional or non-directional spectral wave data***

Code figure		Code figure	
0	Non-directional	1	Directional

1744

I_m *Indicator for method of calculation of spectral data*

Code figure		Code figure	
1	Longuet-Higgins (1964)	4	Maximum entropy method
2	Longuet-Higgins (F_3 method)	5–9	Reserved
3	Maximum likelihood method		

1747

I_p *Indicator for type of platform*

Code figure		Code figure	
0	Sea station	2	Aircraft
1	Automatic data buoy	3	Satellite

1761

I_1 *Name of country or international agency which operates the satellite*

Code figure		Code figure	
0	European Community	3	Russian Federation
1	Japan	4	India
2	USA	5–9	Reserved

2582

M_iM_i *Identification letters of the report*

M_jM_j *Identification letters of the part of the report or the version of the code form*

Code form		M_iM_i				M_jM_j				
		Land station	Sea station	Aircraft	Satellite	Part A	Part B	Part C	Part D	No distinction
FM 12–X Ext.	SYNOP	AA								XX
FM 13–X	SHIP		BB							XX
FM 14–X Ext.	SYNOP MOBIL	OO								XX
FM 18–X	BUOY		ZZ							YY
FM 20–VIII	RADOB	FF	GG			AA	BB			
FM 32–IX	PILOT	PP				AA	BB	CC	DD	
FM 33–IX	PILOT SHIP		QQ			AA	BB	CC	DD	
FM 34–IX	PILOT MOBIL	EE				AA	BB	CC	DD	
FM 35–X Ext.	TEMP	TT				AA	BB	CC	DD	
FM 36–X Ext.	TEMP SHIP		UU			AA	BB	CC	DD	
FM 37–X Ext.	TEMP DROP			XX		AA	BB	CC	DD	
FM 38–X Ext.	TEMP MOBIL	II				AA	BB	CC	DD	
FM 39–VI	ROCOB	RR								XX
FM 40–VI	ROCOB SHIP		SS							XX
FM 41–IV	CODAR			LL						XX
FM 62–VIII Ext.	TRACKOB		NN							XX
FM 63–IX	BATHY		JJ							XX
FM 63–X Ext.	BATHY		JJ							YY
FM 64–IX	TESAC		KK							XX
FM 65–IX	WAVEOB		MM							XX
FM 67–VI	HYDRA	HH								XX
FM 85–IX	SAREP	CC	DD			AA	BB			
FM 86–VIII Ext.	SATEM				VV	AA	BB	CC	DD	
FM 87–VIII Ext.	SARAD				WW					XX
FM 88–X	SATOB				YY					XX

3333

Q_c *Quadrant of the globe*

Code figure	Latitude	Longitude
1	North	East
3	South	East
5	South	West
7	North	West

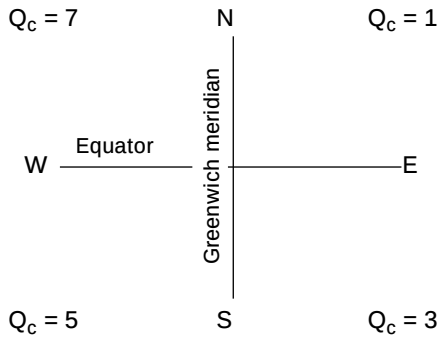

N o t e : The choice is left to the observer in the following cases:

— When the ship is on the Greenwich meridian or the 180th meridian ($L_oL_oL_oL_o$ = 0000 or 1800 respectively):
Q_c = 1 or 7 (northern hemisphere) or
Q_c = 3 or 5 (southern hemisphere);

— When the ship is on the Equator ($L_aL_aL_a$ = 000):
Q_c = 1 or 3 (eastern longitude) or
Q_c = 5 or 7 (western longitude).

4800

x *Exponent for spectral wave data*

Code figure		Code figure	
0	10^{-5}	5	10^{0}
1	10^{-4}	6	10^{1}
2	10^{-3}	7	10^{2}
3	10^{-2}	8	10^{3}
4	10^{-1}	9	10^{4}

ANNEX III

PROBABILITY DISTRIBUTIONS FOR WAVE HEIGHTS

The following distributions are briefly described in the order shown (see Johnson and Kotz, 1970, *inter alia*, for further details):

- Normal or Gaussian
- Log-normal
- Gamma
- Weibull
- Exponential
- Rayleigh
- Generalized extreme value (GEV)
- Fisher-Tippett Type I or Gumbel
- Fisher-Tippett Type III
- Generalized Pareto

The symbols $\bar{x}$ and s are used for the mean and standard deviation of the series x_i (i = 1, n), i.e.:

$$\bar{x} = \frac{\sum x_i}{n}$$

$$s^2 = \frac{\sum (x_i - \bar{x})^2}{n-1}$$

where Σ indicates summation over i (i = 1, n).

The symbol Γ has its usual meaning as the gamma function:

$$\Gamma(z) = \int_{t=0}^{\infty} t^{z-1} e^{-t}\, dt; \quad \Gamma'(z) = \frac{d\Gamma}{dz}$$

Values are widely tabulated.

1. Normal or Gaussian distribution

$$f(x) = \frac{1}{\sqrt{2\pi}\beta} \exp\left[-\frac{(x-\alpha)^2}{2\beta^2}\right] \quad -\infty < x < \infty$$

mean = α

variance = β^2

Probability paper

$$x = \Phi^{-1}(p) \quad \left[\Phi(x) = \int_{-\infty}^{x} \frac{1}{\sqrt{2\pi}} \exp\left(\frac{-x^2}{2}\right) dx\right]$$

$$y = (h)$$

Moments estimators

$$\tilde{\alpha} = \bar{x}$$

$$\tilde{\beta} = s$$

Maximum likelihood estimators

$$\hat{\alpha} = \bar{x}$$

$$\hat{\beta} = \sqrt{\frac{\sum (x_i - \bar{x})^2}{n}}$$

The function Φ (known as the standard normal distribution) is widely tabulated.

2. Log-normal distribution

The two-parameter log-normal distribution is given by:

$$f(x) = \frac{1}{x\beta\sqrt{2\pi}}\exp\left[-\frac{(\log x-\alpha)^2}{2\beta^2}\right] \quad x>0$$
$$= 0 \qquad \text{otherwise}$$
$$\text{mean} = \exp\left[\alpha+\frac{\beta^2}{2}\right]$$
$$\text{variance} = \exp[2\alpha]\exp\left[\beta^2\right]\left(\exp\left[\beta^2\right]-1\right)$$

Probability paper

$$x = \Phi^{-1}(p) \quad \left[\Phi(x)=\int_{-\infty}^{x}\frac{1}{\sqrt{2\pi}}\exp\left(\frac{-x^2}{2}\right)dx\right]$$
$$y = \log(h)$$

Maximum likelihood estimators

$$\hat{\alpha} = \frac{1}{n}\sum \log x_i$$
$$\hat{\beta} = \sqrt{\frac{1}{n}\sum(\log x_i - \hat{\alpha})^2}$$

The three-parameter log-normal is produced by replacing x by $x - \theta$ and is defined on $[\theta, \infty)$. Estimation is more complex.

3. Gamma distribution

$$f(x) = \frac{x^{\alpha-1}}{\beta^\alpha\Gamma(\alpha)}\exp(-\frac{x}{\beta}) \quad \alpha, \beta, x > 0$$
$$= 0 \qquad \text{otherwise}$$
$$\text{mean} = \alpha\beta$$
$$\text{variance} = \alpha\beta^2$$

Probability paper cannot be used for estimation with the gamma distribution.

Moments estimators

$$\tilde{\alpha} = \frac{\bar{x}^2}{s^2}$$
$$\tilde{\beta} = \frac{s^2}{\bar{x}}$$

Maximum likelihood estimators

$$\frac{1}{n}\sum \log x_i = \log\hat{\beta}+\Psi(\hat{\alpha})$$
$$\bar{x} = \hat{\alpha}\hat{\beta}$$

where $\Psi(x) = \Gamma'(x)/\Gamma(x)$. These equations have to be solved numerically.

The three-parameter gamma is produced by replacing x by $x - \theta$ and is defined on $[\theta, \infty)$. Estimation is more complex.

4. Weibull distribution

$$f(x) = \beta\left(\frac{x}{\alpha}\right)^{\beta-1}\frac{1}{\alpha}\exp\left[-\left(\frac{x}{\alpha}\right)^{\beta}\right] \quad \alpha, \beta, x > 0$$

$$= 0 \qquad \text{otherwise}$$

$$F(x) = 1-\exp\left[-\left(\frac{x}{\alpha}\right)^{\beta}\right] \qquad x > 0$$

$$= 0 \qquad x < 0$$

$$\text{mean} = \alpha\Gamma\left(\frac{1}{\beta}+1\right)$$

$$\text{variance} = \alpha^2\left[\Gamma\left(\frac{2}{\beta}+1\right) - \left\{\Gamma\left(\frac{1}{\beta}+1\right)\right\}^2\right]$$

Probability paper

$$x = \log\left[-\log(1-p)\right]$$

$$y = \log(h)$$

Maximum likelihood estimators

$$\hat{\alpha} = \left(\frac{\sum x_i^{\beta}}{n}\right)^{\frac{1}{\beta}}$$

$$\hat{\beta} = \left(\frac{\sum x_i^{\beta}\log(x_i)}{\sum x_i^{\beta}} - \frac{\sum\log(x_i)}{n}\right)^{-1}$$

These equations have to be solved numerically.

The three-parameter Weibull is produced by replacing x by $x - \theta$ and is defined on $[\theta, \infty)$. Estimation is more complex.

5. Exponential distribution

$$f(x) = \frac{1}{\alpha}\exp\left(-\frac{x}{\alpha}\right) \quad \alpha, x > 0$$

$$= 0 \qquad \text{otherwise}$$

$$F(x) = 0 \qquad x < 0$$

$$= 1-\exp\left(-\frac{x}{\alpha}\right) \quad x > 0$$

$$\text{mean} = \alpha$$

$$\text{variance} = \alpha^2$$

Probability paper

$$x = -\log(1-p)$$

$$y = h$$ (Any line must go through the origin.)

Moments and maximum likelihood estimators

$$\tilde{\alpha} = \hat{\alpha} = \bar{x}$$

The two-parameter exponential is produced by replacing x by $x - \theta$ and is defined on $[\theta, \infty)$. Estimation is more complex. The exponential distribution is a special case of the Gamma ($\alpha = 1$) and Weibull ($\beta = 1$) distributions.

6. Rayleigh distribution

$$f(x) = \frac{x}{\alpha^2}\exp\left(-\frac{x^2}{2\alpha^2}\right) \quad \alpha,\ x > 0$$
$$= 0 \qquad \text{otherwise}$$
$$F(x) = 0 \qquad x < 0$$
$$= 1-\exp\left(-\frac{x^2}{2\alpha^2}\right) \quad x > 0$$
$$\text{mean} = \alpha\sqrt{\frac{\pi}{2}}$$
$$\text{variance} = 2\alpha^2\left(1-\frac{\pi}{4}\right)$$

Probability paper

$$x = \log\left[-\log(1-p)\right]$$
$$y = \log(h)$$

All lines have slope O.5.

Moments estimators

$$\tilde{\alpha} = \frac{\bar{x}}{\sqrt{\pi/2}}$$

Maximum likelihood estimators

$$\tilde{\alpha} = \sqrt{\frac{\sum x_i^{\,2}}{2n}}$$

The two-parameter Rayleigh is produced by replacing x by $x - \theta$ and is defined on $[\theta, \infty)$. Estimation is more complex. The Rayleigh distribution is a special case of the Weibull distribution ($\beta = 2$, $\alpha = \sqrt{2}\alpha$).

7. Generalized extreme value (GEV) distribution

$$F(x) = 0 \qquad x < \alpha+\frac{\beta}{\theta} \text{ and } \theta < 0$$
$$= \exp\left[-\left(1-\theta\frac{x-\alpha}{\beta}\right)^{\frac{1}{\theta}}\right]$$
$$= 1 \qquad x > \alpha+\frac{\beta}{\theta} \text{ and } \theta > 0$$
$$\text{mean} = \alpha+\frac{\beta}{\theta}\left[1-\Gamma(1+\theta)\right] \qquad \theta \neq 0$$
$$= \alpha+\gamma\beta \ (\gamma = \text{Euler's constant} = 0.5772...) \quad \theta = 0$$
$$\text{variance} = \left(\frac{\beta}{\theta}\right)^2\left[\Gamma(1+2\theta)+\Gamma^2(1+\theta)\right] \qquad \theta \neq 0$$
$$= \beta^2\frac{\pi^2}{6} \qquad \theta = 0$$

For methods of estimation, see NERC (1975).

8. Fisher-Tippett Type I (FT-I) (or Gumbel) distribution

$$f(x) = \frac{1}{\beta}\exp\left[-\frac{x-\alpha}{\beta} - \exp\left(-\frac{x-\alpha}{\beta}\right)\right] \qquad \beta > 0$$

$$F(x) = \exp\left[-\exp\left(-\frac{x-\alpha}{\beta}\right)\right]$$

$$\text{mean} = \alpha + \gamma\beta \quad (\gamma = \text{Euler's constant} = 0.5772...)$$

$$\text{variance} = \beta^2\frac{\pi^2}{6}$$

Probability paper

$$x = -\log[-\log(p)]$$

$$y = h$$

Moments estimators

$$\alpha = x - \gamma\bar{\beta}$$

$$\beta = \sqrt{6}\frac{s}{\pi}$$

Maximum likelihood estimators

$$\alpha = -\beta\log\left[\frac{1}{n}\sum\exp\left(-\frac{x_i}{\beta}\right)\right]$$

$$\beta = \frac{1}{n}\sum x_i - \frac{\sum x_i\exp\left(-\frac{x_i}{\beta}\right)}{\sum\exp\left(-\frac{x_i}{\beta}\right)}$$

These equations have to be solved numerically.

A detailed description and comparison of the various methods of estimation for the FT-I distribution are given in Carter and Challenor (1983). The FT-I is a special case of the GEV ($\theta = 0$).

9. Fisher-Tippett Type III (FT-III) distribution

$$f(x) = \beta\left(\frac{\theta-x}{\alpha}\right)^{\beta-1}\frac{1}{\alpha}\exp\left[-\left(\frac{\theta-x}{\alpha}\right)^{\beta}\right] \qquad x<\theta$$

$$= 0 \qquad \text{otherwise}$$

$$F(x) = \exp\left[-\left(\frac{\theta-x}{\alpha}\right)^{\beta}\right] \qquad x<\theta$$

$$= 1 \qquad x>\theta$$

$$\text{mean} = \theta - \alpha\Gamma\left(\frac{1}{\beta}+1\right)$$

$$\text{variance} = \alpha^2\left[\Gamma\left(\frac{2}{\beta}+1\right) - \left\{\Gamma\left(\frac{1}{\beta}+1\right)\right\}^2\right]$$

Probability paper

$$x = \log\left[-\log(1-p)\right]$$
$$y = \log(\theta - h)$$

Probability plotting can only be used to estimate θ by plotting several lines and using some goodness-of-fit criterion (see text for details).

The FT-III distribution is a special case of the GEV ($\theta < 0$). For this reason, it is advisable to use the estimation techniques referenced for the GEV. If the transformation X = –X is applied to the FT-III, a three-parameter Weibull distribution is obtained.

10. Generalized Pareto distribution

$$f(x) = \frac{1}{\alpha}\left(1-\beta\frac{x}{\alpha}\right)^{\frac{1}{\beta-1}} \qquad x>0$$
$$= 0 \qquad \text{otherwise}$$

This distribution is the asymptotic distribution for exceedances over a level (in a similar way to the GEV for extremes). For details of its use and estimators, see Smith (1984). The exponential distribution is a special case with $\beta = 0$.

ANNEX IV

THE PNJ (PIERSON-NEUMANN-JAMES, 1955) WAVE GROWTH CURVES

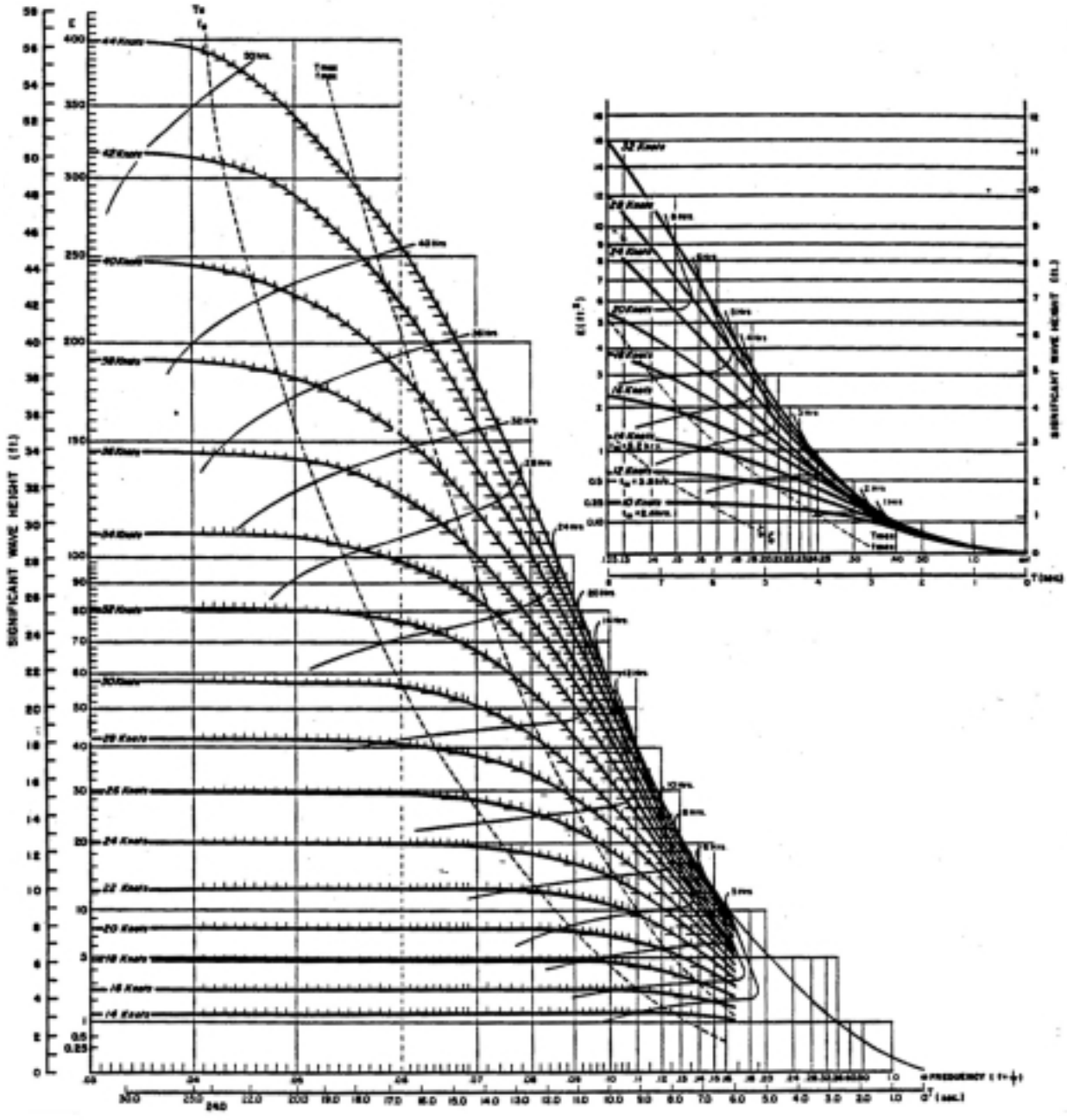

Duration graph. Distorted co-cumulative spectra for wind speeds from 10 to 44 knots as a function of the duration

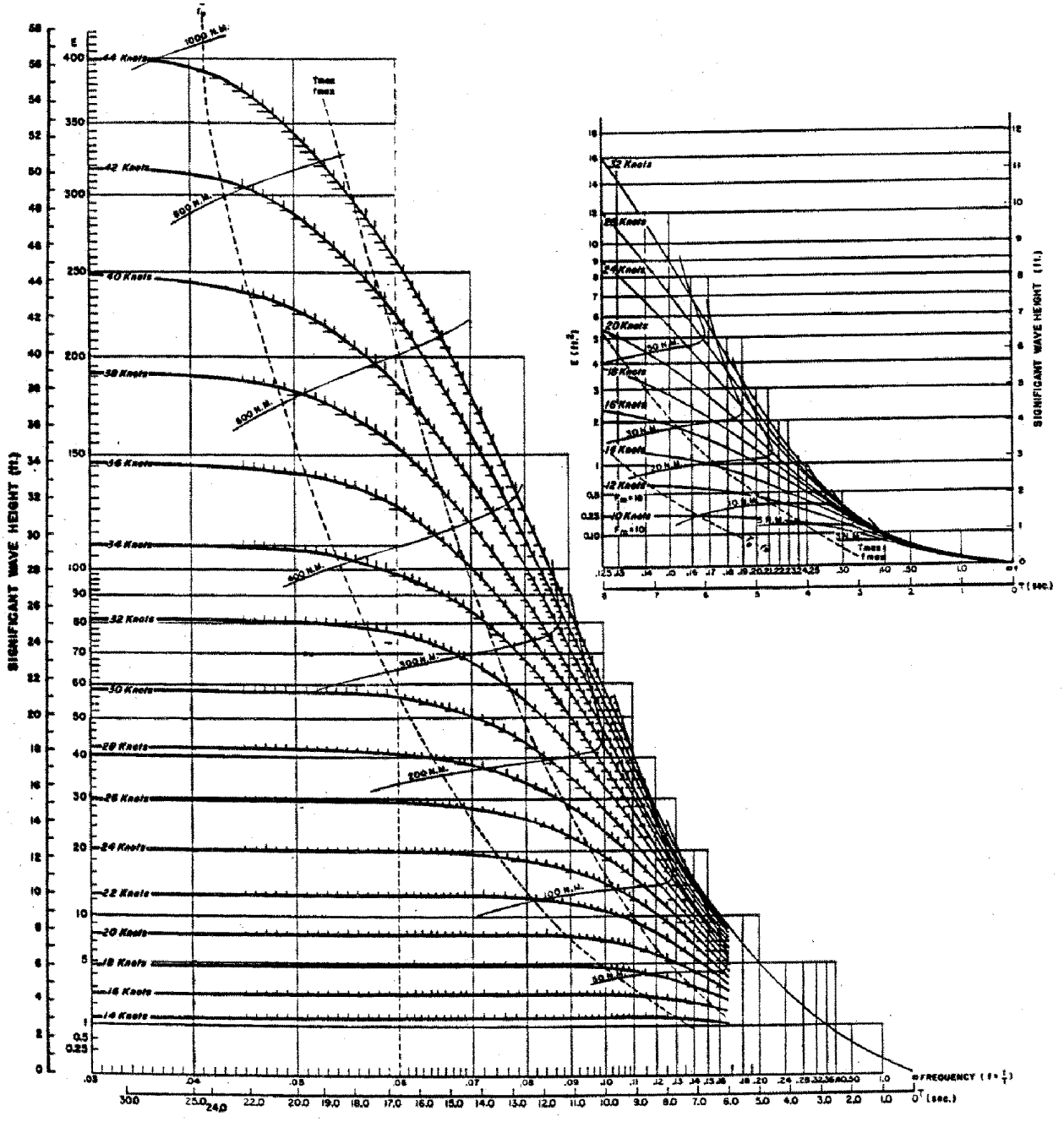

Fetch graph. Distorted co-cumulative spectra for wind speeds from 10 to 44 knots as a function of the fetch

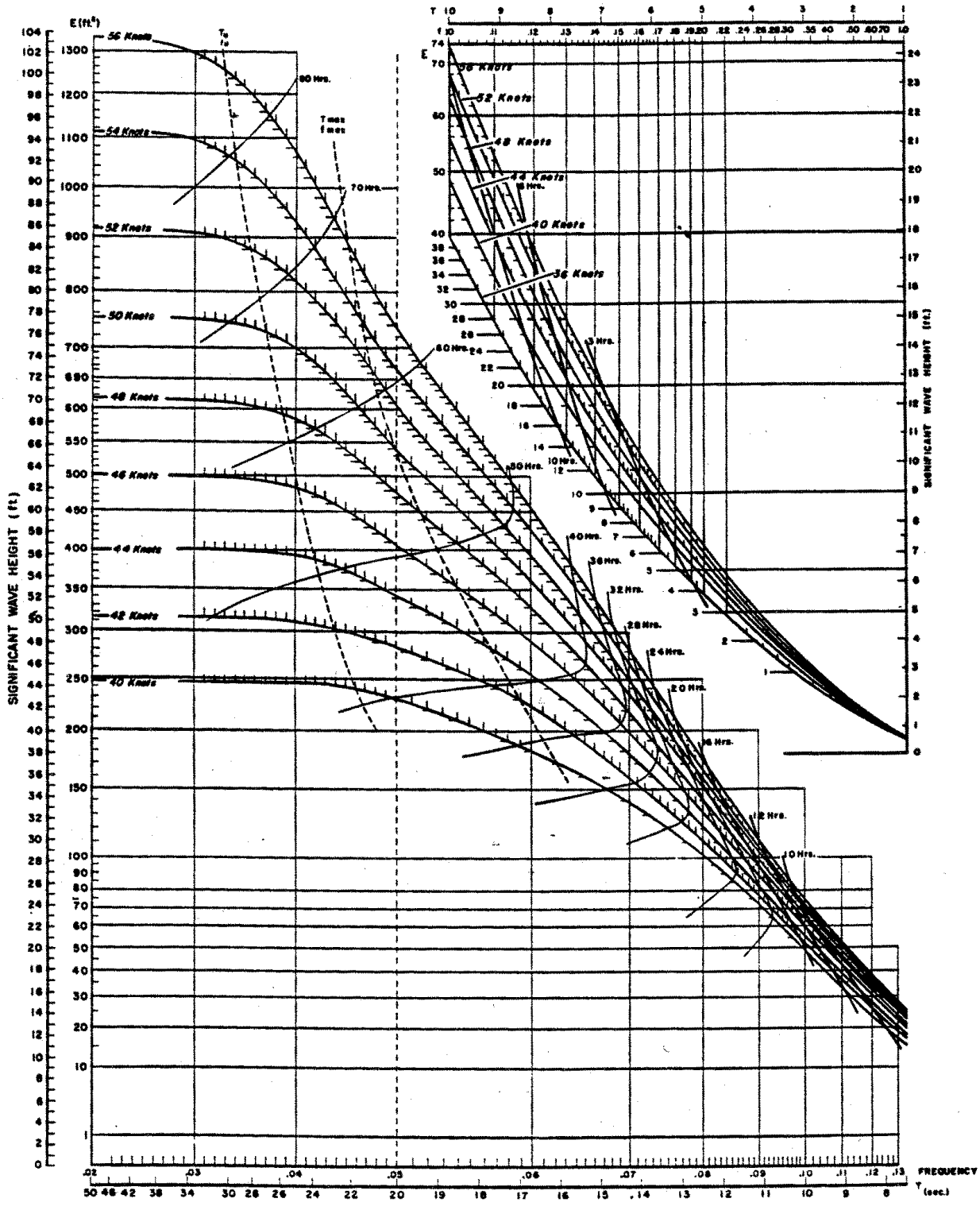

Duration graph. Distorted co-cumulative spectra for wind speeds from 36 to 56 knots as a function of the duration

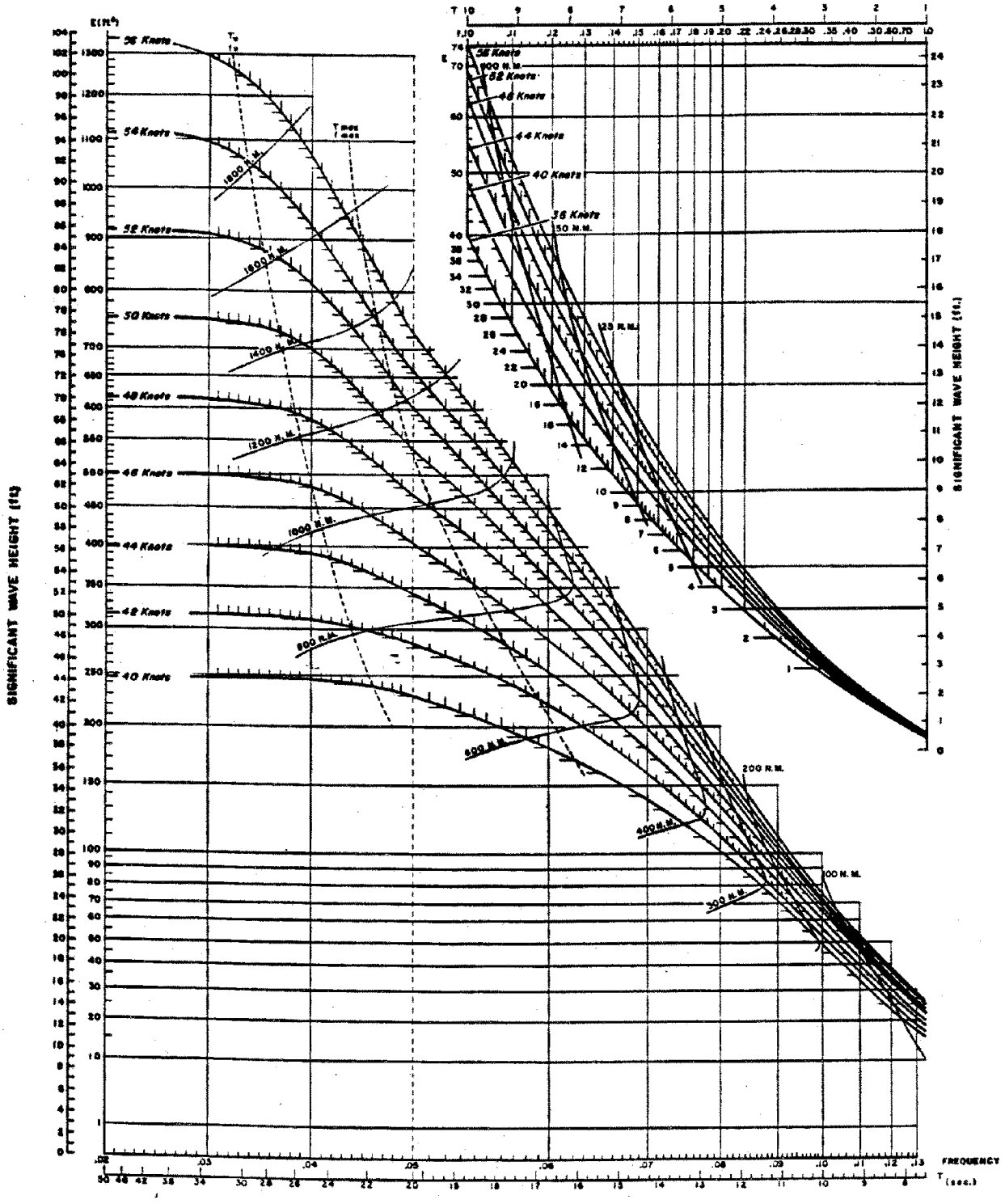

Fetch graph. Distorted co-cumulative spectra for wind speeds from 36 to 56 knots as a function of the fetch

REFERENCES

Abbott, M. B., H. H. Petersen and O. Skovgaard, 1978: Computations of short waves in shallow water. *Proc. 16th Coastal Engineering Conference*, Hamburg, Germany, 414–433.

Abreu, M., A. Larazza and E. B. Thornton, 1992: Non-linear transformation of directional wave spectra in shallow water. *J. Geophys. Res*., 97(C10), 15,579–15,589.

Allender, J., T. Audunson, S. F. Barstow, S. Bjerken, H. E. Krogstad, P. Steinbakke, L. Vartdal, L. Borgman and C. Graham, 1989: The WADIC Project: A comprehensive field evaluation of directional wave instrumentation. *Ocean Engineering*, 161, 505–536.

AWS, 1995: *Forecasters guide to tropical meteorology*. Air Weather Service, Illinois, USA, AWS TR 240, Updated by Colin S. Ramage. August 1995, 462 pp.

Bacon, S. and D. J. T. Carter, 1991: Wave climate changes in the North Atlantic and North Sea. *Int. J. of Climatology*, 11, 545–558.

Barnett, T. P., 1968: On the generation, dissipation and prediction of ocean wind-waves. *J. Geophys. Res*., 73, 513–529.

Barrick, D. E. and J. F. Gower (Eds.), 1986: Special issue on HF radar oceanography. *IEEE Jour. Oceanic Eng*., April l986.

Barstow, S. F., 1995: Wave climate assessment by satellite remote sensing. *Proc. Fifth International Offshore and Polar Engineering Conf.* (*ISOPE-1995*), The Hague, Netherlands, June 1995.

Barstow, S. F. and T. Kollstad, 1991: Field trials of the Directional Waverider. *Proc. First International Offshore and Polar Engineering Conf.* (*ISOPE-1991*), Edinburgh, Scotland, August 1991.

Barstow, S. F., O. Haug and T. van der Vlugt, 1994(*a*): A field validation of a Directional Waverider in a SEAWATCH buoy. *Proc. of the Oceans '94 Conf*., Brest, France, Sept. 1993, Vol 2, 32–37.

Barstow, S. F., T. I. Bern, S. Bjerken, T. I. Brate, O. Haug, O. G. Houmb and H. E. Krogstad, 1994(*b*): World wave climatologies from satellite altimeters. *Proc. of the OCEANS '94 Conf*., Brest, France, Sept. 1993, Vol. 2., 64–68.

Battjes, J. A., 1972: Long-term wave height distributions at seven stations around the British Isles. *Deut. Hydrogr. Z.*, 25(4), 179–189.

Battjes, J. A. and J. P. F. M. Janssen, 1978: Energy loss and set-up due to breaking in random waves. *Proc. 16th Coastal Engineering Conference*, Hamburg, Germany, 569–587.

Battjes, J. A., Y. Eldeberky and Y. Won, 1993: Spectral Boussinesq modelling of breaking waves. *Proc. 2nd Int. Symp. on Ocean Wave Measurements and Analysis*, New Orleans, USA, 813–820.

Beale, R. C., 1981: Spatial evolution of ocean wave spectra. In: *Spaceborne synthetic aperture radar for oceanography*, R. Beale, P. De Leonibus, E. Katz (Eds), The Johns Hopkins Oceanographic Studies, 7, The Johns Hopkins University Press, 110–127.

Bendat, J. S. and A. G. Piersol, 1971: *Random data: analysis and measurement procedures*. Wiley Interscience, New York.

Berkhoff, J. C. W., 1972: Computation of combined refraction-diffraction. *Proc. 13th Coastal Engineering Conference*, 471–490.

Bjerke, P. L. and K. Torsethaugen, 1989: *Environmental conditions on the Norwegian Continental Shelf, Barents Sea*. SINTEF NHL Report No. STF60 A89052, Trondheim, Norway.

Blackadar, A. K., 1965: A simplified two-layer model of the baroclinic neutral atmospheric boundary layer. *Air Force Cambridge Res. Lab. Report*, 65-531, 49–65.

Blackman, R. B. and J. W. Tukey, 1959: *The measurement of power spectra from the point of view of communications engineering*. Dover, New York.

Booij, N., L. H. Holthuijsen and P. H. M. de Lange, 1992: The penetration of short-crested waves through a gap. *Proc. 23rd Coastal Engineering Conference*, 1044–1052.

Borgman, L. E., 1963: Risk criteria. *J. Waterways, Harbors and Coastal Eng. Div.,* ASCE, 89, (WW3), 1–35.

Borgman, L. E., 1973: Probabilities for highest wave in hurricane. *J. Waterways, Harbors and Coastal Eng. Div.,* ASCE, 99 (WW2), 185–207.

Borgman, L. E. and D. T. Resio, 1982: Extremal statistics in wave climatology. A.R. Osborne and P.M. Rizzoli (Eds.). *Topics in ocean physics*. North-Holland Publ. Co., 439–471.

Bouws, E. and J. A. Battjes, 1982: A Monte Carlo approach to the computation of refraction of water waves. *J. Geophys. Res*., 87(C8), 5718–5722.

Bouws, E., H. Günther, W. Rosenthal and C. L. Vincent, 1985: Similarity of the wind-wave spectrum in finite depth water. 1 – Spectral form. *J. Geophys. Res*., 90(C1), 975–986.

Breivik, L. A. and M. Reistad, 1992: *Use of ERS-1 altimeter wave products at DNMI. Evaluation of wave heights and wind speeds. Assimilation in a numerical wave model*. Technical Report No. 101, The Norwegian Meteorological Institute.

Brooks, R. M. and W. D. Corson, 1984: *Summary of archived Atlantic coast wave information study pressure, wind, wave and water level data*. WIS Report 13. Waterways Experiment Station, Vicksburg, MS, USA.

Brown, R. A. and W. T. Liu, 1982: An operational large-scale marine planetary boundary layer model. *J. Appl. Meteor*., 21, 261–269.

Burroughs, L. D., 1984: *Great Lakes near-shore wind predictions from Great Lakes MOS wind guidance*. NOAA Tech. Memorandum, NWS TDL 74.

Businger, J. A., J. C. Wyngaard, Y. Izumi and E. F. Bradley, 1971: Flux-profile measurements in the atmospheric surface layer. *J. Atmos. Sci*., 28, 181–189.

Canadian Climate Center, 1989: *Proc. 2nd International Workshop on Wave Hindcasting and Forecasting*, Vancouver, B.C., CCC, Downsview, Ontario.

Canadian Climate Center, 1991: *Wind/wave hindcast extremes for the east coast of Canada*. Volume I. Prepared under contract no. KM169-7-6678 by MacLaren Plansearch Limited and Oceanweather Inc., 109 pp plus appendices.

Canadian Climate Center, 1992(*a*): *Proc. 3rd International Workshop on Wave Hindcasting and Forecasting*, Montreal, Que., CCC, Downsview, Ontario.

Canadian Climate Center, 1992(*b*): *Wind/wave hindcast extremes for the west coast of Canada*. Downsview, Ontario, M3H 5T4. 143 pp plus appendices.

Cardone, V. J., 1969: *Specification of the wind distribution in the marine boundary layer for wave forecasting*. Geophysical Sciences Laboratory, TR-69-1. New York University.

Cardone, V. J., 1978: *Specification and prediction of the vector wind of the United States continental shelf for application to an oil slick trajectory program*. Final report, Contract T-34530, The City College of the City University of New York.

Cardone, V. J., W. J. Pierson and E. G. Ward, 1976: Hindcasting the directional spectrum of hurricane-generated waves. *J. Petrol. Tech*., 28, 385–394.

Carter, D. J. T. 1993: *Estimating extreme wave heights in the NE Atlantic from GEOSAT data*. Health and Safety Executive Offshore Tech. Report: OTH 93 396. HMSO London, 24 pp.

Carter, D. J. T. and P. G. Challenor, 1981(*a*): Estimating return values of environmental parameters. *Quart. J. Royal Met. Soc*., 107, 259–266.

Carter, D. J. T. and P. G. Challenor, 1981(*b*): *Estimating return values of wave height*. Inst. of Oceanographic Sciences, 116.

Carter, D. J. T. and P. G. Challenor, 1983: Methods of fitting the Fisher-Tippett Type I extreme value distribution. *Ocean Eng*., 10, 191–199.

Carter, D. J. T., and L. Draper, 1988: Has the north-east Atlantic become rougher? *Nature*, 332, 494.

Carter, D. J. T., P. G. Challenor, and P. D. Cotton, 1994: Estimating extreme values of significant wave heights from altimeter data. *Proc. WMO/IOC tech. conf. on space-based observations*. Bergen, Norway, Sept. 1993. WMO, Geneva, TD-No. 649, 63–70.

Carter D. J. T., P. G. Challenor and M. A. Srokosz, 1992: An assessment of GEOSAT wave height and wind speed measurements. *J. Geophys. Res*., 97, 11383–11392.

Carter, D. J. T., S. Foale and D. J. Webb, 1991: Variations in global wave climate throughout the year. *Int. J. Remote Sensing*, 12(8), 1687–1697.

Carter, D. J. T., P. G. Challenor, J. A. Ewing, E. G. Pitt, M. A. Srokosz and M. J. Tucker, 1986: *Estimating wave climate parameters for engineering applications*. Offshore Tech. Report OTH 86/228, HMSO, London.

Cartwright, D. E, and M. S. Longuet-Higgins, 1956: The statistical distribution of the maxima of a random function. *Proc. Royal Soc*. London, A237, 212–232.

Cavaleri, L., 1993: *Meteorological requirements for wave modelling*. WMO Marine Meteorology and Related Oceanographic Activities Report, 29, WMO/TD-No. 583.

Cavaleri, L. and P. M. Rizzoli, 1981: Wind wave prediction in shallow water: theory and applications. *J. Geophys. Res*., 86, 10961–10973.

CERC: Coastal Engineering Research Center, 1973, 1977, 1984: *Shore protection manual*. Waterways Experiment Station, US Army Corps of Engineers.

Challenor, P. G. and D. J. T. Carter, 1983: Monthly extreme air temperatures at Rothamsted. *J. Climat*., 3, 395–404.

Challenor P. G., S. Foale and D. J. Webb, 1990: Seasonal changes in the global wave climate measured by the GEOSAT altimeter. *Int. J. Remote Sensing*, 11, 2205–2213.

Charnock, H., 1955: Wind stress on a water surface. *Quart. J. Royal Met. Soc*., 81, 639.

Chelton, D. B., K. J. Hussey and M. E. Parke, 1981: Global satellite measurements of water vapour, wind speed and wave height. *Nature*, 294, 529–532.

Clancy, R. M., J. E. Kaitala and L. F. Zambresky, 1986: The Fleet Numerical Oceanography Centre Global Spectral Ocean Wave Model. *Bull. Amer. Meteor. Society*, 67(5), 498–512.

Clarke, R. H. and G. D. Hess, 1974: Geostrophic departures and the functions A and B of Rossby Similarity Theory. *Boundary Layer Met*., 7(3), 267–287.

Clarke, R. H. et al., 1971: *The Wangara experiment: boundary layer data*. Commonwealth Scientific and Industrial Research Organization, Division of Meteorological Physics, Technical Paper 19, Australia.

Cooley, J. W. and J. W. Tukey, 1965: An algorithm for machine calculation of complex Fourier series. *Math. Comput*., 19, 297–301.

Corson, W. D. et al., 1981: *Atlantic coast hindcast; deep water significant wave information*. U.S. Army Corps of Engineers, Waterways Experiment Station, Wave Info. Study for US Coastlines, WIS, Rep. 2, 856 pp.

Crapper, G. D., 1984: *Introduction to water waves*. Publ. Ellis Harwood.

Dattatri, J., 1973: Waves off Mangalore Harbor – west coast of India. *J. Waterways, Harbors and Coastal Eng. Div. ASCE*, 99(WW1), 39–58.

Dingemans, M. W., M. J. F. Stive, J. Bosma, H. J. de Vriend and J. A Vogel, 1986: Directional nearshore wave propagation and induced currents. *Proc. 20th Coastal Engineering Conference*, 1092–1106.

Dobson, F. W., 1982: *Review of reference height for and averaging time of surface wind measurements at sea*. WMO Marine Meteorology and Related Oceanographic Activities Report, 3.

Donelan, M., 1982: The dependence of the aerodynamic drag coefficients on wave parameters. *Proc. First Int. Conf. on Meteorology and Air-sea Interaction of the Coastal Zone*, The Hague, Netherlands, Amer. Meteor. Soc., 381–387.

Donelan, M. A., J. Hamilton and W. H. Hui, 1985: Directional spectra of wind generated waves. *Phil. Trans. Royal Soc*., A315, 509–562.

Dorrestein, R., 1960: Simplified method of determining refraction coefficients for sea waves. *J. Geophys. Res*., 65, 637–642.

Dorrestein, R., 1962: Wave set-up on a beach. *Proc. Second Tech. Conf. on Hurricanes*, Miami Beach, Washington DC, 230–24l.

Draper, L., 1963: Derivation of a 'design wave' from instrumental records of sea waves. *Proc. Inst. Civ. Eng*., London, 26, 291–304.

Draper, L., 1966: The analysis and presentation of wave data — a plea for uniformity. *Proc. 10th Int. Conf. on Coastal Eng*., Tokyo. ASCE, 1, 1–11.

Eid, B. M., C. M. Morton, V. J. Cardone and J. A. Greenwood, 1989: Development and evaluation of a wave climate database for the east coast of Canada. *Proc. 2nd International Workshop on Wave Hindcasting and Forecasting*, Vancouver, B.C., 140–150.

Eide, L. I., M. Reistad and J. Guddal, 1985: *Database for computed wind and wave parameters for the North Sea, Norwegian Sea and Barents Sea, each sixth hour for the years 1955–1981*. Norwegian Meteorological Institute, Bergen.

Ewing, J. A., 1971: A numerical wave prediction model for the North Atlantic Ocean. *Deut. Hydrogr. Z*., 24, 241–261.

Ewing, J. A. 1986: Presentation and interpretation of directional wave data. *Underwater Technology*, 12, 17–23.

Feit, D. H. and N. A. Pore, 1978: Objective wind forecasting and verification on the Great Lakes. *J. of Great Lakes Res*., 4(1), 10–18.

Feldhausen, P. H., S. K. Chakrabarti and B. W. Wilson, 1973: Comparison of wave hindcasts at weather station J for North Atlantic storm of December, 1959. *Deut. Hydrogr. Z*., 26(1), 10–16.

Fisher, R. A. and L. H. C. Tippett, 1928: Limiting forms of the frequency distribution of the largest or smallest member of a sample. *Proc. Camb. Phil. Soc*., 24, 180–190.

Forristall, G. J., 1978: On the statistical distribution of wave heights in a storm. *J. Geophys. Res*., 83, 2353–2358.

Francis, P .E., 1987: The North European Storm Study (NESS). *Proc. Int'l Workshop on Wave Hindcasting and Forecasting*, Halifax, Nova Scotia, 23–26 September 1986. Environmental Studies Revolving Fund. Report Series No. 065, Ottawa, 370 pp, 295–302.

Freilich, M. H. and P. G. Challenor, 1994: A new approach for determining fully empirical altimeter wind speed model function. *J. Geophys. Res*., 99, 25051–25062.

Galambos, J., 1978: *The asymptotic theory of extreme order statistics*. J. Wiley and Sons.

Georges, T. M. and J. A. Harlan, 1994: Military over-the-horizen radars turn to ocean monitoring. *MTS Journal*, 27(4), 31–38.

Gerling, T. W., 1992: Partitioning sequences and arrays of directional wave spectra into component wave systems. *J. Atmos. Oceanic Technol*., 9, 444–458.

Gilhousen, D. B., 1987: A field evaluation of NDBC moored buoy winds. *J. Atmos. Oceanic Technol*., 4, 94–104.

Glahn, H. R. and D. A. Lowry, 1972: The use of model output statistics (MOS) in objective weather forecasting. *J. Appl. Meteor*., 11, 1203–1210.

Goda, Y., 1970: Numerical experiments on wave statistics with spectral simulation. *Report of the Port and Harbour Res. Inst*., 9(3), 3–57.

Goda, Y., 1978: The observed joint distribution of periods and heights of sea waves. *Proc. 16th Coastal Engineering Conference*, Hamburg, Germany, 227–246.

Goda, Y., 1979: A review on statistical interpretation of wave data. *Report of the Port and Harbour Res. Inst*., 18(1), 5–32.

Golding, B., 1983: A wave prediction system for real-time sea state forecasting. *Quart. J. Royal Met. Soc*., 109, 393–416.

Gröen P. and R. Dorrestein, 1976: Zeegolven. *KNMI Opstellen op Oceanografisch en Maritiem Meteorologisch Gebied*, 11, 124 pp.

Grønlie, Ø., D. C. Brodtkorb and J. Wøien, 1984: MIROS: A microwave remote sensor for the ocean surface. *Norwegian Maritime Research Quart. Rev*., 12(3), 24–28.

Gumbel, E. J., 1958: *Statistics of extremes*. Columbia Univ. Press, New York.

Haltiner, G. J. and F. L. Martin, 1957: *Dynamic and physical meteorology*. McGraw-Hill Book Company.

Haltiner, G. J. and R. T. Williams, 1980: *Numerical prediction and dynamic meteorology*. John Wiley & Sons.

Hamilton, G. D., 1990: *Guide to moored buoys and other ocean data acquisition systems*. WMO Marine Meteorology and Related Oceanographic Activities Report, 16, WMO/TD-750.

Haring, R. E. and J. C. Heideman, 1978: Gulf of Mexico rare wave return periods. *Offshore Technology Conference*, Paper 3230.

Hasselmann, D. E., M. Dunckel, and J. A. Ewing, 1980: Directional wave spectra observed during JONSWAP (1973). *J. Phys. Oceanogr*., 10, 1264–1280.

Hasselmann, K., 1962: On the non-linear energy transfer in a gravity wave spectrum. 1: General theory. *J. Fluid Mech*., 12, 481–500.

Hasselmann, K., 1974: On the spectral dissipation of ocean waves due to whitecapping. *Boundary Layer Meteor*., 6, 107–127.

Hasselmann, K., S. Hasselmann, C. Brüning and A. Speidal, 1991: Interpretation and application of SAR wave image spectra in wave models. pp 117–124 in Beal R. C. (Ed.) *Directional ocean wave spectra*, Johns Hopkins Univ. Press, Baltimore. 218 pp.

Hasselmann, K., D. B. Ross, P. Müller and W. Sell, 1976: A parametric wave prediction model. *J. Phys. Oceanogr*., 6(2), 200–228.

Hasselmann, K., T. P. Barnett, E. Bouws, H. Carlson, D. E. Cartwright, K. Enke, J. A. Ewing, H. Gienapp, D. E. Hasselmann, P. Kruseman, A. Meerburg, P. Muller, D. J. Olbers, K. Richter, W. Sell and H. Walden, 1973: Measurements of wind-wave growth and swell decay during the Joint North Sea Wave Project (JONSWAP). *Deut. Hydrogr. Z*., A8(12).

Hasselmann, S., and K. Hasselmann, 1981: *A symmetrical method of computing the non-linear transfer in a gravity-wave spectrum*. Hamburger Geophysikalische Einzelschriften, Reihe A: Wiss. Abh. 52, 163 pp.

Hasselmann, S. and K. Hasselmann, 1985: Computations and parameterizations of the non-linear energy transfer in a gravity wave spectrum. Part I. A new method for efficient calculations of the exact non-linear transfer integral. *J. Phys. Oceanogr*., 15, 1369–1377.

Hasselmann, S., K. Hasselmann, J. H. Allender and T. P. Barnett, 1985: Computations and parameterizations of the non-linear energy transfer in a gravity wave spectrum. Part II: Parameterizations of the non-linear energy transfer for application in wave models. *J. Phys. Oceanogr*., 15(11), 1378–1391.

HMSO, 1985: *Waves recorded at ocean weather station Lima, December 1975–November 1981*. Offshore Tech. Report, OTH 84 204, Her Majesty's Stationary Office, London.

Hogben, N., 1990: Overview of global wave statistics. Chapter II in *Encyclopedia of Fluid Mechanics*, Volume 10: Surface and groundwater phenomena, Gulf Publishing Co., Houston.

Hogben, N. and D. J. T. Carter, 1992: Estimation of wave heights: a review of guidance issued by the Department of Energy. *Underwater Technology*, 18(1), 15–23.

Hogben, N., N. M. C. Dacunha and G. F. Olliver, 1986: *Global wave statistics*. Unwin Brothers for British Maritime Tech. Ltd.

ISSC, 1979: Report of Committee I.1: (Environmental conditions). *7th International Ship Structures Congress*, Paris.

Isaacson, M. de St.Q. and N. G. Mackenzie, 1981: Long-term distribution of ocean waves: a review. *J. Waterways, Port, Coastal and Ocean Divn.*, ASCE, 107(WW2), 92–109.

Jansen, P. C. M., 1986: Laboratory observations of the kinematics in the aerated region of breaking waves. *Coastal Engineering*, 9, 453–477.

Janssen, P. A. E. M, 1991: Quasi-linear theory of wind-wave generation applied to wave forecasting. *J. Phys. Oceanogr*., 21, 1631–1642.

Jardine, T. P. and F. R. Latham, 1981: An analysis of wave height records from the NE Atlantic. *Quart. J. Royal Met. Soc*., 107, 4l5–426.

Jenkins, A. D., 1992: A quasi-linear eddy-viscosity model for the flux of energy and momentum to wind waves using conservation-law equations in a curvilinear coordinate system. *J. Phys. Oceanogr*., 22, 844–858.

Jenkins, G. M. and D. G. Watts, 1968: *Spectral analysis and its applications*. Holden-Day.

Jenkinson, A. F., 1955: The frequency distribution of the annual maximum (or minimum) values of meteorological elements. *Quart. J. Royal Met. Soc*., 81, 158–171.

Johnson, N. L. and S. Kotz, 1970: *Continuous univariate distributions*. John Wiley and Sons, New York.

Jones, W. L., L. C. Schroeder, D. H. Boggs, E. M. Bracalente, R. A. Brown, G. J. Dame, W. J. Pierson and F. J. Wentz, 1982: The SEASAT-A scatterometer: the geophysical evaluation of remotely sensed wind vectors over the ocean. *J. Geophys. Res*., 87(C5), 3297–3317.

Kanamitsu, M., J. Alpert, K. Kampana, P. Caplan, D. Deaven, M. Iredell, B. Katz, H.-L. Pan, J. Sela and G. White, 1991: Recent changes implemented into the global forecast system at NMC. *Weather and Forecasting*, 6(3), 415–424.

Khandekar, M. L., 1989: *Operational analysis and prediction of ocean wind waves*. Coastal and Estuarine Studies, No. 33, Springer-Verlag, 214 pp.

Khandekar, M. L. and V. Swail, 1995: Storm waves in Canadian waters: A major marine hazard. *Atmosphere-Ocean*, 33, 329–357.

Khandekar, M. L., R. Lalbeharry and V. Cardone, 1994: The performance of the Canadian Spectral Ocean Wave Model (CSOWM) during the Grand Banks ERS-1 SAR wave spectra validation experiment. *Atmosphere-Ocean*, 32, 31–60.

Komen, G. J., S. Hasselmann, and K. Hasselmann, 1984: On the existence of a fully developed wind-sea spectrum. *J. Phys. Oceanogr*., 14, 1271–1285.

Komen, G. J., L. Cavaleri, M. Donelan, K. Hasselmann, S. Hasselmann and P. A. E. M. Janssen, 1994: *Dynamics and modelling of ocean waves*. Cambridge University Press, 532 pp.

Krishna, K., 1981: A two-layer first order closure model for the study of the baroclinic atmospheric boundary layer. *J. Atmos. Sci*., 38, 1401–1417.

Lacombe, H., 1965: *Cours d'oceanographie physique*, Gauthier-Villars, Paris, 392 pp.

Laing, A. K., 1985: An assessment of wave observations from ships in southern oceans. *J. Clim. Appl. Meteorol*., 24, 481–494.

Large, W. G. and S. Pond, 1981: Open ocean momentum flux measurements in moderate to strong winds. *J. Phys. Oceanogr*., 11(3), 324–336.

Lazanoff, S. M. and N. Stevenson, 1975: *An evaluation of a hemispherical operational wave spectra model*. Tech. Note 75-3, Fleet Numerical Weather Central, Monterey, Calif.

LeBlond, P. H. and L. A. Mysak, 1978: *Waves in the ocean*. Elsevier, Amsterdam.

Lefevre, J. M., J. Barckicke and Y. Menard, 1994: A significant wave height dependent function for Topex/Poseidon wind speed retrieval. *J. Geophys. Res*., 99, 25035–25049.

Lighthill, J., 1978: *Waves in fluids*. Cambridge University Press.

Lionello, P., H. Gunther and P. A. E. M. Janssen, 1992: *Assimilation of altimeter data in a global third generation wave mode*l, Technical Report No. 67, European Centre for Medium Range Weather Forecasts, ECMWF.

Lindau, R., 1994: A New Beaufort Equivalent Scale. *Proc. International COADS Wind Workshop*, Kiel, Germany, May 1994, 232–249.

Liu, W. T., K. B. Katsaros and J. A. Businger, 1979: Bulk parameterization of air-sea exchanges of heat and water vapour including the molecular constraints at the interface. *J. Atmos. Sci*., 36. 1722–1735.

Long, P. E. et al., 1978: *The state of the techniques development laboratory's boundary layer model*. NOAA Tech. Memorandum NWS TDL 66.

Longuet-Higgins, M. S., 1952: On the statistical distribution of the heights of sea waves. *J. Marine Res*., 11, 245–266.

Longuet-Higgins, M. S. and R. W. Stewart, 1962: Radiation stress and mass transport in gravity waves, with applications to "surf beats". *J. Fluid. Mech*., 13, 481–504.

Maat, N., C. Kraan and W. A. Oost, 1991: The roughness of wind waves. *Boundary Layer Meteor*., 54, 89–103.

MacLaren Plansearch Ltd. and Oceanweather, Inc., 1992: *Beaufort Sea extreme waves study*. Environmental Studies Research Funds Report, ESRF-114. National Energy Board, Calgary, Alberta.

Madsen, P. A., and O. R. Sorensen, 1993: Bound waves and triad interactions in shallow water, *J. Ocean Engineering*, 20(4), 359–388.

Mathiesen, M., Y. Goda, P. J. Hawkes, E. Mansard, M. J. Martin, E. Peltier, E. F. Thompson, and G. van Vledder, 1994: Recommended practice for extreme wave analysis. *J. Hydr. Res*., 32(6), 803–814.

Mei, C. C., 1989: *The applied dynamics of ocean surface waves*. World Scientific Publ., Advanced Series on Ocean Engineering – Volume 1, 740 pp.

Mendenhall, B. R., 1967: *A statistical study of frictional wind veering in the planetary boundary layer*. Atmospheric Science Paper 116, Dept. of Atmos. Sci, Colorado State University.

Mesinger, F., Z. I. Janjic, S. Nickovic and D. Gavrilov, 1988: The step-mountain coordinate: Model description and performance for cases of alpine lee cyclogenesis and for a case of an Applalachian redevelopment. *Monthly Weather Review*, 116, 1493–1518.

Miles, J. W., 1957: On the generation of surface waves by shear flows. *J. Fluid Mech*., 3, 185–204.

Miles, J. W., 1960: On the generation of surface waves by turbulent shear flows. *J. Fluid Mech*., 7, 469–478.

Mitsuyasu, H., F. Tasai, T. Suhara, S. Mizuno, M. Okhuso, T. Honda, and K. Rikiishi, 1975: Observations of the directional spectrum of ocean waves using a cloverleaf buoy. *J. Phys. Oceanogr*., 5, 750–760.

Monin, A. S. and A. M. Obukhov, 1954: Basic laws of turbulent mixing in the ground layer of the atmosphere. *Akad. Nauk. SSSR Geofiz. Inst. Tr*., 151, 163–181.

Munk, W. H., 1951: Origin and generation of waves. *Proc. First Coastal Engineering Conference*, Long Beach, Calif., 1–4.

NOAA, 1990: *Coastal-marine automated network (C-MAN) NWS users guide*. US Dept. of Commerce.

Neu, H. J. A., 1984: Interannual variations and longer-term changes in the sea state of the North Atlantic from 1970 to 1982. *J. Geophys. Res*., 89(C4), 6397-6402.

NERC, 1975: *Flood studies report*. Vol. 1 – Hydrological studies. Natural Environment Research Council, London.

Olsen, E., S. F. Barstow and K. Selanger, 1991: *Wave data collection, Efate, Vanuatu, November–December 1990*, Oceanographic Company of Norway Report OCN R-91076.

O'Reilly, W. C., T. H. C. Herbers, R. J. Seymour and R. T. Guza, 1995: A comparison of directional buoy and fixed platform measurements of Pacific swell. Submitted to J. Atmos. Oceanic Technol.

Overland, J. E. and W. H. Gemmill, 1977: Prediction of marine winds in the New York bight. *Monthly Weather Review*, 105, 1003–1008.

Phillips, D. W. and J. G. Irbe, 1978: *Lake to land comparison of wind, temperature, and humidity of Lake Ontario during the International Field Layer for the Great Lakes*. CLI 2-77, Atmospheric Environment Service, Environment Canada.

Phillips, O. M., 1957: On the generation of waves by a turbulent wind. *J. Fluid Mech*., 2, 417–445.

Phillips, O. M., 1958: The equilibrium range in the spectrum of wind-generated waves. *J. Fluid Mech*., 4, 426–434.

Pickands, J. III, 1975: Statistical inference using extreme order statistics. *Ann. Stat*., 3, 119–131.

Pierson, W. J., 1979: *TWINDX: A planetary boundary layer model for the winds in extratropical and tropical ocean areas*. Contract no. N00014-77-C-0206. Naval Environ. Pred. Res. Cen., Monterey, California, USA.

Pierson, W. J., 1982: *The Spectral Ocean Wave Model (SOWM): a northern hemisphere computer model for specifying and forecasting ocean wave spectra*. David Taylor Naval Research and Development Center, DTNSRDC-82-011, Bethesda, MD, USA.

Pierson, W. J., 1990: Examples of, reasons for, and consequences of the poor quality of wind data from ships for the marine boundary layer: implications for remote sensing. *J. Geophys. Res*., 95, 13313–13340.

Pierson, W. J. and L. Moskowitz, 1964: A proposed spectral form for fully developed wind-seas based on the similarity theory of S. A. Kitaigorodskii. *J. Geophys. Res*., 69(24), 5181–5190.

Pierson, W. J., G. Neumann, and R. W. James, 1955: *Practical methods for observing and forecasting ocean waves by means of wave spectra and statistics*. US Navy Hydrographic Office Pub., 603.

Pierson, W. J., L. J. Tick and L. Baer, 1966: Computer-based procedure for preparing global wave forecasts and wind field ananysis capable of using wave data obtained by a spacecraft. *Proc. Sixth Naval Hydrodynamics Symp*., Washington, 499–533.

Pontes, M. T., Athanssoulis, S. F. Barstow, L. Cavaleri, B. Holmes, D. Mollison and H. Oliveira-Peres, 1995: *Proc 14th Int. Offshore Mechanics and Arctic Eng. Conf. (OMAE'95)*, Copenhagen, Denmark, June 1995, 155–161.

Resio, D. T., 1978: Some aspects of extreme wave prediction related to climatic variation. *Proc. 10th Offshore Tech. Conf*., Houston, Texas, III, OTC 3278.

Resio, D. T., W. Perrie, S. Thurston and J. Hubbertz, 1992: A generic third-generation wave model: AL. *Proc. 3rd International Workshop on Wave Hindcasting and Forecasting*, Montreal, Que., 102-114.

Richards, T. L., H. Dragert and D. R. MacIntyre, 1966: Influence of atmospheric stability and over-water fetch on the winds over the lower Great Lakes. *Monthly Weather Review*, 94, 448–453.

Richardson, L. F., 1922: *Weather prediction by numerical process*. Cambridge University Press, Reprinted Dover 1965.

Ris, R. C., L. H. Holthuijsen and N. Booij, 1994: A spectral model for waves in the near shore zone, *Proc. 24th Coastal Engineering Conference*, October, 1994, Kobe, Japan, ASCE, 68–78.

Rivero, O. R., M. L. Lloret and E. A. Collini, 1974: Pronostico automatico de olas en el Atlantico sur. *Boletin del Servicio de Hidrografia Naval*, Vol X, No. 2

Rivero, O. R., C. E. del Franco Ereno and G. and N. Possia, 1978: Aleunos resultados de la aplicacion de un prognostico de olas en el Atlantico sur. *Meteorologica*, Vol VIII, IX, 331–340.

Roll, H. U. 1965: *Physics of the marine atmosphere*, Academic Press

Romeiser, R., 1993: Global validation of the wave model WAM over a one-year period using GEOSAT wave height data. *J. Geophys. Res*., 98(C3), 4713–4726.

Rye, H., 1977: The stability of some currently used wave parameters. *Coastal Eng*., 1, 17–30.

Sanders, F. 1990: Surface analysis over the oceans – searching for sea truth. *Weather and Forecasting*, 5, 596–612.

Sarpkaya, T. and M. Isaacson, 1981: *Mechanics of wave forces on offshore structures*. Van Nostrand Reinhold Co.

Schäffer, H. A., R. Deigaard and P. Madsen, 1992: A two-dimensional surf zone model based on the Boussinesq equations, *Proc. 23rd Coastal Engineering Conference*, 576–589.

Schwab, D. J., 1978: Simulation and forecasting of Lake Erie storm surges. *Monthly Weather Review*, 106, 1476–1487.

Sela, J. G., 1982: *The NMC spectral model*. NOAA Technical Report NWS 30.

Shearman, E. D. R., 1983: Radio science and oceanography. *Radio Sci*., 18(3), 299–320.

Shearman, R. J., 1983: The Meteorological Office main marine data bank. *Marine Observer*, 53, 208–217.

Shearman, R. J. and A. A. Zelenko 1989: *Wind measurements reduction to a standard level*. WMO Marine Meteorology and Related Oceanographic Activities Report, 22, WMO/TD-311.

Shemdin, O. H., K. Hasselmann, S. V. Hsiao, and K. Herterich, 1978: Non-linear and linear bottom interaction effects in shallow water. In: *Turbulent fluxes through the sea surface; wave dynamics and prediction*. Plenum Press, 347–372.

Shemdin, O. H., S. V. Hsiao, H. E. Carlson, K. Hasselman and K. Schulze, 1980: Mechanisms for wave transformation in finite depth water, *J. Geophys. Res*., 85(C9), 5012–5018.

Ship and Ocean Foundation, 1990, 1991. *Study of ocean waves and related surface winds for ship-building*. Tokyo, Japan.

Simmons, A. J., D. M. Burridge, M. Jarraud, C. Girard and W. Wergen, 1988: The ECMWF medium-range prediction models. Development of the numerical formulations and the impact of the increased resolution. *Meteor. Atmos. Phys*, 40, 28–60.

Slutz, R. J., S. J. Lubker, J. D. Hiscox, S. D. Woodruff, R. L. Jenne, D. H. Joseph, P. M. Steurer and J. D. Elms, 1985. *Comprehensive Ocean-Atmosphere Data Set (COADS), Release 1*, NOAA/ERL, Boulder, Colorado.

Smith, R. L., 1984: Threshold methods for sample extremes. In: Statistical extremes and applications. J. Tiago de Oliveira (Ed.). *Proc. NATO Advanced Study Inst. Conf.*, Vimeiro, Portugal 1983. D. Reidel, Dordrecht, 621–638.

Snodgrass, F. E., G. W. Groves, K. F. Hasselmann, G. R. Miller, W. H. Munk, and W. H. Powers, 1966: Propagation of ocean swell across the Pacific. *Phil. Trans. Royal Soc.* A, 259, 431–497.

Snyder, R. L., and C. S. Cox, 1966: A field study of the wind generation of ocean waves. *J. Marine Res*., 24(2), 141–178.

Snyder, R. L., F. W. Dobson, J. A. Elliott and R. B. Long, 1981: Array measurements of atmospheric pressure fluctuations above surface gravity waves. *J. Fluid Mech*., 102, 1–59.

Sommerfeld, A., 1896: Mathematische Theorie der Diffraction. *Math. Ann*., 47, 317-374 (from Wiegel, 1964).

Spillane, K. T. and P. E. Dexter, 1976: Design waves and wind in the Australian tropics. *Australian Meteor. Mag*., 24(2), 37–58.

Stanton, B. R., 1984: *Return wave heights off South Uist estimated from seven years of data*. Institute of Oceanographic Sciences, 164, 54 pp.

Stull, R. B. 1988: *An introduction to boundary layer meteorology*. Kluwer Academic Publishers. Dortrecht, Boston, London, 666 pp.

Sverdrup, H. U. and W. H. Munk, 1947: *Wind, sea and swell: theory of relations for forecasting*. H.O. Pub. 601, US Navy Hydrographic Office, Washington, D.C., 44 pp.

SWAMP Group, 1985: *Ocean wave modelling*. Plenum Press, 256 pp.

Taylor, P. K., E. Kent, M. Yelland and B. Moat, 1994: The accuracy of wind observations from ships. *Proc. International COADS Wind Workshop*, Kiel, Germany, May 1994, 132–151.

Thomas, J. P., 1988: Retrieval of energy spectrum from measured data for assimilation into a wave model. *Quart. J. Royal Met. Soc*., 114, 781–800.

Thomasell, A. and J. G. Welsh, 1963: *Studies of the specification of surface winds over the ocean*. Travelers Research Center, IMC, 7049–88.

Tiedtke, M. et al., 1979: *ECMWF model parameterization of subgrid scale processes*. ECMWF Technical Report, 10.

Tolman, H. L., 1990: Wind wave propagation in tidal seas. Doctoral Thesis, Delft Univ. Tech.

Tolman, H. L., 1994: Wind-waves and moveable-bed bottom-friction. *J. Phys. Oceanogr*., 24(5), 994.

Tournardre, J. and R. Ezraty 1990: Local climatology of wind and sea state by means of satellite radar altimeter measurements. *J. Geophys. Res*., 95, 18255–18268.

Tucker M. J., 1956: A shipborne wave recorder. *Trans. Inst. Nav. Archt.*, London, 98(1), 236–250.

Tucker, M. J., 1989: An improved “Battjes” method for predicting the probability of extreme waves. *Applied Ocean Research*, 4, 212–218.

Tucker, M. J. 1991: *Waves in ocean engineering: measurement, analysis, interpretation*. Ellis Horwood, Chichester, UK. 431 pp.

Tucker, M. J. 1993: Recommended standard for wave data sampling and near-real-time processing. *Ocean Engineering*, 20, 459–474.

Uji, T., 1984: A coupled discrete wave model MRI-II. *J. Oceanographical Society of Japan*, 40, 303–313.

US Navy, 1983: *Hindcast spectral ocean wave model climatic atlas: North Atlantic Ocean*. Prepared by Naval Oceanography Command Detachment, Asheville, NC, USA.

US Navy, 1985: *Hindcast spectral ocean wave model climatic atlas: Pacific Ocean*. Prepared by Naval Oceanography Command Detachment, Asheville, NC, USA.

US Navy 1990: *Hindcast spectral ocean wave model climatic atlas: Mediterranean Sea*. Prepared by Naval Oceanography Command Detachment, Asheville, NC, USA.

Vartdal, L., H. E. Krogstad and S. F. Barstow, 1989: Measurement of wave properties in extreme seas during the WADIC experiment. *Proc. 21st Offshore Tech. Conf.*, Houston, Texas, May 1989. 73–82.

Verploegh, G., 1967: Observation and analysis of the surface wind over the ocean. *KNMI, Mededelingen en Verhandelingen*, 89.

Visser, P. J., 1984: Uniform longshore current measurements and calculations. *Proc. 19th Coastal Engineering Conference*, Houston, 2l92–2207.

Vogel, J. A., A. C. Radder and J. H. de Reus, 1988: Verification of numerical wave propagation models in tidal inlets, *Proc. 21st Coastal Engineering Conference*, 433–447.

WAMDI Group (S. Hasselmann, K. Hasselmann, E. Bauer, P. A. E. M. Janssen, G. Komen, L. Bertotti, P. Lionello, A. Guillaume, V. C. Cardone, J. A. Greenwood, M. Reistad, L. Zambresky, J. A. Ewing), 1988: The WAM model – a third generation wave prediction model, *J. Phys. Oceanogr*., 18, 1775–1810.

Ward, E. G., L. E. Borgman and V. J. Cardone, 1978: Statistics of hurricane waves in the Gulf of Mexico. *Proc. 10th Offshore Tech. Conf.*, Houston, Texas, III, 1523–1536 (OTC 3229). (Also in J. of Petroleum Technology, 1979, 632–642.)

Wiegel, R. L., 1964: *Oceanographical engineering*. Prentice Hall, Englewood Cliffs, N.J.

Wilkerson, J. C. and M. D. Earle, 1990: A study of differences between environmental reports by ships in the voluntary observing program and measured from NOAA buoys. *J. Geophys. Res*., 95, 3373–3385.

Witter, D. L. and D. B. Chelton, 1991: A GEOSAT altimeter wind speed algorithm and a method for altimeter wind speed algorithm development. *J. Geophys. Res*., 96, 8853–8860.

WMO, 1970: *The Beaufort scale of wind force*. Marine Science Affairs, 3 (out of print).

WMO, 1976: *Handbook on wave analysis and forecasting*. WMO No. 446 (out of print).

WMO, 1985, 1991, 1994(*a*): *National reports on wave measuring techniques, numerical wave models and intercomparison*. WMO Marine Meteorology and Related Oceanography Activities Report 12, & Suppls. 3, 4. WMO Wave Programme, WMO/TD-No. 35.

WMO, 1988: *Guide to wave analysis and forecasting*. 1st edition. WMO No. 702, Geneva, Switzerland.

WMO, 1990: *Manual on marine meteorological services*. 2nd edition. WMO No. 558, Geneva, Switzerland.

WMO, 1994(*b*): *Guide to the applications of marine climatology*. WMO No. 781, Geneva, Switzerland.

WMO, 1995: *Manual on codes*. WMO No. 306.

WMO, 1996: *Guide to meteorological instruments and methods of observation*. WMO No. 8.

Wu, J., 1980: Wind-stress coefficients over sea surface near neutral conditions: a revisit. *J. Phys. Oceanogr*., 10, 727–740.

Wu, J., 1982: Wind-stress coefficients over sea surface from breeze to hurricane. *J. Geophys. Res*., 87, 9704–9706.

Wyatt, L. R. and G. Holden, 1994: Limits in direction and frequency resolution for HF radar ocean wave directional spectra measurements. *The Global Atmosphere-Ocean System*, 2, 265–290.

Wyatt, L. R., J. Venn, M. D. Moorhead, G. B. Burrows, A. M. Ponsford and J. van Heteren, 1985: HF radar measurements of significant wave height and mean period during NURWEC. In: *Evaluation, comparison and calibration of oceanographic instruments. Advances in underwater technology and offshore engineering*. Graham and Trotman, London, 209–222.

Young, I. R. and G. J. Holland, 1996: *Atlas of the oceans: wind and wave climate*. Pergamon, 246 pp + CD-ROM.

SELECTED BIBLIOGRAPHY

CERC, 1984: Coastal Engineering Research Center, 1973, 1977, 1984: *Shore protection manual*. Waterways Experiment Station, US Army Corps of Engineers.

Crapper, G. D., 1984: *Introduction to water waves*. Publ. Ellis Harwood, 224 pp.

Hogben, N., N. M. C. Dacunha and G. F. Olliver, 1986: *Global wave statistics*. Unwin Brothers for British Maritime Tech. Ltd.

Kinsman, B., 1965: *Wind waves, their generation and propagation on the ocean surface*. Prentice-Hall Inc., Englewood Cliffs, New Jersey. Reprinted by Dover Publ. 1984, 676 pp.

Khandekar, M. L., 1989: *Operational analysis and prediction of ocean wind waves*. Coastal and Estuarine Studies No. 33, Springer-Verlag, New York, 214 pp.

Kitaigorodskii, S. A., 1970: *The physics of air sea interaction*. Gidrometeorologicheskoe Izdatel'stvo, Leningrad, (translated from Russian). Israel Programme for Scientific Translations, Jerusalem.

Komen, G. J., L. Cavaleri, M. Donelan, K. Hasselmann, S. Hasselmann and P. A. E. M. Janssen, 1994: *Dynamics and modelling of ocean waves*. Cambridge University Press, 532 pp.

Lighthill, J., 1978: *Waves in fluids*. Cambridge University Press, 504 pp.

Massel, S. R., 1994: *Ocean waves: their physics and prediction*. World Scientific Publ., Advanced Series in Ocean Engineering, 350 pp.

Pierson, W. J., G. Neumann, and R. W. James, 1955: *Practical methods for observing and forecasting ocean waves by means of wave spectra and statistics*. US Navy Hydrographic Office Pub., 603, 284 pp.

Stoker, J. J., 1957: *Water waves*. Interscience, New York, 567 pp.

Tucker, M. J. 1991: *Waves in ocean engineering: measurement, analysis, interpretation*. Ellis Horwood, Chichester, UK. 431 pp.

Young, I. R. and G. J. Holland, 1996: *Atlas of the oceans: wind and wave climate*. Pergamon, 246 pp + CD-ROM.

INDEX

Page(s)